ENHANCEMENTS TO
THE DAMAGE LOCATING VECTOR METHOD
FOR STRUCTURAL HEALTH MONITORING

TRAN VIET ANH

NATIONAL UNIVERSITY OF SINGAPORE

2009

ENHANCEMENTS TO
THE DAMAGE LOCATING VECTOR METHOD
FOR STRUCTURAL HEALTH MONITORING

TRAN VIET ANH

BEng, MEng (UCE, Viet Nam)

A THESIS SUBMITTED

FOR THE DEGREE OF DOCTOR OF PHILOSOPHY

DEPARTMENT OF CIVIL ENGINEERING

NATIONAL UNIVERSITY OF SINGAPORE

2009

To my parents,

Acknowledgements

First and foremost, I would like to express my special thanks to my advisor, Professor Quek Ser Tong, for his patience and encouragement that carried me on through difficult times. Prof. Quek's advice had not only made this study possible but also a very fruitful learning process for me. His complete understanding and deep insight have been the key factors to my academic growth over my PhD candidature.

I would also like to acknowledge Dr. Duan Wenhui and Dr. Hou Xiaoyan for their invaluable discussion and friendship during my research and study. Discussion with them greatly enhances the process of tackling the problems encountered during my research progress.

Additionally, I am grateful to all staffs and officers at the Structural Concrete Laboratory, NUS, especially, Ms Tan Annie, Mr. Ow Weng Moon, and Mr. Ishak Bin A Rahman, for their time and assistance in making this research possible.

Besides, I wish to express my sincere gratitude to the National University of Singapore offering me the financial aid for my study.

Finally and most importantly, I would like to acknowledge the special love, support and understanding I have received from my family.

Table of Contents

Summary

The main objective of this thesis is to develop the Damage Locating Vector (*DLV*) method further for structural damage detection by (a) extending its formulation to accommodate multi-stress state elements and the variation of internal forces and element capacity along element length; (b) proposing two schemes to identify damaged elements for the case of imperfect measurements; (c) proposing a simple algorithm to assess the severity of the identified damaged elements; (d) proposing two algorithms to detect damage for the case where the applied static and dynamic loads are unknown; (e) introducing an algorithm to identify faulty signals; and (f) integrating wireless sensor network into the *DLV* method where the issue of intermittent loss during wireless transmission of raw data packets from the sensor nodes to the base station is addressed.

Firstly, the normalized cumulative energy (*NCE*) of each element is proposed as damage indicator instead of the normalized cumulative stress (*NCS*) in the original *DLV* method to extend to cases where the structure contains frame elements. Secondly, since measurement of input excitation is expensive or in some cases impossible, damage detection using the *DLV* method and unknown excitation is developed. For the static case, the unknown to be solved is limited to a fixed factor between the loading at the reference and the damaged states. This is practical since the magnitudes of the static loads when performing for the reference and the damaged states are usually constant for convenient implementation but need not be the same since they are performed at two different times which may be months or years apart. For the dynamic case, the structural stiffness matrix may be determined directly from the measured accelerations without knowing the details of the input excitations. By using the

Newmark-β method to relate velocity and displacement vectors at different time steps to the initial values, a system of nonlinear equations is formulated based on the equations of motion of the structure at different points in time. Newton-Raphson method is then used to solve the system of nonlinear equations with the stiffness coefficients as unknowns. Both algorithms assume that the locations of the actuators and sensors are known. Thirdly, two schemes are proposed to identify the actual damaged elements from a larger set of potential damaged elements (*PDE*) arising from imperfect data, namely, an intersection scheme and a two-stage analysis. The first algorithm, which is robust for cases where the number of sensors used is relatively large, makes use of the common elements in different sets of potential damaged elements computed based on various combinations of sensor readings to identify the actual damaged elements. The second algorithm, which is effective for cases where the number of sensors available is limited, locates possible damaged regions using the change in structural flexibility and then analyzes the damaged regions using the *DLV* method. Fourthly, an algorithm to assess the damage severity of the identified damaged elements is developed. In this algorithm, the first singular value of a flexibility matrix which is constructed using a numerical model of the structure is iteratively adjusted such that it corresponds to that derived from the measured data by changing the stiffnesses of the identified damaged elements using a penalty function method.

Even though a robust damage detection algorithm is available, the damage detection results may still not be reliable if the sensor is faulty or data are of low quality. An algorithm is proposed to assess the quality of measured data (or the *in-situ* sensors) by making use of signals from various sets of sensors to form different flexibility matrices. Singular value decompositions are performed on these matrices to

identify the non-zero singular values (*NZV*) and the relative quality among different sets can be deduced. The set which produces the smallest *NZV* is considered as associated with healthy sensors and sensors which do not belong to this set may be considered as faulty. The algorithm can identify multiple faulty sensors simultaneously and is applicable for the cases where structure is either damaged or healthy. The feasibility of the algorithm is illustrated using simulated and measured data from a 3-D modular truss structure.

Traditionally, to collect structural response data, either displacement transducers or accelerometers are employed. Wireless sensors are becoming popular as measured responses collected from conventional sensors wired to the data acquisition system can be costly to install and maintain, and may interfere with the operations of the structure. The transmission of individual packet of data from each sensor using radio frequency to the base station usually experiences intermittent loss based on commercially available system. An algorithm to reconstruct the lost data values is introduced. Discrete Fourier transform (*DFT*) is employed to identify the significant frequencies of the measured data and the Fourier coefficients are determined by least-squares fit of the measured values in an iterative manner to reconstruct an approximated complete signal. The algorithm is found robust for the case where signals with 30% of lost data can be reconstructed with less than 10% 'error' in the lost portions. This approach is slightly different from the recent non-commercial systems where each sensor board is equipped with substantial memory and a firmware for *DFT* to pre-process the data before transmission. This recent innovation by other researchers also has limitations which have yet to be fully resolved.

The enhancements to the *DLV* method are illustrated using (a) simulated data from a 2-D warehouse structure which comprises truss elements as well as beam and

column elements with varied and constant cross-sectional areas; and (b) experimental data from two 3-D modular truss structures.

Keywords: damage detection, damage locating vector, normalized cumulative energy, wireless sensor, transmission loss, sensor validation.

List of Tables

List of Figures

List of Symbols

Latin letters

$\mathbf{a}$	=	acceleration vector
b	=	width of beam
$\mathbf{d}$	=	structural displacement vector
$\dot{\mathrm{d}}$	=	first time differentiate of displacement d (or velocity)
$\ddot{\mathrm{d}}$	=	second time differentiate of displacement d (or acceleration)
$\mathbf{f}$	=	force vector
h	=	height of beam element
i	=	imaginary number
n	=	structural degree of freedoms
ne	=	number of structural elements
$ndlv$	=	number of damage locating vector
nf	=	number of frequency contained in applied force
ns	=	number of sensors used
$\mathbf{q}_1$, $\mathbf{q}_2$	=	Boolean matrix
r	=	number of input
s	=	singular value
t	=	time
$\mathbf{u}$	=	input force vector in time domain
$\mathbf{v}$	=	velocity vector
$\mathbf{x}$	=	state vector
$\mathbf{y}$	=	output vector
$\mathbf{A}$	=	discrete state matrix; cross sectional area

$\mathbf{A}_c$ = continuous state matrix

$\mathbf{B}$ = input influence matrix at discrete-time state

$\mathbf{B}_2$ = input influence matrix characterizing the locations and types of inputs

$\mathbf{B}_c$ = input influence matrix at continuous-time state

$\mathbf{C}$ = output influence matrix for state vector

$\mathbf{C}_a$ = output influence matrix for acceleration

$\mathbf{C}_d$ = output influence matrix for displacement

$\mathbf{C}_v$ = output influence matrix for velocity

$\mathbf{D}$ = direct transition matrix at discrete-time state

$\mathbf{D}_d$ = structural damping matrix

$\overline{\mathrm{D}}_d$ = structural modal damping matrix

DLV = damage locating vector

E = modulus of elasticity (Young modulus); energy

NCE = Normalized Cumulative Energy

ERA = Eigensystem Realization Algorithm

$\mathbf{F}$ = structural flexibility matrix

$\mathbf{F}_u$ = structural flexibility matrix of reference (undamaged or intact) state

$\mathbf{F}_\Delta$ = relative change in flexibility matrix

$\mathbf{F}_d$ = structural flexibility matrix of altered (damaged or reinforced) state

G = shear modulus; gain matrix

$\mathbf{H}$ = Hankel matrix

I = moment of inertial of section

$\mathbf{I}$ = identity matrix

$\mathbf{K}$ = structural stiffness matrix

$\mathbf{K}_u$ = structural stiffness matrix at reference (undamaged or intact) state

$\mathbf{K}_d$ = structural stiffness matrix at altered (damaged or reinforced) state

$\overline{\mathbf{K}}$ = structural modal stiffness matrix

L = length of element

L_1 = Length of elements in unaltered part of structure

L_2 = Length of elements in altered part of structure

$\mathbf{M}$ = structural mass matrix

$\overline{\mathbf{M}}$ = structural modal stiffness matrix

N_1 = internal axial force in unaltered part of structure

N_2 = internal axial force in altered part of structure

$\mathbf{O}$ = zeros matrix

P = force

$\mathbf{P}$ = force vector

Q_1 = internal shear force in unaltered part of structure

Q_2 = internal shear force in altered part of structure

SNR = Signal to Noise Ratio

T = structural period

$\mathbf{U}$ = left singular matrix; input matrix

$\mathbf{V}$ = right singular matrix

$\mathbf{Y}$ = Markov parameters

$\overline{\mathbf{Y}}$ = observed Markov parameters

Greek letters

Δt = discrete time step

δ = displacement

ε = sensitivity of equipment

Ξ = energy

$\bar{\Xi}$ = normalized cumulative energy

$\delta\mathbf{F}$ = matrix of relative change in flexibility

λ = eigenvalue

Λ = eigenvalue matrix

ρ = material mass density

ψ = arbitrary normalized eigenvector

Ψ = eigenvector matrix

π = Pi

σ = element stress

Σ = singular value matrix

ν = poison ratio

ξ = number of observed point in time domain

ω = structural frequency

Other symbols

$\dagger$ = pseudo-inverse

$\widehat{(\bullet)}$ = estimated value of $(\bullet)$

CHAPTER 1

INTRODUCTION

Our daily life depends heavily on infrastructures such as buildings, bridges, and offshore platforms. Through years of operation, these infrastructures may suffer from aging, corrosion, change in loading and environmental conditions, earthquake, and terrorist attack, leading to damage. Early detection of damage in infrastructures can help to increase the safety and reliability of existing structures, provide authorities with necessary measures to extend the service life of the infrastructures and reduce cost, or in some extreme cases, minimize catastrophic failures and loss of lives. Interests in monitoring the occurrence of damages as well as their severity can be substantiated by the intensity of research being carried out in recent years. Thorough review on the development of structural damage detection can be found in Doebling et al. (1996), Zou et al. (2000), Auweraer and Peeters (2003), Chang et al. (2003), Worden and Dulieu-Barton (2004), Alvandi and Cremona (2006), Kerschen et al. (2006), Yan et al. (2007), Worden et al. (2007), Worden et al. (2008), Nasrellah (2009), and Soong and Cimellaro (2009).

In this chapter, the definition of damage and the different methods for structural damage detection are discussed. A review of published works in structural damage detection as well as their applicability and limitations is summarized, leading to the formulation of the objectives and scope of this study. This chapter ends with a description of the layout of this thesis.

1.1 DAMAGE IN STRUCTURE

Damage in a system in general is a negative change introduced into the system. In civil engineering context, damage is defined as the degradation of material, the reduction in quality of boundary condition, or the breakage of connections. These damages are caused by many different sources such as corrosion, aging, earthquake, fire, and changes in loading and environmental conditions as lifestyle and technology advancements.

Structural damage has been studied thoroughly and different classifications of structural damage have been proposed. Barer and Peters (1970) introduced six common types of damage, namely (1) brittle damage, (2) fatigue damage, (3) corrosion fatigue, (4) stress corrosion cracking, (5) crevice carrion, and (6) galvanic corrosion. Schiff (1990) proposed another classification of damage for structures comprising six different types of damages, namely (1) elastic damage, (2) damage of brittle material, (3) fatigue damage, (4) brittle damage, (5) damage due to elastic instability, and (6) damage due to excessive deflection.

Detailed studies on various damages in structures have been performed to quantify the physical state of damage, its causes and effects. Damage in reinforced concrete structures under fire is found to be dependent on the bond characteristics, the length of elements, the behaviour of steel material, and the size of fire compartment (Izzuddin and Elghazouli, 2004; Elghazouli and Izzuddin, 2004; Wong, 2005; Kodur and Bisby; 2005). Damage in cold-formed beams and columns is attributed mainly to the local buckling effect which is usually not the case for hot-rolled beams and columns. The latter failure is usually attributed to the inadequate capacity of a section of structural members (Delatte, 2005). Damage in structures due to underground blast is found largely dependent on both spatial variation effect

and structure-ground interaction effect caused by blast-induced motion (Wu and Hao, 2005a-b). Damage in buildings under terrorist attacked by planes crashed is attributed not only to the impact by the airplanes but also the fire and the weakening of steel and concrete material under fire (Omika et al., 2005).

The simplest way to simulate damage in numerical study is to reduce the Young's moduli of members (Law et al., 1998) or element stiffness (Yang and Huang, 2007). Although this does not cover all kinds of damage, it is sufficient for evaluation of many practical situations. Hence for experimental studies, most researchers either introduce a cut (Vo and Haldar, 2005) or change affected member from a larger cross-sectional area to a smaller cross-sectional area (Gao et al., 2007).

The varying physical cause and development of damage in structure has partly resulted in different methods for structural damage detection being proposed by researchers. These various methods will be briefly reviewed in the following sections.

1.2 LITERATURE REVIEW

The aim of a structural damage detection tool can be classified into four levels (Doebling et al., 1996):

(*i*) detect the presence of damage as it occurs,

(*ii*) determine the location of the damage,

(*iii*) assess the damage severity, and in some cases

(*iv*) predict the remaining service life of the structure.

To achieve this aim, identification methods and solution techniques have been evolved. The methods are generally classified into (a) non model-based and (b) model-based.

The solution techniques, which are commonly employed, include Least Square Estimation (LSE) method, Kalman Filter (KF) method, Extended Kalman Filter (EKF) method, Genetic Algorithm (GA) method. Predicting the remaining service life of the structure which is classified as a level (*iv*) stage of structural health monitoring (*SHM*), usually relates to structural design assessment, fatigue analysis, and fracture mechanics, and is only performed after structural damage detection has been completed and is not considered in this report.

Non model-based methods employ response data obtained from two different states of the structure, reference and damaged, in order to detect and localize damage without involving a detailed analytical model of the structure and can usually achieve level (*ii*) solution, namely determining the location of damage. Model-based methods attempt to update the analytical model of the structure using measured response data at various states of the structure in order to assess structural damage. Such methods are capable of assessing the damage severity, complete a level (*iii*) analysis. If an analytical model of the structure is not available, model-based methods can make use of analytical equations where the unknowns to be solved are parameters of the structure. The main difference between the two classes of methods is therefore the dependency on the parameterized analytical model or equations of the structure. Some of these identification methods and solution techniques for structural damage detection are briefly reviewed in the following.

1.2.1 Non model-based damage detection

Non model-based methods for structural damage detection may be the oldest methods to assess the damage of existing structures and are still commonly used today due to their simplicity. Looking at structural components to search for cracks and

damages is classified as visual inspection method (Bray and McBride, 1992; Dry, 1996; Pang and Bond, 2005; Fraser, 2006). Listening to the audible variations in response to the tapping on structural surface to determine if voids or debonding exists is denoted as tap test (Cawley et al., 1991; Lipetzky et al., 2003). Visualizing the interior of structure to assess the existence of crack using X-ray or Gamma ray is grouped under the name of X-ray or Gamma ray methods (Jama et al., 1998; Balasko et al., 2004; Thornton, 2004). Measuring the state of stress using ultrasonic guided wave or eddy current can also locate cracks in structures (Green, 2004; Tsuda, 2006; Lee et al., 2006).

With rapid advancement in information technology, sophisticated methods have been proposed to assess structural damage. Measuring the traveling time of a signal through existing structural component (Quek et al., 2003); identifying the presence of spikes or impulses in the time-frequency of a signal after performing wavelet transform (WT) or Hibert-Huang Transform (HHT) (Hou et al., 2000; Lu and Hsu, 2002; Rajasekaran and Varghese, 2005; Yang et al., 2004; Xu and Chen, 2004) forms the basis of a class of methods to localize damage in structure and in some cases the severity and geometry of the damage. For example, Yang et al. (2003a-b) employed Hibert-Huang spectral analysis to identify linear structure and locate damage using either (*i*) normal modes, or (*ii*) complex modes. From the measured response data of a free vibration structure at only one *DOF*, empirical mode decomposition (*EMD*) is employed to identify modal responses. Hilbert transform is then performed on each modal response to estimate the instantaneous amplitude and phase angle time histories. Subsequently, the natural frequencies and damping ratios of the structure are identified using a linear least-squares fit procedure. When the measurements at all *DOF* of structure are available, by comparing the magnitudes and phase angles computed from

measurements at different *DOF*, structural mode shapes, physical mass, damping and stiffness matrices can be evaluated. To further demonstrate the feasibility of HHT technique to detect structural damage, Quek et al. (2003) used the signal after passing through the HHT algorithm to locate damages in beams and plates. The damage is detected based on simple wave propagation consideration using changes in flight times, velocities and frequencies. Some difficulties in applying the HHT technique were also discussed such as signal end effects, and the criterion to terminate the shifting process. From these studies, HHT appears to be a good signal processing tool for damage detection in dealing with actual measurements which contain noise.

Methods using change in modal properties such as natural frequencies or mode shape to localize damage are also classified as non model-based methods (Yuen, 1985; Lin, 1995; Pandey et al., 1991; Khan et al., 2000). Because modal information reflects global properties, change in modal parameters might not be optimal to detect damage of a localized nature. Alternatively, change in mode shape curvature (Alampalli et al., 1997; Wahab and De Roeck, 1999) and change in modal strain energy (Shi et al., 2000, 2002) have also been utilized to detect damage. Moreover, model updating methods, which map the modal properties of an analytical model to the modal properties of the measured model for structural damage detection, have also been explored (Fritzen and Jennewein, 1998; Wahab et al., 1999; Halling et al., 2001). Since measuring natural frequencies alone is faster and more economical than measuring mode shape values, natural frequencies can be selected as variables to be updated (Maeck et al., 2000). To increase accuracy and speed up the solution process, combination of frequencies and mode shape values have been integrated into the objective function which needs to be updated (Jaishi and Ren, 2005). To relax mapping the analytical frequency and mode shape value of every mode to those of the synthesized model and to provide more

information within a desired frequency range, frequency response function (FRF) has been employed as updating variables (Cha and Tuck-Lee, 2000).

Despite the successes of non model-based methods, there are concerns about their practicality in detecting structural damage. Visual inspection methods are subjective and dependent on experience of the inspectors and the results are significantly affected by environmental conditions such as temperature and humidity. Tap test is only applicable to assess local damage at the surface of the structure. X-ray, Gamma-ray, and ultrasonic guided wave methods require skilled engineers and raise great concerns about safety and health issues on the operators. Methods based on time traveling of guided signal or the presence of abrupt changes in decomposed signals are suitable for homogeneous components whereas practical issues with regards to composites has yet to be satisfactorily resolved. Methods based on change in modal parameters can only provide reliable results for some simple problems such as cantilever beam, simply supported beam, single bay truss structure, and cantilever plate (Tenek et al., 1995; Salawu and Williams, 1995; Swamidas and Chen, 1995; Ratcliffe, 1997; Farrar and James, 1997; Diaz and Soutis, 1999; Narayana and Jebaraj, 1999; Ray and Tian, 1999; Qu et al., 2006). The modal-based methods have been found to be (*i*) dependent on the geometry of damage, and (*ii*) not sensitive to damage severity (Chen et al., 1995; Banks et al., 1996). Meanwhile, model updating methods which are based on modal parameters have difficulty providing accurate solutions because the objective function usually converges to a local maximum (Jaishi and Ren, 2005).

1.2.2 Model-based damage detection

Model-based damage detection methods, which exploit the physical model of the undamaged structure or the analytical equations containing parameters to be identified, together with the response data at various states of the structure to assess structural damage, may overcome some limitations of non model-based methods such as the dependence on the experience of the inspectors, the restricted application on homogeneous structures. Model-based methods for structural damage detection can generally be classified into two approaches, namely (1) static response based methods; and (2) dynamic response based methods.

(1) ***Detect damage using static response***

Methods using static response for identification of structural parameters and damage detection are amongst the simplest formulations (Liu and Chian, 1997; Sanayei and Saletnik, 1996a-b; Liang and Hwu, 2001). To generate structural deformations, a static load is utilized. Static response in term of either displacement or strain can be measured using displacement transducers or strain gauges, respectively. The damage identification problem is then converted into an optimization problem in which the objective function to be minimized is the error norm of structural equilibrium in terms of either nodal forces or nodal displacements, from which the structural parameters can be identified. By comparing the current structural parameters with those at the reference or undamaged state, damage elements, if any, and their severity can be assessed. Generally, the advantages of methods based on static response over those based on dynamic response are that (*i*) the model is simple; and (*ii*) data storage is manageable. No assumption on mass or damping is required, implying that less errors and uncertainties are introduced into the model. The quantity of data captured is small compared to dynamic response data (Ling, 2004).

Sanayei and Scampoli (1991) mapped the analytical stiffness matrix which is derived from the finite element model (FEM) of the structure onto the measured stiffness matrix which is computed from the force and displacement measurements. The mapping process is performed by minimizing the difference in every component of the upper right triangle of the analytical stiffness matrix with its counterpart in the measured stiffness matrix. The variables to be identified are the structural parameters such as cross-sectional areas, moment of inertia. The optimization problem was solved by an iterative Least Square Estimation (LSE) algorithm from which structural parameters can be estimated. Numerical examples of a pier-deck model consisting of a doubly-reinforced orthogonal slab supported by cap beams showed its ability to estimate structural parameters correctly. The proposed method is found attractive due to its simplicity. However, the number of measured points should be larger than the number of unknown parameters to guarantee a proper solution.

Banan et al. (1994a-b) proposed two algorithms to estimate the member parameters such as cross-sectional areas and Young's moduli of a finite element model of the structure with known topology and geometry from measured displacements under known static load. The problem is transformed into a constrained optimization formulation in which the discrepancy between either displacements or forces of the finite element model and the measurements at the measured points is used as the objective function. The least square minimization of the objective function is solved by an iterative quadratic programming approach. The proposed method is capable of estimating structural parameters for the case of incomplete spatial measurements. Hjelmstad and Shin (1997) further developed the method to detect structural damage accounting for measurement errors using a Monte Carlo model. Although zero-mean white noise with root mean square (*RMS*) of 5% was introduced to all measurements,

multiple damaged elements can still be identified with high confidence (approximately 96% probability).

Despite the feasibility of methods based on static response to assess structural damage, they have yet to be widely used in practice. It may be attributed to the fact that (*i*) civil structures are usually large and/or complex with extremely high stiffnesses which may require exceptionally large static load to generate measurable deflections; (*ii*) reference locations are required to measure deflections which might be impractical to implement in reality for structures such as bridges, offshore platforms, and space structures; and (*iii*) static response based methods are sensitive to measurement errors.

(2) ***Detect damage using dynamic response***

Methods to detect damage in structure based on dynamic response are widespread due to their significant advantages such as: (*i*) it is adequate to excite an existing structure with a small amplitude dynamic load (relative to the required magnitude of the static load) or in some circumstances, natural sources such as wind, earthquake, and moving vehicle can be employed; (*ii*) the use of acceleration responses eliminate the need for a fixed physical reference such as that required by measurement of deflection; and (*iii*) dynamic response based methods can accommodate higher level of measurement error compared to static response based methods or in some cases where the measurements are taken long enough, the effect of zero-mean white noise may automatically cancel out for some methods (Chang et al., 2003). Methods for structural damage detection using dynamic response can be further classified into: (*a*) methods using change in stiffness or flexibility matrix; (*b*) substructure methods; and (*c*) other methods.

(*a*) *Methods using change in stiffness or flexibility matrix*

Based on a numerical model of the structure with "original" values of the parameters, the structural stiffness/flexibility matrix can be computed. From the measured dynamic responses of structure, the "corresponding" structural stiffness/flexibility matrix can be formulated. If the two matrices are significantly different, it may be attributed to the presence of damage. The numerical stiffness/flexibility matrix is modified by changing the values of the structural parameters such that some criteria are satisfied. These modified values can then be used to deduce the elements that are damaged as well as their severity.

Escobar et al. (2005) proposed a method to locate and estimate the severity of damage using changes in stiffness matrix. The latter is used with the penalty function method in an iterative scheme to estimate the change in stiffness contribution factor of each element to the global stiffness from the undamaged to the damaged state. Element(s) with large reduction of stiffness contribution factor over a period of time is classified as being damaged and the corresponding contribution factor is used to assess elemental damage severity. Three numerical examples, namely a ten-story one-bay frame, a ten-story five-bay frame and a two-storey 3-D one-bay by one-bay frame were used to illustrate the effectiveness of the proposed method. Damaged scenarios were generated by reducing the stiffness of affected columns from 10% to 45% while noise level of up to 10% was also introduced. The method has been shown to be capable of assessing both damaged elements and their severity accurately. However, the applicability of the method to detect damaged elements other than column elements such as beam and brace elements has not been addressed.

Chase et al. (2005) also developed an algorithm for continuous monitoring of the state of a structure. It is assumed that mass and damping are time invariant while stiffness keeps changing from one time step to another. Shear structures of 4, 12 and

120 degrees of freedom (*DOF*) were utilized for both theoretical formulation and numerical simulation. The change in structural stiffness matrix ($\Delta\mathbf{K}$) was divided into n (n is the number of stories) sub-matrices of the same size with the global stiffness matrix containing entry of 1, -1 and 0, each of which is multiplied by an unknown parameters α_i (i = 1, 2,…, n). For instance, the change in structural stiffness matrix for a 3-*DOF* shear structure can be expressed as

$$\Delta\mathbf{K} = \sum_{i=1}^{3} \alpha_i \, \Delta\mathbf{K}_i = \alpha_1 \begin{bmatrix} 1 & 0 & 0 \\ 0 & 0 & 0 \\ 0 & 0 & 0 \end{bmatrix} + \alpha_2 \begin{bmatrix} 0 & -1 & 0 \\ -1 & 1 & 0 \\ 0 & 0 & 0 \end{bmatrix} + \alpha_3 \begin{bmatrix} 0 & 0 & 0 \\ 0 & 0 & -1 \\ 0 & -1 & 1 \end{bmatrix} \quad (1.1)$$

The unknowns α_i at each time step are identified by utilizing adaptive recursive least squares filter based on the minimization of the discrepancy between applied force vector and the force calculated from structural responses. From the identified α_i, the structural stiffness at each time step is estimated. The damaged elements and their severity are then extracted based on their contribution to the global stiffness (vector α_i). Using a benchmark 3-D steel structure (4-story, each story 0.9 m tall, 2-bay by 2-bay in plane each bay with 1.25m long), four damaged patterns were studied, namely (*i*) all braces in the 1st story removed; (*ii*) all braces in the 1st and the 3rd stories removed; (*iii*) one brace in the 1st story removed; and (*iv*) one brace in each of the 1st and the 3rd stories removed. Results showed the feasibility and robustness of the method in detecting structural damage with short convergence time (maximum convergence time required is 1.56 seconds after damage occurred). However, the decomposition of the matrix of change in stiffness into n sub-matrices of the same size, the assumption of lumped mass matrix, and the assumption of damping as proportional to the stiffness matrix are suitable mostly for simple shear structures.

To accurately construct the stiffness matrix from dynamic responses requires the excitation of both lower and higher modes which is difficult in practice (Pandey

and Biswas, 1994; Gao and Spencer, 2002). Hence, methods based on change in flexibility matrix which can bypass this difficulty have been proposed (Alvin et al., 2003; Alvandi and Cremona, 2006). Pandey and Biswas (1994) used measured acceleration responses and applied load history to identify structural natural frequencies and mode shapes. Structural flexibility matrix can be constructed with high accuracy using only a few lower modes as follows

$$\mathbf{F} = \sum_{i=1}^{nm} \frac{1}{\omega_i^2} \boldsymbol{\psi}_i \boldsymbol{\psi}_i^T \tag{1.2}$$

where $\mathbf{F}$ is the estimated flexibility matrix, ω_i the i^{th} frequency, $\boldsymbol{\psi}_i$ the i^{th} mode shape, *nm* the number of modes used to form the flexibility matrix which is much smaller than the number of structural *DOF*. Based on the starting point where flexibility starts to change and the maximum change in flexibility coefficients between the intact and the damaged states, damage locations and severity can be monitored. For cantilever beam, the commencement of damage is identified by the starting point where flexibility starts to increase. For simply supported beam or free-free beam (after removing rigid body modes), maximum change in flexibility indicates the location of damage. A simply-supported beam was experimentally performed to illustrate its suitability for practical application. The applicability of the method for more complex structures has not been fully addressed. Bernal (2002) used the change in flexibility matrix to compute the so-called Damage Locating Vector (*DLV*) which is then used to localize damage. When the *DLV* is treated as a static force vector onto the reference structural model, zero-stress field is observed at the damaged regions, providing a means to identify structural damage. The method has been shown feasible both numerically and experimentally using truss structures (Bernal, 2002; Gao et al., 2007). It is attractive to observe that the method is applicable for both static and dynamic

response. However, performance of the method for structures comprising multi-stress state elements has not been fully addressed.

Despite the promising of the methods based on change in flexibility matrix to assess structural damage, it must be noted that (*i*) they are much less sensitive to the cases where damage is close to supports or damage located far away from excitation locations (Alvandi and Cremona, 2006); (*ii*) they require a large number of sensors (such that at least the first three modes are properly captured) to locate damaged regions correctly (Alvin et al., 2003); and (*iii*) their applicability to real and/or complicated structures which contain many *DOF* and elements remains of a great concern (Doebling, et al., 1996). Methods based on substructure concept, which may mitigate some of these difficulties will be reviewed next.

(*b*) *Substructure methods*

Recognizing that existing structures are usually large and/or complicated, substructure methods have been proposed to identify structural parameters on a "divide and conquer" principle (Koh et al., 1991; Koh et al., 1999). The structure is divided into substructures either with or without overlap. A set of equations of motion and observation equations is formulated for each substructure. This system of equations is solved using Extended Kalman filter with Weighted Global Iteration (EK-WGI) to obtain parameters of the substructures. The EK-WGI method requires measurements of displacements and velocities at all interface *DOF* in the first generation of substructure methods though accelerations are commonly measured in practice. This requirement is relaxed in Koh et al. (2003a-b) by the use of Genetic Algorithm (GA) to solve the above-mentioned system of equations, where acceleration measurements at all interface *DOF* are still required. This requirement is completely relaxed in Koh et al. (2003c) by employing GA algorithm to minimize the difference in the interface force

vectors which are formulated using different sets of measured responses. Michael (2006) further improved the substructure methodology to encompass the case of output only problem. However, measurements collocated with and adjacent to the *DOF* where the forces are applied are required.

It is noted that all substructure methods have been proposed and illustrated using shear structures with both numerical and experimental examples, where identification of damage is limited to columns or story stiffnesses only. Application of substructure methods to detect damage in general frame structures which comprise beam, column and brace elements have not been fully addressed.

(*c*) *Other methods*

There are methods in the literature which cannot be classified easily into the above-mentioned two categories. These include optimization based methods, Neural Network (*NN*) based methods, output only methods, and nonlinear methods. These methods will be briefly reviewed in this section.

Optimization based methods: When excitation forces and structural responses at all *DOF* are available, an over-determined system of equations can be formulated based on the equations of motion of structure at different time steps to solve for unknowns including system mass, damping and stiffness coefficients. To solve this system of equations, many techniques are available and have been attempted, such as Least Square Estimation (LSE) method, Conjugate Gradients Square (CGS) method, Minimum Residual (MR) method, Generalized Minimum Residual (GMR) method, Quasi-minimal Residual (QR) method, based on which structural parameters can be estimated (Hac and Spanos, 1990). For the cases where only limited responses are measured, Kalman Filter (KF), which is a technique to minimize the estimated error covariance of state vectors (including velocities and displacements) using a predictor-

corrector type estimator, can be employed. The KF essentially contains two stages: time update and measurement update. The former projects the current state estimation ahead in time; the latter adjusts the projected estimation by the actual measurements at that time. When the system of equations contain nonlinear terms as commonly encountered in structural health monitoring problem since structural parameters are embedded into the state variables, Extended Kalman Filter (EKF) can be employed. The EKF is actually the KF where the model in real time (first stage) is linearized using previous estimation. However, when processing EKF algorithm, some poles corresponding to unknown structural parameters of the linearized state equations might lie on the imaginary axis, leading to unstable solution (Evensen, 1994). Unstable or even divergent results may also be observed if the system is highly nonlinear (Moradkhani et al., 2005). To overcome such limitation, Monte Carlo based KF, denoted as Ensemble Kalman Filter (EnKF), has been developed (Reichle et al., 2002; Moradkhani et al., 2005). In the EnKF model, the estimation of *a priori* model covariance is not required in the updating step (second stage). Instead, Monte Carlo method is used to approximate the error covariance evolution equation to forecast the error. However, the authors also acknowledge that computational intensity remains challenging for large systems.

Alternatively, GA technique, which is a search machine that minimizes the difference between the measured and simulated signal (usually accelerations or nodal forces) based on the random variation and selection of a population of solutions, can be employed. The advantages of GA over traditional optimization techniques such as LSE and EKF are that (*i*) it can provide global optimal solution since it searches from a population of points rather than a single point; and (*ii*) it can be applied for discontinuous or discrete problems where derivation of objective function is expensive

or not available. Computational intensity is the only concern in the implementation of GA algorithm to real problems.

Neural network methods: Neural network based methods rooted from the study of biological neurons in which measurements are matched to a set of trained samples representing different types of damage (Waszczyszyn and Ziemianski, 2001). Neural network based methods are particularly suitable for problems where significant data-base on different damaged scenarios is available but explicit algorithm is not easy to obtain. However, the mapping process is only accurate if the pattern matches one of the samples in the training set. Training the *NN* with all possible damaged scenarios of a structure is time consuming if not impossible since the latter are practically infinite. To mitigate this limitation, support vector machine (SVM) is invoked as a mechanical learning system which uses a hypothetic space of linear function in a high dimensional feature space (Wang, 2005). Nevertheless, the extremely large size of the Kernel matrix, and the slow speed of the training and testing process still remain challenging for the popularity of the *NN* based methods.

Output only methods: Output only based methods have been developed to mitigate the requirement of input time history measurements since measuring input is sometimes expensive or impossible. Such methods can make use of natural sources to excite structures such as ambient vibration, and earthquake excitation. Many output only based methods have been developed, such as methods based on modal analysis (Beck and Jennings, 1980), methods based on Fourier analysis (Torkamani and Ahmadi, 1988), methods based on adaptive filtering (Safak, 1989 a-b), methods based on substructure concept (Michael, 2006). Amongst many of them, a finite-element based procedure to identify structural parameters and to assess damage severity at element level with unknown input excitation has been shown promising (Wang and

Haldar, 1994, 1997; Ling and Haldar, 2004; Vo and Haldar, 2005; Katkhuda and Haldar, 2005). From the response measurements, the error vector can be formulated using the equations of motion of the structure at different time steps (assuming that mass matrix is known) as follows

$$\mathbf{E} = \mathbf{M}\ddot{\mathbf{d}} + \mathbf{D}_d\dot{\mathbf{d}} + \mathbf{K}\mathbf{d} - \mathbf{f} \tag{1.3}$$

where $\mathbf{M}$, $\mathbf{D}_d$, $\mathbf{K}$ are structural mass, damping, stiffness matrices, respectively; $\mathbf{d}, \dot{\mathbf{d}}, \ddot{\mathbf{d}}$ the displacement, velocity, acceleration vectors, respectively; and $\mathbf{f}$ the input force vector. Since the input force vector is unknown, the first step of the algorithm is to estimate the input signal from initial guesses of the structural parameters and applied force. The second step of the algorithm is to estimate the structural parameters using the estimated load in the first step. The process is iterated until the estimated input signals converge with a pre-determined tolerance. Finally, the dynamic properties of the structure in terms of stiffness and damping at the element level are estimated. Performance of the method is illustrated through both numerical examples of shear buildings and frame structures with 5% noise, and experimental examples of a simply supported beam structure. It is interesting to realize that the proposed method is simple and robust even though the input excitation is unknown and limited measured responses are contaminated with noise. Further investigation on the performance of the proposed method has been carried out successfully on more complicated structures as reported in Haldar (2009 a & b), Haldar (2008), Katkluda and Haldar (2008), Martinez et al. (2008), giving the method a prospect of becoming a popular tool for structural damage detection.

An alternative to the above class of methods was suggested by Quek et al. (1999) using an eigenspace algorithm for structural identification of tall buildings subjected to ambient excitations. This method requires only the measurement of response time-

history which is then decomposed into subspace matrices using QR decomposition and Quotient *SVD* technique. Least Square approach is adopted to obtain a solution which is non-unique, and the desired solution is computed by applying similarity transformation. The advantages of the proposed method are that it is non-iterative and that the initial values for parameters are not required. The only disadvantage of this method is the requirement of measurement at all *DOF* of structure which might not be available in practice.

A comparison between the cases of output-only versus input/output data processing for structural identification and damage assessment has been carried out by Mevel et al. (2006). The two methodologies were applied in both the subspace-based methods and error prediction methods using real in-flight measured data of an aircraft provided by Avions Marcel Dassault within the Eurêka project FLITE. It is shown that the input/output methods perform better than the output-only methods using the real data in term of stability of system order identification. It is therefore recommended that input sensors should be used where possible and the trade-off is between increased estimation accuracy and sensor cost.

Nonlinear methods: After damage occurs, structural responses are usually nonlinear such as the presence of cracks that open and close under operational loads, damage caused by losing joints and connections, damage caused by delamination in bonded layered materials, damage caused by material nonlinearity associated with excessive deformation. Hence, structural damage detection methods could be more practical if they take into account the nonlinear behavior of the structure. Many methods for structural damage detection accounting for nonlinear behavior of the structure have been explored, such as the restoring force surface method (Masri and Caughey, 1979; Crawley and Aubert, 1986), the gradient descent method (Nelles,

2001), and the EKF-based method (Nelles, 2001). Recently, Yang and his co-workers have developed a method to track the change in structural damping, mass and stiffness caused by damage which can account for the nonlinearity behavior of the structure using the LSE approach (Yang and Lin, 2004, 2005). In the proposed algorithm, the objective function needed to be minimized is the sum of relative change in the structural parameter vectors including stiffness, damping ratio, and mass when the structure changes from one time instant to the next. The idea behind the proposed algorithm is that the optimal solution of structural parameters should follow the most direct path (the path with minimum variation) from one time instant to another in order to get rid of oscillations in the results. Solving all optimization problems from the initial time step to the present time step, the changes in the values of the structural parameters with time can be tracked and deductions on structural damage can be made. It is interesting to observe that the proposed method is also applicable to track the gradual changes of structural parameters. A major limitation of the proposed methodology is the need to measure the structural responses at all *DOF*. To overcome this limitation, the sequential nonlinear least square estimation (SNLSE) algorithm was proposed (Yang et al., 2005; Yang et al, 2007; Yang and Huang, 2007). Unlike the traditional EKF method, the unknowns in terms of the structural parameters ($\boldsymbol{\theta}$) and state vector ($\mathbf{X}$) are estimated in two consecutive steps. In the first step, the structural parameters $\boldsymbol{\theta}$ are estimated using the LSE method based on the assumption that the state vector $\mathbf{X}$ is known. Because the state vector $\mathbf{X}$ is actually unknown, results in the first step produces $\boldsymbol{\theta}$ as a function of $\mathbf{X}$. In the second step, the discrepancy between measured and estimated force vector is again minimized using recursive LSE (RLSE) method. Since $\boldsymbol{\theta}$ are functions of unknown state vector $\mathbf{X}$, the objective function to be minimized in the second step is highly nonlinear with respect to $\mathbf{X}$. The stability and

convergence of the proposed SNLSE method were demonstrated through numerical examples comprising 1, 2, and 5 *DOF* structures (Yang et al., 2005). It is appealing to find that the proposed SNLSE method is applicable to monitor both nonlinear elastic structures and nonlinear hysteretic structures. The proposed SNLSE method was then further applied to the case of unknown excitation and limited measured accelerations with excellent results as shown in Yang et al. (2007) and Yang and Huang (2007). However, the application of the proposed methodology to a more complicated structure other than spring-dash-pot and shear structures has not been investigated both numerically and experimentally.

Although much effort has been made to popularize the nonlinear based methods for structural damage detection, limitations still exist. Firstly, nonlinear damage detection methods lack generalization capacity. Each typical structure requires a specific nonlinear model. Hence, the solution is problem dependent. One technique which can perform well for this structure may not work for another (Farrar et al., 2007). Secondly, nonlinear based methods are usually computationally cumbersome, expensive and require definitions of many input parameters. The more input parameters the methods require, the greater the dependence of the output on the input, leading to the reduction in their robustness. Thirdly, nonlinear based methods are exposed to limitation of mathematical framework since most of the available formulations have been developed based on linearity assumption such as the framework for vector space theory. Fourthly, technical limitation also poses a challenge on the evolution of nonlinear based methods. For example, the amplitude of excitation affects significantly the nonlinear behavior of the structure; combination of various sources of nonlinearity in a method for structural damage detection is questionable.

In summary, amongst all the methods for structural damage detection in the literature, the *DLV* method emerges as the potential one because it can be used with either static or dynamic responses; it can identify both single and multiple damaged elements; when using with dynamic responses, it is able to operate with approximate modal data and truncated modal basis. In the following section, the development of the *DLV* method over the past few years will be briefly reviewed.

1.2.3 Detect damage using damage locating vector method

Bernal (2002) proposed the *DLV* method for structural damage localization that belongs to the model-based approach. The method does not use the change in mode shapes or frequencies. Instead, a load vector that produces the same displacements at the reference and damaged states, the so-called *DLV*, is developed to identify damaged elements. In other words, no additional stresses are generated in damaged elements if the *DLV* is applied onto the reference structural model. This characteristic of the *DLV* is utilized to locate damaged elements. A systematic procedure to compute the *DLV* was introduced by Bernal and Gunes (2004). Performance of the *DLV* method has been illustrated both numerically and experimentally using truss structures (Bernal, 2002; Gao et al., 2007). However, only single damaged element was examined in the experiment, leaving the case of multiple damaged elements uncertain.

Sim et al. (2008) further examined the efficiency of the *DLV* method under the presence of model uncertainties using 13 and 39 *DOF* plane truss structures. From the investigation, they recommended that the value of 0.1 should be taken as the threshold to classify damaged from undamaged elements with the probability of less than 5% of "false negative" (defined as when the damaged element is not present within the set of identified potential damaged elements) based on the assumption that the Young's

moduli of all elements are statistically independent variables, each with a coefficient of variation, δ_E, of 10%.

Recognizing the potential of the *DLV* method, improvements have been made to enhance its popularity. Firstly, it has been further developed to accommodate the case of unknown excitation by (*i*) using modal mass scaling from known mass perturbation (Bernal, 2004); (*ii*) constructing a matrix proportional to the flexibility matrix at sensor locations (Duan et al., 2005); (*iii*) assuming that the structural "mass" does not change when the structure changes from the reference to the damaged state (Gao and Spencer, 2006); or (*iv*) using a structural stochastic model (Bernal, 2006). Secondly, it has been further developed to detect structural damage online by introducing the distributed computing strategy (DCS) (Gao, 2005). The concept of the DCS is that (*i*) a number of sensors close to each other are combined to form a local community in which one sensor is selected as the manager sensor; (*ii*) the manager sensor collects information from all sensors in the community and assess the "health" of structural members monitored by the community using the *DLV* method; and (*iii*) information about damaged elements monitored by the community is interacted with information of neighbouring communities before sending to the base station for decision making.

Although huge effort has been made to popularize the *DLV* method as a tool for structural damage interrogation, further research is still needed to (*i*) apply the method to structures which comprise members with multi-stress state and varied cross-sectional areas along element lengths; (*ii*) identify the actual damaged elements in the set of potential damaged elements (*PDE*) due to the lack of perfect and/or complete information; and (*iii*) assess the damage severity of identified damaged elements.

In summary, significant progress has been made on the structural damage detection using either static or dynamic responses in the last two decades, fuelled in

part by the advancement in sensor and data acquisition technologies. In line with this, the recent development and application of wireless sensor technology in the context of damage detection would be a natural field of investigation with respect to the practical implementations. Robustness of a particular damage detection method may perhaps be increased by using better quality sensors that have been developed or methods to validate the quality of the sensor data before being used for damage identification would enhance confidence in detection technology. Literature review on these two aspects will be briefly introduced in the following two sections.

1.2.4 Sensor validation

To detect structural damage, structural responses need to be measured and their quality plays a crucial role on the accuracy of the damage detection result. Validating the quality of measured signals or the "health" of the *in situ* sensors is thus a challenging problem and has attracted many researchers (Qin et al., 1997; Leahy et al., 1997; Friswell and Inman, 1999; Hsiao, 2005). A thorough review on the developments of sensor fault detection can be found in Feng et al. (2007). Various approaches can be employed to validate sensor integrity, such as using error function, Principle Component Analysis (*PCA*), or neural network (*NN*).

Additive and multiplicative errors are two common manifestations of faults in sensors (Abdelghani and Friswell, 2004). The former, which may result for example from the direct current (*DC*) offsets in electronic equipments, is usually modeled as a constant amplitude shift in the signal. This additive amplitude shift is not known *a priori*. For multiplicative error, its amplitude is often proportional to the true value of the measured signal and may result from an error in the coefficient of the calibration equation, for example, an error in the slope of the fitted calibration line.

For a structure under zero-mean white noise excitations, its dynamic response usually has zero-mean over a sufficiently long period. This facilitates the estimation of the additive error (Friswell and Inman, 1999; Abdelghani and Friswell, 2004). Specifically, from response measurements of *ns* sensors, response measurement of sensor *j* (*j* = 1, 2, …, *ns*) can be estimated using the remaining measurements of (*ns* - 1) sensors. The difference between the measured and the estimated signal at sensor *j* produces the residual function for that sensor. If the mean value of the residual function for sensor *j* is significantly different from zero for a sufficiently long period, sensor *j* is classified as faulty. However, the threshold value to classify non-zero mean value of the residual function produced by a faulty sensor from the value produced by noise and uncertainties has not been clearly suggested.

To detect multiplicative error, the concept of error function, which is commonly constructed by subtracting the measurements from the estimated values of a sensor based on readings of the remaining sensors, can be utilized. Abdelghani and Friswell (2007) assumed that if the structural modal matrix (**Φ**) is available, the acceleration responses at all *ns* sensors can be estimated as

$$\widehat{\mathbf{Y}} = \mathbf{\Phi}\mathbf{\Phi}^{\dagger}\mathbf{Y} \tag{1.4}$$

where "†" represents the pseudo-inverse; $\mathbf{Y}$ and $\widehat{\mathbf{Y}}$ are the measured and estimated acceleration responses at all *ns* sensors. If sensor *j* is suspected as faulty, $\mathbf{\Phi}$, $\mathbf{Y}$ and $\widehat{\mathbf{Y}}$ are partitioned as follows

$$\mathbf{\Phi} = \begin{bmatrix} \mathbf{\Phi}_0 \\ \mathbf{\Phi}_j \end{bmatrix}, \mathbf{Y} = \begin{bmatrix} \mathbf{Y}_0 \\ \mathbf{Y}_j \end{bmatrix} \text{ and } \widehat{\mathbf{Y}} = \begin{bmatrix} \widehat{\mathbf{Y}}_0 \\ \widehat{\mathbf{Y}}_j \end{bmatrix} \tag{1.5}$$

where $\boldsymbol{\Phi}_j$, $\mathbf{Y}_j$ and $\widehat{\mathbf{Y}}_j$ are the jth row and $\boldsymbol{\Phi}_0$, $\mathbf{Y}_0$ and $\widehat{\mathbf{Y}}_0$ the matrices containing the remaining rows of $\boldsymbol{\Phi}$, $\mathbf{Y}$ and $\widehat{\mathbf{Y}}$, respectively. Two residual functions are defined as follows

$$\boldsymbol{\gamma}_j^0 = \widehat{\mathbf{Y}}_0 - \mathbf{Y}_0 \tag{1.6}$$

$$\boldsymbol{\varsigma}_j = \boldsymbol{\Phi}_0(\boldsymbol{\Phi}_0)^{\dagger}\mathbf{Y}_0 - \widehat{\mathbf{Y}}_0 = \overline{\mathbf{Y}} - \widehat{\mathbf{Y}}_0 \tag{1.7}$$

where $\overline{\mathbf{Y}}$ is the estimated responses at all sensors except sensor j computed using $\boldsymbol{\Phi}_0$ and $\mathbf{Y}_0$. From Eqs. (1.6) and (1.7), the correlation index is proposed as

$$\rho_j = \frac{E(\boldsymbol{\varsigma}_j^T \boldsymbol{\gamma}_j^0)}{\sqrt{E(\|\boldsymbol{\varsigma}_j\|^2)}} \tag{1.8}$$

where $E(.)$ denotes the expectation of (.). Faulty sensor is considered as associated with the maximum correlation index. Because only the maximum ρ_j is considered, only one faulty sensor can be identified at a time. In addition, a threshold is needed to distinguish ρ_j which results from faulty sensor from that resulting from noise and uncertainties.

Li et al. (2007) defined the error function in a different manner. The set of *ns* sensors used is divided into two groups, namely functional and faulty, to identify the instances of failures for sensors in the faulty group. If sensor j belongs to the faulty group, the quality of the measurement by sensor j from time steps $(k - p)$ to k can be assessed by forming the following matrix

$$\mathbf{W}_d^j = \begin{bmatrix} \mathbf{y}_d^j(k-p) & \mathbf{y}_d^j(k-p+1) & \cdots & \mathbf{y}_d^j(k) \\ \mathbf{y}_d^0(k-p) & \mathbf{y}_d^0(k-p+1) & \cdots & \mathbf{y}_d^0(k) \end{bmatrix} \tag{1.9}$$

where $\mathbf{y}_d^j$ are the readings of the suspected faulty sensor j; and $\mathbf{y}_d^0$ the readings from the group of the working sensors. A similar matrix can be formed for the case where all sensors are healthy as

$$\mathbf{W}_u^j = \begin{bmatrix} \mathbf{y}_u^j(k-p) & \mathbf{y}_u^j(k-p+1) & \cdots & \mathbf{y}_u^j(k) \\ \mathbf{y}_u^0(k-p) & \mathbf{y}_u^0(k-p+1) & \cdots & \mathbf{y}_u^0(k) \end{bmatrix} \tag{1.10}$$

The *SVD* of $\mathbf{W}_u^j$ is given by

$$\mathbf{W}_u^j \xrightarrow{SVD} \mathbf{U} \cdot \mathbf{\Sigma} \cdot \mathbf{V}^T = \begin{bmatrix} \mathbf{U}_1 & \mathbf{U}_2 \end{bmatrix} \begin{bmatrix} \mathbf{\Sigma}_1 & \\ & \mathbf{0} \end{bmatrix} \begin{bmatrix} \mathbf{V}_1^T \\ \mathbf{V}_2^T \end{bmatrix} \tag{1.11}$$

Pre-multiplying both sides of Eq. (1.11) by $\mathbf{U}^T$ and invoking the orthonormal property of $\mathbf{U}$ gives

$$\mathbf{U}_2^T \mathbf{W}_u^j = \mathbf{0} \tag{1.12}$$

Using column *i* of $\mathbf{U}_2^T$, the error function for the suspected sensor *j* can be defined as

$$\mathbf{e}_j = (\mathbf{U}_2^i)^T \mathbf{W}_d^j \tag{1.13}$$

It can be seen that if all the sensors are healthy, then $\mathbf{e}_j = \mathbf{0}$ for all *i* because $\mathbf{W}_u^j$ and $\mathbf{W}_d^j$ share the same base vector for the left singular value null space. The presence of non-zero values in $\mathbf{e}_j$ indicates faults in sensor *j*. However, the issue of a non-zero criterion even if the sensor is healthy due to the presence of noise and uncertainties has not been fully addressed since no threshold has been suggested to demarcate non-zero values caused by faulty sensors from those caused by noise and uncertainties. Furthermore, the method requires the measurements where all of the sensors are in "healthy" conditions.

Another attractive technique is the use of Principle Component Analysis (*PCA*) to detect, isolate and reconstruct faulty signal (Dunia et al., 1996; Pranatyasto and Qin, 2001; Kerschen et al., 2005). The procedure proposed by Kerchen et al. (2005) starts by dividing the entire measured signal $\mathbf{S}_0$ (whose base vector can be computed) into *nseg* segments. The base vector for each of these segments $\mathbf{S}_i$ (i = 1, 2, …, *nseg*) can also be computed. The angle between the base vector of the entire space $\mathbf{S}_0$ and that of

each subspace $\mathbf{S}_i$ is computed. If the angle is greater than a pre-defined upper limit, there exists faulty signal in that segment and vice versa. To identify the portion of faulty signal, one segment of signal at a time is discarded from the entire analysis and the angle between the new base vectors of the entire space $\mathbf{S}_0$' and each subspace $\mathbf{S}_i$' is re-calculated. The angle should be minimal if the discarded signal is faulty. The advantages of this method are that it can work for nonlinear structural behavior and can also identify approximately the times when the faults occur. However, the method requires lengthy signal. In addition, since only one segment of signal is discarded from $\mathbf{S}_0$ and S_i to formulate $\mathbf{S}_0$' and $\mathbf{S}_i$', only one segment of each faulty sensor can be identified at a time. The procedure of removing one segment at a time and reiterating can be too time-consuming that the method may lose its appeal for practical application.

Neural network (*NN*) has also been employed to assess faulty sensors (Napolitano et al., 1998; Mesbahi, 2001; Rizzo and Xibilia, 2002, Campa et al., 2008). From the current measured data at all sensors, the reading of sensor *j* can be estimated as (Mesbahi, 2001)

$$\hat{y}_j = sig\left[\sum_{i=1}^{h} sig\left(\sum_{k=1}^{ns} y_k W_{i,k}^1 + c_i\right) W_{j,k}^2 + b_j\right] \tag{1.14}$$

where $sig(y) = 1/(1+e^{-y})$; h and ns are the hidden and input nodes of the *NN*, respectively; y_k the reading of sensor k (k = 1, 2, …, ns); and W^1, W^2, c, and b the network weights. The confidence level for the reading of sensor j, y_j, can be defined as

$$CL_j = 1 - \frac{\left|\hat{y}_j - y_j\right|}{\hat{y}_j} \tag{1.15}$$

A close to zero value of CL_j implies that sensor j is faulty whereas a close to one value indicates that sensor j is healthy. The detection of faulty sensor procedure is integrated

into a 3-layer feed-forward artificial neural network which is trained using the back-propagation method. The algorithm has been demonstrated to be able to perform online detection of faults for various types of sensors such as thermocouples, pressure transducers, and flow meters. However, the classification of a value which is close to one or zero has not been clearly suggested.

Similarly, Campa et al. (2008) adopted *NN* to estimate the output of sensor *j* at a time instance as

$$\hat{y}_j = \sum_{i=1}^{nf} w_i e^{-(y_j-\mu_i)^2/2\sigma_i^2} \tag{1.16}$$

where y_j is the measured data by sensor *j* at the current time instant; *nf* the number of basis functions for the *NN*; μ_i and σ_i the mean and variance of the *i*th basis function, respectively; and w_i its weight. The residue for sensor *j* is defined as

$$R_j = y_j - \hat{y}_j \tag{1.17}$$

When R_j exceeds a pre-defined threshold, sensor *j* is classified as faulty and vice versa. The procedure is embedded into a hybrid *NN* which comprises a radial basis function *NN* and a resource allocating network. The *NN* is trained using a set of measured data where different types of failures are artificially injected. The hybrid structure *NN* is particularly relevant when nonlinear characteristics are captured by the data. The method has been shown to be applicable for speed sensors, torque sensors, and pressure transducers.

Recognizing that identifying the cause of the fault in a sensor is even more difficult than identifying the faulty sensor (Henry and Clarke, 1993), an attempt to assess the nature of the fault in the sensor, such as gain fault, bias fault, spike fault, and noise fault, has been carried out by Rizzo and Xibilia (2002) using *NN*. In this method, four criteria to assess displacement sensor *j* are proposed, namely,

(a) maximum value (together with the criterion (b) to assess gain and step faults)

$$M_j = \max_k \left[y_j(k) \right] \tag{1.18}$$

(b) average value (used in conjunction with (a))

$$A_j = \frac{1}{ns} \sum_{j=1}^{ns} y_j(k) \tag{1.19}$$

(c) maximum absolute difference value at one time step (to assess spike fault), and

$$P_j = \max_k \left| y_j(k) - y_j(k-1) \right| \tag{1.20}$$

(d) sum of *FFT* sample between frequencies f_1 and f_2 (to assess noise fault)

$$N_j = \sum_{f=f_1}^{f_2} Y_j(f) \quad \text{where } Y_j(f) = FFT\{y_j(k)\} \tag{1.21}$$

in which $y_j(k)$ is the measured displacement at discrete time index k by sensor j. From numerous sets of trained data, a multi-layer perceptron *NN* is trained and the ranges for these criteria are specified. If one or some criteria for sensor j are out of the specified ranges, sensor j is classified as faulty and the causes are identified. For example, if both the maximum and the average exceed their ranges, the sensor is classified as having gain and step faults; if the maximum difference absolute value at one time step exceeds its range, the sensor has a spike fault; if the sum of *FFT* sample between frequencies f_1 and f_2 exceeds its range, the sensor is considered as too noisy. If other combination of the criteria is satisfied, multiple causes of a faulty sensor can be identified accordingly.

Despite recent rapid development in sensor validation algorithms, their application to enhance the reliability of damage detection remains challenging. Two major problems have not been fully addressed, namely (*i*) integrating the sensor validation algorithm to identify "unsuitable" signals besides detecting structural damage; and (*ii*) identifying multiple faulty sensors simultaneously.

1.2.5 Detect damage with wireless sensors

In practical damage detection implementation, sensors are sparsely distributed over the structure to be monitored and wired to a central multi-channel data logging system. The cost of installing and maintaining such traditional wired sensors is high and they may interfere with the normal operations of the structure (Lynch, 2004). For example, to monitor a building, Celebi (2002) assessed that the average cost per sensor in a multi-channel system is US$5,000. To monitor the Tsing Ma suspension bridge in Hong Kong, a monitoring system containing more than 350 sensing channels costs more than US$8,000,000 (Farrar, 2001). To overcome such disadvantages of traditional wired sensors, wireless sensors are being implemented (Lynch et al., 2003; Lynch and Loh, 2006; Park et al., 2006; Spencer et al., 2008) and various improvements have been reported in the last few years such as the introduction of different transmission topologies, the improvement on the sampling frequency (Nagayama, 2007; Lynch, 2004; Hou et al., 2008). However, concerns about adaptation and practical implementation such as power supply, network management, cross-talk, data integrity and transmission speed remain challenging. Though the data captured on board by the wireless sensors has been digitized, transmitting data packets from various sensor nodes to the base station using radio frequency (RF) commonly experiences intermittent loss. The causes of data loss may be explained by (a) data packets from more than one sensor reach the base station simultaneously, (b) distances between the sensor nodes and the base station are out of the communication range, and (c) acknowledgement (ACK) messages of the lost packets are over-written. If the ACK messages indicating the lost packet numbers are not received by the sensor node, the lost packets are not resent. The quality of data received at the base station affects the

reliability of the structural health monitoring system and emerges as a major challenge in the integration of wireless sensors into an existing structural damage detection method.

When transmitting the measured data from the sensor nodes to the base station, Nagayama (2007) noted that the percentage of data loss is random and can be as high as 86%. This poses a huge hurdle in enhancing a damage detection system using wireless sensors and must be overcome to a level that reliability of the entire system is acceptable at a practical level. Two improvements are being pursued to solve this problem. The first improvement is the introduction of more efficient transmission protocols through better hardware and software in the wireless sensor systems to bring down the percentage of loss data to a minimum (Lynch, 2004; Mechitov et al., 2004; Nagayama, 2007). Once the percentage of loss data is not large, then a second level of improvement becomes feasible, by adjusting the spurious or missing data values to match the overall characteristics of the intact portions of the signal (Marks, 1983; Yuito and Matsuo, 1989; Marvasti et al., 1992).

With regards to the first level of improvement, Mechitov et al. (2004) proposed the use of tree topology with Mica2 mote sensors for reliable communication. In this topology, the sensor sends a group of data packets and then waits for the acknowledgement (ACK) message from the receiver. If the sender does not receive ACK message, the same group of packets is resent. Otherwise the sender moves on to send the next group of data packets. If one packet in the group is lost, all packets in that group are resent, reducing the efficiency of the proposed topology. For more efficient transmission topology, Nagayama (2007) proposed the Automatic Repeat reQuest (ARQ) prototype for data transmission problem. The idea behind the proposed prototype is that: (*i*) the sender transmits all data packets to the receiver; (*ii*) the

receiver stores all data in a buffer zone; and (*iii*) on receiving the last packet, the receiver sends message indicating which packets are lost to the sender and only those lost packets are resent. Advantage of the proposed prototype is that the number of ACK messages and the number of messages need to be resent is reduced significantly. However, this may be feasible for short records only and the maximum record length which this approach can provide reliable signal needs to be ascertained.

With regards to the second level of improvement, Bhuptani and Khosla (2006) proposed the use of interpolation and extrapolation procedure based on least square approximation to estimate the lost values. Although the method is simple and able to provide reasonable estimates, it is unable to produce good results for cases of consecutive lost data points, as exhibited by the loss of an entire packet of data during transmission. Hsu and Lo (2006) proposed an iterative scheme using Fourier Transform and boundary-matched concept to estimate lost data. The measured signal is first pre-processed by superposing with a computed signal such that the periodicity and continuity conditions of the signal are satisfied. Discrete Fourier Transformed (DFT) is then performed on this signal to obtain the significant frequencies and the corresponding Fourier coefficients. Applying inverse DFT on the identified significant frequencies and the corresponding Fourier coefficients and then subtracting the added signal in the pre-processing step from the results, the lost data are estimated. The procedure is iterated until the discrepancy of estimated lost values between two consecutive iterations is negligible. Though the method is verified successfully using a sinusoid signal with rapid convergence speed, its applicability to signals containing consecutive lost values and the typical associated errors have not been investigated.

Although attempts have been made to integrate wireless sensors into damage detection systems, there are rooms for improvements to enhance its reliability in practical situations.

1.2.6 Summary of findings

From the above review, some non model-based methods, such as visual inspection method, tap test method, X-ray method, and Gamma-ray method, are found time consuming and labor intensive whereas some other non model-based methods, such as methods based on traveling time of guided signals and modal based methods, are found suitable for homogeneous and simple structures. Model-based methods using static response are usually found simple in formulation with few assumptions and should be utilized to explore the insights of newly developed methods. Whereas, model-based methods using change in the stiffness matrix may require the excitation to span over a wide range of frequencies to capture sufficient number of mode shapes which is hard to excite and control in practice. Methods based on the change in flexibility matrix necessitate a large number of sensors for precise evaluation of modal parameters, making the methods expensive for practical application. However, since the flexibility matrix can easily be obtained for a reduced-order model of the structure, change in flexibility-based methods can be employed to assess damaged regions with limited sensors. Methods based on substructure concept are only applicable for shear structures. Amongst all model-based methods for structural damage detection, the *DLV* method appears to be promising and has room for further development into a practical tool. It can be applied using either static or dynamic responses and can provide reasonable results with limited data since it possesses the advantage of the methods

based on change in flexibility matrix which requires the excitation of only few lower modes in order to estimate reasonably accurate flexibility matrix.

Over a period of use, it is practically impossible to ensure that all the sensors are in good working condition. Automatic detection of faulty sensors and/or contaminated data is needed in a structural health monitoring system. Pre-processing of the data through a sensor validation algorithm has been proposed but two major problems have not been fully addressed, namely (*i*) identifying faulty sensors besides detecting structural damage, and (*ii*) identifying multiple faulty sensors simultaneously.

Using wired sensors in structures may not be always possible, or if possible may interfere with the normal operations of the structure. In addition, long wires are often needed and problems such as noise, integrity, maintenance and cost are real issues to content with. Additions and enhancements to a wired multi-channel system are often quite limited. Although wireless sensor network can overcome the problems and limitations associated with a wired system, there are practical issues that need to be addressed before it becomes an attractive alternative. One significant issue that needs to be addressed urgently is the enhancement of the quality of the data.

1.3 OBJECTIVES AND SCOPE OF STUDY

The main objective of this thesis is to develop the *DLV* method further by (a) extending its formulation to include frame elements in the structure, (b) proposing a strategy to identify damaged elements for the case of imperfect measurements, (c) identifying faulty data/sensor in the context of the *DLV* method, and (d) integrating wireless sensor network into the method where the issue of intermittent loss of data is addressed. To achieve the main objective, the scope of this study includes the following.

1. Structures comprising frame and truss elements will be considered, namely a 2-D warehouse structure. Besides the different types of elements, the variation of internal forces and corresponding capacities within each component will be taken into account. Both numerical and experimental examples will be used in this study for structures with single and multiple damaged elements.
2. Imperfect information arising from noise and the limited number of sensors used will result in the *DLV* method liable to give inaccurate results or results that have poor resolution. Often, other elements besides those damaged are also identified as being damaged. Two schemes to identify the actual damaged elements from the set of potential damaged elements (*PDE*) will be proposed. The first scheme makes use of the intersection of available sets of *PDE* obtained from different combinations of number of sensors to filter out actual damaged elements. The second scheme first identifies damaged regions using the relative change in flexibility matrices and then zooms into each damaged region to locate the actual damaged elements using the *DLV* method.
3. A simple algorithm to estimate the severity of damaged elements will be proposed and investigated. The flexibility matrix ($\mathbf{F}_n$) which is constructed using numerical model of the structure at the reference state is mapped to the flexibility matrix ($\mathbf{F}_d$) which is computed from measured data of the structure at the current (damaged) state by using penalty function method to minimize the difference between the first singular values of the two flexibility matrices. The variables to be estimated in the minimization process are the stiffnesses of the damaged elements. When $\mathbf{F}_n$ approaches $\mathbf{F}_d$, the severity of the damaged elements could be assessed. Single and multiple damaged elements will be investigated using numerical data of a 2-D warehouse structure and experimental data of a 3-D modular truss structure.

4. This study will extend the *DLV* method for cases where the loads, either static or dynamic, are not measured or known. For unknown static load cases, an algorithm will be proposed to estimate the ratio between the magnitudes of the static loads at the reference and damaged state, from which the *DLV* can be computed to assess structural damage. For unknown dynamic load cases, an algorithm to construct the structural stiffness matrix from response accelerations will be proposed. The algorithm makes use of Newmark-β method to relate the displacements and velocities between different time steps in terms of their initial values. This results in a system of nonlinear equations when equilibrium is imposed at all *DOF*, from which the stiffness matrix is formulated. Based on the change in stiffness matrix, the *DLV* can be calculated for damage localization purpose.
5. An algorithm for sensor validation will be proposed where multiple faulty sensors can be identified simultaneously, to ensure the robustness of the *DLV* method. From all measured signals, combinatorial sets of the same number of signals are formed. For each set, the change in the flexibility matrix relative to that of the reference or undamaged structure is computed and singular value decomposition (*SVD*) is performed to estimate the number of non-zero singular values (*NZV*). The set which produces the smallest *NZV* is taken as associated with sensors considered to be healthy whereas sensors which do not belong to this combination are suspected to be faulty. The performance of the sensor validation algorithm will be illustrated using both simulated and experimental data obtained from a 3-D modular truss structure monitored by sensors, some of which are faulty.
6. An algorithm to correct for packets of lost data as exhibited in wireless mote sensors will be proposed based on numerically simulated data and then illustrated using physically measured data. The algorithm is based on the concept of

significant frequencies in the signal whereby Fourier transform is used in a proposed iterative scheme. The numerical simulation will cover various possible scenarios to ensure that the algorithm is sufficiently robust. A 3-D modular truss structure using 7 wireless mote sensors including 1 base station will be physically experimented and the data examined for their percentage of losses and then corrected. The signals are then used to locate the damaged elements, if any.

It should be mentioned that real experiments on existing infrastructures such as buildings, bridges, offshore platforms would be ideal but often the authorities do not allow or welcome such work being done on their structures. Furthermore, such experiments are expensive and difficult to control due to interference from the normal operations associated with such infrastructures. For this reason, the experiments are performed in the Structures and Concrete Laboratory within the Department of Civil Engineering at the National University of Singapore.

1.4 ORGANIZATION OF THESIS

This thesis comprises six chapters. Chapter 1 summarizes the different types of damage in structures and the importance of structural damage detection in practical applications. Literature review on works related to structural damage detection is discussed, including the different approaches that have been taken, and the methods of solutions of equations that have been proposed. In particular, the work performed with respect to the *DLV* method is examined. Works related to sensor validation and the use of wireless sensors in structural health monitoring systems is reviewed. The objective and scope of this study are outlined.

Chapter 2 presents the detection of structural damage using *DLV* and static response. The concept and physical discussion on the *DLV* method is first reviewed.

Enhancements to the *DLV* method are then presented to (*i*) extend the application of the *DLV* method to structures comprising multi-state stress elements; (*ii*) detect actual damaged elements when measurements are imperfect; (*iii*) differentiate between damaged and strengthened structure; (*iv*) assess the severity of the identified damaged elements; and (*v*) extend the *DLV* method to the case where the applied static load is unknown. Numerical and experimental examples of a 2-D warehouse structure and a 3-D modular truss structure, respectively, are performed to assess the performance of these enhancements.

Chapter 3 presents the application of the *DLV* method to detect structural damage using dynamic response with either known or unknown excitation. The formulation of either flexibility or stiffness matrix from structural dynamic responses is a critical component in the application of the *DLV* method using dynamic response. A procedure to form the flexibility matrix with respect to the sensor locations using the Eigensystem Realization Algorithm (*ERA*) and known excitation presented in Bernal and Gunes (2004) is summarized. An algorithm to formulate the structural stiffness matrix from acceleration responses only is then proposed. Besides, a simple algorithm for optimal sensor placement is proposed to (*i*) identify the optimal configuration to place the available sensors, and (*ii*) estimate the minimum number of sensors required by the *DLV* method for reliable damage detection results. The feasibility of these methodologies is illustrated numerically using simulated response from a 2-D warehouse structure and experimentally using measured data from a 3-D modular truss structure.

Chapter 4 presents an algorithm for sensor validation in the context of the *DLV* method. What constitutes faulty sensor for both displacement transducers and accelerometers are defined. The application of *SVD* in the sensor validation algorithm

with different combinations of measurements to obtain the number of non-zero singular values (*NZV*), from which faulty sensors are identified, is demonstrated. The feasibility of the proposed algorithm is illustrated using both simulated and experimental data from a 3-D modular truss structure.

Chapter 5 presents the integration of wireless sensors into the *DLV* method to detect structural damage. Essential to the integration is the improvement of the quality of measured data after being transmitted from the sensor nodes to the base station. An algorithm to estimate lost values based on measured values using Fast Fourier Transform (FFT) and inverse FFT is proposed. Parametric study on the performance of the proposed algorithm is carried out numerically. The feasibility of the integration is then investigated experimentally using measured data from a 3-D modular truss structure with six wireless sensors and one base station.

Chapter 6 summarizes the findings and conclusions of this study. The directions for further study are then proposed.

CHAPTER 2

DAMAGE DETECTION VIA *DLV* USING STATIC RESPONSES

2.1 INTRODUCTION

The literature review in Chapter 1 highlighted that despite the effectiveness of the damage locating vector (*DLV*) method in assessing structural damage there exist challenges in its practical application. Firstly, the composite "stress" values to use within the *DLV* method framework have been illustrated for truss structures, but its extension to general structural type has not been fully addressed. For example, to assess damage in frame structure, all internal forces components such as moment, shear, axial force and their variation within each element length as well as their corresponding capacities must be considered. Secondly, the set of potential damaged elements (*PDE*) usually contains both actual damaged and some undamaged elements because the number of sensors available for structure damage detection does not cover all the structural *DOF* to satisfy the condition of observability. This is due either to the unavailability or malfunctioning of sensors. Some parts of the structure may not be accessible for monitoring. Hence, detecting the actual damaged elements needs to be addressed. Thirdly, the *DLV* method has not been developed to assess the damage severity of the identified damaged elements. This limitation also exists in methods such as those based on change in mode shape and flexibility (Alvandi and Cremona, 2006).

In this chapter, the normalized cumulative energy (*NCE*) of each element is proposed as the criterion to determine the damaged elements based on the *DLV* method. This is an extension of the original *DLV* method where the normalized

cumulative stress (*NCS*) is used. To address the second limitation of the *DLV* method, two schemes to detect actual damaged elements are introduced. For the third limitation, a procedure to assess the severity of each identified damaged element is suggested where the penalty function method is adapted. Finally, an algorithm to detect structural damage using the *DLV* method with unknown static load is suggested. Numerical example of a 2-D warehouse structure and a laboratory experiment using a 3-D modular truss structure are presented to illustrate the performance of the proposed enhancements to the *DLV* method.

2.2 SUMMARY OF THE *DLV* METHOD

2.2.1 Concept of *DLV*

Consider a linear elastic structure with *ns* sensors attached. Let $\mathbf{F}_u$ and $\mathbf{F}_d$ denote the (*ns* × *ns*) flexibility matrices constructed with respect to the sensor locations for the reference and the altered structures, respectively. Assume that there exists a set of (*ns* × 1) static load $\mathbf{P}$ ($\neq \mathbf{0}$) such that when they are applied to the reference and the altered structures, the work done is identical; that is,

$$0.5\mathbf{P}^T\left(\mathbf{F}_d\,\mathbf{P}\right)=0.5\mathbf{P}^T\left(\mathbf{F}_u\,\mathbf{P}\right) \quad \text{or} \quad \left(\mathbf{F}_d-\mathbf{F}_u\right)\mathbf{P}=\mathbf{F}_\Delta\,\mathbf{P}=0 \quad (2.1)$$

Equation (2.1) is satisfied if (*i*) $\mathbf{F}_\Delta = \mathbf{0}$, or (*ii*) $\mathbf{F}_\Delta$ rank deficient and $\mathbf{P}$ is the basis of the null space of $\mathbf{F}_\Delta$. The first case implies $\mathbf{F}_u = \mathbf{F}_d$, which means that the structure is unaltered. The latter implies that the changes are confined to elements whose energies are always zero under $\mathbf{P}$. That is, $\mathbf{P}$ effectively does not induce any additional energy on the altered elements and is by definition a *DLV*. This is further elaborated in Appendix A.

2.2.2 Determination of *DLV*

In general, **P** is extracted by performing singular value decomposition (*SVD*) on $\mathbf{F}_\Delta$ in Eq. (2.1), where the latter is the change in flexibility matrix with respect to the sensor locations from the reference to the altered state; that is,

$$\mathbf{F}_\Delta \xrightarrow{SVD} \mathbf{U}\cdot\mathbf{\Sigma}\cdot\mathbf{V}^T = \begin{bmatrix}\mathbf{U}_1 & \mathbf{U}_0\end{bmatrix}\begin{bmatrix}\mathbf{\Sigma}_1 & \mathbf{0}\\ \mathbf{0} & \mathbf{\Sigma}_0\end{bmatrix}\begin{bmatrix}\mathbf{V}_1^T & \mathbf{V}_0^T\end{bmatrix}^T \qquad (2.2)$$

in which $\mathbf{\Sigma}$ is the singular value matrix, $\mathbf{\Sigma}_1$ the sub-matrix of $\mathbf{\Sigma}$ containing all non-zero singular values (*NZV*), $\mathbf{\Sigma}_0$ the sub-matrix of $\mathbf{\Sigma}$ containing all zero singular values; and **U** and **V** the left and right singular matrices, respectively. Using the orthonormal property of **V**,

$$\begin{bmatrix}\mathbf{V}_1^T & \mathbf{V}_0^T\end{bmatrix}^T\begin{bmatrix}\mathbf{V}_1 & \mathbf{V}_0\end{bmatrix} = \mathbf{I} \qquad (2.3)$$

where **I** is the identity or unit matrix, and post-multiplying both sides of Eq. (2.2) by **V** gives

$$\begin{bmatrix}\mathbf{F}_\Delta\mathbf{V}_1 & \mathbf{F}_\Delta\mathbf{V}_0\end{bmatrix} = \begin{bmatrix}\mathbf{U}_1\mathbf{\Sigma}_1 & \mathbf{0}\end{bmatrix} \qquad (2.4)$$

From Eq. (2.4), $\mathbf{F}_\Delta\mathbf{V}_0 = \mathbf{0}$. Comparing with Eq. (2.1) implies

$$\mathbf{P} \equiv \mathbf{V}_0 \text{ or } DLV \equiv \mathbf{V}_0 \qquad (2.5)$$

In summary, $\mathbf{F}_\Delta$ is first computed and then decomposed to obtain $\mathbf{V}_0$ as the matrix of *DLV*s.

The *SVD* performed using Eq. (2.2) is based on the change in flexibility matrix and the resulting *DLV* has force as the physical quantity. If the change in stiffness matrix is used instead, then the resulting *DLV* obtained after *SVD* has displacement as the physical quantity. The mathematical justification for this is given in Appendix B.

2.2.3 Physical meaning of *DLV*

To provide physical insight into the *DLV* method, a numerical example using a simple truss containing two elements (see Fig. 2.1) is employed. At the reference state, both elements have the same Young's modulus $E_1 = E_2 = E$, cross-sectional area $A_1 = A_2 = A$; and length $L_1 = L_2 = 5$ m. At the altered state, the cross-sectional area of element 1 is reduced to $\beta_1 A$ ($\beta_1 < 1$) all along the length of the element while the cross-sectional area of element 2 remains unchanged. Assume that two sensors are available to measure the displacements in both u_1 and u_2 directions where a unit load is applied to node 3 at u_1 and u_2 directions, one at a time.

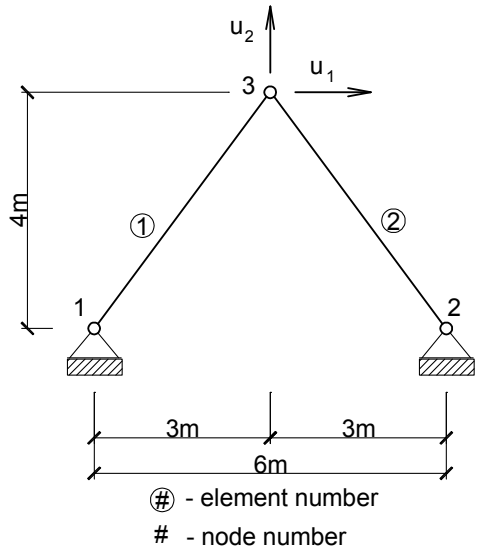

Fig. 2.1. Two-element truss structure

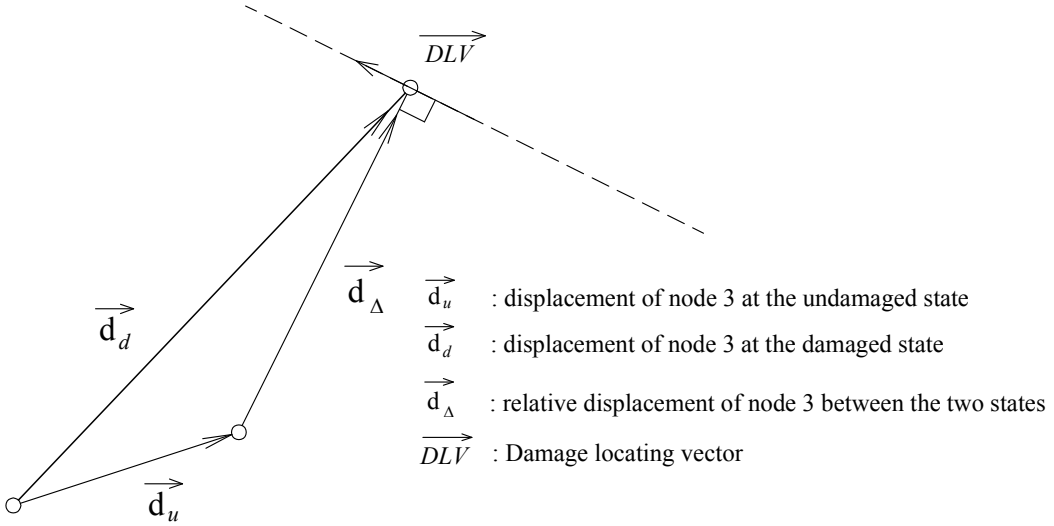

Fig. 2.2. Direction of *DLV* in relation with relative change in displacement vector

The flexibility matrices with reference to the sensor locations for the reference ($\mathbf{F}_u$) and the altered ($\mathbf{F}_d$) states are formulated as

$$\mathbf{F}_u = \frac{1}{EA}\begin{bmatrix} 6.94 & 0 \\ 0 & 3.91 \end{bmatrix} \text{ and } \mathbf{F}_d = \frac{1}{EA}\begin{bmatrix} \dfrac{3.47(1+\beta_1)}{\beta_1} & \dfrac{2.60(1-\beta_1)}{\beta_1} \\ \dfrac{2.60(1-\beta_1)}{\beta_1} & \dfrac{1.95(1+\beta_1)}{\beta_1} \end{bmatrix} \quad (2.6)$$

and the change in flexibility matrix between the two states is

$$\mathbf{F}_\Delta = \mathbf{F}_d - \mathbf{F}_u = \frac{1-\beta_1}{\beta_1 EA}\begin{bmatrix} 3.47 & 2.60 \\ 2.60 & 1.95 \end{bmatrix} \quad (2.7)$$

Singular value decomposition of $\mathbf{F}_\Delta$ yields

$$\mathbf{F}_\Delta \xrightarrow{SVD} \mathbf{U}\cdot\mathbf{\Sigma}\cdot\mathbf{V}^T = \frac{1-\beta_1}{\beta_1 EA}\begin{bmatrix} -0.8 & -0.6 \\ -0.6 & 0.8 \end{bmatrix}\begin{bmatrix} 5.43 & 0 \\ 0 & 0 \end{bmatrix}\begin{bmatrix} -0.8 & 0.6 \\ -0.6 & -0.8 \end{bmatrix} \quad (2.8)$$

Following Eqs. (2.4) and (2.5), the *DLV* is extracted as

$$DLV = \begin{bmatrix} 0.6 & -0.8 \end{bmatrix}^T \quad (2.9)$$

The relative change in displacement at node 3 due to the 2 unit loads applying at node 3 in u_1 and u_2 directions between the reference and the altered states is given by

$$\mathbf{d}_\Delta = \mathbf{F}_\Delta \begin{Bmatrix} 1 \\ 1 \end{Bmatrix} = \frac{1-\beta_1}{\beta_1 EA}\begin{bmatrix} 6.07 & 4.55 \end{bmatrix}^T \tag{2.10}$$

Taking the scalar product of the *DLV* in Eq. (2.9) and $\mathbf{d}_\Delta$ in Eq. (2.10) gives

$$DLV^T \times \mathbf{d}_\Delta = \begin{bmatrix} 0.6 & -0.8 \end{bmatrix} \times \frac{1-\beta_1}{\beta_1 EA}\begin{bmatrix} 6.07 \\ 4.55 \end{bmatrix} \approx 0 \tag{2.11}$$

implying orthogonality between the *DLV* and the relative displacement vector, as illustrated in Fig. 2.2. In other words, the *DLV* is a set of forces such that the net work done on the reference and the altered structure is zero.

2.3 FORMATION OF FLEXIBILITY MATRIX AT SENSOR LOCATIONS

Consider an *n-DOF* structure with *ns* displacement sensors attached. Unless non-contact laser instrument is used, displacement transducers can only be employed if there is a stiff or fixed reference frame on which they can be mounted. Nevertheless, assume that one can measure the displacements at all *ns* sensor locations when a load *P* is applied at *DOF j* where there is a sensor attached ($j \in ns$). The compatibility conditions at all *DOF* of the structure can be expressed as

$$\mathbf{d} = \mathbf{F}\,\mathbf{f} \tag{2.12}$$

where $\mathbf{F}$ is the ($n \times n$) structural flexibility matrices; $\mathbf{f} = \mathbf{B}_2 P$ the ($n \times 1$) applied force vector in which $\mathbf{B}_2$ is the ($n \times 1$) input influence matrix to map *P* to the structural *DOF*; and $\mathbf{d}$ the ($n \times 1$) nodal displacement vector. Extracting the compatibility conditions at the *ns* sensor locations from Eq. (2.12) gives

$$\begin{bmatrix} d_{1j} \\ d_{2j} \\ \vdots \\ d_{jj} \\ \vdots \\ d_{nsj} \end{bmatrix} = \begin{bmatrix} \delta_{11} & \delta_{12} & \cdots & \delta_{1j} & \cdots & \delta_{1n} \\ \delta_{21} & \delta_{22} & \cdots & \delta_{2j} & \cdots & \delta_{2n} \\ \cdots & \cdots & \cdots & \cdots & \cdots & \cdots \\ \delta_{j1} & \delta_{j2} & \cdots & \delta_{jj} & \cdots & \delta_{jn} \\ \cdots & \cdots & \cdots & \cdots & \cdots & \cdots \\ \delta_{ns1} & \delta_{ns2} & \cdots & \delta_{nsj} & \cdots & \delta_{nsn} \end{bmatrix} \begin{bmatrix} 0 \\ 0 \\ \vdots \\ P \\ \vdots \\ 0 \end{bmatrix} \tag{2.13}$$

where d_{ij} is the displacement at *DOF i* due to a load P and δ_{ij} the displacement at *DOF i* due to a unit load applied to the structure at *DOF j* ($i, j = 1, 2, \ldots, ns$). Equation (2.13) can be rewritten as

$$\begin{bmatrix} d_{1j} \\ d_{2j} \\ \vdots \\ d_{jj} \\ \vdots \\ d_{ns\,j} \end{bmatrix} = \begin{bmatrix} \delta_{1j}P \\ \delta_{2j}P \\ \vdots \\ \delta_{jj}P \\ \vdots \\ \delta_{ns\,j}P \end{bmatrix} \quad \text{or} \quad \begin{bmatrix} \delta_{1j} \\ \delta_{2j} \\ \vdots \\ \delta_{jj} \\ \vdots \\ \delta_{ns\,j} \end{bmatrix} = \begin{bmatrix} d_{1j}/P \\ d_{2j}/P \\ \vdots \\ d_{jj}/P \\ \vdots \\ d_{ns\,j}/P \end{bmatrix} \tag{2.14}$$

By shifting the load P through all the *ns* monitored *DOF* and measuring the corresponding displacement vectors at the *ns* sensor locations, all columns of the flexibility matrix with respect to the sensor locations ($\mathbf{F}_s$) can be calculated and assembled as

$$\mathbf{F}_s = \begin{bmatrix} \delta_{11} & \delta_{12} & \cdots & \delta_{1\,ns} \\ \delta_{21} & \delta_{22} & \cdots & \delta_{2\,ns} \\ \cdots & \cdots & \cdots & \cdots \\ \delta_{ns1} & \delta_{ns2} & \cdots & \delta_{ns\,ns} \end{bmatrix} = \begin{bmatrix} d_{11}/P & d_{12}/P & \cdots & d_{1\,ns}/P \\ d_{21}/P & d_{22}/P & \cdots & d_{2\,ns}/P \\ \cdots & \cdots & \cdots & \cdots \\ d_{ns1}/P & d_{ns2}/P & \cdots & d_{ns\,ns}/P \end{bmatrix} \tag{2.15}$$

If shifting the load through all the *ns* measured *DOF* is not possible but *n* sets of independent static load vectors are available, by changing the magnitude of the static load at a convenient *DOF* while leaving the magnitudes of the static load at the other *DOF* unchanged, the flexibility matrix with respect to the sensor locations can still be formulated using the measured displacements.

It is noted that the formulation of flexibility matrix presented above is still valid if the application of a moment and the measurement of nodal rotation by angular sensor are available. Practically, nodal rotation measurement is usually difficult and expensive. To ease the implementation of the *DLV* method, this study considers the measurement of nodal displacements only.

2.4 NORMALIZED CUMULATIVE ENERGY AS DAMAGE INDICATOR

If column *i* of the *DLV* matrix is applied to the reference structure model, the energy induced in element *j*, denoted as Ξ_{ji}, can be computed as

$$\Xi_{ji} = \int_{L_j} \frac{M_{ji}^{\ 2}}{2E_j I_j} ds + \int_{L_j} \nu \frac{Q_{ji}^{\ 2}}{2G_j A_j} ds + \int_{L_j} \frac{N_{ji}^{\ 2}}{2E_j A_j} ds \qquad (2.16)$$

where M_{ji}, Q_{ji}, N_{ji} are internal moment, shear and axial force, respectively, within element *j* due to column *i* of the *DLV*; L_j its length; ν its Poison's ratio and E_jI_j, G_jA_j, E_jA_j its flexural, shear, and axial stiffness, respectively, in which E_j is its Young's modulus and G_j its shear modulus. Equation (2.16) takes into account the presence of different types of internal forces (M_{ji}, Q_{ji}, N_{ji}) within element *j* and the variation of internal forces and element stiffness (E_jI_j, G_jA_j, E_jA_j) along the length the element. The cumulative energy of element *j* due to the entire *DLV* matrix ($\mathbf{V}_0$) is

$$\Xi_j = \sum_{k=1}^{ndlv} \Xi_{jk} \qquad (2.17)$$

where *ndlv* is the number of columns in $\mathbf{V}_0$ and *ndlv* < *ns*. The normalized cumulative energy (*NCE*) of element *j* is defined as

$$\overline{\Xi}_j = \frac{\Xi_j}{\Xi_m} \qquad (2.18)$$

where $\Xi_m = \max_{all\ j}\left(\Xi_j\right)$.

In the case of truss structures, Eq. (2.16) becomes

$$\Xi_{ji} = \int_{L_j} \frac{N_{ji}^{\ 2}}{2E_j A_j} ds = \frac{N_{ji}^{\ 2} L_j}{2E_j A_j} = \sigma_{ji}^2 \frac{A_j L_j}{2E_j} \qquad (2.19)$$

where σ_{ji} is the stress induced in element *j* by column *i* of $\mathbf{V}_0$. Re-writing Eq. (2.19) gives

$$\sigma_{ji} = \sqrt{\Xi_{ji} \times \frac{2E_j}{A_j L_j}} \tag{2.20}$$

The normalized cumulative stress (*NCS*) of element *j* in the original *DLV* method proposed by Bernal (2002) is defined as

$$\overline{\sigma}_j = \frac{\sigma_j}{\sigma_m} \text{ where } \sigma_j = \sum_{k=1}^{ndlv} \sigma_{jk} \text{ and } \sigma_m = \max_{all\ j}(\sigma_j) \tag{2.21}$$

To visualize the relationship between *NCE* and *NCS*, consider the simplest case where the entire truss structure is composed of elements with the same modulus, length and cross-sectional area, and *ndlv* = 1. From Eqs. (2.17) - (2.21),

$$\overline{\Xi}_j = \left(\overline{\sigma}_j\right)^2 \tag{2.22}$$

Other than this special case, theoretical comparison between *NCE* and *NCS* is not available, meaning that the *NCE* and the *NCS* are not the same.

The set of *PDE* comprises those elements with $\overline{\Xi}_j = 0$. In reality, due to the presence of noise and uncertainties, the *NCE* of damaged elements may not exactly be zero and a near-zero threshold is needed for practical applications. Based on the study by Sim et al. (2008), if the value of 0.1 is used as the *NCS* threshold, then the probability of "false negative" (corresponding to the case when the damaged element is not within the set of identified *PDE*) is less than 5% assuming that the Young's moduli of all elements are statistically independent variables, each with a coefficient of variation, δ_E, of 10%. The same basis is adopted in this study and the square value of the *NCS* threshold value is employed as *NCE* threshold. Based on the limited numerical and experimental examples performed, the value of 0.01 has been shown to be robust.

Integrating over element length to obtain Ξ_{ji} may reduce the sensitivity of the damage indicator but makes the method manageable. Normalizing Ξ_{ji} over the

element length may facilitate comparison between elements of different lengths, as will be illustrated in Section 2.9.2.

2.5 DIFFERENTIATING DAMAGED AND STRENGTHENED MEMBER

Consider the truss structure in Section 2.2.3 where the $DLV = [0.6\ -0.8]^T$ has been computed. Applying the *DLV* to the reference structural model as a nodal load vector as shown in Fig. 2.3, the *NCE* of the two elements can be computed as

$$\bar{\Xi}_1 = 0;\ \bar{\Xi}_2 = 1 \tag{2.23}$$

from which element 1 is deduced as being damaged. It is noted that if the axial stiffness (*EA*) of element 1 is increased (strengthened), $\beta_1 > 1$ and Eq. (2.7) still holds. Equation (2.8) becomes

$$\mathbf{F}_\Delta \xrightarrow{SVD} \mathbf{U}\cdot\mathbf{\Sigma}\cdot\mathbf{V}^T = \frac{\beta_1 - 1}{\beta_1 EA}\begin{bmatrix} -0.8 & -0.6 \\ -0.6 & 0.8 \end{bmatrix}\begin{bmatrix} 5.43 & 0 \\ 0 & 0 \end{bmatrix}\begin{bmatrix} 0.8 & -0.6 \\ 0.6 & +0.8 \end{bmatrix} \tag{2.24}$$

leading to $DLV = [-0.6\ \ 0.8]^T$. Hence, the results in Eq. (2.23) remain unchanged. The question is how to determine whether the altered member is damaged or strengthened.

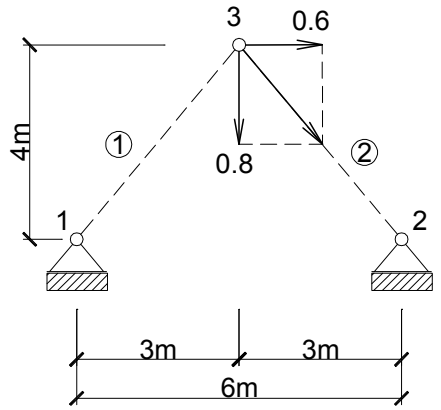

Fig. 2.3. Applying *DLV* onto reference structural model

From the identified flexibility matrices with respect to the sensor locations at the reference ($\mathbf{F}_u$) and the damaged ($\mathbf{F}_d$) states, an indicator to differentiate damaged and strengthened member is defined as

$$\delta_{\Delta} = \frac{\delta_{mm}^{d} - \delta_{mm}^{u}}{\delta_{mm}^{u}} \times 100\% \tag{2.25}$$

where $\left|(\delta_{mm}^{d} - \delta_{mm}^{u}) / \delta_{mm}^{u}\right| = \max_{all\ i} \left|(\delta_{ii}^{d} - \delta_{ii}^{u}) / \delta_{ii}^{u}\right|$, in which δ_{ii}^{u} and δ_{ii}^{d} are elements *i* on the diagonals of $\mathbf{F}_u$ and $\mathbf{F}_d$, respectively; $i = 1, 2, \ldots, ns$; $m \in ns$; and $|(\bullet)|$ the absolute value of $(\bullet)$. Since a unit load is applied one at a time directly onto the structure at *DOF i* to compute δ_{Δ}, the dominator in Eq. (2.25), $\delta_{ii}^{u} \neq 0$. Tua (2005) noted that the flexibility of the structure increases with damage, resulting in $\delta_{\Delta} > 0$; and the flexibility of the structure decreases with strengthening, resulting in $\delta_{\Delta} < 0$. Hence, positive δ_{Δ} is proposed to represent damaged structure and negative δ_{Δ} is proposed to represent strengthened structure.

For the truss used in Section 2.2.3, $\delta_{\Delta} = 0.5(1-\beta_1)/\beta_1$. If $0 < \beta_1 < 1$, implying that the truss is damaged, $\delta_{\Delta} > 0$. On the contrary, if $\beta_1 > 1$, implying that the truss is strengthened, $\delta_{\Delta} < 0$.

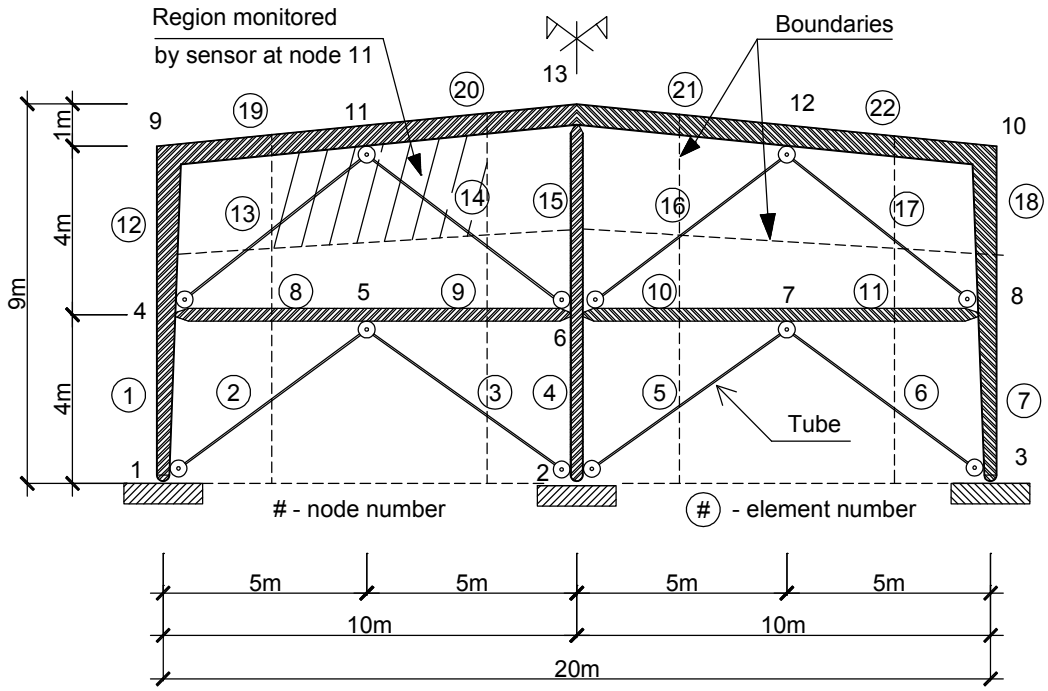

Fig. 2.4. 2-D warehouse structure

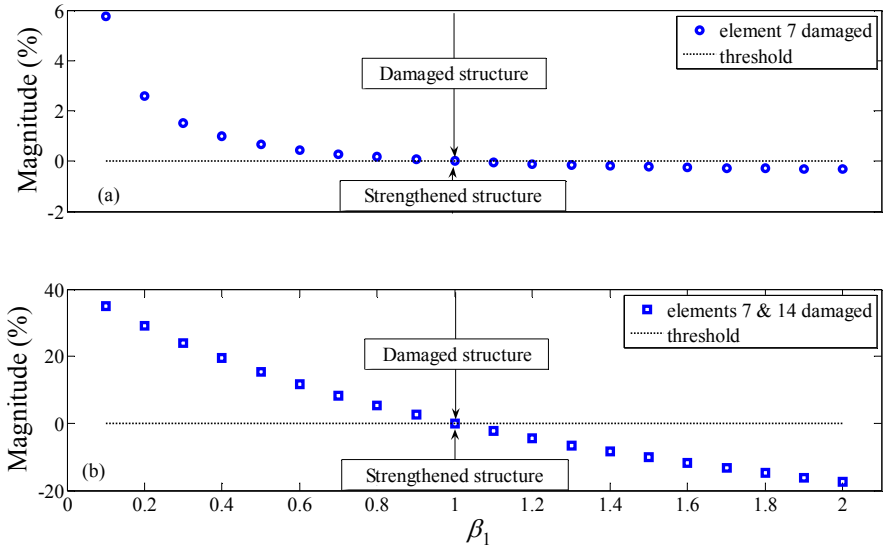

Fig. 2.5. Relationship between δ_Λ and: (a) alteration in element 7 (β_1); and (b) alteration in elements 7 (β_1) and 14 ($\beta_2 = \beta_1$). (2-D warehouse structure; $0 < \beta_1, \beta_2 < 1$: element damaged; $1 < \beta_1, \beta_2$: element strengthened)

Table 2.1. Specifications for members of 2-D warehouse structure

Element numbers		Height (mm)	Width (mm)	Flange thickness (mm)	Web thickness (mm)	Young's modulus (10^{11}Nm^{-2})	Moment of inertia (10^{-8} m^4)	Cross-sectional area (10^{-4}m^2)
1, 7	lower end	300	300	16	10	2.10	20982	122.8
	upper end	450	300	16	10	2.10	51312	137.8
12, 18	lower end	450	300	16	10	2.10	51312	137.8
	upper end	600	300	16	10	2.10	97145	152.8
4, 15		300	300	16	10	2.10	20982	122.8
19, 20, 21, 22		500	300	16	10	2.10	64784	142.8
8, 9, 10, 11		300	300	16	10	2.10	20982	122.8
2, 3, 5, 6, 13, 14, 16, 17		Tubular sections				2.10	4	2.0

For further illustration, a 2-D warehouse structure shown in Fig. 2.4 is considered. The specifications of the structural elements are listed in Table 2.1. Assuming that 10 displacement sensors are available to monitor horizontal displacements at nodes (4, 6, 8, 9, 10, 13) and vertical displacements at nodes (5, 7, 11, 12). Two cases of alterations will be investigated, namely (a) element 7 is altered; and (b) elements (7, 14) are altered. Alteration in element 7 is simulated by multiplying its flexural stiffness (EI) along the length of the element with a coefficient β_1 whereas alteration in element 14 is generated by multiplying its axial stiffness (EA) along the length of the element with a coefficient β_2. For this illustration, results of δ_Δ for some values of $\beta_2 = \beta_1$ ranging from 0.1 to 2 at the intervals of 0.1 are plotted in Fig. 2.5. From Fig. 2.5, if $\beta_1 < 1$, meaning that the members are damaged, $\delta_\Delta > 0$; if $\beta_1 > 1$, meaning that the members are strengthened, $\delta_\Delta < 0$. It is also observed that $|\delta_\Delta|$ increases monotonically with the damage severity. In addition, increasing member stiffness results in smaller variation of $|\delta_\Delta|$ compared to decreasing the same amount of member stiffness. For instance, increasing 50% flexural stiffness of element 7 results in variation of $|\delta_\Delta| = 0.2\%$ whereas decreasing 50% flexural stiffness of element 7 results in variation of $|\delta_\Delta| = 0.7\%$. The variation of $|\delta_\Delta|$ is almost linear where the

members are strengthened or slightly damaged whereas δ_Δ increases rapidly if damage severity is close to 100% (β_1 is close to zero).

To investigate the presence of both damaged and strengthened members in the structure on δ_Δ, the same procedure as above is performed where β_1 and β_2 are varied from 0.1 to 2 at the intervals of 0.1. Results in Fig. 2.6 indicate that δ_Δ can provide correct conclusion if both elements (7, 14) are damaged or strengthened simultaneously. For example, if both elements (7, 14) are damaged with $\beta_1 = \beta_2 = 0.1$, $\delta_\Delta = 35.0\%$; if both elements (7, 14) are strengthened with $\beta_1 = \beta_2 = 2$, $\delta_\Delta = -17.4\%$. However, if element 7 is damaged and element 14 is strengthened or element 7 is strengthened and element 14 is damaged, δ_Δ cannot provide reliable conclusion. For instance, if element 7 is strengthened with $\beta_1 = 2$ and element 14 is damaged with $\beta_2 = 0.1$, $\delta_\Delta = 34.9\%$ and an incorrect conclusion that the structure is damaged will be issued; if element 7 is damaged with $\beta_1 = 0.1$ and element 14 is strengthened with $\beta_2 = 2$, $\delta_\Delta = -17.3\%$ and an incorrect conclusion that the structure is strengthened will be issued.

In short, the procedure for structural damage detection includes two steps: (1) detect altered elements; and (2) differentiate whether the altered elements are damaged or strengthened. An indicator was proposed to address the latter and shown good performance for the case where structure is either damaged or strengthened. However, the indicator cannot provide reliable result if both damaged and strengthened members present simultaneously. Nevertheless, strengthening in an existing structure is usually done purposely and can be recorded. Identifying strengthened members is therefore less critical compared to identifying damaged members which are not known *a priori*. Hence, the major concern of this report is the identification of damaged elements in structure assuming that strengthen members if any are known before hand. The

baseline data of the structure can be updated once repair is made and then use as that corresponding to the undamaged state so that the procedure presented in this thesis remains applicable.

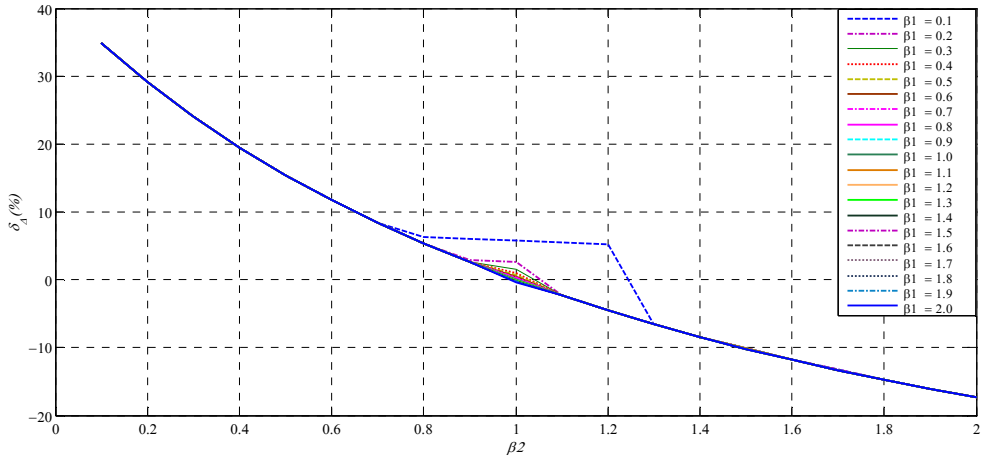

Fig. 2.6. Relationship between δ_Δ and alterations in elements 7 (β_1) and 14 (β_2). (2-D warehouse structure; $0 < \beta_1, \beta_2 < 1$: element damaged; $1 < \beta_1, \beta_2$: element strengthened)

2.6 IDENTIFYING ACTUAL DAMAGED ELEMENTS

2.6.1 Intersection scheme

In the *DLV* method, if limited number of sensors are used, the set of *PDE* identified will contain both actual damaged and some undamaged elements (Bernal, 2002). The intersection scheme is formulated to filter out the actual damaged elements by taking the intersection of all potential sets derived using data from various combinations of sensors. The scheme is summarized in Fig. 2.7.

Starting with *ns* sensors, a set of *PDE* is first computed and denoted as the current intersected damaged set (*IDS*). Next, by using only data from *ns*-1 sensors which are close to members in the *IDS* set, another set of *PDE* can be identified. By taking the common elements from this *PDE* and the *IDS*, a new *IDS* is obtained. This procedure can be repeated for a different sets of *ns*-1 sensors (since there are *ns* possible sets of *ns*-1 sensors) to get a new *IDS*. If the old and the new *IDS* are identical, the elements in the *IDS* are identified as the actual damaged elements and the identification process is taken as completed. The process is also terminated if the new *IDS* is a null set, implying that there is no damaged element in the structure. If 2 consecutive *IDS* are not identical and the combinations of *ns*-1 sensors are exhausted, then combinations of *ns*-2 sensors are next considered until the criterion of 2 consecutive repeated *IDS* are met. The termination criterion can be increased to requiring higher number of consecutive identical *IDS* to ensure robustness of the method at the expense of computational cost. Based on extensive study with different numerical examples (see Section 2.9.1), including data with added noise, it is found that the 2 identical consecutive *IDS* criterion is robust.

The scheme works provided that *ns* is greater than 2 since at least 2 measurements are required to form a matrix before any *SVD* can be performed to

compute the *DLV*. With *ns* = 2, only 1 set of *PDE* can be computed and no subsequent combination of sensors is available to filter out the actual damaged elements.

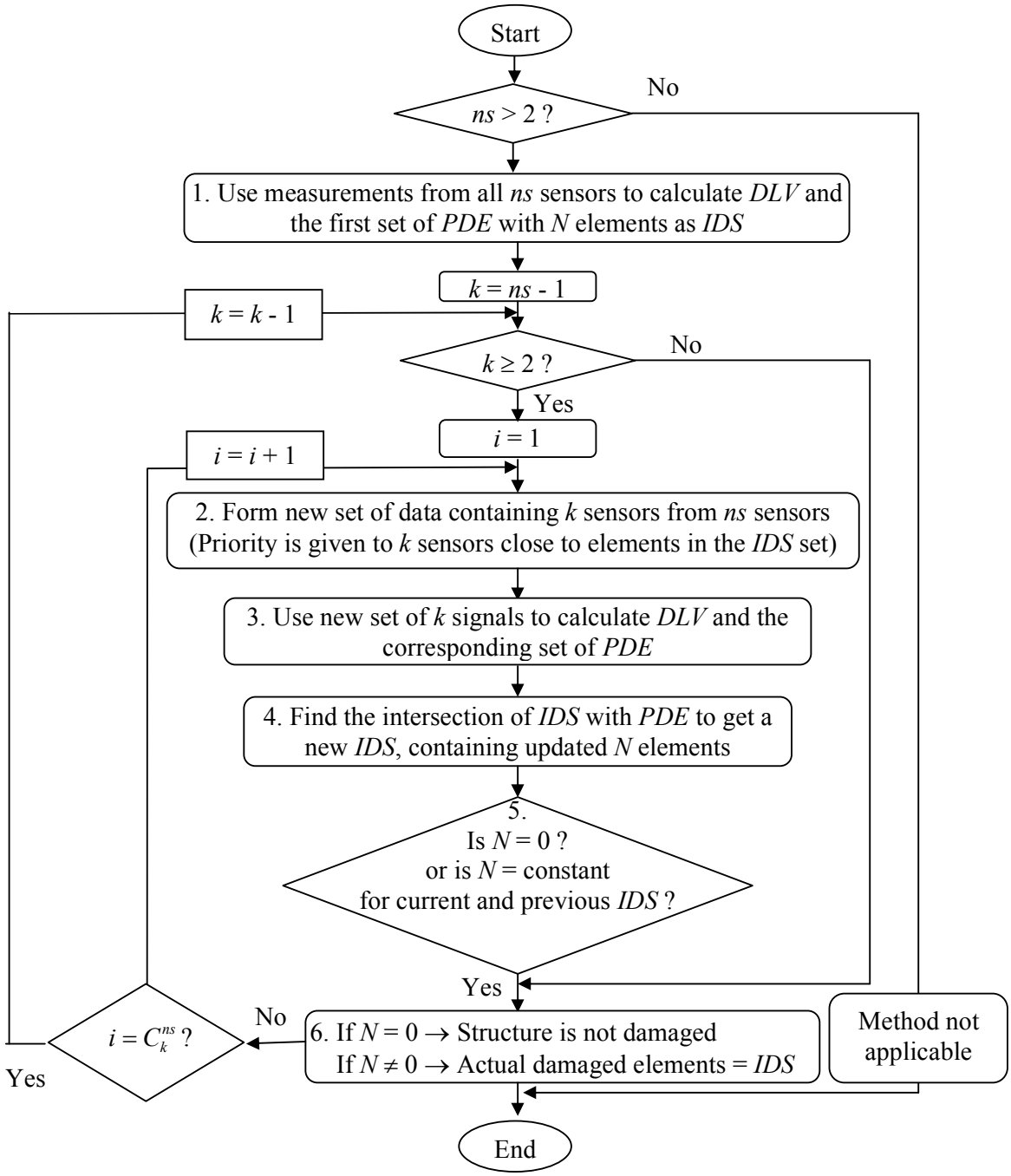

Fig. 2.7. Flow chart for intersection scheme to identify actual damaged elements

2.6.2 Two-stage analysis

In structures with many elements and degrees of freedom (*DOF*), if the number of sensors used is small, the number of combinations to analyze before reliable results are obtained using the intersection scheme may be quite formidable. Hence, a two-stage analysis is proposed whereby potential damaged regions are first identified based on the relative change in flexibility matrix and the individual regions are then analyzed using the *DLV* method to identify the actual damaged elements.

For a structure with sensors attached at various locations, the sensors may be viewed as capturing information mostly of structural members in its vicinity. If the perpendicular bisector between pairs of sensors are drawn, then the polygon around (or interval between) each sensor may be taken as the region covered by that sensor. Any structural element encompassed or intersected by the polygon (or interval) is considered as significantly contributing to the data captured by the enclosed sensor relative to the other sensors.

From the identified flexibility matrices with respect to the sensor locations at the reference ($\mathbf{F}_u$) and the damaged ($\mathbf{F}_d$) states, damaged region index vector is defined as

$$\delta\mathbf{F} = \left[\delta_1^{\Delta} \quad \delta_2^{\Delta} \quad \cdots \quad \delta_{ns}^{\Delta} \right] \times 100\% \tag{2.26}$$

where $\delta_i^{\Delta} = \left(\delta_{ii}^d - \delta_{ii}^u \right) / \delta_{ii}^u$, in which δ_{ii}^u and δ_{ii}^d are elements *i* on the diagonals of $\mathbf{F}_u$ and $\mathbf{F}_d$, respectively; and i = 1, 2, …, *ns*. Since the unit load is applied one at a time directly onto the structure at *DOF i* to compute component *i* of $\delta\mathbf{F}$, the denominator in Eq. (2.26), $\delta_{ii}^u \neq 0$. As the presence of damage in structure increases its flexibility, applying a unit load to *DOF i* at both the reference and damaged states gives $\left| \delta_{ii}^u \right| \leq \left| \delta_{ii}^d \right|$. Note that if δ_{ii}^u is negative, δ_{ii}^d is also negative, resulting in non-negative δ_i^{Δ}. The vector $\delta\mathbf{F}$ will be null if there is no change in the structure from its reference

state. Hence, any non-zero entry in $\delta\mathbf{F}$ indicates some form of damage. If the values in Eq. (2.26) are plotted on the structural layout, by comparing values between neighbouring sensor locations, local maxima can be identified, which is likely to indicate that there is(are) damaged element(s) in the region covered by the associated sensor.

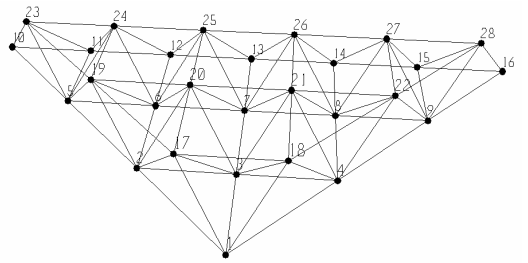

a) 3-D truss model with node numbers

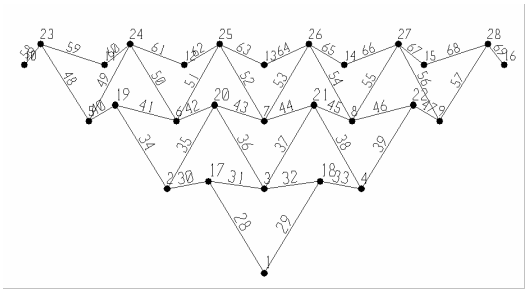

b) Node and web element numbers

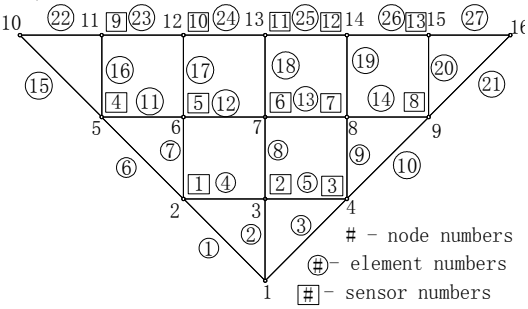

c) Node and element numbers at bottom flange, and sensor numbers (inside rectangular boxes)

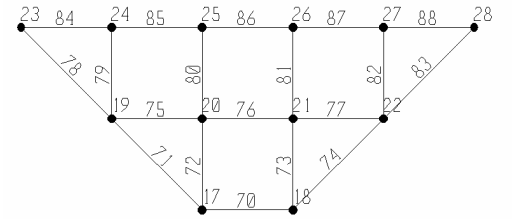

d) Element & node numbers at top flange

Fig. 2.8. 3-D modular truss structure model

Table 2.2. Summary of materials and geometries for 3-D modular truss members

Truss members	ϕ (mm)	Thickness (mm)	Length (mm)	Quantity	Material	Elastic modulus (N/m^2)
Top flange	46	1.6	1000	15	Steel	2.1×10^{11}
Top flange	46	1.6	1414	4	Steel	2.1×10^{11}
Web	22	1.0	1000	42	Aluminum	6.8×10^{10}
Bottom flange	46	1.6	1000	21	Steel	2.1×10^{11}
Bottom flange	46	1.6	1414	6	Steel	2.1×10^{11}

Table 2.3. Maximum coefficients of $\delta\mathbf{F}$ for 6.5% noise added: 3-D modular truss structure (structure healthy)

Set No.	Sensors at nodes	Number of samples	Max ($\delta\mathbf{F}$) Mean	Max ($\delta\mathbf{F}$) Standard deviation
1	[3,4,5,6,7,8,9,11,12,13,14,15]	30	0.0571	0.0288
2	[2,4,5,6,7,8,9,11,12,13,14,15]	30	0.0541	0.0165
3	[2,3,5,6,7,8,9,11,12,13,14,15]	30	0.0576	0.0235
4	[2,3,4,6,7,8,9,11,12,13,14,15]	30	0.0491	0.0217
5	[2,3,4,5,7,8,9,11,12,13,14,15]	30	0.0542	0.0185
6	[2,3,4,5,6,8,9,11,12,13,14,15]	30	0.0577	0.0238
7	[2,3,4,5,6,7,9,11,12,13,14,15]	30	0.0551	0.0225
8	[2,3,4,5,6,7,8,11,12,13,14,15]	30	0.0394	0.0211
9	[2,3,4,5,6,7,8,9,12,13,14,15]	30	0.0574	0.0259
10	[2,3,4,5,6,7,8,9,11,13,14,15]	30	0.0522	0.0212
11	[2,3,4,5,6,7,8,9,11,12,14,15]	30	0.0559	0.0186
12	[2,3,4,5,6,7,8,9,11,12,13,15]	30	0.0471	0.0205
13	[2,3,4,5,6,7,8,9,11,12,13,14]	30	0.0511	0.0204
14	[2,3,4,5,6,7,8,9,11,12,13,14,15]	30	0.0560	0.0213

In practice, even if there is no damage in the structure, when a unit load is applied to both the reference and the damaged structures, non-zero entries in $\delta\mathbf{F}$ may still exist due to measurement inaccuracy and the presence of noise. A near-zero threshold is therefore applied to ensure that healthy regions are not wrongly identified as damaged regions. This threshold is in fact problem dependent, and is a function of the type of structure and the number of sensors used. As an illustration, a 3-D modular truss comprising 88 elements and 28 nodes, pin-supported at the three bottom corners is used to generate structural flexibility matrices at sensor locations for both the reference ($\mathbf{F}_u$) and the damaged ($\mathbf{F}_d$) states. The truss model is shown in Fig. 2.8 and its members' properties and geometries are given in Table 2.2. Thirteen displacement sensors are used to monitor the vertical displacements of all nodes at the lower chord of the truss. Consider the case when the truss is healthy ($\mathbf{F}_u = \mathbf{F}_d$) and monitored by 12 sensors. It will be shown in Section 4.2.1 that the maximum noise level in the flexibility matrices which the *DLV* method can accommodate in this set-up before the

results become unreliable is 6.5%. In this example, zero-mean white noise with root mean square (*RMS*) of 6.5% are added to contaminate the simulated flexibility matrices, $\mathbf{F}_u$ and $\mathbf{F}_d$, based on which the maximum entry of $\delta\mathbf{F}$ is computed. Since the true value is supposed to be zero, this maximum entry indicates the threshold beyond which the structure may be considered as damaged. The procedure is repeated 30 times and results are summarized in Table 2.3. The first 13 sets in Table 2.3 are for the case where 12 sensors are used and the maximum of the mean value is less than 0.059 with standard deviation less than 0.029. A reasonable threshold of 0.06 may be used for this case, although one may argue that to increase robustness of the method, a threshold of 0.03 corresponding to one standard deviation below the mean may be applied as the demarcation criterion. If 13 sensors are used and the ultimate zero-mean white noise with *RMS* of 11.5% beyond which the *DLV* method can be considered unreliable is used to contaminate the flexibility matrices, the results in the last row of Table 2.3 indicate that the same threshold may still be used. If 7 sensors are used and the upper limit zero-mean white noises with *RMS* of 3.5% are added, the maximum of the mean value reduces to 0.044 with standard deviation of 0.013. A threshold of 0.03 at approximately one standard deviation below the mean may be selected as the criterion to demarcate between a healthy and a potentially damaged structures. For specific applications, numerical simulations may first be performed introducing noise to the measured signal based on the data acquisition accuracy to estimate the appropriate threshold to adopt.

It is possible that actual damaged elements may not be identified using the two-stage analysis scheme if the effect of damage on the change in structural flexibility matrix is less than the near-zero threshold used. This usually corresponds to cases where the damage is minor to be of concerned, such as that due to fine cracks or slight

damage in non-critical elements. For example, for the 3-D modular truss with element 86 damaged, using 12 sensors, the damage has to exceed 7% of the axial stiffness before the threshold of 0.03 is crossed.

Using the change in flexibility matrix to identify possible damaged regions in the first stage has advantage over the use of change in mode shape commonly found in the literature. The latter is usually computed based on the difference between the identified mode shapes at the reference and damaged states. For example, Ewins (2000) defined the Coordinate Modal Assurance Criterion (**COMAC**) as

$$\mathbf{COMAC}(i) = \frac{\left[\sum_{j=1}^{nm}\left(\mathbf{\Phi}_{ij}^{u}\mathbf{\Phi}_{ij}^{d}\right)\right]^2}{\left[\sum_{j=1}^{nm}\left(\mathbf{\Phi}_{ij}^{u}\right)^2\right]\left[\sum_{j=1}^{nm}\left(\mathbf{\Phi}_{ij}^{d}\right)^2\right]} \tag{2.27}$$

where $\mathbf{\Phi}_{ij}$ is mode shape value at coordinate i of mode shape j; nm the number of identified mode shapes; and superscripts u and d denote the reference and the damaged states. Component i of the **COMAC** should be unity if the structure is healthy. When component i of **COMAC** is different from unity, it gives an indication of a possible damaged region at the monitored coordinate i. However, the change in flexibility matrix increases monotonically with increasing severity of damage while the change in mode shape values is not necessarily monotonic, especially if damage is severe or covers a large area of the structure (Tua, 2005).

In the second stage of the analysis, the *DLV* method is performed to identify a set of *PDE* which contains both the actual damaged and some undamaged elements. Since the presence of damaged elements will generate local maxima at the appropriate entries of $\delta\mathbf{F}$, only those elements in the set of *PDE* corresponding to elements associated with the identified damaged regions in the first stage are confirmed as being damaged.

2.7 ASSESSING DAMAGE SEVERITY

Performing the *DLV* method, the damaged elements can be identified. An iterative scheme adopting the penalty function method is used to assess the severity of the identified damaged elements in terms of axial stiffness for truss members and flexural stiffnesses for frame members. From the measured displacement responses, the structural flexibility matrix of its current state ($\mathbf{F}_d$) is formulated following the procedure presented in Section 2.3. Based on the reference structure, a finite element (*FE*) model of the structure can be constructed. For the case where the stiffnesses of some elements are damaged, the same program is used with the modified stiffnesses to obtain the modified structural flexibility matrix, denoted as $\mathbf{F}_n$. If there is only one damaged element then by direct computation based on a few postulated modified stiffness and checking whether $\mathbf{F}_n$ approaches $\mathbf{F}_d$, the damage severity at the element level can be deduced. For the case where there are two or more damaged elements, $\mathbf{F}_n$ is mapped to $\mathbf{F}_d$ by minimizing the difference in some of their representative characteristics, such as eigenvalues and eigenvectors, in order to deduce damage severity of the damaged elements. However, eigenvalues and eigenvectors are found not sensitive to structural damage and for some cases non-uniqueness solution may be observed if the structure is symmetric (Lu and Law, 2007). Singular values of flexibility matrix, which are easy to compute and sensitive to the matrix disturbance, are explored in this section. The special characteristic of singular values of a matrix is that they are non-negative and are placed in decreasing order of magnitude. Under matrix disturbance, all singular values will be affected although the level of affection is not the same. Hence, to minimize the difference in singular values of $\mathbf{F}_n$ and $\mathbf{F}_d$ or to map $\mathbf{F}_n$ to $\mathbf{F}_d$, the following three objective functions are considered, namely

(1) Mean of normalized difference in singular values of $\mathbf{F}_n$ and $\mathbf{F}_d$

$$z = \frac{1}{ns}\sum_{i=1}^{ns}\left|\frac{s_d(i)-s_n(i)}{s_n(i)}\right|\times 100\% \tag{2.28}$$

(2) Normalized difference in the first (maximum) singular values between $\mathbf{F}_n$ and $\mathbf{F}_d$ (since the first singular value of a matrix is the most affected singular value when the matrix is disturbed)

$$z = \frac{\left|s_d(1)-s_n(1)\right|}{s_n(1)}\times 100\% \tag{2.29}$$

(3) Root mean square of normalized difference in singular values of $\mathbf{F}_n$ and $\mathbf{F}_d$

$$z = \sqrt{\frac{1}{ns}\sum_{i=1}^{ns}\left[\frac{s_d(i)-s_n(i)}{s_n(i)}\right]^2}\times 100\% \tag{2.30}$$

where $s_n(i)$ and $s_d(i)$ are the ith singular value of $\mathbf{F}_n$ and $\mathbf{F}_d$, respectively; i = 1, 2, …, ns; and ns the number of sensors used. The results of the three above-mentioned objective functions for the 2-D warehouse structure (Fig. 2.4 and Table 2.1) and the 3-D modular truss structure (Fig. 2.8 and Table 2.2) for the case of single damaged element are plotted in Figs. 2.9 and 2.10. In general, a reduction in element stiffness produces the maximum change in the second objective function. For example, for the 2-D warehouse structure, the magnitudes of the three objective functions are 3.0%, 7.2% and 6.3% (corresponding to 10% reduction in flexural stiffness of element 8), respectively, which is maximum at the second objective function. There are 4 elements which produce the largest magnitudes at the third objective function, namely elements (2, 3, 5, 6). For such cases, however, the difference in magnitudes between the second and the third objective functions are not significant.

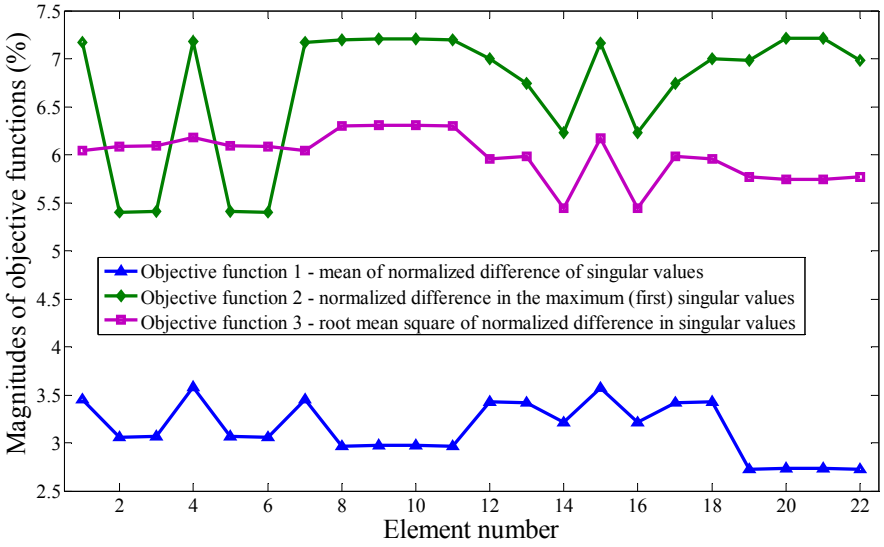

Fig. 2.9. Objective function values for different damaged elements with 10% reduction in element stiffness of 2-D warehouse structure

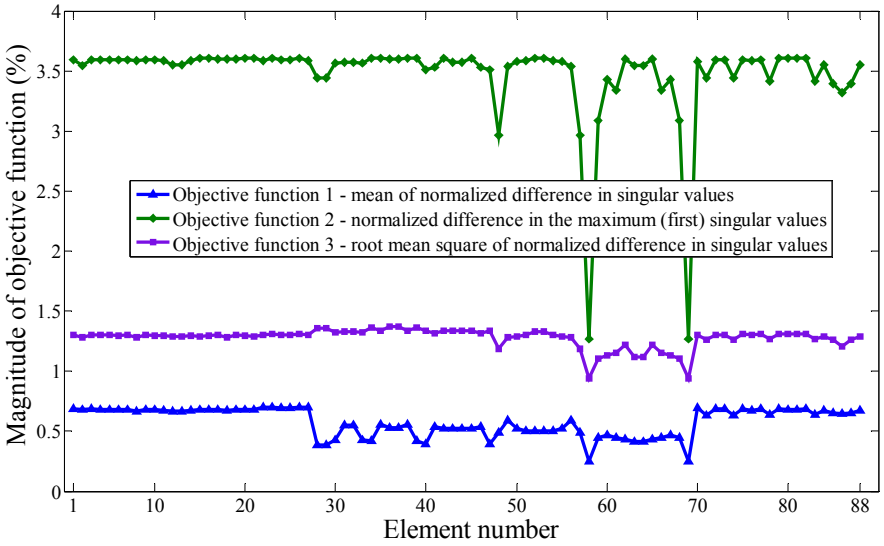

Fig. 2.10. Objective function values for different damaged elements with 10% reduction in axial stiffness of 3-D modular truss structure

From the above observation, the change in the first singular value of a matrix is found the most sensitive to the disturbance of structural flexibility matrix caused by the presence of damage. Minimizing the difference between the first singular values of $\mathbf{F}_n$ and $\mathbf{F}_d$ is proposed as criterion to map $\mathbf{F}_n$ to $\mathbf{F}_d$, resulting in the estimation of damage severity of the damaged elements. Therefore, normalized difference in the first singular values between $\mathbf{F}_n$ and $\mathbf{F}_d$ will be selected as the objective function to be minimized.

The algorithm starts by forming a set of structural parameters $\boldsymbol{\theta}$ comprising stiffnesses of the *nd* identified damaged elements based on the reference structure as

$$\boldsymbol{\theta} = \begin{bmatrix} (EX)_1 & (EX)_2 & \cdots & (EX)_{nd} \end{bmatrix}^T \tag{2.31}$$

where $(EX)_i$ is the axial stiffness or the flexural stiffness of element i if element i is truss or frame element, respectively, in which i = 1, 2, …, and *nd* is the number of damaged elements. From $\boldsymbol{\theta}$ and measured displacement responses, $\mathbf{F}_n$ and $\mathbf{F}_d$ are formulated, based on which the objective function to be minimized z can be computed following Eq. (2.29).

In penalty function method (Friswell and Mottershead, 1995), the objective function in Eq. (2.29) can be approximated by neglecting the higher order components as

$$\hat{z} = \mathbf{S} \times \delta\boldsymbol{\theta} \tag{2.32}$$

where $\mathbf{S}$ is the structural sensitivity matrix and $\delta\boldsymbol{\theta}$ the modification of $\boldsymbol{\theta}$ such that $\mathbf{F}_n$ approaches $\mathbf{F}_d$. The structural sensitivity matrix can be computed as

$$\mathbf{S} = \frac{\partial z}{\partial \boldsymbol{\theta}} \approx \frac{\delta z^0}{\delta \boldsymbol{\theta}^0} = \left[\frac{\delta z^0}{\delta (EX)_1^0} \quad \frac{\delta z^0}{\delta (EX)_2^0} \quad \cdots \quad \frac{\delta z^0}{\delta (EX)_{nd}^0} \right]^T \tag{2.33}$$

where $\delta\boldsymbol{\theta}^0$ is a small disturbance of $\boldsymbol{\theta}$ or $\delta\boldsymbol{\theta}^0 = \left[\delta(EX)_1^0 \quad \delta(EX)_2^0 \quad \cdots \quad \delta(EX)_{nd}^0\right]^T$; in which $\delta(EX)_i^0$ is the small disturbance in stiffness of damaged element *i*; and δz^0 the variation of *z* due to the small disturbance $\delta\boldsymbol{\theta}^0$.

To estimate $\delta\boldsymbol{\theta}$, the discrepancy between the actual and the approximated normalized difference in maximum singular values of $\mathbf{F}_n$ and $\mathbf{F}_d$ is estimated as follow

$$\varepsilon = z - \hat{z} = z - \mathbf{S} \times \delta\boldsymbol{\theta} \tag{2.34}$$

Applying least square estimation (*LSE*) method on Eq. (2.34) gives

$$\delta\boldsymbol{\theta} = \mathbf{S}^{\dagger} z \tag{2.35}$$

where "†" denotes pseudo-inverse. The stiffnesses of the *nd* damaged elements are updated as

$$\boldsymbol{\theta} = \boldsymbol{\theta} + \delta\boldsymbol{\theta} \tag{2.36}$$

The procedure is iterated until a pre-defined tolerance is reached, that is,

$$\min\left\{\begin{array}{l} \sqrt{\dfrac{\delta\boldsymbol{\theta}^T \times \delta\boldsymbol{\theta}}{\boldsymbol{\theta}^T \times \boldsymbol{\theta}}} \times 100\% \\ \left|\dfrac{z_i - z_{i-1}}{z_i}\right| \times 100\% \end{array}\right\} \le Tol \tag{2.37}$$

where *Tol* is pre-defined tolerance; z_i and $z_{i\text{-}1}$ the values of the objective function at iterations *i* and *i* - 1.

It is noted that the number of variables to be estimated in the proposed procedure (*nd*) is much smaller compared to the number of variables to be estimated in other matching procedures available in the literature which includes all coefficients of stiffness and damping matrices (Liu and Shepard Jr., 2004; Chen and Li, 2004; Lu and Law, 2006, 2007), making it more feasible and robust. Besides, the computation of the singular values to evaluate the objective function in the current approach is more

computationally efficient compared to the computation of eigenvalues and eigenvectors adopted in the literature.

2.8 DETECT DAMAGE WITH UNKNOWN STATIC LOAD

To formulate the flexibility matrix using the measured displacements following the procedure presented in Section 2.3, a known static load is shifted through all monitored locations. Although the procedure can still be employed if the static load applied at each *DOF* is different, the static load is usually selected to be constant to ease the implementation and computation process. However, the magnitude of the static load need not be the same when performing for the reference and the damaged structures as they may be done at different times which may be months or years apart. In some extreme cases, the magnitudes of the static loads are even unknown. In such cases, modifications are required in order to perform the *DLV* method to assess structural damage.

Let P_u and P_d denote the unknown static loads being applied onto the reference and the damaged structures, respectively, and that displacement responses at *ns* sensor locations are measured. The flexibility matrices with respect to the sensor locations for the reference ($\mathbf{F}_u$) and the damaged ($\mathbf{F}_d$) structures can be written as follows

$$\mathbf{F}_u = \frac{1}{P_u}\begin{bmatrix} d_{11}^u & d_{12}^u & \cdots & d_{1ns}^u \\ d_{21}^u & d_{22}^u & \cdots & d_{2ns}^u \\ \vdots & \vdots & \ddots & \vdots \\ d_{ns1}^u & d_{ns2}^u & \cdots & d_{ns\ ns}^u \end{bmatrix} = \frac{1}{P_u}\mathbf{U}_u \tag{2.38}$$

$$\mathbf{F}_d = \frac{1}{P_d}\begin{bmatrix} d_{11}^d & d_{12}^d & \cdots & d_{1ns}^d \\ d_{21}^d & d_{22}^d & \cdots & d_{2ns}^d \\ \vdots & \vdots & \ddots & \vdots \\ d_{ns1}^d & d_{ns2}^d & \cdots & d_{ns\ ns}^d \end{bmatrix} = \frac{1}{P_d}\mathbf{U}_d \tag{2.39}$$

where d_{ij}^{u} and d_{ij}^{d} are the displacements at *DOF i* due to loads P_u and P_d at *DOF j* at the reference and the damaged states, respectively; superscripts *u* and *d* are associated with the reference and damaged states; and $\mathbf{U}_u$ and $\mathbf{U}_d$ the displacement matrices with respect to the sensor locations of the reference and the damaged structures, respectively, that is,

$$\mathbf{U}_u = \begin{bmatrix} d_{11}^{u} & d_{12}^{u} & \cdots & d_{1ns}^{u} \\ d_{21}^{u} & d_{22}^{u} & \cdots & d_{2ns}^{u} \\ \vdots & \vdots & \ddots & \vdots \\ d_{ns1}^{u} & d_{ns2}^{u} & \cdots & d_{ns\,ns}^{u} \end{bmatrix} \text{ and } \mathbf{U}_d = \begin{bmatrix} d_{11}^{d} & d_{12}^{d} & \cdots & d_{1ns}^{d} \\ d_{21}^{d} & d_{22}^{d} & \cdots & d_{2ns}^{d} \\ \vdots & \vdots & \ddots & \vdots \\ d_{ns1}^{d} & d_{ns2}^{d} & \cdots & d_{ns\,ns}^{d} \end{bmatrix} \tag{2.40}$$

Based on measured displacements, $\mathbf{U}_u$ and $\mathbf{U}_d$ can be formulated following Eq. (2.40) whereas $\mathbf{F}_u$ and $\mathbf{F}_d$ are not computable since P_u and P_d are not known. Following Section 2.2.2, the *DLV* can not be computed since $\mathbf{F}_\Delta$ is not available. Equation (2.1) can be re-written here for easier reference

$$(\mathbf{F}_d - \mathbf{F}_u)\,\mathbf{P} = \mathbf{F}_\Delta\,\mathbf{P} = \mathbf{0} \tag{2.41}$$

where $\mathbf{P}$ is *DLV*. Assume that there exists a constant α such that

$$P_u = \alpha\, P_d \tag{2.42}$$

Multiplying both sides of Eq. (2.41) with P_u and invoking Eq. (2.42) gives

$$P_u(\mathbf{F}_d - \mathbf{F}_u)\,\mathbf{P} = (P_u\mathbf{F}_\Delta)\,\mathbf{P} = \mathbf{0} \rightarrow (\alpha P_d\mathbf{F}_d - P_u\mathbf{F}_u)\,\mathbf{P} = \mathbf{0} \rightarrow (\alpha\mathbf{U}_d - \mathbf{U}_u)\,\mathbf{P} = \mathbf{U}_\Delta\mathbf{P} = \mathbf{0} \tag{2.43}$$

where

$$\mathbf{U}_\Delta = \alpha\,\mathbf{U}_d - \mathbf{U}_u = P_u\mathbf{F}_\Delta \tag{2.44}$$

From Eq. (2.44), performing *SVD* on $\mathbf{U}_\Delta$ and $\mathbf{F}_\Delta$ produces the same right singular matrix. Hence, the set of *DLV*s can also be computed by replacing $\mathbf{F}_\Delta$ by $\mathbf{U}_\Delta$ in Eqs. (2.2) - (2.5). The remaining requirement is to estimate α such that Eq. (2.42) is satisfied.

The distinguishing feature of α which satisfies Eq. (2.42) is that: if the structure is not damaged, $\mathbf{U}_\Delta = \mathbf{F}_\Delta = \mathbf{0}$; if the structure is damaged, $\mathbf{F}_\Delta$ is rank-deficient, hence following Eq. (2.44), $\mathbf{U}_\Delta = P_u\mathbf{F}_\Delta$ is also rank-deficient. In both cases, α which satisfies Eq. (2.42) produces the smallest summation of singular values of $\mathbf{U}_\Delta = \alpha\mathbf{U}_d - \mathbf{U}_u$. Thus, α can be estimated by minimizing the following sum of singular values of $\mathbf{U}_\Delta$

$$z_\alpha = \sum_{i=1}^{ns} s_\Delta(i) \tag{2.45}$$

where $s_\Delta(i)$ is the ith singular value of $\mathbf{U}_\Delta = \alpha\mathbf{U}_d - \mathbf{U}_u$. The minimization problem in Eq. (2.45) can be executed without any difficulty using the function 'fminbnd' in Matlab. Upon estimating α, the *DLV* set can be computed by replacing $\mathbf{F}_\Delta$ by $\mathbf{U}_\Delta$ in Eqs. (2.2) -(2.5). Consequently, the *DLV* method can be employed to detect structural damage.

2.9 NUMERICAL AND EXPERIMENTAL ILLUSTRATION

Numerical example of a 2-D warehouse structure is performed to illustrate the *NCE*-based *DLV* method in Section 2.9.1. Experimental example of a 3-D modular truss structure is then carried out to assess the performance of the *DLV* method with measured data in Section 2.9.2.

2.9.1 Numerical example

A 2-D warehouse structure shown in Fig. 2.4 is simulated to generate displacement responses. The structure comprises (a) beams and columns with either constant or varied cross-sectional areas; and (b) truss members. The specifications of the structural members are listed in Table 2.1. Two cases of damage are investigated, namely (1) element 14 is damaged; and (2) elements (7, 14) are damaged. Damage in

element 7 is simulated by imposing a 20% reduction in its flexural stiffness for the whole length of the element whereas for element 14, a 20% reduction in axial stiffness along the whole length of the element is imposed to simulate its damage. Static loads P_u and P_d, assumed unknown, are applied on the reference and the damaged structures, respectively, and the horizontal displacement responses at nodes (4, 6, 8, 9, 10, 13) and vertical displacement responses at nodes (5, 7, 11, 12) are monitored. By shifting P_u and P_d through all the monitored *DOF*, the displacements at sensor locations are recorded and shown in Table 2.4 based on which the displacement matrices $\mathbf{U}_u$ and $\mathbf{U}_d$ are formulated. The procedure presented in Section 2.8 is next employed to estimate α in Eq. (2.42). Upon estimating $\alpha = 2$, the change in displacement matrix $\mathbf{U}_\Delta = \alpha\mathbf{U}_d - \mathbf{U}_u$ can be computed. Replacing $\mathbf{F}_\Delta$ by $\mathbf{U}_\Delta$ in Eqs. (2.2) - (2.5), a set of 9 *DLV*s is identified.

***i*) Intersection scheme to identify actual damaged elements**

Applying the *DLV* set onto the reference structural model as nodal force vectors with respect to the sensor locations, the *NCE* of all elements are evaluated and the set of *PDE* which includes elements (14, 17) is identified. Therefore, the current *IDS* contains elements (14, 17) and *ne* = 2. By omitting data from the sensor at node 4 which is far away from elements (14, 17) in the current *IDS*, the flexibility matrices with respect to the remaining 9 sensor locations are computed from which a set of 8 *DLV*s is identified. By applying these *DLV*s onto the reference structural model as nodal force vectors, the *NCE* of all elements are computed and the set of *PDE* which contains element 14 is identified. Intersecting the set of *PDE* and the current *IDS* which contains elements (14, 17) produces element 14 as the new *IDS* (*ne* = 1). Similarly, by omitting the readings of the sensor at node 10, which is far away from elements 14 in the current *IDS*, instead of the sensor at node 4, another set of *PDE*

containing elements (12, 14, 16) is identified. Intersecting the identified *PDE* with the current *IDS* which contains element 14 only gives element 14 as the new *IDS* (*ne* = 1). Since the *IDS* is the same for 2 consecutive steps, the iteration is terminated and the actual damaged element 14 is identified correctly. The procedure is summarized in the upper portion of Table 2.5. Similarly for the case where elements (7, 14) are damaged, the feasibility of the intersection scheme is confirmed by the results in the upper portion of Table 2.6.

Table 2.4. Simulated displacements for 2-D warehouse structure (10^{-3} mm)

		Static load at node									
		4	5	6	7	8	9	10	11	12	13
		Reference structure									
Displacement sensors at nodes	4	112.62	0.02	108.33	0.00	107.00	124.58	123.49	1.71	2.58	123.87
	5	0.02	273.61	0.01	0.06	0.01	0.10	0.06	0.45	0.23	0.11
	6	108.33	0.01	111.55	0.00	110.10	124.23	123.34	-0.47	2.46	123.63
	7	0.00	0.06	0.00	273.61	-0.01	-0.06	-0.11	0.23	0.45	-0.11
	8	107.00	0.01	110.10	-0.01	116.27	124.42	123.69	-0.41	0.23	123.91
	9	124.58	0.10	124.23	-0.06	124.42	232.38	225.57	-19.64	19.03	227.83
	10	123.49	0.06	123.34	-0.11	123.69	225.57	232.35	-19.06	19.72	227.81
	11	1.71	0.45	-0.47	0.23	-0.41	-19.64	-19.06	103.67	-24.00	-18.90
	12	2.58	0.23	2.46	0.45	0.23	19.03	19.72	-24.00	103.40	18.95
	13	123.87	0.11	123.63	-0.11	123.91	227.83	227.81	-18.90	18.95	230.09
		Damaged structure (element 14 damaged)									
Displacement sensors at nodes	4	56.35	0.01	54.20	0.00	53.54	62.63	62.07	0.53	1.40	62.27
	5	0.01	136.80	0.01	0.03	0.01	0.05	0.03	0.22	0.12	0.06
	6	54.20	0.01	55.81	0.00	55.08	62.42	61.97	-0.53	1.33	62.12
	7	0.00	0.03	0.00	136.80	0.00	-0.03	-0.05	0.11	0.22	-0.05
	8	53.54	0.01	55.08	0.00	58.17	62.55	62.18	-0.53	0.23	62.29
	9	62.63	0.05	62.42	-0.03	62.55	119.18	115.69	-12.70	10.52	116.87
	10	62.07	0.03	61.97	-0.05	62.18	115.69	119.00	-12.32	10.84	116.78
	11	0.53	0.22	-0.53	0.11	-0.53	-12.70	-12.32	54.60	-12.97	-12.29
	12	1.40	0.12	1.33	0.22	0.23	10.52	10.84	-12.97	52.04	10.47
	13	62.27	0.06	62.12	-0.05	62.29	116.87	116.78	-12.29	10.47	117.96
		Damaged structure (elements 7 & 14 damaged)									
Displacement sensors at nodes	4	56.35	0.01	54.20	0.00	53.54	62.63	62.08	0.53	1.40	62.27
	5	0.01	136.80	0.01	0.03	0.01	0.05	0.03	0.22	0.12	0.06
	6	54.20	0.01	55.81	0.00	55.08	62.42	61.97	-0.53	1.33	62.12
	7	0.00	0.03	0.00	136.81	0.00	-0.04	-0.06	0.11	0.25	-0.06
	8	53.54	0.01	55.08	0.00	58.17	62.56	62.18	-0.53	0.23	62.30
	9	62.63	0.05	62.42	-0.04	62.56	119.20	115.70	-12.69	10.48	116.89
	10	62.08	0.03	61.97	-0.06	62.18	115.70	119.01	-12.32	10.81	116.79
	11	0.53	0.22	-0.53	0.11	-0.53	-12.69	-12.32	54.60	-12.97	-12.29
	12	1.40	0.12	1.33	0.25	0.23	10.48	10.81	-12.97	52.12	10.42
	13	62.27	0.06	62.12	-0.06	62.30	116.89	116.79	-12.29	10.42	117.99

Table 2.5. Damage detection of 2-D warehouse structure - Intersection scheme (element 14 damaged)

		Set of sensors includes sensors at nodes	No. of *DLV*	*PDE*	Eliminated elements	*IDS*	*ne*
	ns =10	[4, 5, 6, 7, 8, 9, 10, 11, 12, 13]	9	[14, 17]		[14, 17]	2
k =*ns* -1=9	*i* =1	[5, 6, 7, 8, 9, 10, 11, 12, 13]	8	[14]	17	[14]	1
	i =2	[4, 5, 6, 7, 8, 9, 11, 12, 13]	8	[12, 14, 16]		[14]	1
	i =3	[4, 6, 7, 8, 9, 10, 11, 12, 13]	8	[4, 14]		[14]	1
	i =4	[4, 5, 7, 8, 9, 10, 11, 12, 13]	8	[1, 2, 7, 14, 20]		[14]	1
	i =5	[4, 5, 6, 8, 9, 10, 11, 12, 13]	8	[12, 14]		[14]	1
	i =6	[4, 5, 6, 7, 9, 10, 11, 12, 13]	8	[14, 16]		[14]	1
	i =7	[4, 5, 6, 7, 8, 10, 11, 12, 13]	8	[14]		[14]	1
	i =8	[4, 5, 6, 7, 8, 9, 10, 11, 12]	8	[12, 14, 16]		[14]	1
	i =9	[4, 5, 6, 7, 8, 9, 10, 12, 13]	8	[12, 14]		[14]	1
	i =10	[4, 5, 6, 7, 8, 9, 10, 11, 13]	8	[14, 17]		[14]	1

Table 2.6. Damage detection of 2-D warehouse structure - Intersection scheme (elements 7 & 14 damaged)

		Set of sensors includes sensors at nodes	No. of *DLV*	*PDE*	Eliminated elements	*IDS*	*ne*
	ns =10	[4, 5, 6, 7, 8, 9, 10, 11, 12, 13]	9	[1, 4, 7, 13, 14]		[1, 4, 7, 13, 14]	5
k =*ns* -1=9	*i* =1	[4, 5, 6, 7, 8, 9, 11, 12, 13]	8	[7, 12, 14]	1, 4, 13	[7,14]	2
	i =2	[4, 5, 6, 7, 8, 10, 11, 12, 13]	8	[1, 7, 13, 14, 17]		[7,14]	2
	i =3	[5, 6, 7, 8, 9, 10, 11, 12, 13]	8	[2, 7, 8, 14]		[7,14]	2
	i =4	[4, 6, 7, 8, 9, 10, 11, 12, 13]	8	[3, 7, 14		[7, 14]	2
	i =5	[4, 5, 7, 8, 9, 10, 11, 12, 13]	8	[2, 7, 8, 14]		[7, 14]	2
	i =6	[4, 5, 6, 8, 9, 10, 11, 12, 13]	8	[7, 14, 17]		[7, 14]	2
	i =7	[4, 5, 6, 7, 9, 10, 11, 12, 13]	8	[7, 13, 14, 17]		[7, 14]	2
	i =8	[4, 5, 6, 7, 8, 9, 10, 12, 13]	8	[3,7,12,14,19,21]		[7, 14]	2
	i =9	[4, 5, 6, 7, 8, 9, 10, 11, 13]	8	[7, 14]		[7, 14]	2
	i =10	[4, 5, 6, 7, 8, 9, 10, 11, 12]	8	[2,7,14,20]		[7, 14]	2

To demonstrate that two consecutive identical *IDS* is adequate to stop the iteration described in Section 2.6.1, the remaining 8 combinations resulting from omitting readings of one sensor at a time are considered and the identified *PDE* is listed in the lower portion of Table 2.5 for the case where element 14 is damaged. The *IDS* contains only element 14 for all cases, confirming the suitability of the proposed termination criterion. The same computation is performed for the case where elements

(7, 14) are damaged and yields the same conclusion as results shown in the lower portion of Table 2.6.

To investigate the effect of noise on the performance of the proposed methodology, the above examples are used and zero-mean white noise with *RMS* equals to 5% of the *RMS* of the simulated displacements is added to all simulated response displacements to generate contaminated data. From contaminated data, the method presented in Section 2.8 is employed to identify the unknown constant α, from which $\Delta\mathbf{U}$ is computed following Eq. (2.44). Performing *SVD* on $\Delta\mathbf{U}$ gives a set of 7 *DLV*s. Applying these *DLV*s onto the reference structural model as nodal force vectors, the *NCE* of all elements are computed and the first set of *PDE* comprising 6 elements (4, 6, 12, 13, 14, 17) is identified. These 6 elements are assigned as the current *IDS* (*ne* = 6). By omitting the readings of the sensor at node 4, which is not close to member of the current *IDS*, and employing the method in Section 2.8 on the remaining 9 sensor readings, $\Delta\mathbf{U}$ is computed, based on which *SVD* is performed to identify another set containing 5 *DLV*s. Applying these *DLV*s onto the reference structural model as nodal force vectors, the *NCE* of all elements are evaluated and the set of *PDE* which includes elements (1, 8, 10, 14) is identified. Taking the intersection between the set of *PDE* and the current *IDS* which contains elements (4, 6, 12, 13, 14, 17) gives element 14 as the new *IDS* (*ne* = 1). Similarly, by omitting the readings of the sensor at node 10 which is not close to the only member of the current *IDS* instead of the sensor at node 4, another set of *PDE* comprising elements (5, 14, 16) is identified. The intersection of the set of *PDE* and the current *IDS* which contains element 14 only produces element 14 as the new *IDS* (*ne* = 1). Since the *IDS* for the 2 consecutive steps are identical, the iteration is stopped, concluding that the actual damage is in element 14. The procedure is summarized in the upper portion of Table 2.7. Performing the same procedure for

the other 8 combinatorial sets of sensors by dropping one sensor record each time, the results in the lower portion of Table 2.7 confirm that only element 14 is damaged, reinforcing the criterion of 2 consecutive identical *IDS* to stop the iteration in Section 2.6.1. The same computation is performed for the case where elements (7, 14) are damaged and the results in Table 2.8 support the feasibility of the intersection scheme.

Table 2.7. Damage detection of 2-D warehouse structure - Intersection scheme (element 14 damaged, 5% noise)

		Set of sensors includes sensors at nodes	No. of *DLV*	*PDE*	Eliminated elements	*IDS*	*ne*
	ns=10	[4, 5, 6, 7, 8, 9, 10, 11, 12, 13]	7	[4, 6, 12, 13, 14, 17]		[4, 6, 12, 13, 14, 17]	6
$k = ns - 1 = 9$	i=1	[5, 6, 7, 8, 9, 10, 11, 12, 13]	5	[1,8,10,14]	4,6,12,13,17	[14]	1
	i=2	[4, 5, 6, 7, 8, 9, 11, 12, 13]	5	[5,14,16]		[14]	1
	i=3	[4, 6, 7, 8, 9, 10, 11, 12, 13]	5	[14]		[14]	1
	i=4	[4, 5, 7, 8, 9, 10, 11, 12, 13]	5	[7, 14]		[14]	1
	i=5	[4, 5, 6, 8, 9, 10, 11, 12, 13]	5	[5,6,14]		[14]	1
	i=6	[4, 5, 6, 7, 9, 10, 11, 12, 13]	5	[10,11,12,14,15]		[14]	1
	i=7	[4, 5, 6, 7, 8, 10, 11, 12, 13]	5	[1,8,9,14,16,21]		[14]	1
	i=8	[4, 5, 6, 7, 8, 9, 10, 11, 12]	5	[14,15,19,20]		[14]	1
	i=9	[4, 5, 6, 7, 8, 9, 10, 12, 13]	5	[14,18]		[14]	1
	i=10	[4, 5, 6, 7, 8, 9, 10, 11, 13]	5	[7,14]		[14]	1

Table 2.8. Damage detection of 2-D warehouse structure - Intersection scheme (elements 7 & 14 damaged, 5% noise)

		Set of sensors includes sensors at nodes	No. of *DLV*	*PDE*	Eliminated elements	*IDS*	*ne*
	ns=10	[4, 5, 6, 7, 8, 9, 10, 11, 12, 13]	9	[1,4,6,7,11,14,18,22]		[1,4,6,7,11,14,18,22]	8
$k=ns-1=9$	i=1	[4, 5, 6, 7, 8, 9, 11, 12, 13]	8	[2,5,7,12,14,15,16,21]	1,4,6,11,18,22	[7,14]	2
	i=2	[4, 5, 6, 7, 8, 10, 11, 12, 13]	8	[1,3,7,11,13,14,17]		[7,14]	2
	i=3	[5, 6, 7, 8, 9, 10, 11, 12, 13]	8	[2,4,7,13,14,15,16,19,20]		[7,14]	2
	i=4	[4, 6, 7, 8, 9, 10, 11, 12, 13]	8	[2,3,5,7,8,12,14,17,21]		[7, 14]	2
	i=5	[4, 5, 7, 8, 9, 10, 11, 12, 13]	8	[2,7,13,14]		[7, 14]	2
	i=6	[4, 5, 6, 8, 9, 10, 11, 12, 13]	8	[3,7,14,17,19,20,21,22]		[7, 14]	2
	i=7	[4, 5, 6, 7, 9, 10, 11, 12, 13]	8	[5,6,7,13,14,17]		[7, 14]	2
	i=8	[4, 5, 6, 7, 8, 9, 10, 12, 13]	8	[3,7,8,9,12,14,15,16,17,18,19,21]		[7, 14]	2
	i=9	[4, 5, 6, 7, 8, 9, 10, 11, 13]	8	[7, 8,14]		[7, 14]	2
	i=10	[4, 5, 6, 7, 8, 9, 10, 11, 12]	8	[5,7,9,12,13,14,15,16,20]		[7, 14]	2

***ii*) Two-stage analysis to identify actual damaged elements**

For the cases where the number of sensors used is much smaller than the number of structural *DOF*, the number of combinations needed in the intersection scheme before reliable result is realized may be astounding. In such cases, the two-stage

analysis can be employed where damaged regions are identified in the first step by examining the change in flexibility matrix and then to zoom in the damaged regions to identify damaged elements by using the *DLV* method in the second step. Performance of the two-stage analysis in identifying damaged elements is examined next.

Upon identifying α and $\Delta\mathbf{U}$, the damage region index vector ($\delta\mathbf{F}$) has not been computed following Eq. (2.26) yet. If set P_d = 1, one obtains P_u = 2, the flexibility matrices at the reference and the damaged states can be computed using Eqs. (2.38) - (2.39), based on which Eq. (2.26) can be employed to obtain $\delta\mathbf{F}$. In Fig. 2.4, the dash lines demarcate the regions "represented" by the corresponding displacement transducers. For example, the region for displacement transducer at node 11 is illustrated by the hatched area which includes elements (13, 14, 19, 20).

Case of One Damaged Element

For the case where element 14 is damaged, from the flexibility matrices with respect to the 10 sensor locations for both the reference and the damaged states, $\delta\mathbf{F}$ is computed and plotted in Fig. 2.11, where the maximum at a sensor location can be identified by examining the values for all the nearest sensors that encircle this location. For example at node 6, one has to compare its value against those at nodes (5, 7, 13), where it is obvious that its value is less than the value at node 13. On the other hand for node 11, its value is the largest compared to the values at its surrounding sensor nodes (5, 9, 13). The same procedure also yields the value at node 10 as the other local maximum. Hence, there are 2 possible damaged regions as represented by the regions corresponding to the 2 local maxima at nodes (10, 11). In the second step, performing *SVD* on the change in the flexibility matrix, a set of 9 *DLV*s is computed. Applying these *DLV*s onto the reference structure as nodal force vectors, the *NCE* of all elements can be computed and the set of *PDE* which comprises elements (12, 14) is identified as

shown in the upper portion of Table 2.9. Although the set of *PDE* comprises elements (12, 14), only element 14 falls within the possible damaged regions identified in the first step and is therefore taken as being damaged.

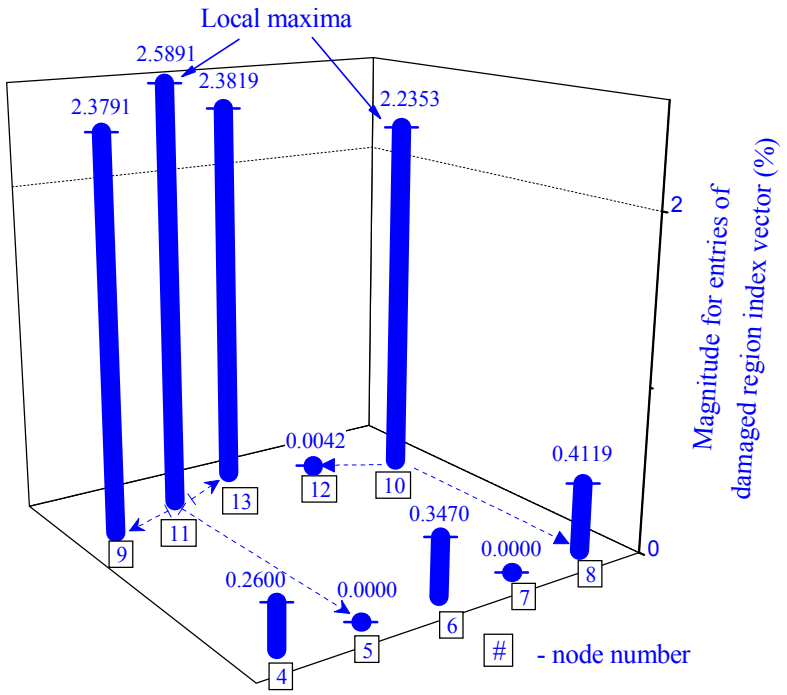

Fig. 2.11. Damage indices for 2-D warehouse structure (element 14 damaged)

Table 2.9. Damage detection of 2-D warehouse structure: Two-stage analysis scheme

		Damaged regions at nodes	Sensors at nodes	Potential damaged elements								
noise free	Element 14 damaged	10, 11	[4, 5, 6, 7, 8, 9, 10, 11, 12, 13]				12	14				
	Elements 7 & 14 damaged	8, 11	[4, 5, 6, 7, 8, 9, 10, 11, 12, 13]	1		7	12	14				
5% noise	Element 14 damaged	10, 11	[4, 5, 6, 7, 8, 9, 10, 11, 12, 13]		4			14		16	17	
	Elements 7 & 14 damaged	8, 11	[4, 5, 6, 7, 8, 9, 10, 11, 12, 13]	1	4	7	12	14	15	16	17	18

Case of Two Damaged Elements

Similarly, for the case where elements (7, 14) are damaged, from the identified flexibility matrices with respect to the 10 sensor locations, $\delta\mathbf{F}$ is computed and shown in Fig. 2.12. Following the same procedure with the case where element 14 is damaged, 2 local maxima are identified, indicating 2 possible damaged regions around nodes (8, 11). The *DLV* method is then applied on the flexibility matrices obtained, giving the set of *PDE* containing elements (1, 7, 12, 14) as shown in the upper portion of Table 2.9. Element 7 is associated with the sensor at node 8 and element 14 is associated with the sensor at node 11 whereas elements (1, 12) are not associated with the 2 probable damaged regions. Hence, the two-stage analysis is able to identify the correct damaged elements in an efficient manner.

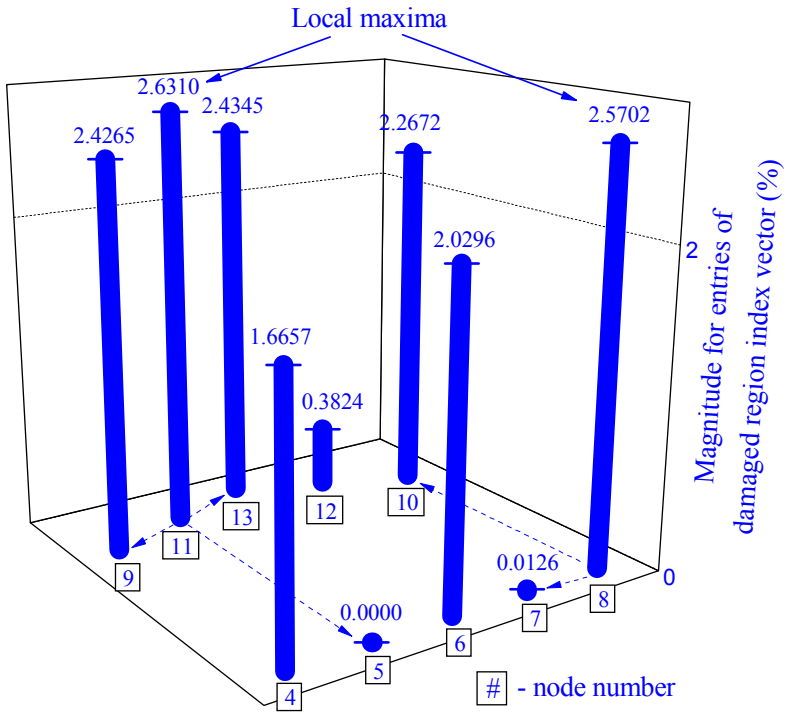

Fig. 2.12. Damage indices for 2-D warehouse structure (elements 7 & 14 damaged)

Case of Three Damaged Elements

The methodology is applicable for more than 2 damaged elements. The case where elements 7, 14 and 21 are damaged is illustrated. The computed $\delta\mathbf{F}$ values are plotted in Fig. 2.13 where 3 local maxima are observed at sensor nodes 8, 11 and 12. Applying the *DLV* method identifies correctly the 3 damaged elements.

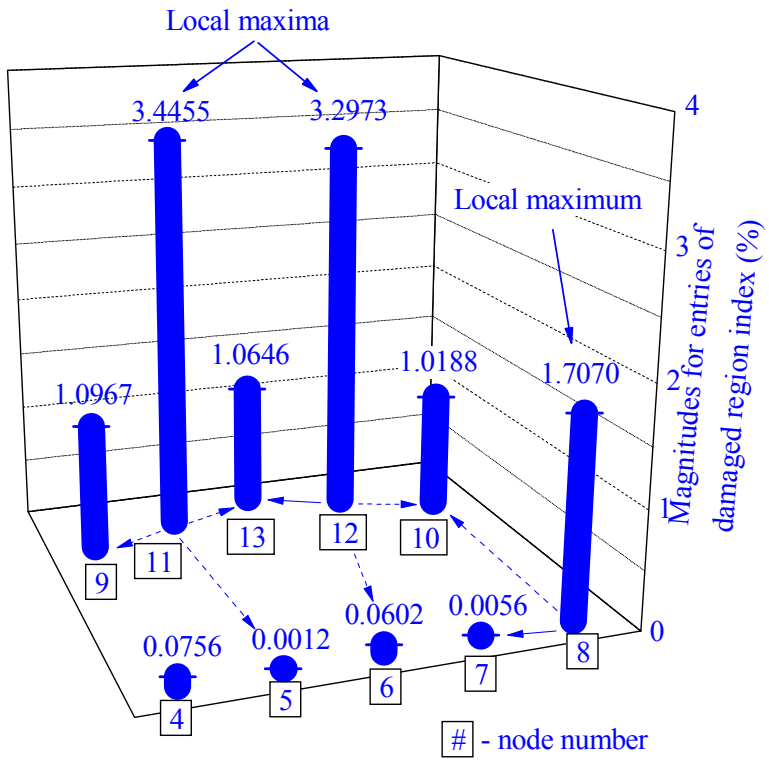

Fig. 2.13. Damage indices for 2-D warehouse structure (elements 7, 14 & 21 damaged)

Case of adjacent members damaged

Since damage is reflected by the local maxima in the two-stage analysis scheme, it may be suspected that the presence of two or more adjacent damaged elements may not be detected. In order to investigate this allegation, two cases of adjacent damaged elements will be investigated, namely (1) elements (14, 20) damaged; and (2) elements (12, 13, 19) damaged. For consistency with the previous cases, damage in element 14

is simulated by reducing 20% its axial stiffness (*EA*) all along the length of the element whereas damage in elements 12, 13, 19 and 20 is simulated by reducing 20% of their flexural stiffnesses (*EI*) within the whole length of the elements.

For case (1) where elements (14, 20) are damaged, from the flexibility matrices with respect to the 10 sensor locations for both the reference and the damaged states, $\delta\boldsymbol{F}$ is computed and plotted in Fig. 2.14 where a local maximum at node 11 is observed. Performing the *DLV* method in the second step of the two-stage analysis scheme gives elements (2, 14, 20) as the set of *PDE* which is shown in the upper portion of Table 2.10. However, only elements (14, 20) are classified as damaged since they fall within the identified damaged region is the first step. Similarly, the adjacent damaged elements in case (2) can also be identified correctly using the two-stage analysis scheme as results shown in Fig. 2.15 and the lower portion of Table 2.10.

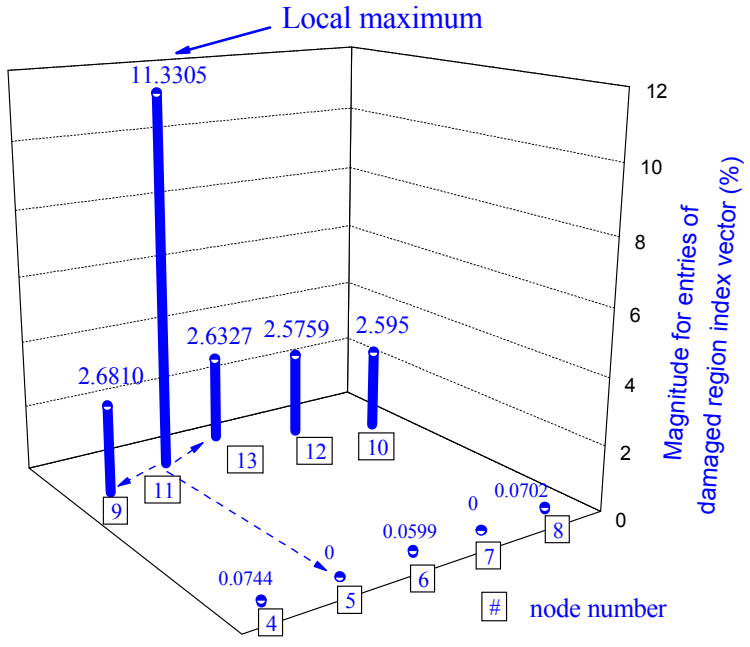

Fig. 2.14. Damage indices for 2-D warehouse structure (elements 14 & 20 damaged)

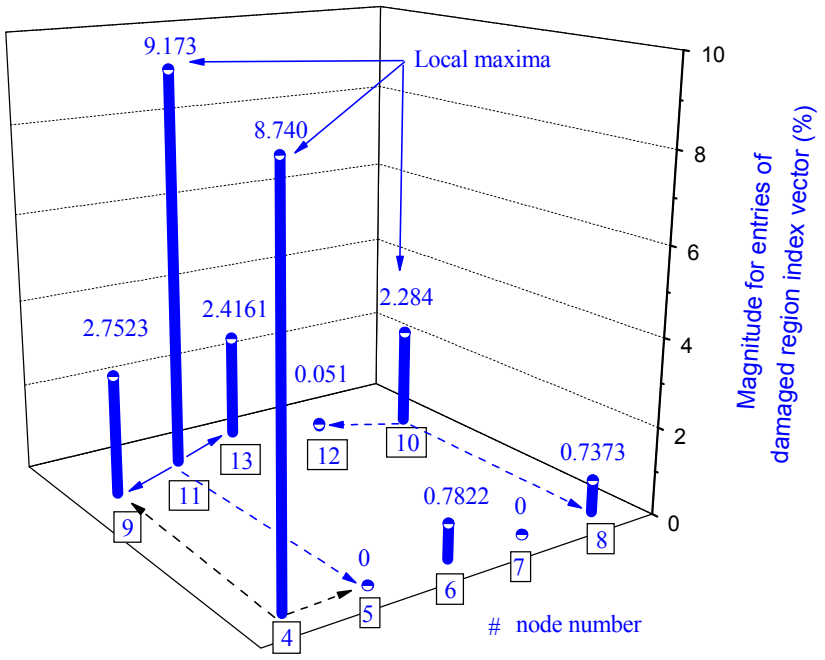

Fig. 2.15 Damage indices for 2-D warehouse structure (elements 12, 13&19 damaged)

Table 2.10. Damage detection of 2-D warehouse structure: Two-stage analysis scheme

	Damaged regions at nodes	Sensors at nodes	Potential damaged elements					
Elements (14, 20) damaged	11	[4, 5, 6, 7, 8, 9, 10, 11, 12, 13]	2			14		20
Elements (12, 13, 19) damaged	4, 10, 11	[4, 5, 6, 7, 8, 9, 10, 11, 12, 13]		12	13		19	

Damage Identification with Noisy Data

The above analysis assumes that the data captured is free of noise. In the case of noisy data, the threshold below which damaged regions may be wrongly identified has to be set, and the maximum error beyond which the *DLV* method is no longer robust needs to be estimated. For the case where element 14 is damaged with 20% reduction in axial stiffness, the simulated displacements at the 10 sensor locations are contaminated with zero-mean white noise for both the reference and the damaged

states. The procedure presented in Section 2.8 is performed to estimate α, from which the change in displacement matrix is computed and the set of *DLV*s identified. Different cases of *RMS* value of the noise are studied, from 1% to 30% at intervals of 0.5%. Applying the *DLV*s onto the reference structural model as nodal force vectors, the *NCE* of all elements are computed and the set of *PDE* identified. It is observed that when the error exceeds 8.5%, element 14 is excluded from the set of *PDE*, leading to erroneous conclusion. Performing the same procedure for the single damaged element cases (each prescribed with 20% reduction in axial stiffness or flexural stiffness corresponding to truss or frame element to simulate damage) for all elements of the 2-D warehouse structure, the results in Fig. 2.16 indicate a threshold of 8.5% for reliable detection.

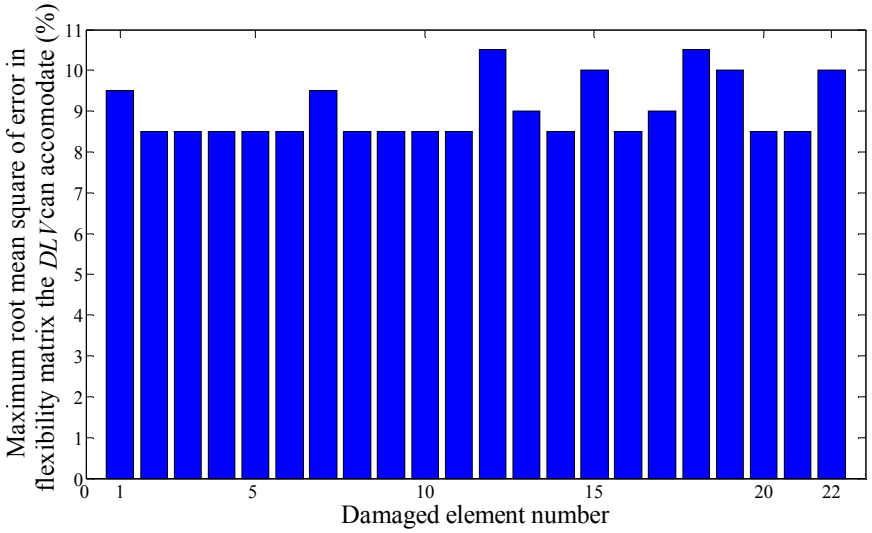

Fig. 2.16. Thresholds for error in flexibility matrix below which the *DLV* method can accommodate for various single damaged elements (2-D warehouse structure)

For the case where the structure is healthy, adding zero-mean white noise with *RMS* equal to 8.5% of the *RMS* of the flexibility matrices at both the reference and the damaged states to simulate contaminated flexibility matrices, non-zero entries in $\delta\mathbf{F}$

can be computed and the maximum is recorded. The procedure is repeated 30 times and the mean maximum value of 0.023 is observed with standard deviation of 0.017. Hence, if a local maximum of $\delta\mathbf{F}$ is greater than 0.023 (or 0.006 if one standard deviation below the mean is advocated instead), then one may suspect that there is damage within the region associated with this local maximum.

To investigate the feasibility of the two-stage analysis under noisy data, zero-mean white noise with *RMS* equal to 5% of the *RMS* of the simulated displacements is added to all simulated displacements to generate contaminated data. The procedure presented in Section 2.8 is used to identify α. By setting $P_d = 1$, the flexibility matrices at the reference and the damaged states can be computed using Eqs. (2.38), (2.39) and (2.42). For the case where element 14 is damaged, the values of $\delta\mathbf{F}$ are computed and plotted in Fig. 2.17. The same 2 possible damaged regions are identified, namely corresponding to the sensors at nodes (10, 11), which agree with the case without noise in Fig. 2.11. With noise, the local maximum at node 11 becomes less distinctive. From the identified flexibility matrices at the reference and the damaged states, the *DLV* method is applied, giving a set of *PDE* which comprises elements (4, 14, 16, 17) as shown in the lower portion of Table 2.9. Of the 4 elements identified in the set of *PDE*, only element 14 falls within the probable damaged regions identified in the previous step and is therefore classified as damaged. Comparing with the results where there is no noise, the set of *PDE* is larger. If the noise level added is 10% instead of 5%, the 2 damaged regions identified will be those corresponding to nodes (9, 10) instead of nodes (10, 11). Applying the *DLV* method in the second step yields incorrect results. Hence, it is essential to establish the tolerable noise level associated with the damage identification method used.

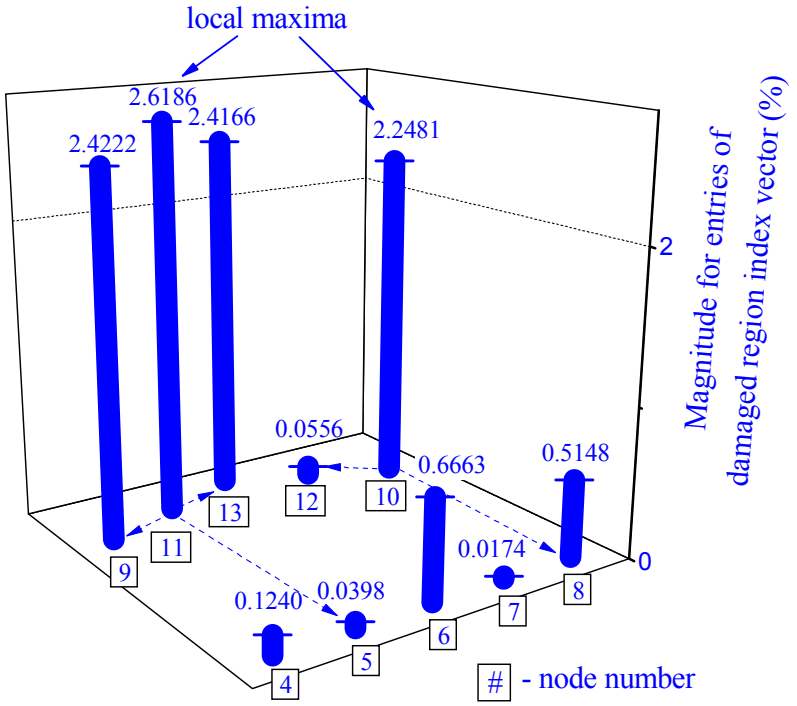

Fig. 2.17. Damage indices for 2-D warehouse structure (element 14 damaged, 5% noise)

For the case where elements (7, 14) are damaged and 5% noise is added, the same 2 local maxima at nodes (8, 11) are identified with node 11 being less distinctive than that for the case without noise, as shown in Fig. 2.18. Based on the contaminated flexibility matrices, the *DLV* method produces 9 *PDE*, namely (1, 4, 7, 12, 14, 15, 16, 17, 18) as shown in the lower portion of Table 2.9. The size of *PDE* set has increased from 4 for the case without noise to 9. Nevertheless, intersecting the set of *PDE* with the elements in the identified damaged regions gives elements (7, 14) as damaged. If the noise level is increased to 10% (beyond the 8.5% robustness limit discussed earlier), node 11 is no longer classified as associated with a damaged region, leading to inaccurate damage detection results.

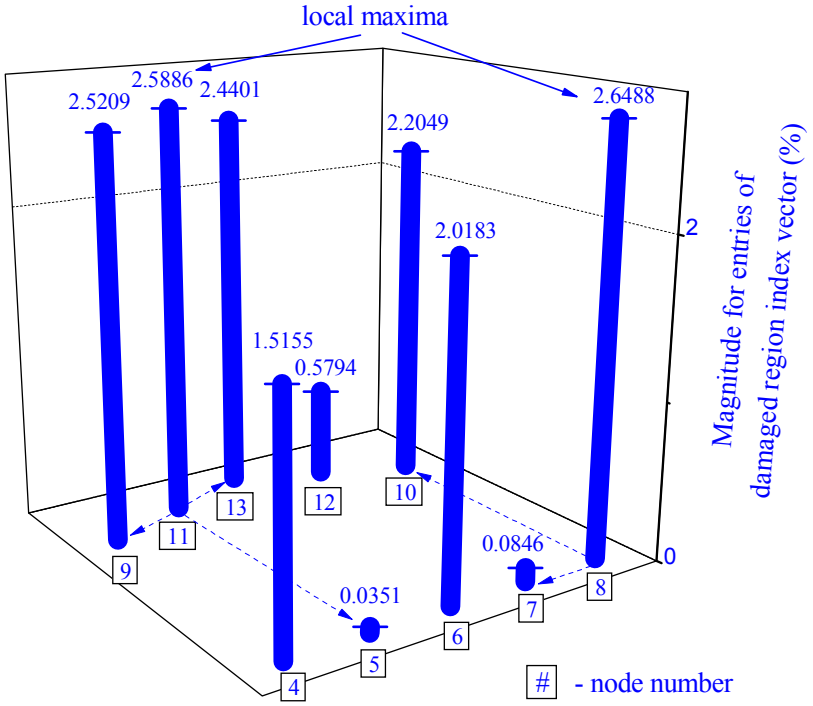

Fig. 2.18. Damage indices for 2-D warehouse structure (elements 7 & 14 damaged, 5% noise)

***iii*) Assessing damage severity**

After the damaged elements are identified, the damage severity can be assessed using the procedure presented in Section 2.7. For the case where element 14 is damaged, only one variable needs to be estimated, that is the axial stiffness of element 14. Starting from the axial stiffness of element 14 at the reference state $(EA)_{14} = 4.26 \times 10^7$ (N), the algorithm needed 5 iterations before Eq. (2.37) is satisfied with $Tol = 10^{-2}$ as shown in Fig. 2.19a. The identified stiffness of element 14 is $(EA)_{14} = 3.46 \times 10^7$ (N) compared to the exact value of 3.44×10^7 (N), which is less than 1% difference. In this case, the second equation of Eq. (2.37) governs. If the algorithm is continued, the variable monotonically approaches the exact value though the relationship between the number of iterations and the identified error is not linear. For example, at iteration 12^{th}, the difference between the identified and the exact axial stiffness of element 14 is 0.21%; that is, $(EA)_{14} = 3.45 \times 10^7$ (N).

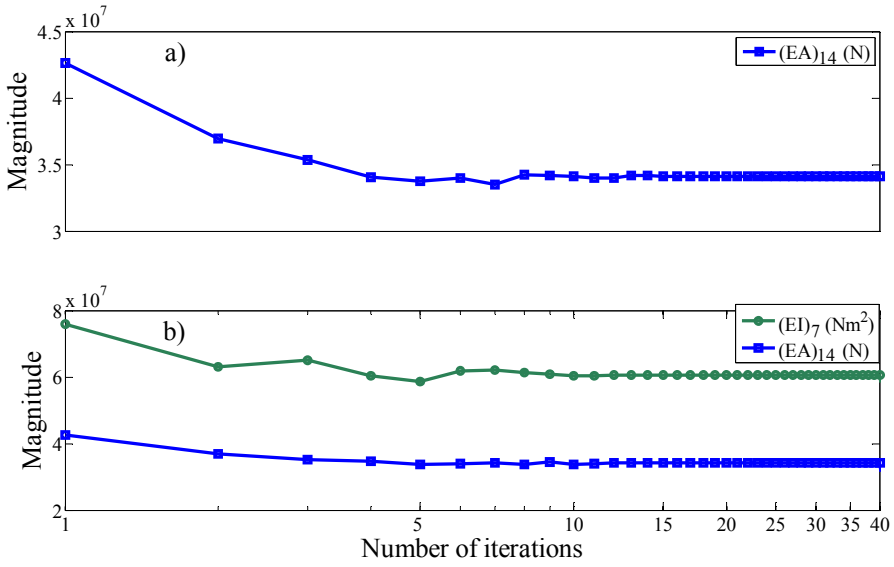

Fig. 2.19. Relationship between estimated element stiffnesses and number of iterations: (a) element 14 damaged; and (b) elements 7 & 14 damaged

For the case where elements (7, 14) are damaged, the unknowns to be estimated include the flexural stiffness of element 7 and the axial stiffness of element 14. Applying the procedure presented in Section 2.7 with the values of the stiffnesses of the damaged elements at the reference state as initial guess, the results obtained are plotted in Fig. 2.19b. If the tolerance of 10^{-2} is used to stop the iteration in Eq. (2.37), 6 iterations are required. The identified stiffnesses of elements (7, 14) are $(EI)_{14} = 6.12 \times 10^7$ (Nm^2) and $(EA)_{14} = 3.46 \times 10^7$ (N) compared to the exact values of 3.44×10^7 (N) and 6.07×10^7 (Nm^2), respectively, resulting in less than 1% difference. If the algorithm is continued, the stiffnesses of the damaged element approach the exact values monotonically, illustrating the stability of the procedure.

The feasibility of the procedure is confirmed for the case where simulated displacements are contaminated with 5% noise based on the results shown in Fig. 2.20. With noise, it took the procedure more iterations to achieve the same pre-defined threshold value of 10^{-2} in Eq. (2.37). For example, for the case where element 14 is

damaged, 15 iterations are required whereas 13 iterations are required for the case where elements (7, 14) are damaged. Nevertheless, the procedure still provides reasonable results with the stiffnesses of the damaged elements monotonically approaching the exact values.

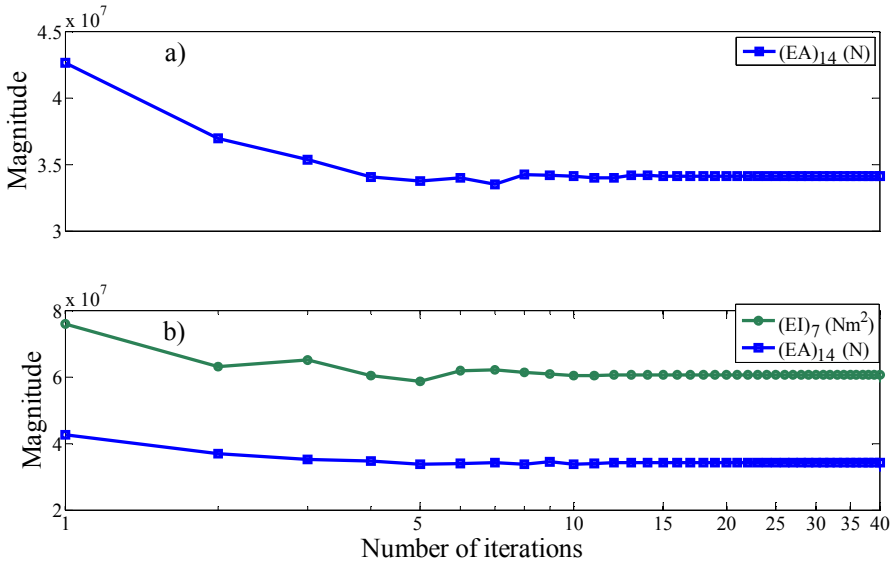

Fig. 2.20. Relationship between estimated element stiffnesses and number of iterations with 5% noise: (a) element 14 damaged; and (b) elements 7 & 14 damaged

2.9.2 Experimental illustration

The 3-D modular truss structure used in Section 2.6.2 is set up experimentally as shown in Fig. 2.21 to investigate the performance of the proposed methodologies. The geometries and mechanical properties of truss members are listed in Table 2.2. Two static loads are utilized to excite the truss at the reference (Fig. 2.21b) and the damaged (Fig. 2.21c) states. Thirteen 10 mm displacement transducers (model CDP) and a data logger (model TDS-303) are employed to monitor the vertical displacements of all nodes at the lower chords of the truss. Two cases of damage are investigated, namely (a) element 86 is damaged; and (b) elements (1, 86) are damaged. Damage is simulated

by changing the affected members from steel ($EA = 4.26 \times 10^7$ N) to aluminum ($EA = 4.51 \times 10^6$ N) tubes (see Table 2.2 for the specifications of the tubes).

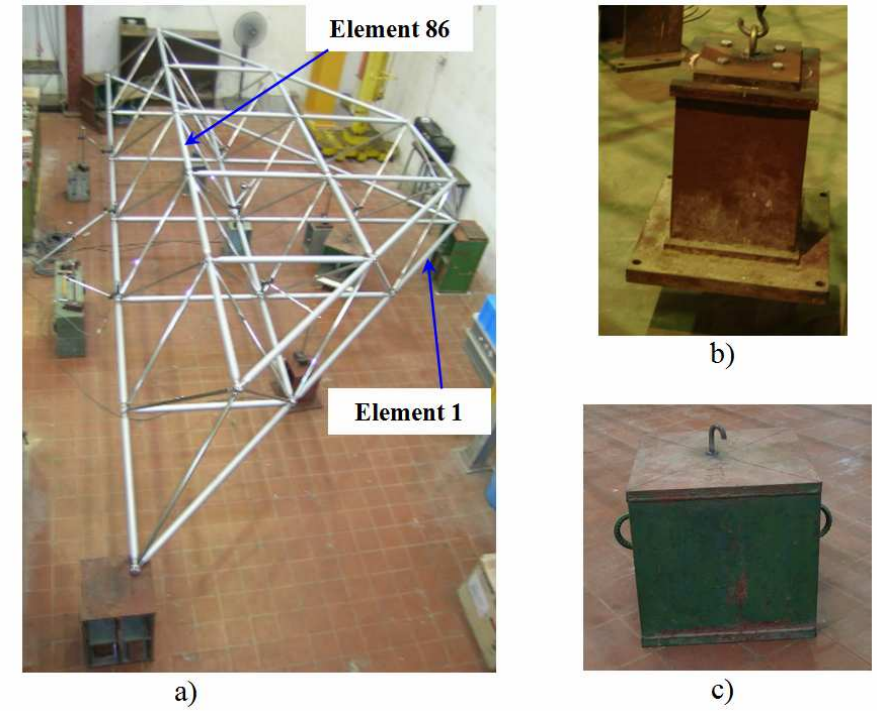

Fig. 2.21. Experimental set-up: a) 3-D modular truss structure; b) static load at reference state; and c) static load at damaged state

Shifting the static loads through all nodes at the lower chord of the truss, the displacements are measured and shown in Table 2. 11, based on which displacement matrices at the reference and the damaged states are formulated. Since the accuracy of the displacement transducer – data logger system is 10^{-3} mm, values in Table 2. 11 have the accuracy of 10^{-3} mm. Besides, positive displacement is associated with downward displacement of a node. Under the application of the static load at some nodes, few nodes move upward, resulting in the presence of negative values in Table 2. 11. Following the procedure presented in Section 2.8, α is estimated as 0.75. Applying *SVD* on $\mathbf{U}_\Delta$ which is computed using Eq. (2.44), the set of *DLV*s is identified.

Table 2. 11. Measured displacements for experimental truss (mm)

		Static load at node												
		2	3	4	5	6	7	8	9	11	12	13	14	15
		Reference structure												
Displacement transducers at nodes	2	2.061	0.637	-0.140	1.161	1.057	0.699	0.296	-0.044	0.409	0.370	0.660	0.743	0.349
	3	0.637	1.062	0.637	0.458	0.651	0.743	0.651	0.458	0.418	0.629	0.719	0.629	0.418
	4	-0.140	0.637	2.061	-0.044	0.296	0.699	1.057	1.161	0.349	0.743	0.660	0.370	0.409
	5	1.161	0.458	-0.044	2.116	1.195	0.691	0.289	-0.109	0.872	0.997	0.849	0.663	0.400
	6	1.057	0.651	0.296	1.195	1.733	1.095	0.691	0.289	1.060	1.475	1.423	1.085	0.646
	7	0.699	0.743	0.699	0.691	1.095	1.673	1.095	0.691	0.883	1.423	1.681	1.423	0.883
	8	0.296	0.651	1.057	0.289	0.691	1.095	1.733	1.195	0.646	1.085	1.423	1.475	1.060
	9	-0.044	0.458	1.161	-0.109	0.289	0.691	1.195	2.116	0.400	0.663	0.849	0.997	0.872
	10	0.409	0.418	0.349	0.872	1.060	0.883	0.646	0.400	2.659	1.799	1.332	0.906	0.484
	12	0.370	0.629	0.743	0.997	1.475	1.423	1.085	0.663	1.799	3.553	2.216	1.389	0.906
	13	0.660	0.719	0.660	0.849	1.423	1.681	1.423	0.849	1.332	2.216	3.551	2.216	1.332
	14	0.743	0.629	0.370	0.663	1.085	1.423	1.475	0.997	0.906	1.389	2.216	3.553	1.799
	15	0.349	0.418	0.409	0.400	0.646	0.883	1.060	0.872	0.484	0.906	1.332	1.799	2.659
		Damaged structure (element 86 damaged)												
Displacement transducers at nodes	2	2.781	0.892	-0.154	1.557	1.481	1.055	0.466	-0.049	0.605	0.607	1.086	1.105	0.524
	3	0.892	1.472	0.892	0.623	0.962	1.152	0.962	0.623	0.634	0.988	1.228	0.988	0.634
	4	-0.154	0.892	2.781	-0.049	0.466	1.055	1.481	1.557	0.524	1.105	1.086	0.607	0.605
	5	1.557	0.623	-0.049	2.824	1.614	0.957	0.407	-0.142	1.180	1.363	1.192	0.917	0.550
	6	1.481	0.962	0.466	1.614	2.468	1.729	1.079	0.407	1.542	2.215	2.347	1.696	0.989
	7	1.055	1.152	1.055	0.957	1.729	2.691	1.729	0.957	1.398	2.322	3.010	2.322	1.398
	8	0.466	0.962	1.481	0.407	1.079	1.729	2.468	1.614	0.989	1.696	2.347	2.215	1.542
	9	-0.049	0.623	1.557	-0.142	0.407	0.957	1.614	2.824	0.550	0.917	1.192	1.363	1.180
	10	0.605	0.634	0.524	1.180	1.542	1.398	0.989	0.550	3.651	2.602	2.143	1.411	0.750
	12	0.607	0.988	1.105	1.363	2.215	2.322	1.696	0.917	2.602	5.130	3.664	2.245	1.411
	13	1.086	1.228	1.086	1.192	2.347	3.010	2.347	1.192	2.143	3.664	6.016	3.664	2.143
	14	1.105	0.988	0.607	0.917	1.696	2.322	2.215	1.363	1.411	2.245	3.664	5.130	2.602
	15	0.524	0.634	0.605	0.550	0.989	1.398	1.542	1.180	0.750	1.411	2.143	2.602	3.651
		Damaged structure (elements 1 & 86 damaged)												
Displacement transducers at nodes	2	2.781	0.893	-0.152	1.554	1.480	1.055	0.467	-0.048	0.602	0.603	1.086	1.104	0.523
	3	0.893	1.474	0.896	0.615	0.958	1.152	0.964	0.625	0.627	0.977	1.228	0.985	0.633
	4	-0.152	0.896	2.787	-0.063	0.459	1.054	1.484	1.562	0.512	1.086	1.087	0.603	0.603
	5	1.554	0.615	-0.063	2.853	1.629	0.958	0.401	-0.152	1.204	1.402	1.190	0.927	0.554
	6	1.480	0.958	0.459	1.629	2.476	1.730	1.076	0.401	1.555	2.235	2.346	1.701	0.992
	7	1.055	1.152	1.054	0.958	1.730	2.691	1.729	0.957	1.399	2.323	3.010	2.322	1.398
	8	0.467	0.964	1.484	0.401	1.076	1.729	2.469	1.616	0.985	1.689	2.347	2.213	1.541
	9	-0.048	0.625	1.562	-0.152	0.401	0.957	1.616	2.827	0.542	0.904	1.193	1.360	1.179
	10	0.602	0.627	0.512	1.204	1.555	1.399	0.985	0.542	3.671	2.635	2.142	1.419	0.754
	12	0.603	0.977	1.086	1.402	2.235	2.323	1.689	0.904	2.635	5.183	3.662	2.258	1.417
	13	1.086	1.228	1.087	1.190	2.346	3.010	2.347	1.193	2.142	3.662	6.016	3.663	2.143
	14	1.104	0.985	0.603	0.927	1.701	2.322	2.213	1.360	1.419	2.258	3.663	5.133	2.603
	15	0.523	0.633	0.603	0.554	0.992	1.398	1.541	1.179	0.754	1.417	2.143	2.603	3.651

***i*) Intersection scheme to identify actual damaged elements**

Using 13 sensors

For the case where element 86 is damaged, applying the set of *DLV*s onto the reference structural model as nodal force vectors at sensor locations, the *NCE* of all

elements are computed and the set of *PDE* which comprises elements (4, 9, 56, 86) is identified. The current *IDS* therefore contains elements (4, 9, 56, 86) and *ne* = 4. By omitting the readings of the sensor at node 15 which is far away from the members of the current *IDS* set, the readings of the remaining 12 sensors are used to formulate the displacement matrices at the reference and the damaged structures. Performing *SVD* on $\mathbf{U}_{\Delta}$, a set of *DLV*s is identified and when applying onto the reference structural model as nodal force vectors yields a set of *PDE* comprising elements (20, 55, 73, 75, 81, 86). Intersecting the set of *PDE* and the current *IDS* which contains elements (4, 9, 56, 86) gives the new *IDS* with element 86 as the only member (*ne* = 1). Similarly, by omitting the readings of the sensor at node 9 which is far away from the members of the current *IDS* set instead of the sensor at node 15, another set of *PDE* comprising elements (41, 45, 86) is identified. Intersecting the set of *PDE* and the current *IDS* which contains element 86 only gives element 86 as the new *IDS* (*ne* = 1). Since the *IDS* for 2 consecutive steps are identical, the iteration is terminated, confirming that the actual damage is in element 86. The procedure is summarized in the upper portion of Table 2.12. Similarly, for the case where elements (1, 86) are damaged, the feasibility of the intersection scheme is illustrated by the results summarized in the lower portion of Table 2.12.

Table 2.12. Damage detection of experimental truss structure - Intersection scheme (13 sensors used)

	Set No.			Set of sensors includes sensors at nodes	No. of *DLV*	*PDE*	Eliminated elements	*IDS*	*ne*
Element 86 damaged	1		*ns* =13	[2,3,4,5,6,7,8,9,11, 12,13,14,15]	10	[4,9,56,86]		[4,9, 56,86]	4
	2	*k*=*ns* -1=12	*i* =1	[2,3,4,5,6,7,8,9,11, 12,13,14]	9	[20,55,73,75, 81,86]	4,9,56	[86]	1
	3		*i* =2	[2,3,4,5,6,7,8,11, 12,13,14,15]	9	[41,45,86]		[86]	1
Elements 1 & 86 damaged	1		*ns* =13	[2,3,4,5,6,7,8,9,11, 12,13,14,15]	9	[1,56,61,70]		[1,56,61, 70,86]	5
	2	*k*=*ns* -1=12	*i* =1	[2,3,4,5,6,7,8,9,11, 12,13,14]	8	[1,20,44,55, 58,86]	56,61	[1,86]	2
	3		*i* =2	[2,3,4,5,6,7,8,11, 12,13,14,15]	8	[1,21,70,86]		[1,86]	2

Using 7 sensors

If only 7 displacement transducers are available and are placed at nodes (3, 6, 7, 8, 12, 13, 14) (see Fig. 2.8c), the intersection scheme is still applicable. For the case where element 86 is damaged, from measured displacements by the 7 sensors, the procedure presented in Section 2.8 is employed to estimate $\alpha = 0.75$. Performing *SVD* on $\mathbf{U}_\Delta$, which is computed using Eq. (2.44), the set of *DLV*s is identified. By applying these *DLV*s onto the reference structural model as nodal force vectors at the sensor locations, the *NCE* of all elements are computed and the set of *PDE* which comprises elements (16, 20, 37, 42, 50, 86) is identified. The current *IDS* therefore contains elements (16, 20, 37, 42, 50, 86) and *ne* = 6. By omitting readings of the sensor at node 8 which is far away from the members of the current *IDS*, the readings of the remaining 6 sensors are used to compute $\mathbf{U}_\Delta$ in Eq. (2.44). Performing *SVD* on $\mathbf{U}_\Delta$, a set of *DLV*s is identified and applied onto the reference structure yields elements (17, 19, 20, 21, 22, 27, 29, 86) as the set of *PDE*. Intersecting the *PDE* with the current *IDS* which includes elements (16, 20, 37, 42, 50, 86) produces elements (20, 86) as the new *IDS* (*ne* = 2). Similarly, by omitting the readings of sensor at node 6, which is far away

from elements (20, 86) in the current *IDS*, instead of the sensor at node 8, another set of *PDE* comprising elements (16, 17, 31, 86) is identified. Taking the intersection between the set of *PDE* and the current *IDS* which comprises elements (20, 86) gives the new *IDS* with element 86 as the only member (*ne* = 1). By omitting the readings of the sensor at node 3, which is far away from element 86 of the current *IDS* set, instead of the sensor at node 6, another set of *PDE* which comprises elements (21, 77, 86) is identified. Intersecting the *PDE* with the current *IDS* which comprises element 86 produces element 86 as the new *IDS* (*ne* = 1). Since the *IDS* for 2 consecutive steps are identical, the iteration is taken as completed, identifying correctly element 86 as being damaged. The whole procedure is summarized in the upper portion of Table 2.13. Similarly for the case where elements (1, 86) are damaged and 7 sensors are used, the feasibility of the intersection scheme is reinforced by the results summarized in the lower portion of Table 2.13. It is observed that with fewer sensors used, more combinations of sensors are required before the damaged elements can be identified following the intersection scheme.

Table 2.13. Damage detection of experimental truss - Intersection scheme (7 sensors used)

	Set No.			Set of sensors includes sensors at nodes	No. of *DLV*	*PDE*	Eliminated elements	*IDS*	*ne*
Element 86 damaged	1		*ns* =7	[3,6,7,8,12,13,14]	4	[16,20,37, 42,50,86]		[16,20,37, 42,50,86	4
	2	*k* =*ns* - 1=6	*i* =1	[3,6,7,12,13,14]	3	[17,19,20,21, 22,27,29,86]	16,37,42,50	[20,86]	2
	3		*i* =2	[3,7,8,12,13,14]	3	[16,17,31,86]	20	[86]	1
	4		*i* =3	[6,7,8,12,13,14]	3	[21,77,86]		[86]	1
Elements 1 & 86 damaged	1		*ns* =7	[3,6,7,8,12,13,14]	4	[1,16,20, 66, 77,86]		[1,16,20, 66,77,86]	7
	2	*k* =*ns* - 1=6	*i* =1	[3,6,7,12,13,14]	3	[1,16,17,59, 60,84,86]	20,66,77	[1,16,86]	3
	3		*i* =2	[3,7,8,12,13,14]	3	[1,18,19,20, 53,82,86]	16	[1,86]	2
	4		*i* =3	[6,7,8,12,13,14]	3	[1,20,37,86]		[1,86]	2

***ii*) Two-stage analysis to identify actual damaged elements**

To mitigate the combining sensors process in the intersection scheme which is especially formidable for the cases where the number of sensors is small compared to the structural *DOF*, the two-stage analysis can be employed. Performance of the two-stage analysis with measured displacement data is investigated in this section for two cases, namely 13 and 7 sensors are used.

Similar to the numerical example, by setting $P_d = 1$, one obtains $P_u = 0.75$. The flexibility matrices at the reference and the damaged structures can be computed using Eqs. (2.38) - (2.39).

Using 13 Sensors with Element 86 Damaged

For case (a) where element 86 is damaged, $\delta\mathbf{F}$ is computed and plotted in Fig. 2.22. It can be observed that the value at node 13 is the maximum compared to those at nodes (7, 12, 14), indicating the possibility of damage in the region defined by the sensor at node 13. Applying the *DLV* procedure, the set of *PDE* identified contains 4 elements (4, 9, 56, 86) as shown in the upper portion of Table 2.14. Since only element 86 is associated with the identified possible damaged region, it is assessed as damaged.

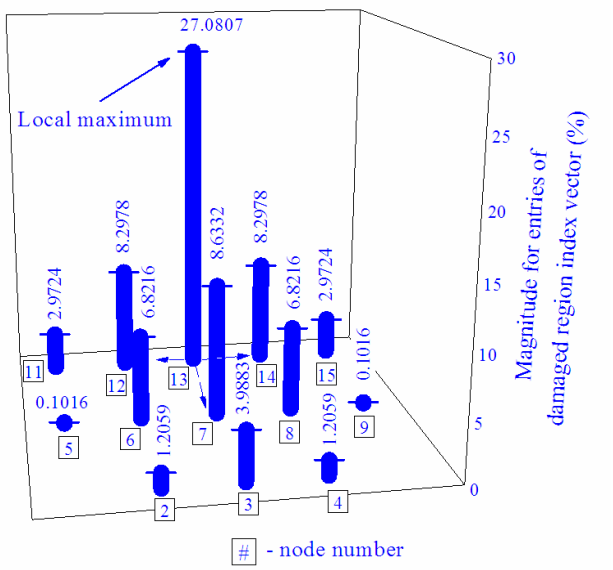

Fig. 2.22. Damage indices for 3-D modular truss structure (element 86 damaged, 13 sensors used)

Table 2.14. Damage detection of experimental truss: Two-stage analysis scheme

		Damaged regions at nodes	Sensors at nodes	Potential damaged elements
13 sensors used	Element 86 damaged	13	[2, 3, 4, 5, 6, 7, 8, 9, 11, 12, 13, 14, 15]	4 9 56 86
	Elements 1 & 86 damaged	2, 13	[2, 3, 4, 5, 6, 7, 8, 9, 11, 12, 13, 14, 15]	1 12 22 27 86
7 sensors used	Element 86 damaged	13	[3, 6, 7, 8, 12, 13, 14]	16 20 37 42 50 86
	Elements 1 & 86 damaged	3, 13	[3, 6, 7, 8, 12, 13, 14]	1 16 20 66 77 86

Using 13 Sensors with Elements (1, 86) Damaged

Similarly for case (b) where elements (1, 86) are damaged, the values of $\delta\mathbf{F}$ are plotted in Fig. 2.23, which shows 2 local maxima at entries corresponding to sensors at nodes (2, 13), indicating 2 possible damaged regions. Performing the *DLV* method in the second stage analysis yields elements (1, 12, 22, 27, 48, 78, 86) in the identified set of *PDE* as shown in the upper portion of Table 2.14. However, only elements (1, 86) are classified as being damaged since they fall within the damaged regions identified in the first stage, which matches the actual situation.

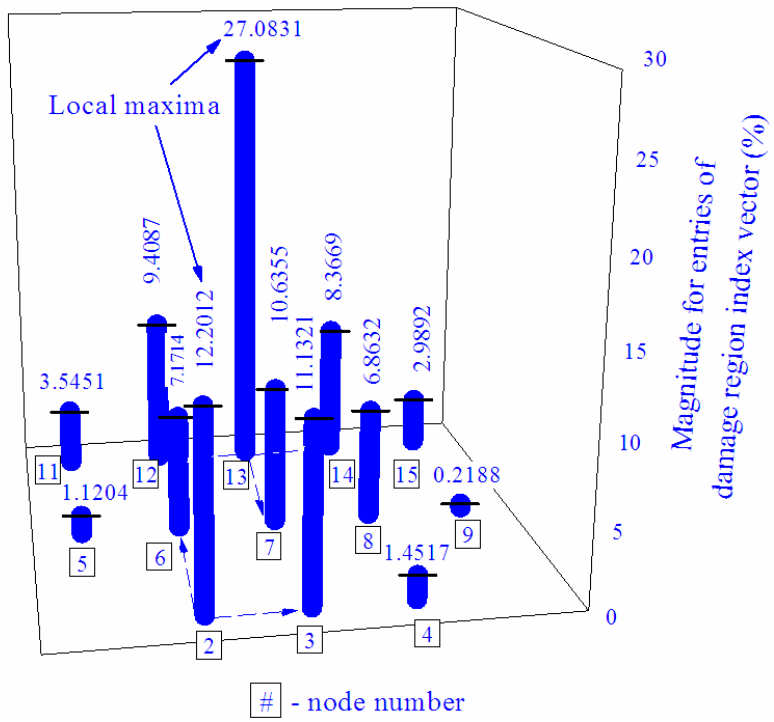

Fig. 2.23. Damage indices for 3-D modular truss structure (elements 1 & 86 damaged, 13 sensors used)

Using 7 Sensors with Element 86 Damaged

If only 7 displacement transducers are available and are placed at nodes (3, 6, 7, 8, 12, 13, 14) (see Fig. 2.8c), the two-stage analysis scheme still works. For the case where element 86 is damaged, the values of $\delta\mathbf{F}$ are plotted in Fig. 2.24, where the region associated with sensor at node 13 is identified as possibly damaged. Employing the *DLV* method in the second stage analysis, the set of *PDE* comprising elements (16, 20, 37, 42, 56, 86) is obtained as shown in the lower portion of Table 2.14. Of the 6 elements identified, only element 86 is associated with the posible damaged region and hence classified as being damaged. Although the number of elements in the *PDE* increases with fewer sensors used, the method is still able to identify the damaged element correctly.

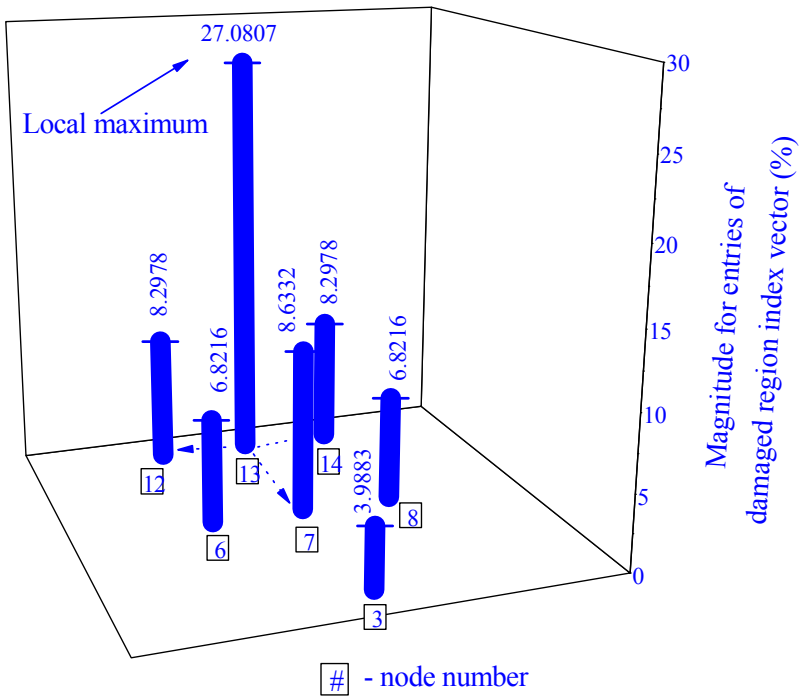

Fig. 2.24. Damage indices for 3-D modular truss structure (element 86 damaged, 7 sensors used)

Using 7 Sensors with Elements (1, 86) Damaged

Similarly, for the case where elements (1, 86) are damaged, results plotted in Fig. 2.25 show that the regions defined by the sensors at nodes (3, 13) are potentially damaged. The *DLV* analysis yields a set of *PDE* comprising elements (1, 16, 20, 66, 77, 86) as shown in the lower portion of Table 2.14. However, only elements (1, 86) fall within the identified damaged regions and are hence classified as being damaged. Again, the size of *PDE* set increases as the number of sensors used decreases, while the method still yields reliable results.

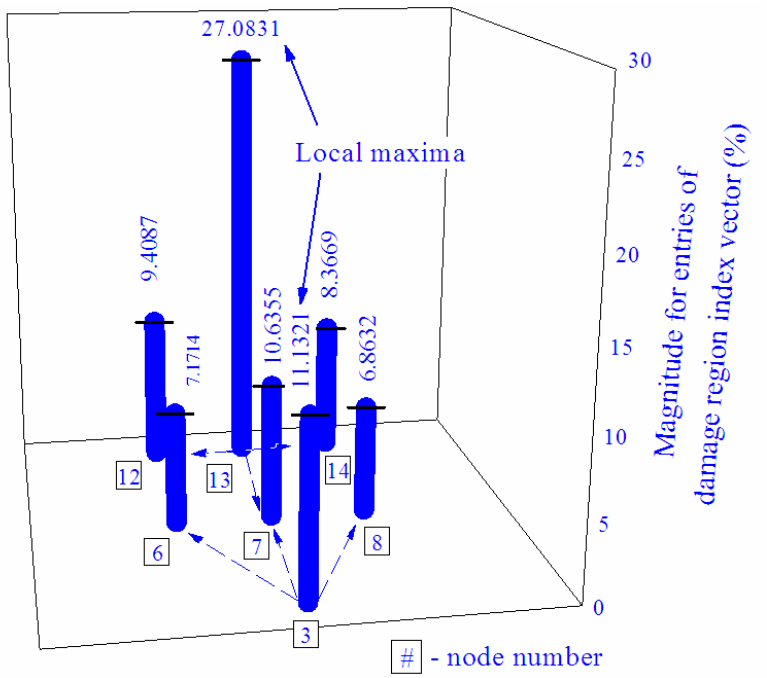

Fig. 2.25. Damage indices for 3-D modular truss structure (elements 1 & 86 damaged, 7 sensors used)

***iii*) Assess damage severity**

For the case where element 86 is damaged, following the procedure presented in Section 2.7 using the axial stiffness of element 86 at the reference state as the initial guess, the computation results are summarized in Fig. 2.26a. It took the algorithm 9 iterations before Eq. (2.37) is satisfied with $Tol = 10^{-2}$. The identified axial stiffness of element 86 is $(EA)_{86} = 4.57\times10^{6}$ (N) compared to the exact values of 4.51×10^{6} (N), which is less than 2% difference. Similarly, the feasibility of the procedure is confirmed for the case where elements (1, 86) are damaged based on the results presented in Fig. 2.26b.

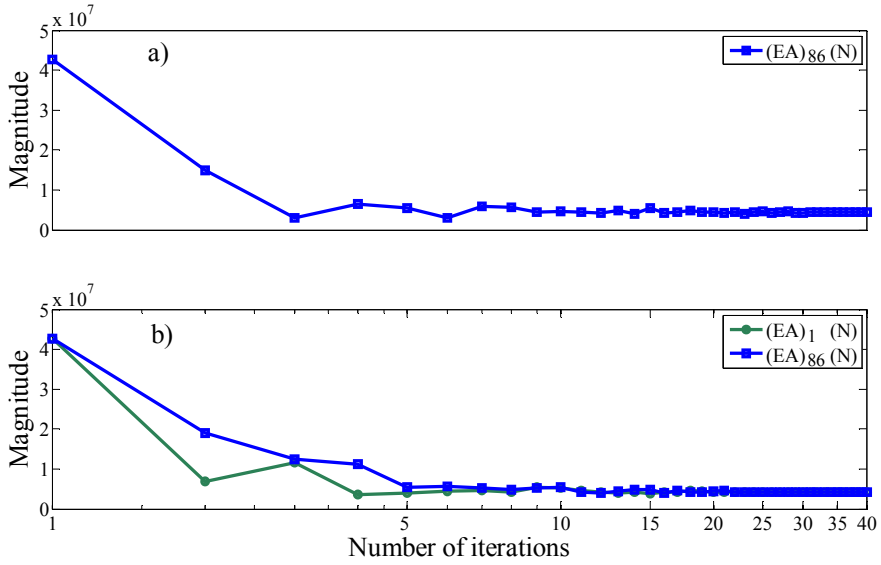

Fig. 2.26. Relationship between identified element stiffnesses and number of iterations for experimental truss: (a) element 86 damaged; and (b) elements 1 & 86 damaged

To assess the effect of integrating over element length on the sensitivity of the damage indicator presented in Section 2.4, the *NCE* of each element is compared with itself normalized by element length (denoted as *NCE*1) for the case where element 86 is damaged. Results in Fig. 2.27 show that both damage indicators, *NCE* and *NCE*1, provide the same set of *PDE* which comprises elements (4, 9, 56, 86) although *NCE*1 is a little more sensitive. This added sensitivity is not worth the increment in the computational process and is therefore not integrated in the *DLV* method.

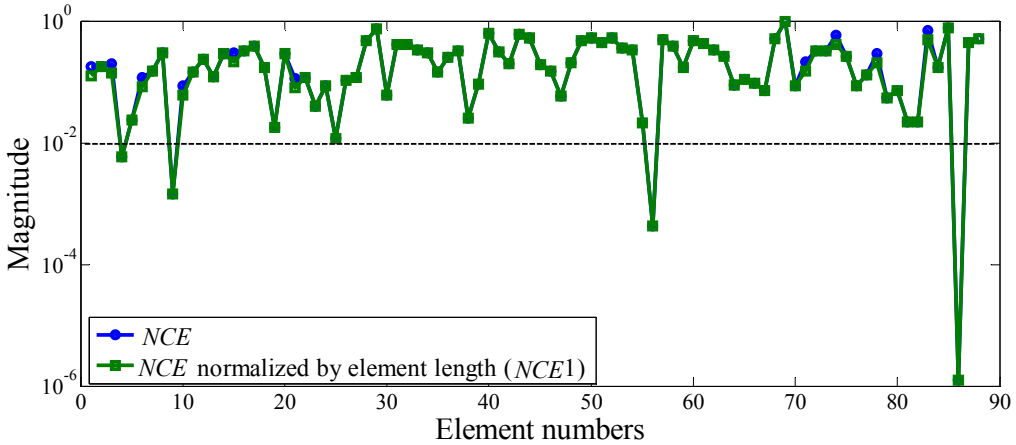

Fig. 2.27. Comparison between *NCE* and *NCE* normalized over element length (*NCE*1) for experimental truss (13 sensors used)

2.10 CONCLUDING REMARKS

The basic concept of the *DLV* method is introduced and its physical insight is discussed based on which enhancements have been made. Firstly, the *NCE* of each element is proposed as damage indicator after the *DLV* set is applied onto the reference structural model as nodal force vectors instead of the *NCS* used in the original *DLV* method. The *NCE* indicator extends the application of the *DLV* method to structures comprising elements with multi-stress state and varied cross-sectional areas along element lengths. Secondly, the sign of the maximum absolute value of the relative change in flexibility matrix is proposed as indicator to differentiate damaged and strengthened structures since the *DLV* method can only identify a set of potentially altered elements. Thirdly, two schemes are introduced to identify the actual damaged elements from the larger set of *PDE* which comprises both actual damaged and some undamaged elements due to imperfect measurements, namely the intersection scheme and the two-stage analysis. The former makes use of the intersection of different sets of *PDE* obtained by performing the *DLV* method for different combinations of measurements. The latter identifies the probable damaged regions first using the change in flexibility matrix. Then, the *DLV* analysis is employed to identify actual damaged elements in the damaged regions. Fourthly, a simple algorithm to estimate the severity of the damaged elements is proposed by adopting the penalty function method in an iterative scheme. The discrepancy between flexibility matrices is used to achieve this objective. Fifthly, an algorithm is proposed to detect structural damage using the *DLV* method with unknown static load. Essential to the algorithm is the determination of a constant α which relates the magnitudes of the static loads at the reference and the damaged states. Upon estimating α, the set of *DLV*s can be computed and the *DLV* analysis can be employed to interrogate structural damage.

Performance of the *NCE*-based *DLV* method is investigated numerically using a 2-D warehouse structure, which comprises frame and truss type elements with both constant and varied cross-sectional areas, for the case where the static loads at the reference and the damaged states are different and unknown. With 10 displacement sensors used and 5% noise, the intersection scheme can provide reliable results within 3 combinations of sensors whereas damage severity of the damaged elements can be estimated with approximately 1% error within about 10 iterations. In an experiment of a 3-D modular truss structure, the intersection scheme can also identify the damaged elements correctly with 7 displacement transducers used and unknown static load. The number of combinations of sensors increases from 3 for the case where 13 sensors are used to 4 for the case where 7 sensors are used. Nevertheless, the damaged elements can still be identified correctly. The two-stage analysis can also identify the damaged elements correctly with 7 sensors used and unknown static load. Damage severity of the damaged elements can be achieved within 2% error in 15 iterations, illustrating the efficiency of the proposed damage severity assessment algorithm.

CHAPTER 3

DAMAGE DETECTION VIA *DLV* AND DYNAMIC RESPONSES

3.1 INTRODUCTION

Although methods based on static responses to detect structural damage are simple conceptually, they are used comparatively less often in practical application. It may be attributed to (1) the requirement of a stiff or fixed reference frame on which displacement transducers can be mounted to measure displacement responses; (2) the requirement of a large applied static load to actuate existing structures since their stiffnesses are usually high; (3) the shifting of heavy static load from one position to another to generate enough readings for the methods to work is time consuming and sometimes introduces uncertainties; and (4) the high sensitivity of the methods to the presence of noise and uncertainties. On the other hand, with the rapid advancement in hardware technology, data storage and computational time are not the major obstacles to prevent the privilege of methods based on dynamic responses to detect structural damage.

In this chapter, the *DLV* method is adapted to assess structural damage using dynamic responses for two cases, namely (1) when the excitation is known; and (2) when the excitation is unknown. The application of the *DLV* method hinges on the computation of the flexibility or stiffness matrix from the dynamic responses. If the excitations force are measured, meaning that input is known, Eigensystem Realization Algorithm (*ERA*) (Juang and Pappa, 1985; Pappa et al., 1993; Juang, 1994) can be employed in conjunction with an algorithm to estimate the flexibility coefficients from state space results (Bernal and Gunes, 2004) to compute the flexibility matrix with

reference to the sensor locations. The procedure is summarized in Section 3.2. If the excitations forces are not measured, Section 3.3 presents an algorithm to estimate the stiffness matrix from acceleration responses. Upon obtaining the flexibility or stiffness matrix, the *DLV* method and the enhancements introduced in Chapter 2 can be utilized to assess structural damage.

As the number and locations of sensors play an important role in improving the accuracy of damage detection results, an algorithm is proposed in Section 3.4 to (a) identify the optimal locations to place the available sensors; and (b) identify the minimum number of sensors which is required to obtain reliable damage detection results by the *DLV* method.

3.2 FORMULATING FLEXIBILITY MATRIX WITH KNOWN EXCITATION

3.2.1 Eigensystem realization algorithm

Ho and Kalman (1965) may be the first researchers who introduced the principle of minimum realization theory which is the originality of the state space realization. The methodology has been substantially extended to identify modal parameters from noisy measurements and is called the Eigensystem Realization Algorithm (*ERA*). In this section, the well-known *ERA* algorithm is used to identify the second order modal model of a system from dynamic responses. Detail derivation of the *ERA* algorithm can be found in Juang and Pappa (1985) and Juang (1994). The key points of *ERA* algorithm which are used to derive the state space realization matrices from dynamic responses of a structure are summarized to facilitate the formulation of the flexibility matrix in the next section.

For an *n-DOF* structure with *r* input excitation points, the equation of motion is represented by

$$\mathbf{M}\ddot{\mathbf{d}} + \mathbf{D}_d\dot{\mathbf{d}} + \mathbf{K}\mathbf{d} = \mathbf{f} \tag{3.1}$$

where $\mathbf{M}$, $\mathbf{D}_d$, $\mathbf{K}$ are the ($n \times n$) mass, damping and stiffness matrices, respectively; $\ddot{\mathbf{d}}$, $\dot{\mathbf{d}}$ and $\mathbf{d}$ the ($n \times 1$) acceleration, velocity and displacement vectors, respectively; and $\mathbf{f} = \mathbf{B}_2\mathbf{u}$ the ($n \times 1$) forcing vector in which $\mathbf{u}$ is the ($r \times 1$) applied load vector and $\mathbf{B}_2$ the ($n \times r$) input influence matrix characterizing the locations of inputs.

In the continuous-time state-space model, Eq. (3.1) can be cast with the state vector $\mathbf{x}$ as the primary variable as (Juang and Pappa, 1985; Juang, 1994)

$$\dot{\mathbf{x}} = \mathbf{A}_c\mathbf{x} + \mathbf{B}_c\mathbf{u} \tag{3.2}$$

where
$$\mathbf{A}_c = \begin{bmatrix} \mathbf{0} & \mathbf{I} \\ -\mathbf{M}^{-1}\mathbf{K} & -\mathbf{M}^{-1}\mathbf{D}_d \end{bmatrix},\ \mathbf{B}_c = \begin{bmatrix} \mathbf{0} \\ \mathbf{M}^{-1}\mathbf{B}_2 \end{bmatrix}, \mathbf{x} = \begin{bmatrix} \mathbf{d} \\ \dot{\mathbf{d}} \end{bmatrix} \tag{3.3}$$

$\mathbf{A}_c$ is the ($2n \times 2n$) state matrix; $\mathbf{B}_c$ the ($2n \times r$) input influence matrix; $\mathbf{x}$ the ($2n \times 1$) state vector; and subscript c stands for continuous model. The output vector $\mathbf{y}$ for the case of ns output points can be written as (Juang and Pappa, 1985; Juang, 1994)

$$\mathbf{y} = \mathbf{C}_a\ddot{\mathbf{d}} + \mathbf{C}_v\dot{\mathbf{d}} + \mathbf{C}_d\mathbf{q} = \mathbf{C}\mathbf{x} + \mathbf{D}\mathbf{u} \tag{3.4}$$

where $\mathbf{C} = \begin{bmatrix} \mathbf{C}_d - \mathbf{C}_a\mathbf{M}^{-1}\mathbf{K} & \mathbf{C}_v - \mathbf{C}_a\mathbf{M}^{-1}\mathbf{D}_d \end{bmatrix}$ and $\mathbf{D} = \mathbf{C}_a\mathbf{M}^{-1}\mathbf{B}_2$; $\mathbf{C}_a$, $\mathbf{C}_v$, $\mathbf{C}_d$ the ($ns \times n$) output influence matrices for acceleration, velocity and displacement, respectively; $\mathbf{C}$ the ($ns \times 2n$) output influence matrix for the state vector $\mathbf{x}$; and $\mathbf{D}$ the ($ns \times r$) direct transmission matrix ($\mathbf{D}$ will disappear if accelerations are not used as output measurements). The presence of $\mathbf{D}$ makes physical sense since a step changes in the input $\mathbf{u}$ will produce a step change in the acceleration of output vector $\mathbf{y}$ (Juang and Pappa, 1985; Juang, 1994).

Equations (3.2) and (3.4) form the continuous-time state-space model of order $2n$ of the dynamic system (Juang and Pappa, 1985; Juang, 1994); that is

$$\begin{cases} \dot{\mathbf{x}} = \mathbf{A}_c\,\mathbf{x} + \mathbf{B}_c\,\mathbf{u} \\ \mathbf{y} = \mathbf{C}\,\mathbf{x} + \mathbf{D}\,\mathbf{u} \end{cases} \tag{3.5}$$

The discrete-time state space model for the system can be written as (Juang, 1994)

$$\begin{cases} \mathbf{x}(k+1) = \mathbf{A}\,\mathbf{x}(k) + \mathbf{B}\,\mathbf{u}(k) \\ \mathbf{y}(k) = \mathbf{C}\mathbf{x}(k) + \mathbf{D}\,\mathbf{u}(k) \end{cases} \tag{3.6}$$

where $$\mathbf{A} = e^{\mathbf{A}_c \Delta t};\ \mathbf{B} = \int_0^{\Delta t} e^{\mathbf{A}_c \tau} d\tau \times \mathbf{B}_c \tag{3.7}$$

and the matrices **A** and **B** in Eq. (3.6), which have the same sizes with their counter parts in the continuous time state defined in Eq. (3.5), describe the input-output relationship through a discrete-time state vector **x**(*k*). Given a vector of discrete input **u**, the output measurement **y** can be obtained through Eq. (3.6).

Juang and Pappa (1985) and Juang (1994) proposed an algorithm to calculate the realization matrices $\mathbf{A}_c$, $\mathbf{B}_c$ and **C** from *r* input and *ns* output vectors, denoted as the *ERA* algorithm. The four major steps of the *ERA* algorithm are summarized next.

Step 1*: Compute the Markov Parameters*

To estimate the Markov parameters, the Fast Fourier Transform (*FFT*) can be employed on the input/output measurements to compute the Frequency Response Fuctions (*FRF*s) which are then used in the Inverse Discrete Fourier Transform (*IDFT*) to compute the sampled pulse response history. An alternative to the computation of the Markov parameters in frequency domain is the computation of the Markov parameters in time domain which is employed in the *ERA* algorithm (Juang and Pappa, 1985; Juang, 1994).

From the measured input and output signals, the Markov parameters can be calculated in either a direct or an indirect manner (Juang and Pappa, 1985; Juang, 1994). In the direct approach, from the input and output measurements, the input matrix and output vector are formulated as

$$\mathbf{U}=\begin{bmatrix} \mathbf{u}(0) & \mathbf{u}(1) & \cdots & \mathbf{u}(4) & \cdots & \mathbf{u}(\xi-1) \\ 0 & \mathbf{u}(0) & \cdots & \mathbf{u}(3) & \cdots & \mathbf{u}(\xi-2) \\ 0 & 0 & \cdots & \mathbf{u}(2) & \cdots & \mathbf{u}(\xi-3) \\ \cdots & \cdots & \cdots & \cdots & \ddots & \cdots \\ 0 & 0 & 0 & 0 & \cdots & \mathbf{u}(0) \end{bmatrix}_{r\xi\times\xi} \tag{3.8}$$

$$\mathbf{y}=\begin{bmatrix}\mathbf{y}(0) & \mathbf{y}(1) & \cdots & \mathbf{y}(4) & \cdots & \mathbf{y}(\xi-1)\end{bmatrix}_{ns\times\xi} \tag{3.9}$$

where ξ is the number of observation points per sensor (that is, points along the time axis); *ns* the number of output measurements; and *r* the number of inputs. Re-writing Eq. (3.6) in a matrix form using the expressions in Eqs. (3.8)-(3.9) gives

$$\underset{(ns\times\xi)}{\mathbf{y}} = \underset{(ns\times r\xi)}{\mathbf{Y}} \cdot \underset{(r\xi\times\xi)}{\mathbf{U}} \tag{3.10}$$

Equation (3.10) expresses the relationship between the input and output time history through Markov parameters (**Y**). The Markov parameters can then be retrieved as a least squares solution of Eq. (3.10) as (Juang and Pappa, 1985; Juang, 1994)

$$\underset{(ns\times r\xi)}{\mathbf{Y}} = \underset{(ns\times\xi)}{\mathbf{y}} \cdot \underset{(\xi\times r\xi)}{\mathbf{U}^{\dagger}} = \begin{bmatrix} \underset{(ns\times r)}{\mathbf{Y}(0)} & \underset{(ns\times r)}{\mathbf{Y}(1)} & \underset{(ns\times r)}{\mathbf{Y}(2)} & \cdots & \underset{(ns\times r)}{\mathbf{Y}(\xi-1)} \end{bmatrix} \tag{3.11}$$

where the superscript "†" denotes pseudo-inversion.

Juang and Pappa (1985) pointed out that the drawback of the direct approach lies on the pseudo-inversion of the input matrix **U** which is usually ill-conditioned if the input signals are not rich in frequencies such as the case of sinusoid excitations. Furthermore, if ξ is too large as usually encountered for lightly damped system, the input matrix **U** also becomes ill-conditioned. To overcome this limitation, an observer matrix is introduced to Eq. (3.6) to form a stable discrete state-space model for the system to be identified (Juang and Pappa, 1985; Juang, 1994).

In the indirect approach, a term $\mathbf{G} \times \mathbf{y}(k)$ is introduced to the right hand side of the first equation in Eq. (3.6) to yield (Juang and Pappa, 1985; Juang, 1994)

$$\mathbf{x}(k+1)=\mathbf{A}(k)+\mathbf{B}u(k)+\mathbf{G}y(k)-\mathbf{G}\mathbf{y}(k)=\left[\mathbf{A}+\mathbf{GC}\right]\mathbf{x}(k)+\left[\mathbf{B}+\mathbf{GD}\right]\mathbf{u}(k)-\mathbf{G}\mathbf{y}(k)$$

or $$\mathbf{x}(k+1)=\overline{\mathbf{A}}\,\mathbf{x}(k)+\overline{\mathbf{B}}\,\mathbf{v}(k) \qquad (3.12)$$

where $\overline{\mathbf{A}}=\mathbf{A}+\mathbf{G}\,\mathbf{C}$, $\overline{\mathbf{B}}=[\mathbf{B}+\mathbf{G}\mathbf{D}, -\mathbf{G}]$, $\mathbf{G}$ the ($2n \times ns$) arbitrary matrix chosen to make $\overline{\mathbf{A}}$ as stable as desired, and

$$\mathbf{v}(k)=\begin{bmatrix}\mathbf{u}(k)\\ \mathbf{y}(k)\end{bmatrix} \qquad (3.13)$$

Mathematically, Eq. (3.12) is identical to the first equation of Eq. (3.6). However, the system matrices and the input vector in Eqs. (3.12) and (3.6) are different. Define

$$\mathbf{V}=\begin{bmatrix}\mathbf{u}(0) & \mathbf{u}(1) & \cdots & \mathbf{u}(p) & \cdots & \mathbf{u}(\xi-1)\\ 0 & \mathbf{v}(0) & \cdots & \mathbf{v}(p-1) & \cdots & \mathbf{v}(\xi-2)\\ 0 & 0 & \cdots & \mathbf{v}(p-2) & \cdots & \mathbf{v}(\xi-3)\\ \cdots & \cdots & \cdots & \cdots & \ddots & \cdots\\ 0 & 0 & 0 & \mathbf{v}(0) & \cdots & \mathbf{v}(\xi-p-1)\end{bmatrix}_{[(r+ns)p+r]\times\xi} \qquad (3.14)$$

where p is a sufficiently large number such that $\overline{\mathbf{A}}^{k} \approx 0$ for all time steps $k \geq p$ which can be done since $\mathbf{G}$ can be arbitrarily chosen (Juang and Pappa, 1985; Juang, 1994). Equation (3.6) can be re-written as

$$\begin{cases}\mathbf{x}(k+1)=\overline{\mathbf{A}}\,\mathbf{x}(k)+\overline{\mathbf{B}}\,\mathbf{v}(k)\\ \underset{ns\times\xi}{\mathbf{y}} = \underset{ns\times[(r+ns)p+r]}{\overline{\mathbf{Y}}} \times \underset{[(r+ns)p+r]\times\xi}{\mathbf{V}}\end{cases} \qquad (3.15)$$

Equation (3.15) is an observer equation if the state $\mathbf{x}(k)$ is considered as an observer state vector and the parameters $\overline{\mathbf{Y}}$ of the system are therefore referred to as the observer Markov parameters (Juang and Pappa, 1985; Juang, 1994). The input-output description in matrix form becomes

$$\underset{(ns\times\xi)}{\mathbf{y}} = \underset{(ns\times[(r+ns)p+r])}{\overline{\mathbf{Y}}} \quad \underset{([(r+ns)p+r]\times\xi)}{\mathbf{V}} \qquad (3.16)$$

where $\mathbf{y}=\begin{bmatrix}\mathbf{y}(0) & \mathbf{y}(1) & \cdots & \mathbf{y}(p) & \cdots & \mathbf{y}(\xi-1)\end{bmatrix}$, and

$$\overline{\mathbf{Y}} = [\mathbf{D} \quad \mathbf{C}\overline{\mathbf{B}} \quad \mathbf{C}\overline{\mathbf{A}}\overline{\mathbf{B}} \quad \ldots \quad \mathbf{C}\overline{\mathbf{A}}^{p-1}\overline{\mathbf{B}}] \tag{3.17}$$

To solve for $\overline{\mathbf{Y}}$ uniquely and to minimize numerical error due to the computation of the pseudo-inversion, all rows of $\mathbf{V}$ must be linearly independent (Juang and Pappa, 1985; Juang, 1994). The least squares solution of Eq. (3.16) has the following form

$$\overline{\mathbf{Y}} = \mathbf{y}\,\mathbf{V}^{\dagger} = \left[\overline{\mathbf{Y}}(0) \quad \overline{\mathbf{Y}}(1) \quad \overline{\mathbf{Y}}(2) \quad \cdots \quad \overline{\mathbf{Y}}(p)\right] \tag{3.18}$$

where $\overline{\mathbf{Y}}(0) = \mathbf{D}$; $\overline{\mathbf{Y}}(k) = \mathbf{C}\overline{\mathbf{A}}^{k-1}\overline{\mathbf{B}}$, …, $\overline{\mathbf{Y}}(p) = \mathbf{C}\overline{\mathbf{A}}^{p-1}\overline{\mathbf{B}}$.

Parameter k of the observer Markov parameter ($\overline{\mathbf{Y}}(k)$) can be partitioned as

$$\overline{\mathbf{Y}}(k) = \mathbf{C}\overline{\mathbf{A}}^{k-1}\overline{\mathbf{B}} = \left[\mathbf{C}(\mathbf{A}+\mathbf{GC})^{k-1}(\mathbf{B}+\mathbf{GD}) \quad -\mathbf{C}(\mathbf{A}+\mathbf{GC})^{k-1}\mathbf{G}\right] \tag{3.19}$$

$$\overline{\mathbf{Y}}(k) = \left[\overline{\mathbf{Y}}^{(1)}(k) \quad -\overline{\mathbf{Y}}^{(2)}(k)\right] \quad (k = 1, 2, \ldots, p) \tag{3.20}$$

The minus sign used for $\overline{\mathbf{Y}}^{(2)}(k)$ in Eq. (3.20) is chosen such that $\overline{\mathbf{Y}}^{(2)}(k) = \mathbf{C}(\mathbf{A}+\mathbf{GC})^{k-1}\mathbf{G}$. It is observed that the first observer Markov parameter $\overline{\mathbf{Y}}(0)$ has a smaller size than the remaining observer Markov parameters. By induction, the relationship between the observer Markov parameters and the System Markov parameters can be obtained

$$\mathbf{Y}(0) = \overline{\mathbf{Y}}(0) = \mathbf{D} \tag{3.21}$$

$$\mathbf{Y}(k) = \overline{\mathbf{Y}}^{(1)}(k) - \sum_{i=1}^{k}\left[\mathbf{Y}^{(2)}(k)\,\mathbf{Y}(k-i)\right] \text{ for } k = 1, 2, \ldots, p \tag{3.22}$$

$$\mathbf{Y}(k) = -\sum_{i=1}^{p}\left[\mathbf{Y}^{2}(i)\,\mathbf{Y}(k-i)\right] \text{ for } k = p+1, p+2, \ldots, \infty \tag{3.23}$$

Equation (3.23) implies that the system has only p independent system Markov parameters since $\mathbf{Y}(k)$ ($k \geq p+1$) is a linear combination of its past p parameters, namely $\mathbf{Y}_{k-1}$, $\mathbf{Y}_{k-2}$, ..., $\mathbf{Y}_{k-p}$.

It is observed that the indirect approach can produce an observer with minimal residue in a least squares sense for a given input/output data measurements for the cases where measurements are contaminated with noise and uncertainties (Juang and Pappa, 1985; Juang, 1994). Hence, the indirect approach has two major advantages compared to the direct approach. Firstly, the number of independent Markov parameters is compressed by the introduction of an observer gain matrix **G**, resulting in a smaller size Hankel matrix (see next step) and enhancing the stability and reducing the amount of computation. Secondly, the increment in stability of the system by introducing an observer gain matrix allows the indirect approach to be applicable for the case of multiple input/output measurements to identify the system Markov parameters. In this study, the indirect approach is adopted to identify the system Markov parameters from the input/output measurements.

Step 2: Form the Hankel Matrix

Once the system Markov parameters **Y** is determined, the generalized Hankel matrix (of size $\alpha\, ns \times \beta\, r$) can be formed as follows (Juang and Pappa, 1985; Juang, 1994)

$$\mathbf{H}(k-1)=\begin{bmatrix} \mathbf{Y}(k) & \mathbf{Y}(k+1) & \mathbf{Y}(k+2) & \cdots & \mathbf{Y}(k+\beta-1) \\ \mathbf{Y}(k+1) & \mathbf{Y}(k+2) & \mathbf{Y}(k+3) & \cdots & \mathbf{Y}(k+\beta) \\ \mathbf{Y}(k+2) & \mathbf{Y}(k+3) & \mathbf{Y}(k+4) & \cdots & \mathbf{Y}(k+\beta+1) \\ \cdots & \cdots & \cdots & \ddots & \cdots \\ \mathbf{Y}(k+\alpha-1) & \mathbf{Y}(k+\alpha) & \mathbf{Y}(k+\alpha+1) & \cdots & \mathbf{Y}(k+\alpha+\beta-2) \end{bmatrix} \quad (3.24)$$

where α and β are chosen such that the rank of the Hankel matrix is not less than the order of the system ($2n$). Juang and Pappa (1985) suggested that $\alpha \geq 2n$, $\beta \geq 2n$. The Hankel matrices for $k = 1$ and $k = 2$ are respectively

$$\mathbf{H}(0)=\begin{bmatrix} \mathbf{Y}(1) & \mathbf{Y}(2) & \mathbf{Y}(3) & \cdots & \mathbf{Y}(\beta) \\ \mathbf{Y}(2) & \mathbf{Y}(3) & \mathbf{Y}(4) & \cdots & \mathbf{Y}(1+\beta) \\ \mathbf{Y}(3) & \mathbf{Y}(4) & \mathbf{Y}(5) & \cdots & \mathbf{Y}(2+\beta) \\ \cdots & \cdots & \cdots & \ddots & \cdots \\ \mathbf{Y}(\alpha) & \mathbf{Y}(\alpha+1) & \mathbf{Y}(\alpha+2) & \cdots & \mathbf{Y}(\alpha+\beta-2) \end{bmatrix} \tag{3.25}$$

$$\mathbf{H}(1)=\begin{bmatrix} \mathbf{Y}(2) & \mathbf{Y}(3) & \mathbf{Y}(4) & \cdots & \mathbf{Y}(\beta+1) \\ \mathbf{Y}(3) & \mathbf{Y}(4) & \mathbf{Y}(5) & \cdots & \mathbf{Y}(\beta+2) \\ \mathbf{Y}(4) & \mathbf{Y}(5) & \mathbf{Y}(6) & \cdots & \mathbf{Y}(\beta+3) \\ \cdots & \cdots & \cdots & \ddots & \cdots \\ \mathbf{Y}(\alpha+1) & \mathbf{Y}(\alpha+2) & \mathbf{Y}(\alpha+3) & \cdots & \mathbf{Y}(\alpha+\beta-1) \end{bmatrix} \tag{3.26}$$

Note that $\mathbf{Y}(0) = \mathbf{D}$ is not included in $\mathbf{H}(0)$, and if $\alpha \geq 2n$ and $\beta \geq 2n$, the matrix $\mathbf{H}(k\text{-}1)$ is of rank $2n$.

Step 3: Decompose the Hankel Matrix $\mathbf{H}(0)$

The *ERA* algorithm (Juang and Pappa, 1985; Juang, 1994) continues by factorizing the Hankel matrix $\mathbf{H}(0)$ using singular value decomposition,

$$\mathbf{H}(0) \xrightarrow{SVD} \mathbf{U}\,\mathbf{\Sigma}\,\mathbf{V}^T \xrightarrow{truncate} \mathbf{U}_{2n}\,\mathbf{\Sigma}_{2n}\,\mathbf{V}_{2n}^T \tag{3.27}$$

where the columns of matrices $\mathbf{U}$ and $\mathbf{V}$ are orthonormal and $\mathbf{\Sigma}$ is a matrix containing singular values

$$\mathbf{\Sigma}=\begin{bmatrix} \mathbf{\Sigma}_{2n} & \mathbf{0} \\ \mathbf{0} & \mathbf{0} \end{bmatrix} \tag{3.28}$$

$$\text{with} \quad \mathbf{\Sigma}_{2n}=\begin{bmatrix} s_1 & & 0 \\ & s_2 & \\ & \ddots & \\ 0 & & s_{2n} \end{bmatrix} \quad \text{in which} \quad s_1 \geq s_2 \geq \cdots s_{2n} > 0 \tag{3.29}$$

$\mathbf{U}_{2n}$ and $\mathbf{V}_{2n}$ are the orthonormal matrices formed by the first $2n$ columns of matrices $\mathbf{U}$ and $\mathbf{V}$, respectively.

Step 4: Construct the Realization Matrices

The realization matrices can be estimated as follows (Juang and Pappa, 1985; Juang, 1994)

$$\hat{\mathbf{A}} = \boldsymbol{\Sigma}_{2n}^{-1/2}\, \mathbf{U}_{2n}^{T}\, \mathbf{H}(1)\, \mathbf{V}_{2n}\, \boldsymbol{\Sigma}_{2n}^{-1/2},\ \hat{\mathbf{B}} = \boldsymbol{\Sigma}_{2n}^{1/2}\, \mathbf{V}_{2n}^{T}\, \mathbf{E}_{r},\ \hat{\mathbf{C}}_{c} = \mathbf{E}_{ns}^{T}\, \mathbf{U}_{2n}\, \boldsymbol{\Sigma}_{2n}^{1/2} \tag{3.30}$$

where $\mathbf{E}_{ns}^{T} = \begin{bmatrix} \mathbf{I}_{ns} & \mathbf{0}_{ns} & \mathbf{0}_{ns} & \cdots & \mathbf{0}_{ns} \end{bmatrix}_{ns \times ns\,\alpha}$ and $\mathbf{E}_{r}^{T} = \begin{bmatrix} \mathbf{I}_{r} & \mathbf{0}_{r} & \mathbf{0}_{r} & \cdots & \mathbf{0}_{r} \end{bmatrix}_{r \times \beta}$ in which $\mathbf{I}_{ns}$, $\mathbf{0}_{ns}$ and $\mathbf{I}_{r}$, $\mathbf{0}_{r}$ are ($ns \times ns$) and ($r \times r$) unit and zero matrices, respectively. The continuous time model can be obtained from the discrete time model through their relationship in Eq. (3.7), that is

$$\mathbf{A}_{c} = \frac{\log(\mathbf{A})}{\Delta t} \quad \text{and} \quad \mathbf{B}_{c} = (\mathbf{A} - \mathbf{I})^{-1}\, \mathbf{A}_{c}\, \mathbf{B} \tag{3.31}$$

Juang and Pappa (1985) and Juang (1994) showed that the major advantage of the *ERA* algorithm to identify the second order modal model of a system is that it does not require the *a priori* knowledge of the system order. For sufficiently low noise level data, the order of the estimated state matrix ($\hat{\mathbf{A}}$) is 2*n*. For the case of noise-free, performing *SVD* on the Hankel matrix reveals exactly 2*n* non-zero singular values (*NZV*). With the presence of noise and measurement error, the Hankel matrix will usually be full rank which generally does not equal to the order of system under test. The purpose of the *ERA* algorithm is to realize a smoothed version of the system realization matrices which closely represents the major characteristics of the system under test. This can be achieved by truncating some relatively small singular values, say $s_{i+1}, \ldots, s_{2n}$ of $\boldsymbol{\Sigma}$. These singular values usually contain more noise information than system information. In other words, the directions determined by $s_{i+1}, \ldots, s_{2n}$ do not significantly affect the degrees of controllability and observability. The reduced model of order *i* after ignoring some small singular values ($s_{i+1}, \ldots, s_{2n}$) is called the robust controllability of the realized system (Juang and Pappa, 1985; Juang, 1994).

3.2.2 Formulation of flexibility matrix

The structural flexibility matrices at the reference and the damaged states need to be formed based on sensor measurements to perform the *DLV* method. From response accelerations and measured excitations, the *ERA* algorithm presented in Section 3.2.1 is employed to extract the state-space realization matrices of the structure, from which a procedure proposed by Bernal and Gunes (2004) is used to compute coefficients of the flexibility matrices. The latter involves three major steps, namely (a) expressing the structural flexibility matrix in term of complex modes; (b) determining the partitioned flexibility matrix from state-space realization; and (c) estimating the diagonal matrix containing the modal normalized constants. Each of these steps will be summarized briefly below as detail derivation can be found in Bernal and Gunes (2004).

(a) Compute Structural Flexibility Matrix in term of Complex Modes

The free vibration of an *n-DOF* structure can be described as

$$\mathbf{M}\ddot{\mathbf{d}} + \mathbf{D}_d\dot{\mathbf{d}} + \mathbf{K}\mathbf{d} = \mathbf{0} \tag{3.32}$$

where the definitions of all variables are identical to those in Eq. (3.1). In general, the eigen-solution of Eq. (3.32) is complex. Let the ($n \times n$) matrices of real eigenvalues and eigenvectors be denoted as $\mathbf{\Lambda}$ and $\boldsymbol{\psi}$, respectively. Equation (3.32) can be re-written into a first-order matrix form as (Bernal and Gunes, 2004)

$$\begin{bmatrix} \mathbf{D}_d & \mathbf{M} \\ \mathbf{M} & \mathbf{0} \end{bmatrix}\dot{\mathbf{x}} = \begin{bmatrix} -\mathbf{K} & \mathbf{0} \\ \mathbf{0} & \mathbf{M} \end{bmatrix}\mathbf{x} \tag{3.33}$$

where $\mathbf{x}$ is the state vector, $\mathbf{x} = \begin{bmatrix} \mathbf{d}^T & \dot{\mathbf{d}}^T \end{bmatrix}^T$. The eigenvalue and eigenvector matrices of Eq. (3.33) can be expressed respectively as (Bernal and Gunes, 2004)

$$\mathbf{\Lambda}_1 = \begin{bmatrix} \mathbf{\Lambda} & \mathbf{0} \\ \mathbf{0} & \mathbf{\Lambda}^* \end{bmatrix} \text{ and } \mathbf{\Phi} = \begin{bmatrix} \boldsymbol{\psi} & \boldsymbol{\psi}^* \\ \boldsymbol{\psi}\mathbf{\Lambda} & \boldsymbol{\psi}^*\mathbf{\Lambda}^* \end{bmatrix} \tag{3.34}$$

where superscript "*" denotes complex conjugate. Let

$$\mathbf{D}_g^{-1} = \mathbf{\Phi}^T \begin{bmatrix} -\mathbf{K} & \mathbf{0} \\ \mathbf{0} & \mathbf{M} \end{bmatrix} \mathbf{\Phi} \tag{3.35}$$

which is a diagonal matrix of modal constants. By noting that

$$\begin{bmatrix} -\mathbf{K}^{-1} & \mathbf{0} \\ \mathbf{0} & \mathbf{M}^{-1} \end{bmatrix} = \begin{bmatrix} -\mathbf{F} & \mathbf{0} \\ \mathbf{0} & \mathbf{M}^{-1} \end{bmatrix} = \mathbf{\Phi} \mathbf{D}_g \mathbf{\Phi}^T = \begin{bmatrix} \boldsymbol{\psi} & \boldsymbol{\psi}^* \\ \boldsymbol{\psi}\mathbf{\Lambda} & \boldsymbol{\psi}^*\mathbf{\Lambda}^* \end{bmatrix} \mathbf{D}_g \begin{bmatrix} \boldsymbol{\psi} & \boldsymbol{\psi}\mathbf{\Lambda} \\ \boldsymbol{\psi}^* & \boldsymbol{\psi}^*\mathbf{\Lambda}^* \end{bmatrix} \tag{3.36}$$

one obtains (Bernal and Gunes, 2004)

$$\mathbf{F} = -\begin{bmatrix} \boldsymbol{\psi} & \boldsymbol{\psi}^* \end{bmatrix} \mathbf{D}_g \begin{bmatrix} \boldsymbol{\psi} \\ \boldsymbol{\psi}^* \end{bmatrix} = -\Upsilon \mathbf{D}_g \Upsilon^T \tag{3.37}$$

where $\Upsilon = \begin{bmatrix} \boldsymbol{\psi} & \boldsymbol{\psi}^* \end{bmatrix}$ is the complex mode shapes of the structure. To obtain $\mathbf{F}$, $\mathbf{D}_g$ needs to be estimated.

(b) Partition Flexibility Matrix from State-Space Realization

From Section 3.2.1, the realization matrices $\mathbf{A}_c, \mathbf{B}_c, \mathbf{C}, \mathbf{D}, \mathbf{A}, \mathbf{B}$ have been identified using acceleration responses and measured input excitations. Performing Fourier transformation on the first equation of Eq. (3.5) yields

$$i\omega \mathbf{x} = \mathbf{A}_c \mathbf{x} + \mathbf{B}_c \mathbf{u}(\omega) \Rightarrow \mathbf{x} = \left[i\omega \mathbf{I} - \mathbf{A}_c \right]^{-1} \mathbf{B}_c \mathbf{u}(\omega) \tag{3.38}$$

Substituting Eq. (3.38) into the second equation of Eq. (3.5) yields

$$\mathbf{y}(\omega) = \left\{ \mathbf{C}\left[\mathbf{I} \cdot i\omega - \mathbf{A}_c \right]^{-1} \mathbf{B}_c + \mathbf{D} \right\} \mathbf{u}(\omega) \tag{3.39}$$

The Fourier transformation of the output vector can be expressed in terms of the displacement vector $\mathbf{y}_D$ as

$$\mathbf{y}(\omega) = (i\omega)^p \, \mathbf{y}_D(\omega) \tag{3.40}$$

where p = 0, 1 or 2 corresponds to the output measurement of displacement, velocity or acceleration, respectively. Substituting Eq. (3.40) into Eq. (3.39) gives

$$\mathbf{y}_D(\omega) = \frac{1}{(i\omega)^p} \left\{ \mathbf{C}\left[\mathbf{I} \cdot i\omega - \mathbf{A}_c \right]^{-1} \mathbf{B}_c + \mathbf{D} \right\} \mathbf{u}(\omega) \tag{3.41}$$

The flexibility matrix relates the inputs to the outputs at $\omega = 0$ (Bernal and Gunes, 2004). By defining $\mathbf{F}_p$ as a suitable partition of the structural flexibility matrix $\mathbf{F}$ such that

$$\mathbf{y}_D(0) = \mathbf{F}_p\, \mathbf{u}(0) \tag{3.42}$$

one obtains

$$\mathbf{F}_p = \underset{\omega \to 0}{Lim}\left[\frac{1}{(i\omega)^p} \left\{ \mathbf{C}\left[\mathbf{I} \cdot i\omega - \mathbf{A}_c\right]^{-1} \mathbf{B}_c + \mathbf{D} \right\} \right] \tag{3.43}$$

i) If $p = 0$, namely output measurement is displacement, $\mathbf{D} = \mathbf{0}$

$$\mathbf{F}_p = \lim_{\omega \to 0}\left[\mathbf{C}\left(\mathbf{I}.i\omega - \mathbf{A}_c\right)^{-1} \mathbf{B}_c \right] = -\mathbf{C}\mathbf{A}_c^{-1}\mathbf{B}_c \tag{3.44}$$

ii) If $p = 1$, namely output measurement is velocity, $\mathbf{D} = \mathbf{0}$

$$\mathbf{F}_p = \lim_{\omega \to 0}\left\{ \frac{1}{i\omega}\left[\mathbf{C}\left(\mathbf{I}.i\omega - \mathbf{A}_c\right)^{-1} \mathbf{B}_c \right] \right\} = \lim_{\omega \to 0}\left\{ -\mathbf{C}\left(\mathbf{I}.i\omega - \mathbf{A}_c\right)^{-2} \mathbf{I}.\mathbf{B}_c \right\} = -\mathbf{C}\mathbf{A}_c^{-2}\mathbf{B}_c \tag{3.45}$$

iii) If $p = 2$, namely output measurement is acceleration, $\mathbf{D} \neq \mathbf{0}$

$$\mathbf{F}_p = \lim_{\omega \to 0}\left\{ \frac{1}{(i\omega)^2}\left[\mathbf{C}\left(\mathbf{I}.i\omega - \mathbf{A}_c\right)^{-1} \mathbf{B}_c + \mathbf{D} \right] \right\} = \lim_{\omega \to 0}\left\{ \frac{1}{2(i\omega)}\left[-\mathbf{C}\left(\mathbf{I}.i\omega - \mathbf{A}_c\right)^{-2} \mathbf{I}.\mathbf{B}_c + 0 \right] \right\}$$
$$\mathbf{F}_p = \lim_{\omega \to 0}\left\{ \frac{1}{2}\left[2\mathbf{C}\left(\mathbf{I}.i\omega - \mathbf{A}_c\right)^{-3} \mathbf{I}.\mathbf{I}.\mathbf{B}_c \right] \right\} = -\mathbf{C}\mathbf{A}_c^{-3}\mathbf{B}_c \tag{3.46}$$

From Eqs. (3.44)-(3.46),

$$\mathbf{F}_p = -\mathbf{C}\,\mathbf{A}_c^{-(p+1)}\mathbf{B}_c \tag{3.47}$$

(c) Compute Diagonal Matrix containing Modal Constants ($\mathbf{D}_g$)

Bernal and Gunes (2004) showed that the complex eigenvector Υ_s for the reduced system, defined with respect to *DOF* at the sensor locations, can be obtained from the matrix $\mathbf{C}$ in Eq. (3.6) and the normalized complex mode shapes in Eq. (3.37) via

$$\Upsilon_s = \mathbf{C}\,\Upsilon \tag{3.48}$$

The flexibility matrix of the reduced system defined at the sensor locations can be retrieved following Eq. (3.37) as

$$\mathbf{F}_s = -\Upsilon_s \mathbf{D}_g \Upsilon_s^T \tag{3.49}$$

Expressing the state matrix $\mathbf{A}_c$ in term of its eigenvalues ($\mathbf{\Lambda}_c$) and eigenvectors (Υ_c), Eq. (3.47) can be rewritten as follows

$$\mathbf{F}_p = -\mathbf{C}\,\Upsilon_c \mathbf{\Lambda}_c^{-(p+1)} \Upsilon_c^{-1} \mathbf{B}_c = -\Upsilon_s \mathbf{\Lambda}_c^{-(p+1)} \Upsilon_c^{-1} \mathbf{B}_c \tag{3.50}$$

Defining $\mathbf{B}_{cc}$ and Υ_{sc}^T are the columns extracted from the columns of $\mathbf{B}_c$ and Υ_s^T corresponding to the *DOF* where the actuators and sensors are collocated, respectively. By comparing the collocated columns of the flexibility matrices in Eqs. (3.49) and (3.50) gives (Bernal and Gunes, 2004)

$$-\Upsilon_s \mathbf{D}_g \Upsilon_{sc}^T = -\Upsilon_s \mathbf{\Lambda}_c^{-(p+1)} \Upsilon_c^{-1} \mathbf{B}_{cc} \tag{3.51}$$

or

$$\mathbf{D}_g \Upsilon_{sc}^T = \mathbf{\Lambda}_c^{-(p+1)} \Upsilon_c^{-1} \mathbf{B}_{cc} \tag{3.52}$$

From Eq. (3.52), the modal normalized constants matrix $\mathbf{D}_g$ can be calculated as (Bernal and Gunes, 2004)

$$\mathbf{D}_g = \mathbf{\Lambda}_c^{-(p+1)} \Upsilon_c^{-1} \mathbf{B}_{cc} \begin{bmatrix} \Upsilon_{sc}(1) & & & 0 \\ & \Upsilon_{sc}(2) & & \\ & & \ddots & \\ 0 & & & \Upsilon_{sc}(2n) \end{bmatrix}^{-1} \tag{3.53}$$

where $\Upsilon_{sc}(k)$, k = 1, 2, …, 2n, is the kth component of column vector Υ_{sc}^T. Upon estimating $\mathbf{D}_g$, the flexibility matrix with respect to the sensor locations can be calculated following Eq. (3.49).

3.3 FORMULATING STIFFNESS MATRIX WITH UNKNOWN EXCITATION

To formulate the flexibility matrix from measured accelerations with unknown excitation, Bernal (2004) proposed the use of a known disturbance mass added to the

structure to evaluate the change in eigensolution with the assumption that the change in structural frequency and mode shape are small under the disturbed mass. From the change in eigensolution due to known disturbed mass, the mass normalized constants are evaluated based on which the flexibility matrix is computed. Alternatively, Gao et al. (2006) assumed that change in the mass normalized constants matrix is negligible when structure changes from the reference to the damaged state. The known mass normalized constants at the reference state can therefore be used to compute the flexibility matrix at the damaged state. While the proposal by Bernal (2004) is inconvenience in practice, the proposal by Gao et al. (2006) may introduce error if the damage is severe. In this section, a direct method is proposed to formulate the structural stiffness matrix based solely on measured accelerations, assuming that the mass matrix is known.

Consider an *n-DOF* structure with *ns* accelerometers attached. Assuming that *r* unknown input forces are actuating the structure, *nc* (≥ 0) of which are collocated with the sensors. The locations of sensors and input forces are assumed known. The equation of motion of the structure can be expressed as shown in Eq. (3.1) and is re-written here for easier reference

$$\mathbf{M}\ddot{\mathbf{d}} + \mathbf{D}_d\dot{\mathbf{d}} + \mathbf{K}\mathbf{d} = \mathbf{f} \tag{3.1}$$

If a sampling time interval of Δt is used, then the structural displacement and velocity responses at time step *j* can be estimated using their values at step (*j*-1) through Newmark-β method as

$$\begin{cases} \dot{\mathbf{d}}_j = \dot{\mathbf{d}}_{j-1} + (1-\gamma)\cdot\Delta t\cdot\ddot{\mathbf{d}}_{j-1} + \gamma\cdot\Delta t\cdot\ddot{\mathbf{d}}_j \\ \mathbf{d}_j = \mathbf{d}_{j-1} + \Delta t\cdot\dot{\mathbf{d}}_{j-1} + (0.5-\beta)\cdot\Delta t^2\cdot\ddot{\mathbf{d}}_{j-1} + \beta\cdot\Delta t^2\cdot\ddot{\mathbf{d}}_j \end{cases} \tag{3.54}$$

where γ and β are the integration constants, taken as $\gamma = 0.50$, $\beta = 0.25$ which corresponds to the case of constant average acceleration within Δt. Written in terms of

the initial conditions $\mathbf{d}_1$ and $\dot{\mathbf{d}}_1$, and the accelerations (*ns* of which are measured and *n-ns* of which are not measured and to be solved up to time step *j*), Eq. (3.54) becomes

$$\begin{cases} \dot{\mathbf{d}}_j = \dot{\mathbf{d}}_1 + B_1 \sum_{i=1}^{j-1} \left(\ddot{\mathbf{d}}_i + \ddot{\mathbf{d}}_{i+1} \right) \\ \mathbf{d}_j = \mathbf{d}_1 + (j-1)\dot{\mathbf{d}}_1 \Delta t + C_1 \sum_{i=1}^{j-1} \left(\ddot{\mathbf{d}}_i + \ddot{\mathbf{d}}_{i+1} \right) + B_1 \Delta t \sum_{i=1}^{j-1} \left[(j-i-1) \left(\ddot{\mathbf{d}}_i + \ddot{\mathbf{d}}_{i+1} \right) \right] \end{cases} \tag{3.55}$$

where $B_1 = 0.5\Delta t$, $C_1 = 0.25\Delta t^2$. In theory, with k_1 time steps of measured accelerations, $k_1 n$ equations can be formulated using Eq. (3.1) as

$$\begin{cases} \mathbf{M}\ddot{\mathbf{d}}_1 + \mathbf{D}_d \dot{\mathbf{d}}_1 + \mathbf{K}\mathbf{d}_1 = \mathbf{f}_1 \\ \mathbf{M}\ddot{\mathbf{d}}_2 + \mathbf{D}_d \dot{\mathbf{d}}_2 + \mathbf{K}\mathbf{d}_2 = \mathbf{f}_2 \\ \cdots\cdots\cdots\cdots\cdots\cdots \\ \mathbf{M}\ddot{\mathbf{d}}_{k_1} + \mathbf{D}_d \dot{\mathbf{d}}_{k_1} + \mathbf{K}\mathbf{d}_{k_1} = \mathbf{f}_{k_1} \end{cases} \tag{3.56}$$

where subscripts 1, 2, …, k_1 denote time steps. Substituting Eq. (3.55) into Eq. (3.56), the unknowns in Eq. (3.56) include: (*i*) 2*n* initial conditions ($\mathbf{d}_1$ and $\dot{\mathbf{d}}_1$ for each of the *n-DOF*); (*ii*) $k_1(n - ns)$ accelerations which are not measured; (*iii*) $n(n + 1)/2$ entries in each of $\mathbf{D}_d$ and $\mathbf{K}$, both of which are symmetric matrices; and (*iv*) $k_1 r$ unknown input forces. To solve for these unknowns and hence obtain $\mathbf{K}$, the number of time steps of acceleration data required is

$$k_1 n \geq n(n+1) + k_1(n - ns) + 2n + k_1 r \Rightarrow k_1 \geq \frac{n(n+3)}{ns - r} \tag{3.57}$$

Since Eq. (3.57) does not depend on the number of collocated sensor-actuator pairs (*nc*), the method overcomes the requirement that at least one collocated sensor-actuator pair must exist in the original *DLV* method. Equation (3.56) is a system of nonlinear equations which can be solved by either the Secant method (Wolfe, 1959) or the Newton-Raphson method (Bathe, 1996). Since the Jacobian matrix can be computed directly, the Newton-Raphson method is employed using the parameters of

the structure at the reference state as initial guess for the unknowns in $\mathbf{D}_d$ and $\mathbf{K}$ to obtain the solution numerically.

For a feel of the number of time steps required, a 10-*DOF* structure (n = 10), excited by 2 actuators (r = 2) and monitored by 3 sensors (ns = 3) gives $k_1 \geq 130$ whereas a 50-*DOF* structure (n = 50), excited by 2 actuators (r = 2) and monitored by 8 sensors (ns = 8) necessitates $k_1 \geq 442$.

The above derivation assumes that (*i*) $ns > r$ (or the number of unknown force time histories) and (*ii*) stiffness and damping do not change within these k_1 time steps. If $ns \leq r$ or the locations of applied loads are not known, this method cannot be used. The smallest value for k_1 is $(n + 3)$. For cases where ns is small and r is not much smaller than ns, k_1 may be extremely large to make the method impractical. If stiffness and damping change slowly (less than 0.1% within k_1 time steps), then the values computed are averaged values, otherwise the results may not accurately represent the stiffness and damping matrices of the damaged structure. If the measured time histories are long, then consecutive segments of k_1 time steps of data may be used and the changes of $\mathbf{D}_d$ and $\mathbf{K}$ with time segments can be monitored. In fact, how the damage evolves with time may be captured, or if only the final state is of interest, the final $\mathbf{K}$ values can be used with knowledge of whether it has stabilized. It is possible to track how damping and stiffness matrices vary with time in greater resolution by using a moving time segment at the expense of significantly larger computational effort.

In formulating the algorithm to estimate the stiffness matrix from acceleration responses, the premise is that unknowns should not be unnecessarily introduced in large size problems to ensure that reliable results are obtained. Hence, it is formulated assuming that the mass matrix is known and is valid if the structure suffers from mild damage and no mass is added to or removed from the structure. In such case, the mass

matrix can be evaluated from a finite element model of the reference structure and then substituted into Eq. (3.56) to form a system of nonlinear equations to solve for the unknown coefficients in the stiffness and damping matrices. If the structure experiences significant change in the mass matrix, then the mass matrix coefficients also need to be estimated. The unknowns in Eq. (3.56) will increase by $n(n + 1)/2$ entries and the number of time steps of acceleration data required to solve for the unknown becomes

$$k_1 n \geq \frac{n(n+1)}{2} \times 3 + k_1(n - ns) + 2n + k_1 r \Rightarrow k_1 \geq \frac{n(3n+7)}{2(ns-r)} \tag{3.57a}$$

From Eq. (3.57), if the number of measured data points along the time axis (k_1) is fixed, the number of required sensors can be computed as follows

$$ns \geq r + \frac{n(n+3)}{k_1} \tag{3.58}$$

Incorporating with the requirement of the intersection scheme in Section 2.6.1 to identify the actual damaged elements from the set of *PDE*, the minimal number of sensors used should be the maximum value of 3 and $[r + n(n+3)/k_1]$.

3.4 OPTIMAL SENSOR PLACEMENT

3.4.1 Background

The accuracy of the stiffness matrix identified using the procedure presented in Section 3.3 depends very much on the quality of the acceleration responses which substantially depend on the number, locations and directions of the sensors used. Optimal sensor placement has therefore attracted many researchers (Naimimohasses et al., 1995; Meo and Zumpano, 2005). The challenging problem of optimal sensor placement is to maximize damage information, that is, sensor locations should be chosen such that they produce reliable and sensitive information on the potential

damage of the structure which is not known *a priori*. To achieve that purpose, the general idea is to estimate the optimal number and locations of sensors such that the resulting measured data are most informative based on the simulated responses of the structure.

To estimate the optimal number of sensors, sensors which correspond to the minimal contribution to a specified objective function will be deselected. For example, the Eigenvalue Vector Product (EVP) (Doebling, 1996) maximizes the vibration energy by eliminating sensors which are placed on the nodal lines of the vibration modes; the Effective Independence (EFI) method (Kammer and Brillhart, 1996) tries to maximize the Fisher information matrix determinant by omitting sensors which contribute the least to the first *nm* targeted mode shapes of the structure. These two classes of methods usually come up with a configuration of sensors which concentrates sensors into the high energy content regions, leading to inaccurate global information of the structures. Alternatively, Liu et al. (2008) used GA algorithm with the fitness function is Modal Strain Engergy (MSE) and Modal Assurance Criterion (MAC) to identify the optimal number of sensors. In particular, from a large number of sensors, mode shapes can be evaluated. By omitting sensor which affects the least on the estimated mode shapes, the new number of sensors is retrieved. The procedure is iterated until a pre-defined error is observed, resulting in optimal number and locations of sensors. However, computational intensive is the major obstacle in applying the method for large structure with many *DOF*.

In the following section, an algorithm is proposed to address 2 issues, namely (1) with *ns* sensor available, find the optimal locations to place the sensors; and (2) find the minimal number of sensors such that damage detection result by the *DLV* method

is reliable. The algorithm is formulated within the frame work of structural damage detection using the *DLV* method.

3.4.2 Optimal sensor placement algorithm

Consider an *n-DOF* structure with *ns* sensors attached. The structural stiffness matrix can be formulated using its parameters at the reference state based on which an (*ns* × *ns*) stiffness matrix, which corresponds to the *ns* sensor locations, can be extracted and denoted as $\mathbf{K}_u$. If the locations of the excitations are known, another stiffness matrix can be formulated following the procedure presented in Section 3.3 using the *ns* simulated acceleration responses and denoted as $\mathbf{K}_n$. The relationship between the number of sensors used and the error in the estimated stiffness matrix can be represented by

$$e_{ns} = \frac{1}{ns^2} \sum_{i=1}^{ns} \sum_{j=1}^{ns} \frac{\left| r_{ij}^u - r_{ij}^n \right|}{r_{ij}^u} \tag{3.59}$$

where r_{ij}^u and r_{ij}^n are the components at row *i* and column *j* of the stiffness matrices $\mathbf{K}_u$ and $\mathbf{K}_n$, respectively.

For an *n-DOF* structure, there are *n*!/[*ns*!(*n*-*ns*)!] configurations where *ns* sensors can be located to monitor acceleration responses. The error in the estimated stiffness matrix for each configuration computed using Eq. (3.59) is used to identify the optimal locations of sensors. The configurations provide the smallest e_{ns} are selected as those which associated with the optimal sensor locations. To minimize the number of sensors used, the above procedure is repeated with one sensor is reduced after each iteration. The number of sensors is considered minimal if e_{ns} exceeds the limit error beyond which the *DLV* method cannot provide reliable results. The whole procedure is summarized in Fig. 3.1.

The procedure works provided that $ns \geq 2$ since it is the requirement to formulate the stiffness matrix from acceleration responses presented in Section 3.3. Incorporating with the requirement of the Intersection Scheme in Section 2.6.1 gives $ns \geq 3$.

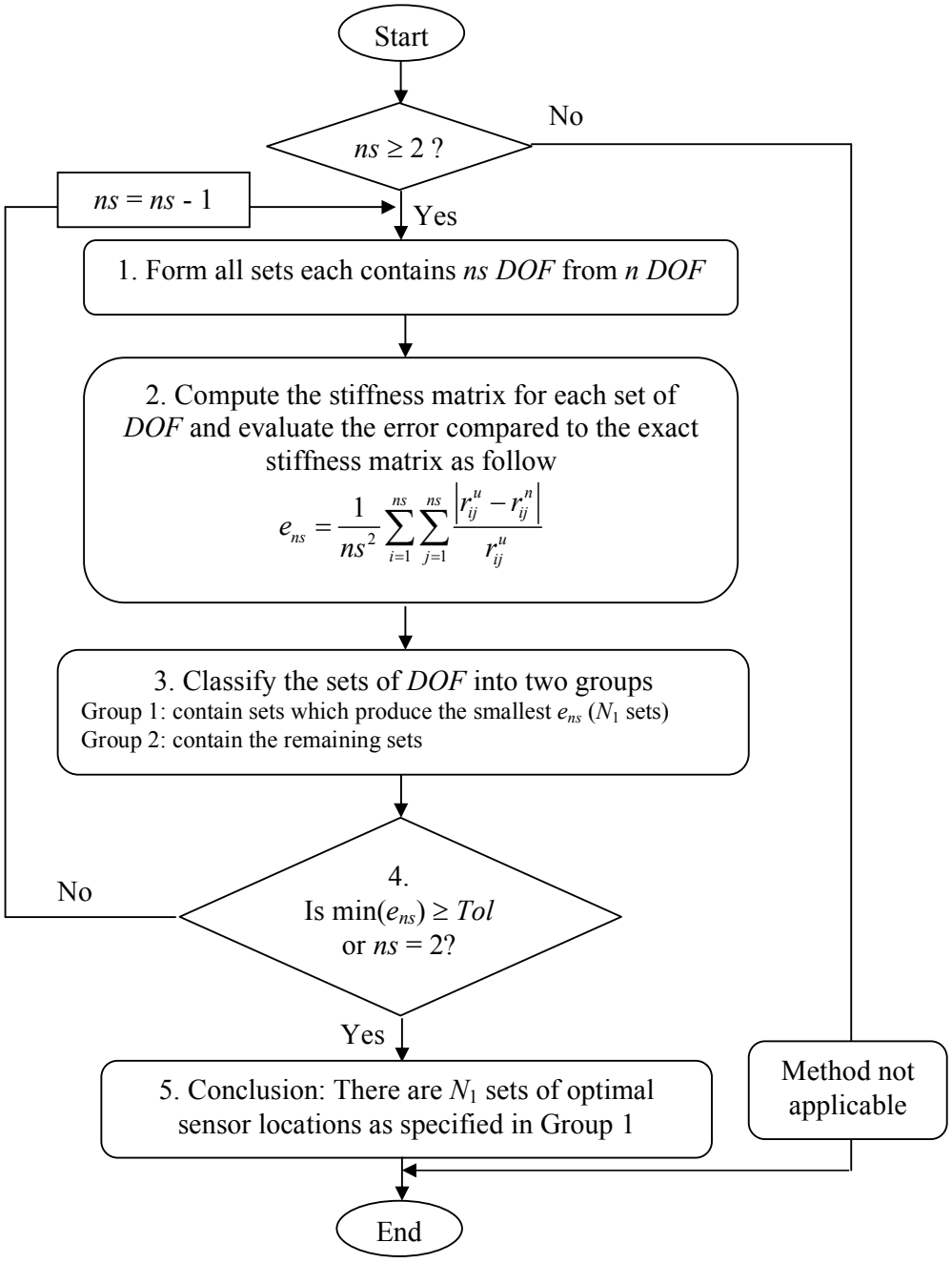

Fig. 3.1. Flow chart for optimal sensor placement

3.5 NUMERICAL AND EXPERIMENTAL EXAMPLES

Performance of the *DLV* method with known excitation can be found in Bernal (2002). This section investigates the performance of the *DLV* method with unknown excitation.

3.5.1 Numerical example

The 2-D warehouse frame structure used in Section 2.5 is considered here (see Fig. 2.4 and Table 2.1). The *DOF* of the structure are shown in Fig. 3.2. Two cases of damage are investigated, namely (a) element 14 is damaged; and (b) elements (7, 14) are damaged. Damage is simulated by imposing a reduction of 20% in the flexural stiffness (*EI*) of column element 7 all along its length whereas for truss member 14, a 20% reduction in axial stiffness (*EA*) all along its length is imposed to simulate its damage. Zero-mean white noise load with *RMS* of 30 N shown in Fig. 3.3 is employed to excite the structure at node 9 horizontally. Acceleration responses horizontally at nodes (4, 6, 8, 9, 10, 13) and vertically at nodes (5, 7, 11, 12) are monitored using a sampling rate of 1kHz. These accelerations are employed directly to identify structural parameters without any post-processing process.

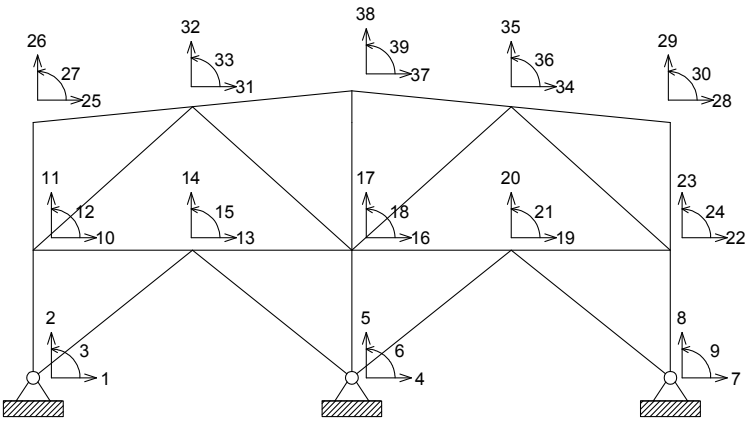

Fig. 3.2. *DOF* of 2-D warehouse structure

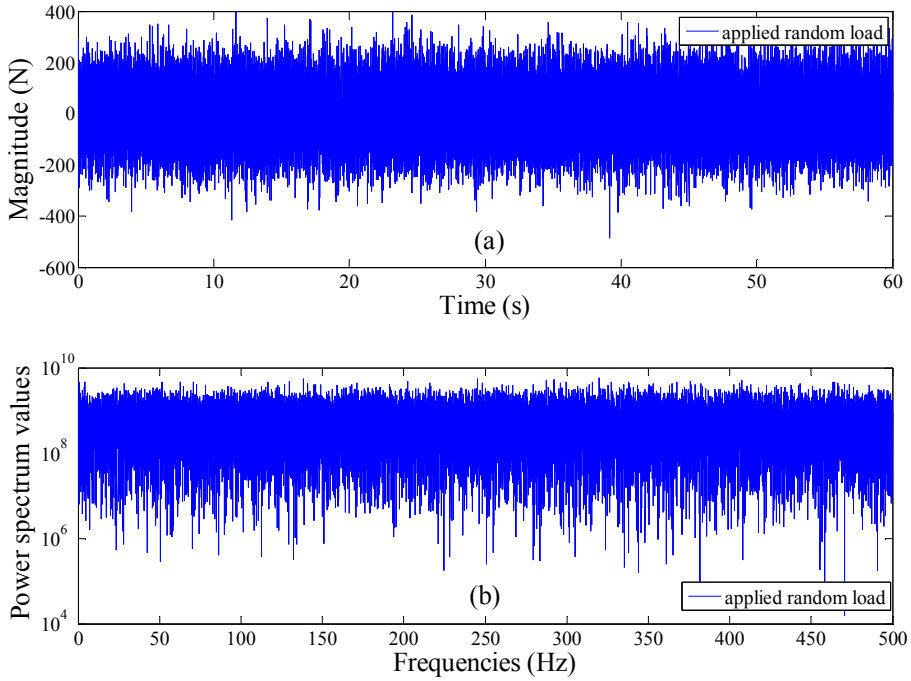

Fig. 3.3. Applied random load onto 2-D warehouse structure with sampling rate of 1 kHz: (a) variation of magnitude with time, and (b) variation of power spectral values with frequencies

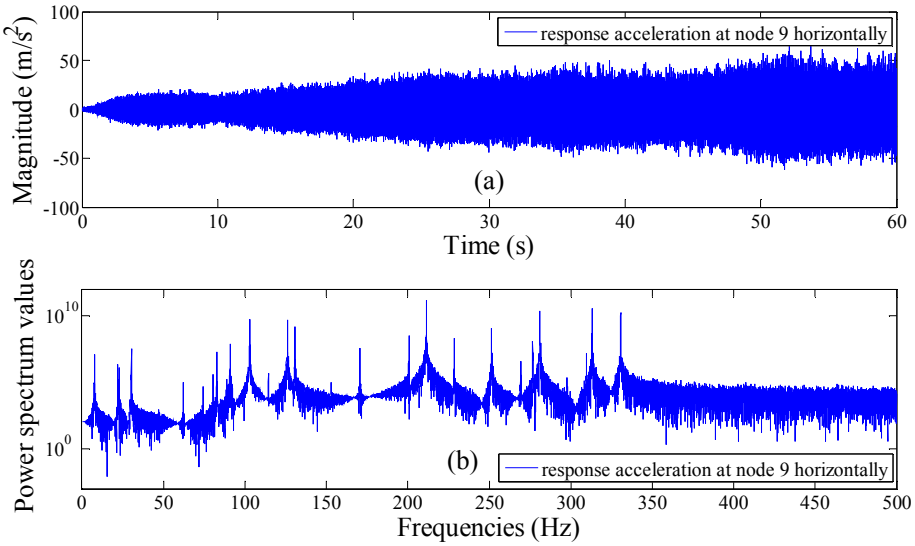

Fig. 3.4. Horizontal response accelerations at node 9: (a) variation of magnitude with time, and (b) variation of power spectral values with frequencies (structure healthy)

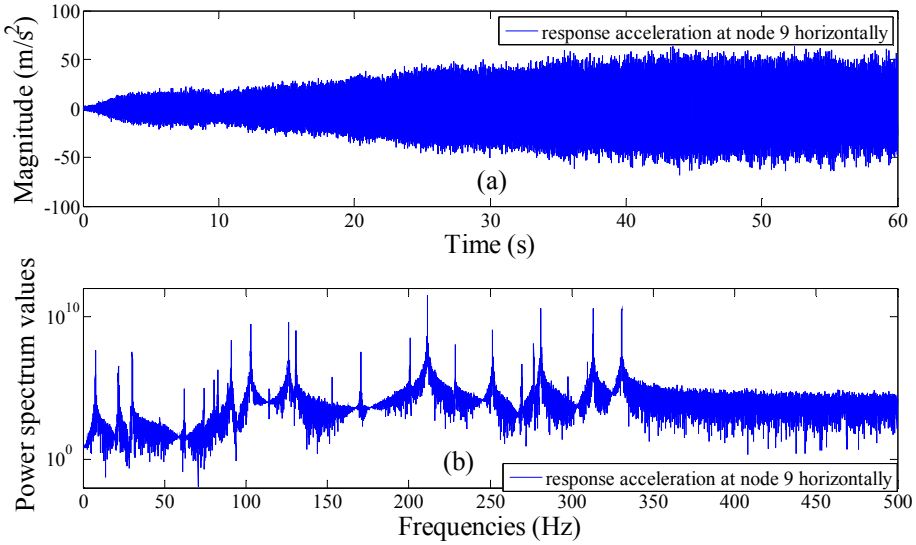

Fig. 3.5. Horizontal response accelerations at node 9: (a) variation of magnitude with time, and (b) variation of power spectral values with frequencies (element 14 damaged)

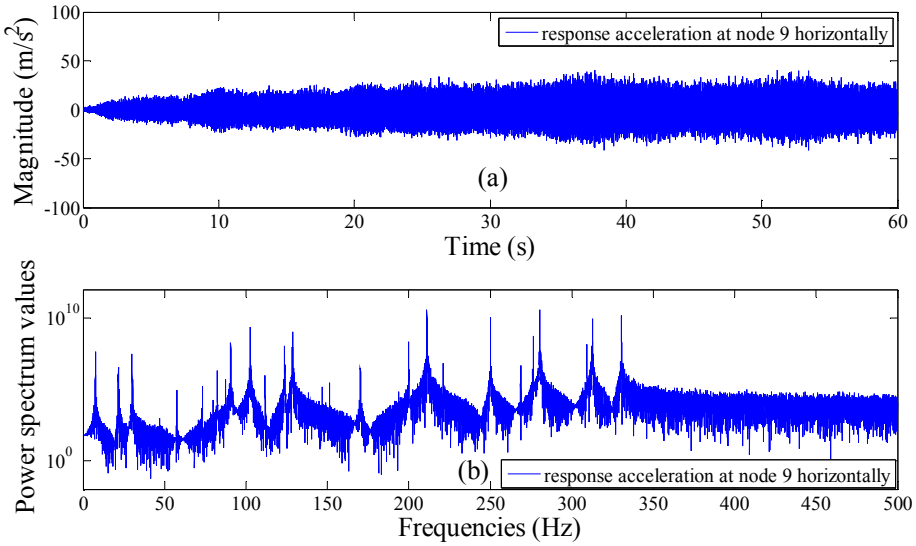

Fig. 3.6. Horizontal response accelerations at node 9: (a) variation of magnitude with time, and (b) variation of power spectral values with frequencies (elements 7 & 14 damaged)

Horizontal acceleration responses at node 9 for different states of the structure are plotted in Figs. 3.3-3.6. Since the structure has 33 unrestrained *DOF* (n = 33), dynamically excited at 1 location (r = 1) and the acceleration responses are measured

by 10 accelerometers (*ns* = 10), each time segment requires 132 time steps following Eq. (3.57). There are 454 time segments altogether. Performing the proposed procedure in Section 3.3 for the three states where (1) the structure is healthy; (2) element 14 is damaged; and (3) elements (7, 14) are damaged, their corresponding structural stiffness matrices identified. From the change in structural stiffness matrix, the *DLV* set is calculated. The intersection scheme proposed in Section 2.6.1 is next employed to identify the actual damaged elements.

For the case where element 14 is damaged, by applying the *DLV* set onto the reference structural model as nodal displacement vectors, the *NCE* of all elements are computed and the set of *PDE* which includes elements (14, 17) is identified. Therefore, the current *IDS* contains elements (14, 17) and *ne* = 2. By omitting data from readings of the sensor at node 4 which is far away from members of the current *IDS*, the stiffness matrix at the remaining 9 sensor locations is computed based on the remaining 9 sensor readings following the method in Section 3.3. Comparing the identified and the reference stiffness matrices, the change in the stiffness matrix is computed. By performing *SVD* on the change in the stiffness matrix, another set of *DLV*s is identified. By applying these *DLV*s onto the reference structural model as nodal displacement vectors, the *NCE* of all elements are computed and the set of *PDE* which contains element 14 is identified. Intersecting the set of *PDE* and the current *IDS* which contains elements (14, 17) produces element 14 as the new *IDS* (*ne* = 1). Similarly, by omitting the readings of the sensor at node 10, which is far away from the only member of the current *IDS*, instead of the sensor at node 4, another set of *PDE* containing elements (12, 14, 17) is identified. Intersecting the identified *PDE* with the current *IDS* which contains element 14 only gives element 14 as the new *IDS* (*ne* = 1). Since the *IDS* is the same for 2 consecutive steps, the iteration is terminated and

element 14 is identified correctly as the actual damaged element. The procedure is summarized in the upper portion of Table 3.1. Similarly for the case where elements (7, 14) are damaged, the feasibility of the method is confirmed by the results shown in the lower portion of Table 3.1.

Table 3.1. Damage detection of 2-D warehouse structure (noise free)

	Set No.			Set of sensors includes sensors at nodes	*PDE*	Eliminated elements	*IDS*	*ne*
Element 14 damaged	1		ns =10	[4, 5, 6, 7, 8, 9, 10, 11, 12, 13]	[14, 17]		[14, 17]	2
	2	$k=ns$ -1=9	i =1	[5, 6, 7, 8, 9, 10, 11, 12, 13]	[14]	17	[14]	1
	3		i =2	[4, 5, 6, 7, 8, 9, 11, 12, 13]	[12, 14, 17]		[14]	1
Elements (7, 14) damaged	1		ns =10	[4, 5, 6, 7, 8, 9, 10, 11, 12, 13]	[1, 4, 7, 13, 14]		[1, 4, 7, 13, 14]	5
	2	$k=ns$ -1=9	i =1	[4, 5, 6, 7, 8, 9, 11, 12, 13]	[7, 12, 14]	1, 4, 13	[7,14]	2
	3		i =2	[4, 5, 6, 7, 8, 10, 11, 12, 13]	[1, 7, 13, 14, 17]		[7,14]	2

Effect of Noise on Damage Detection Results

To investigate the effect of noise on the performance of the proposed methodology, the above example is used and zero-mean white noise with *RMS* of (*i*) 5%, and (*ii*) 10% of the *RMS* of the response accelerations is added to all simulated response accelerations to generate contaminated responses. From contaminated responses, the method in Section 3.3 is employed again to compute the structural stiffness matrices for the three states where (1) the structure is healthy; (2) element 14 is damaged; and (3) elements (7, 14) are damaged. From the change in structural stiffness matrix, *SVD* is employed to identify the set of *DLV*s.

For the case where element 14 is damaged and the acceleration responses contain 5% noise, applying the identified *DLV*s onto the reference structure as nodal

displacement vectors, the *NCE* of all elements are computed and the first set of *PDE* which includes 6 elements (4, 6, 12, 13, 14, 17) is identified. These 6 elements are assigned the current *IDS* (*ne* = 6). By omitting the readings of the sensor at node 4, which is not close to members of the current *IDS* set, and employing the method in Section 3.3 on the remaining 9 sensor readings, the stiffness matrix with respect to the remaining 9 sensor locations is computed. Comparing the identified and the reference stiffness matrices, the change in the stiffness matrix is evaluated, based on which *SVD* is performed to identify another set of *DLV*s. Applying these *DLV*s onto the reference structural model as nodal displacement vectors, the *NCE* of all elements are evaluated and the set of *PDE* which includes elements (1, 8, 10, 14) is identified. Taking the intersection between the set of *PDE* and the current *IDS* which contains elements (4, 6, 12, 13, 14, 17) gives element 14 as the new *IDS* (*ne* = 1). Similarly, by omitting the readings of the sensor at node 10, which is far away from the only member of the current *IDS* set, instead of the sensor at node 4, another set of *PDE* comprising elements (5, 14, 16) is identified. The intersection of the set of *PDE* and the current *IDS* which contains element 14 only produces element 14 as the new *IDS* (*ne* = 1). Since the *IDS* for 2 consecutive steps are identical, the iteration is stopped and element 14 is classified as damaged which matches the actual simulation. The procedure is summarized in the upper portion of Table 3.2. The same computation is performed for the case of 10% noise and the results in the lower portion of Table 3.2 support the feasibility of the proposed methodology. Similar trends are observed for the case where elements (7, 14) are damaged and response accelerations are contaminated with noise where the results are presented in Table 3.3.

Table 3.2. Damage detection of 2-D warehouse structure (element 14 damaged, noise presence)

	Set No.			Set of sensors includes sensors at nodes	*PDE*	Eliminated elements	*IDS*	*ne*
5% noise	1		ns=10	[4, 5, 6, 7, 8, 9, 10, 11, 12, 13]	[4, 6, 12, 13, 14, 17]		[4, 6, 12, 13, 14, 17]	6
	2	$k = ns - 1 = 9$	i = 1	[5, 6, 7, 8, 9, 10, 11, 12, 13]	[1, 8, 10, 14]	[4, 6, 12, 13, 17]	[14]	1
	3		i = 2	[4, 5, 6, 7, 8, 9, 11, 12, 13]	[5, 14, 16]		[14]	1
10% noise	1		ns=10	[4, 5, 6, 7, 8, 9, 10, 11, 12, 13]	[3, 8, 9, 13, 14, 16, 18, 20, 21, 22]		[3, 8, 9, 13, 14, 16, 18, 20, 21, 22]	10
	2	$k = ns - 1 = 9$	i = 1	[5, 6, 7, 8, 9, 10, 11, 12, 13]	[1, 4, 7, 14, 17]	[3, 8, 9, 13, 16, 18, 20, 21, 22]	[14]	1
	3		i = 2	[4, 5, 6, 7, 8, 9, 11, 12, 13]	[5, 7, 14, 19]		[14]	1

Table 3.3. Damage detection of 2-D warehouse structure (elements 7 & 14 damaged, noise presence)

	Set No.			Set of sensors includes sensors at nodes	*PDE*	Eliminated elements	*IDS*	*ne*
5% noise	1		ns=10	[4, 5, 6, 7, 8, 9, 10, 11, 12, 13]	[1, 4, 6, 7, 11, 14, 18, 22]		[1, 4, 6, 7, 11, 14, 18, 22]	8
	2	$k = ns - 1 = 9$	i = 1	[5, 6, 7, 8, 9, 10, 11, 12, 13]	[2, 5, 7, 12, 14, 15, 16, 21]	[1, 4, 6, 11, 18, 22]	[7, 14]	2
	3		i = 2	[4, 5, 6, 7, 8, 9, 11, 12, 13]	[1, 3, 7, 11, 13, 14, 17]		[7, 14]	2
10% noise	1		ns=10	[4, 5, 6, 7, 8, 9, 10, 11, 12, 13]	[1, 4, 6, 7, 12, 14, 15, 16, 18, 22]		[1, 4, 6, 7, 12, 14, 15, 16, 18, 22]	10
	2	$k = ns - 1 = 9$	i = 1	[5, 6, 7, 8, 9, 10, 11, 12, 13]	[2, 5, 7, 11, 13, 14, 20, 21]	[1, 4, 6, 12, 15, 16, 18, 22]	[7, 14]	2
	3		i = 2	[4, 5, 6, 7, 8, 9, 11, 12, 13]	[2, 3, 6, 7, 11, 13, 14, 17, 21, 22]		[7, 14]	2

Effect of Gradual Reduction in Element Stiffness on Damage Detection Results

To investigate the feasibility of the algorithm presented in Section 3.3 in estimating the gradual change in structural parameters, two cases are simulated, namely (a) element 14 is gradually damaged; and (b) elements (7, 14) are gradually damaged. The speed of degradation in element stiffness is 3.78% per second (or equivalently 0.05% reduction in axial stiffness per measurement segment of 132 time steps for element 14 and 0.05% reduction in flexural stiffness per measurement

segment of 132 time steps for element 7). The same random load used above is employed to excite the structure. Acceleration responses at the same 10 *DOF* used above are monitored. For the case where element 14 is gradually damaged, performing the procedure presented in Section 3.3, structural stiffness coefficients are identified with time. Some selected coefficients are plotted in Fig. 3.7. From the difference in identified structural stiffness matrices at the first and the last time segments, the change in structural stiffness is evaluated based on which the *DLV* set is computed. Applying the *DLV* set onto the reference structural model as nodal displacement vectors, the *NCE* of all elements are computed and the set of *PDE* which includes elements (4, 14, 15) is identified as shown in the upper portion of Table 3.4. The 3 elements are assigned as the current *IDS* (*ne* = 3). By omitting the readings of the sensor at node 13, another set of *PDE* containing elements (2, 5, 7, 13, 14, 19) is identified and intersected with the current *IDS* which contains elements (4, 14, 15) gives element 14 as the new *IDS* (*ne* = 1). By omitting the readings of the sensor at node 9 instead of the sensor at node 13, another set of *PDE* which comprises elements (4, 7, 14, 16, 19) is identified. Intersecting the set of *PDE* and the current *IDS*, which comprises element 14, produces element 14 as the new *IDS* (*ne* = 1). Hence, element 14 is classified as being damaged following the criterion of 2 identical *IDS*. The same trend is also observed for the case where elements (7, 14) are gradually damaged based on the results shown in Fig. 3.8 and the lower portion of Table 3.4.

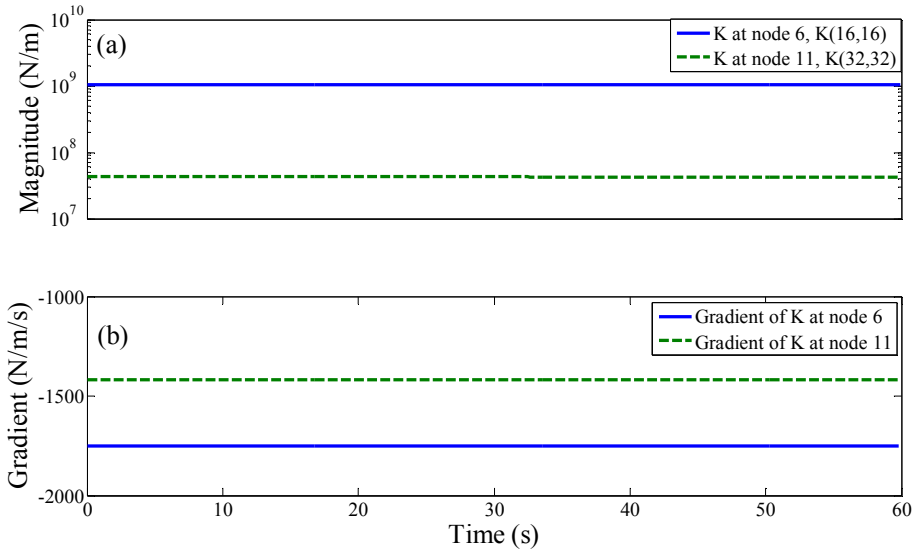

Fig. 3.7. (a) Variation of stiffness coefficients with time; and (b) gradient of variation of stiffness coefficients with time (element 14 damaged)

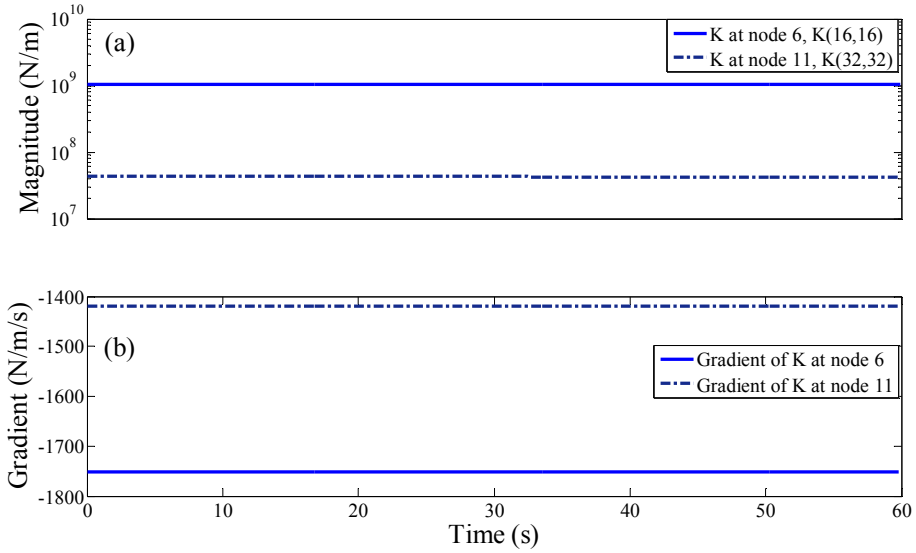

Fig. 3.8. (a) Variation of stiffness coefficients with time; and (b) gradient of variation of stiffness coefficients with time (elements 7 & 14 damaged)

Table 3.4. Damage detection of 2-D warehouse structure (gradual reduction in stiffness parameters)

	Set No.		Set of sensors includes sensors at nodes	*PDE*	Eliminated elements	*IDS*	*ne*
Element 14 damaged	1	ns =10	[4, 5, 6, 7, 8, 9, 10, 11, 12, 13]	[4, 14, 15]		[4, 14, 15]	3
	2	i = 1	[4, 5, 6, 7, 8, 9, 10, 11, 12]	[2, 5, 7, 13, 14, 19]	[4, 15]	[14]	1
	3	i = 2	[4, 5, 6, 7, 8, 10, 11, 12, 13]	[4, 7, 14, 16, 19]		[14]	1
Elements 7 & 14 damaged	1	ns =10	[4, 5, 6, 7, 8, 9, 10, 11, 12, 13]	[2, 4, 6, 7, 13, 14, 15, 17, 19, 20, 21]		[2, 4, 6, 7, 13, 14, 15, 17, 19, 20, 21]	11
	2	i = 1	[4, 5, 6, 7, 8, 9, 10, 11, 12]	[3, 7, 14, 16, 22]	[2, 4, 6, 13, 15, 17, 19, 20, 21]	[7, 14]	2
	3	i = 2	[4, 5, 6, 7, 8, 10, 11, 12, 13]	[3, 4, 5, 7, 14, 16, 22]		[7, 14]	2

$k = ns - 1 = 9$

Effect of Change in Mass of Damaged Elements on Damage Detection Results

To investigate the effect of error induced by the change in the mass of the damaged elements on the damage detection results, the mass density of the damaged elements is reduced from 1% to 100% when the structure changes from the reference to the damaged states. The same excitation force in Fig. 3.3 is used to excite the structure and the same 10 acceleration responses horizontally at nodes (4, 6, 8, 9, 10, 13) and vertically at nodes (5, 7, 11, 12) are monitored. The stiffness of the structure at the reference state can be formulated as before using the procedure presented in Section 3.3. For the case where element 14 is damaged, the procedure presented in Section 3.3 can also be employed to estimate the stiffness matrix with either unknown or known mass assumption. In the latter, the mass matrix of the structure at the reference state is used to estimate the stiffness matrix of the structure at both the reference and the damaged states. Comparison of some identified stiffness coefficients with the exact values is plotted in Fig. 3.9, indicating that the error due to the assumption that the mass does not change when the structure changes from the reference to the damaged state does not significantly affect the accuracy of the estimation results. It is observed that 100% reduction in mass density of element 14

results in approximately 0.6% error in the estimated stiffness matrix, which is acceptable in most damage detection methods. From the difference in the stiffness matrix between the reference and the damaged states computed using the assumption of known mass matrix, the intersection scheme is performed and the damaged element is identified correctly with identical results to the case where the mass of the damaged element is unchanged as shown in Table 3.1.

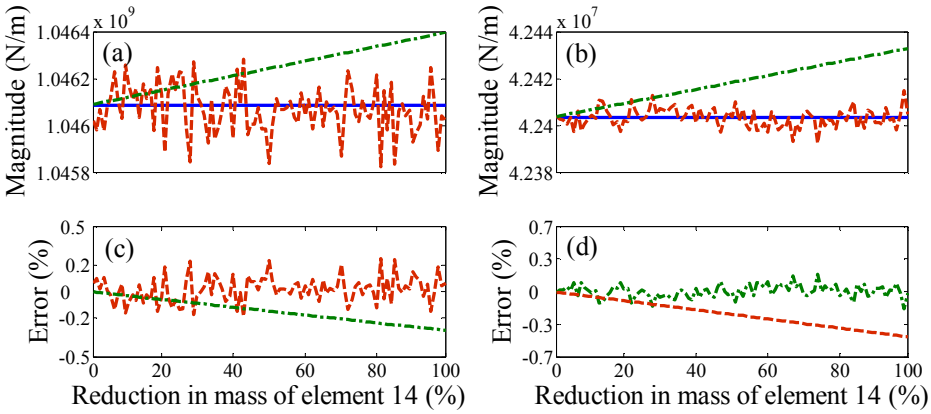

Fig. 3.9. Comparison between exact and estimated stiffness coefficients: (a) K(16,16); (b) K(32,32); and (c) and (d) error between exact and estimated stiffness coefficients for K(16,16) and K(32,32), respectively. Continuous line (—): exact stiffness coefficients; dashed line (---): estimated stiffness coefficients assuming that mass is unknown; and dashed-dotted line (-·-): estimated stiffness coefficients assuming that mass is known (unchanged).

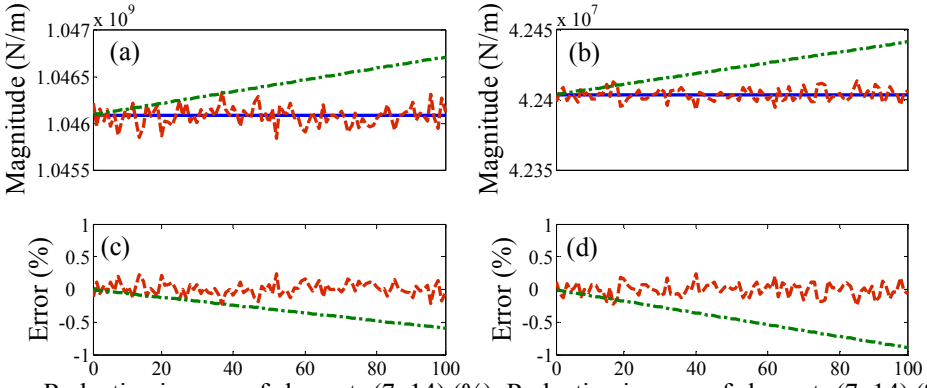

Fig. 3.10. Comparison between exact and estimated stiffness coefficients: (a) K(16,16); (b) K(32,32); and (c) and (d) error between exact and estimated stiffness coefficients for K(16,16) and K(32,32), respectively. Continuous line (—): exact stiffness coefficients; dashed line (---): estimated stiffness coefficients assuming that mass is unknown; and dashed-dotted line (-·-): estimated stiffness coefficients assuming that mass is known (unchanged).

Similarly, for the case where elements (7, 14) are damaged, performing the same procedure as above, the results of some stiffness coefficients identified using the assumption that the mass matrix is unknown and known (unchanged) are compared with the exact values in Fig. 3.10. In this case, using unknown mass assumption to estimate stiffness matrix provides better results than using known (unchanged) mass assumption since the corresponding errors are 0.3% and 0.9% which is associated with the case of 100% reduction in mass density of the damaged elements. However, performing the intersection scheme, the damaged elements are still identified correctly with identical results to the case where the mass of the damaged elements are constant which is shown in Table 3.2.

Performance of the Optimal Sensor Placement Algorithm

To assess the performance of the optimal sensor placement presented in Section 3.4, assuming that the maximum number of sensors available is 10, which are enough to place at all nodes of the structure, the requirements are (*i*) to identify the optimal locations to place the 10 sensors; and (*ii*) to identify the minimum number of sensors which can be used to obtain reliable damage detection results by the *DLV* method. Performing the algorithm in Section 3.4, the optimal locations to place the 10 available sensors are at *DOF* (10, 14, 16, 20, 22, 25, 28, 32, 35, 37) with the corresponding error of 0.12%. The summarized results for the optimal sensor placement are plotted in Fig. 3.11 and Table 3.5. It is observed that the optimal configuration to place the sensors always includes the sensor collocated with the actuator. The maximum error in the identified stiffness matrix for the case where only 2 sensors are used is less than 5%. With only 2 sensors are available and placed at the optimal locations the actual damaged elements can still be identified correctly in the sets of *PDE*. For the case where element 14 is damaged and 2 sensors used, the set of *PDE* includes elements (2,

3, 4, 5, 8, 9, 10, 11, 13, 14) whereas the set of *PDE* comprises elements (2, 3, 4, 5, 6, 7, 8, 9, 10, 11, 13, 14) for the case where elements (7, 14) are damaged and 2 sensors are used. However, no subsequent combination of sensors is available to filter out the actual damaged elements, resulting in false alarm.

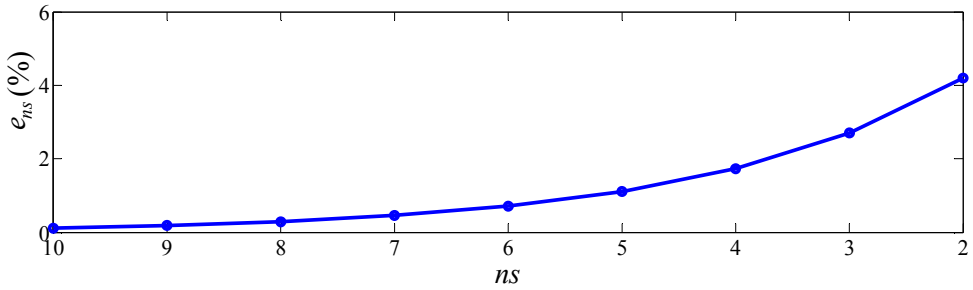

Fig. 3.11. Relationship between number of sensors and error in the identified stiffness matrix for the optimal sensor placement of 2-D warehouse structure

Table 3.5. Optimal sensor placement results for 2-D warehouse structure

ns	Sensors at *DOF*	Sensors at nodes	e_{ns} (%)
10	(10, 14, 16, 20, 22, 25, 28, 32, 35, 37)	(4, 5, 6, 7, 8, 9, 10, 11, 12, 13)	0.1223
9	(10, 14, 20, 22, 25, 28, 32, 35, 37)	(4, 5, 7, 8, 9, 10, 11, 12, 13)	0.1871
8	(10, 14, 22, 25, 28, 32, 35, 37)	(4, 5, 8, 9, 10, 11, 12, 13)	0.2919
7	(10, 22, 25, 28, 32, 35, 37)	(4, 8, 9, 10, 11, 12, 13)	0.4552
6	(10, 22, 25, 28, 32, 37)	(4, 8, 9, 10, 11, 13)	0.7099
5	(10, 22, 25, 28, 37)	(4, 8, 9, 10, 13)	1.1072
4	(10, 25, 28, 37)	(4, 9, 10, 13)	1.7268
3	(25, 28, 37)	(9, 10, 13)	2.693
2	(25, 28)	(9, 10)	4.216

3.5.2 Experiment example

The 3-D modular truss used in Section 2.6.2 with specifications listed in Table 2.2 is set-up in this experiment as shown in Fig. 3.12 to obtain acceleration responses. A shaker with capacity of 75 lbs (334 N) is employed to excite the truss through an amplifier with a capacity of 50 V. Vertical acceleration responses of all nodes at the lower chord of the truss are monitored using 13 accelerometers with capacity of 50 g,

sampled at a rate of 1 kHz. Two cases of damage are investigated, namely (a) element 86 is damaged; and (b) elements (1, 86) are damaged. Damage is simulated by changing the affected members from steel to aluminum tubes (refer to Table 2.2 for specifications of the tubes).

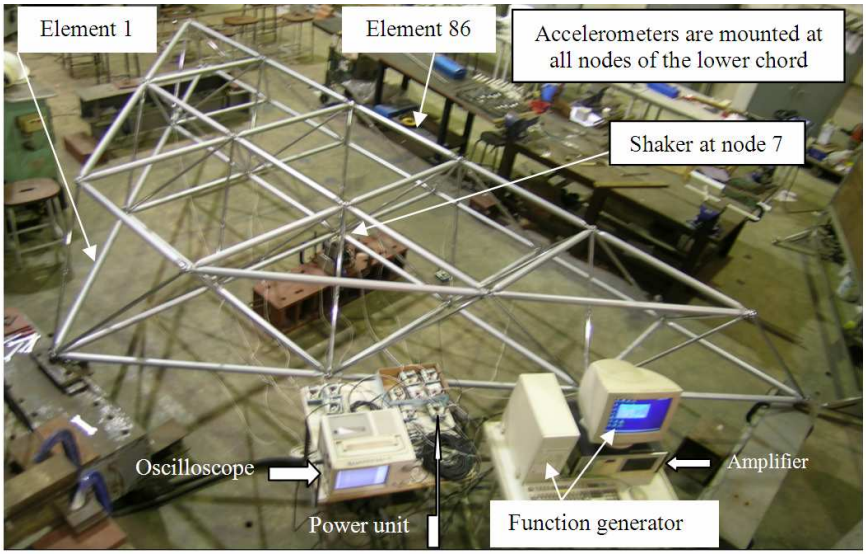

Fig. 3.12. Experimental set-up

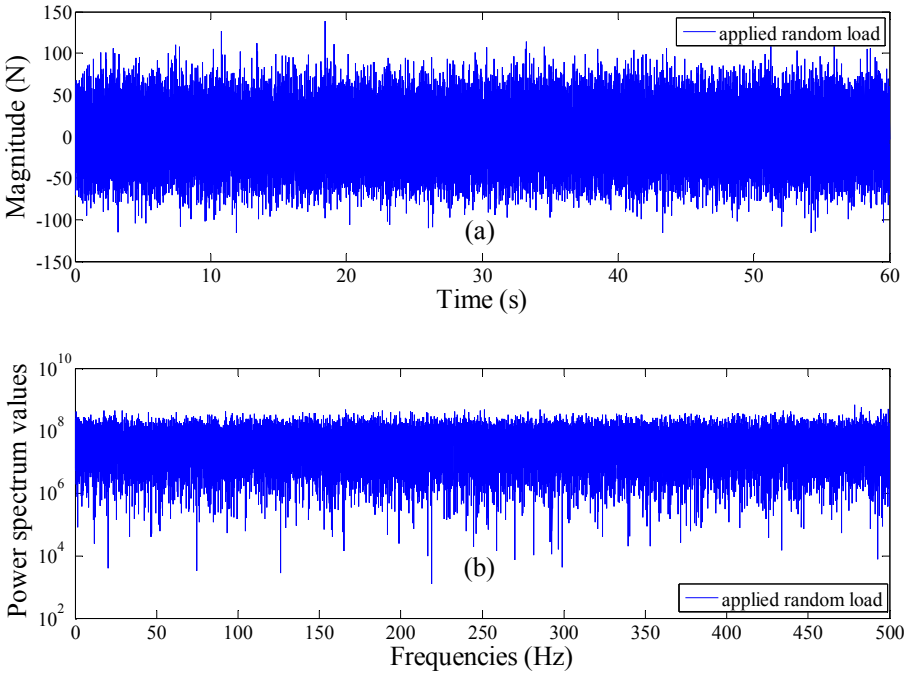

Fig. 3.13. Applied random load onto experimental truss with sampling rate of 1 kHz: (a) variation of magnitude with time, and (b) variation of power spectral values with frequencies (structure healthy)

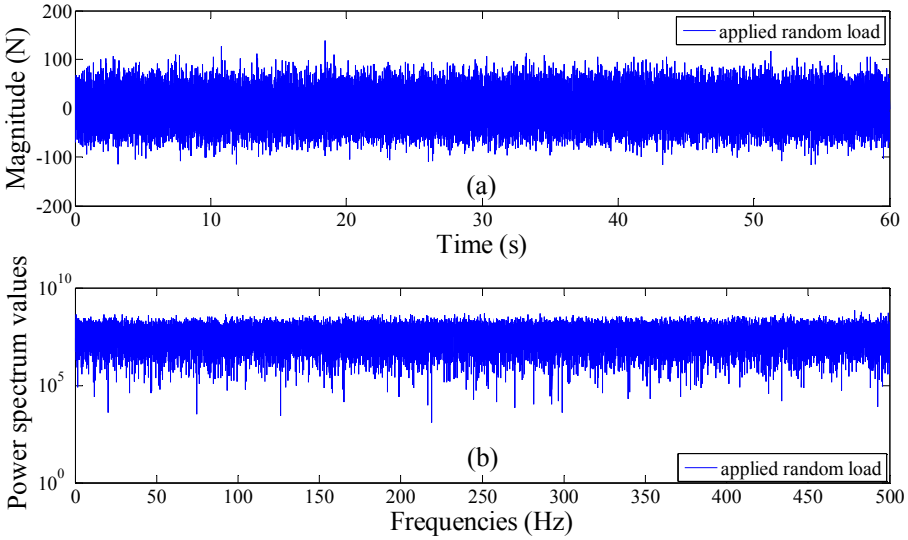

Fig. 3.14. Applied random load onto experimental truss with sampling rate of 1 kHz: (a) variation of magnitude with time, and (b) variation of power spectral values with frequencies (element 86 damaged)

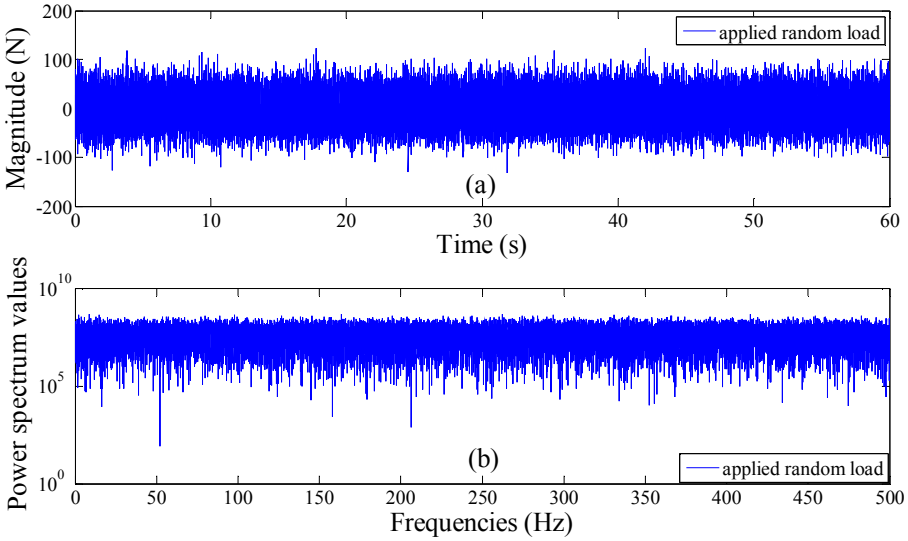

Fig. 3.15. Applied random load onto experimental truss with sampling rate of 1 kHz: (a) variation of magnitude with time, and (b) variation of power spectral values with frequencies (elements 1 & 86 damaged)

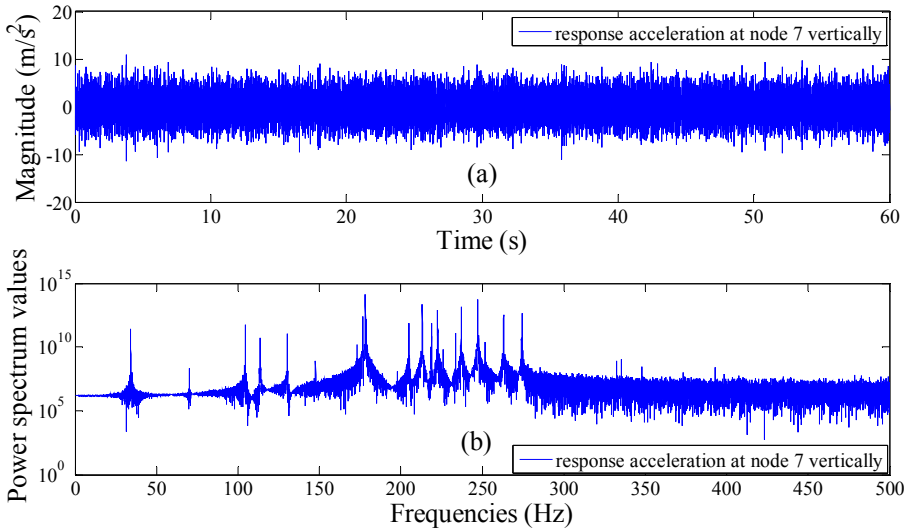

Fig. 3.16. Vertical response accelerations at node 7: (a) variation of magnitude with time, and (b) variation of power spectral values with frequencies (structure healthy)

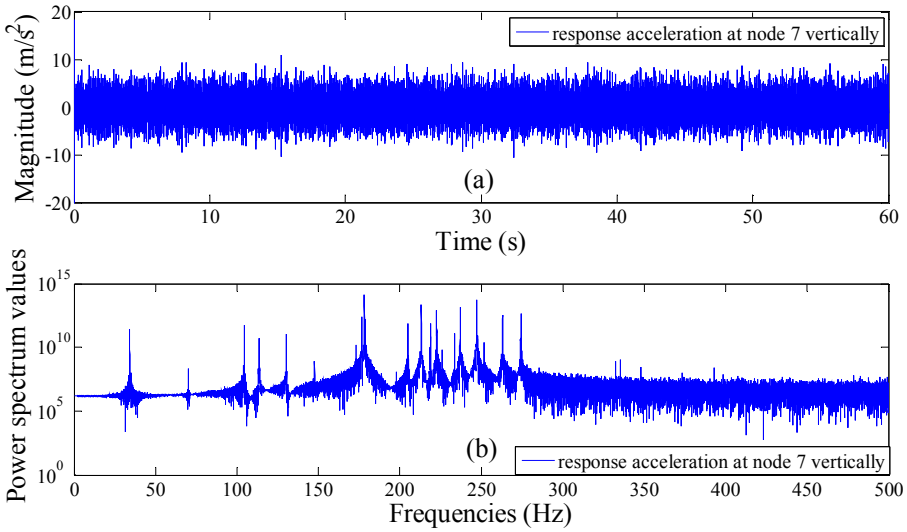

Fig. 3.17. Vertical response accelerations at node 7: (a) variation of magnitude with time, and (b) variation of power spectral values with frequencies (element 86 damaged)

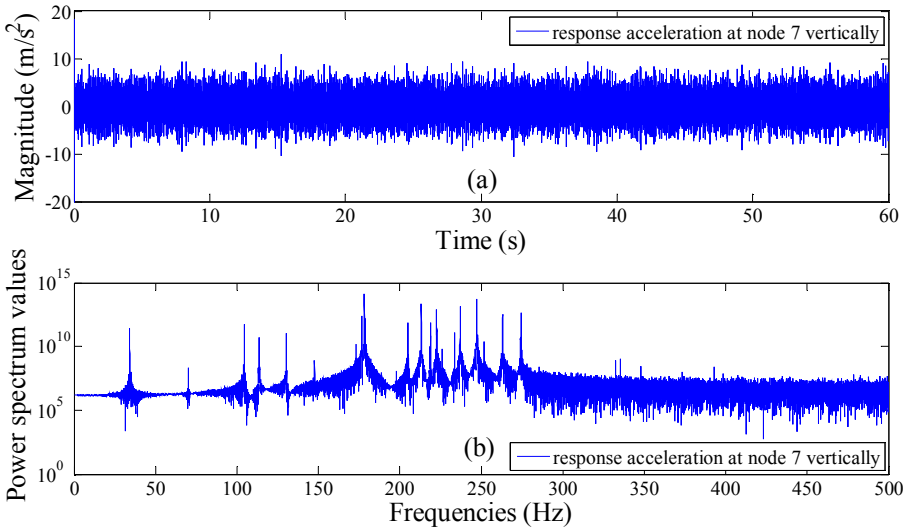

Fig. 3.18. Vertical response accelerations at node 7: (a) variation of magnitude with time, and (b) variation of power spectral values with frequencies (elements 1 & 86 damaged)

Zero-mean white noise loads with *RMS* of 30 N are employed to excite the structure at node 7 vertically. Three states are considered, where (*i*) the structure is healthy; (*ii*) element 86 is damaged; and (*iii*) elements (1, 86) are damaged. The applied loads are plotted in Figs. 3.13-3.15 and will be used later to compare the

structural damage detection results using the *DLV* method with known and unknown excitations. Vertical response accelerations at node 7 where there is a collocated sensor-actuator pair are plotted in Figs. 3.16-3.18 for the 3 different states of the structure.

For the case where element 86 is damaged, from 13 measured accelerations, the procedure presented in Section 3.3 is employed to identify the structural stiffness matrices at the reference and damaged states. From the change in structural stiffness matrix, *SVD* is performed to identify a set of *DLV*s. Applying these *DLV*s onto the reference structure, the *NCE* of all elements are computed and the set of *PDE* which comprises elements (16, 44, 86) is identified. The current *IDS* contains 3 elements (16, 44, 86) and *ne* = 3. By omitting the readings of the sensor at node 15 which is far away from members of the current *IDS* set, the structural stiffness matrix is identified based on the readings of the remaining 12 sensors. By comparing with the stiffness matrix at the reference state, the change in stiffness is computed based on which *SVD* is performed to identify another set of *DLV*s. Applying these *DLV*s onto the reference structure, another set of *PDE* which comprises elements (20, 55, 73, 75, 81, 86) is identified. Intersecting the set of *PDE* with the current *IDS* which contains elements (16, 44, 86) gives element 86 as the new *IDS* (*ne* = 1). Similarly, by omitting the readings of the sensor at node 9, which is far away from the only member of the current *IDS* set, instead of the sensor at node 15, another set of *PDE* which comprises elements (41, 45, 86) is identified. Intersection of the set of *PDE* and the current *IDS* which comprises element 86 only produces element 86 as the new *IDS*. Since the *IDS* for the 2 consecutive steps are identical, the iteration is terminated and element 86 is correctly identified as being damaged. The procedure is summarized in the upper portion of Table 3.6. Similarly, the feasibility of the methodology is confirmed for the

case where elements (1, 86) are damaged based on the results shown in the lower portion of Table 3.6.

Table 3.6. Damage detection of 3-D modular truss structure

	Set No.			Set of sensors includes sensors at nodes	*PDE*	Eliminated elements	*IDS*	*ne*
Element 86 damaged	1		*ns* =13	[2, 3, 4, 5, 6, 7, 8, 9, 11, 12, 13, 14, 15]	[16, 44, 86]		[16, 44, 86]	3
	2	$k = ns-1 = 12$	*i* = 1	[2, 3, 4, 5, 6, 7, 8, 9, 11, 12, 13, 14]	[20, 55, 73, 75, 81, 86]	[16, 44]	[86]	1
	3		*i* = 2	[2, 3, 4, 5, 6, 7, 8, 11, 12, 13, 14, 15]	[41, 45, 86]		[86]	1
Elements 1 & 86 damaged	1		*ns* =13	[2, 3, 4, 5, 6, 7, 8, 9, 11, 12, 13, 14, 15]	[1, 56, 61, 70, 86]		[1, 56, 61, 70, 86]	5
	2	$k = ns-1 = 12$	*i* = 1	[2, 3, 4, 5, 6, 7, 8, 9, 11, 12, 13, 14]	[1, 20, 44, 45, 58, 86]	[56, 61, 70]	[1, 86]	2
	3		*i* = 2	[2, 3, 4, 5, 6, 7, 8, 11, 12, 13, 14, 15]	[1, 21, 70, 86]		[1, 86]	2

To compare the performance of the two procedures based on known and unknown excitations in assessing structural damage, the input excitations and response accelerations of the 13 accelerometers are fed in the procedure presented in Section 3.2 to identify structural flexibility matrices with respect to the sensor locations for the reference and the damaged states. From the change in the flexibility matrix, *SVD* is performed to identify a set of *DLV*s. Applying these *DLV*s onto the reference structure as nodal force vectors at sensor locations, the *NCE* of all elements can be computed and the set of *PDE* is identified. For the case where element 86 is damaged, the *NCE* of all elements computed using the known and unknown input excitations are compared in Fig. 3.19a. With a threshold of 0.01 to discriminate the potential damaged elements from the undamaged elements, the 2 procedures produce the same set of *PDE* though the procedure based on known excitation is a little more sensitive. This result agrees well with the suggestion by Mevel et al. (2003) that the measured input excitations should be included where possible to enhance the reliability of the damage

detection results. The same conclusion is also observed for the case where elements (1, 86) are damaged based on results in Fig. 3.19b.

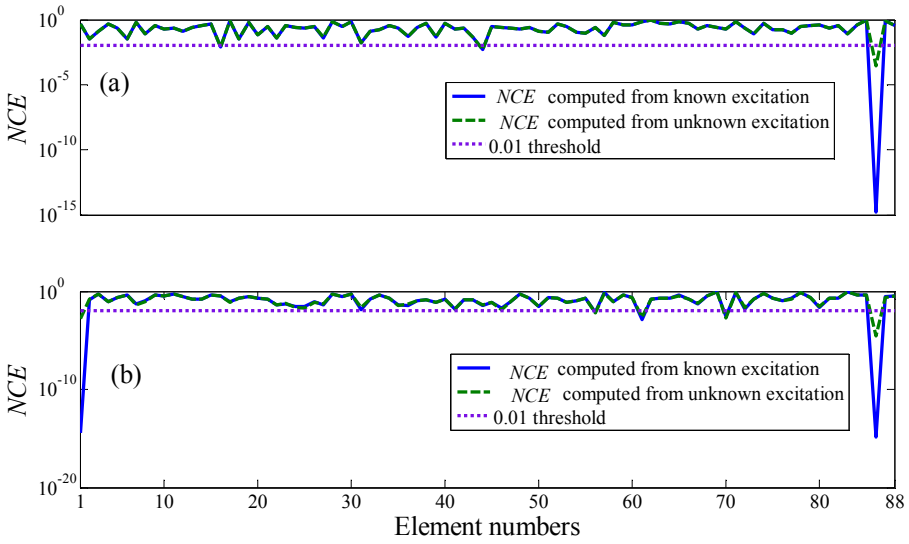

Fig. 3.19. Comparison between *NCE* computed from known and unknown excitation for experiment truss: (a) element 86 damaged; and (b) elements (1, 86) damaged (13 sensors used)

Performance of the Optimal Sensor Placement

To further investigate the performance of the optimal sensor placement for the 3-D modular truss structure, the 13 sensors used in the experiment is considered as the maximum number of sensors available for measuring acceleration responses. The requirements are (*i*) to identify the optimal locations to place the 13 sensors; and (*ii*) to identify the minimum number of sensors which the *DLV* method can still provide reliable results. Two cases will be considered, namely (1) sensors can only be placed at the lower chord of the truss; and (2) sensors can be placed at both the lower and the upper chords of the truss.

Performing the algorithm in Section 3.4, the optimal positions to place the 13 sensors for cases (1) and (2) are at nodes (2, 3, 4, 5, 6, 7, 8, 9, 11, 12, 13, 14, 15) and (3, 6, 7, 8, 12, 13, 14, 20, 21, 24, 25, 26, 27), respectively, in vertical direction. The

minimal number of sensors can be used with the *DLV* method is 2 where the optimal locations to place the 2 sensors are at nodes (7, 13) in vertical direction and the corresponding error is approximately 3%. The summarized results for the optimal sensor placement are shown in Fig. 3.20 and Table 3.7. Comparison of the error using the same number of sensors for case (1) where the sensors can only be placed at the lower chord of the truss and case (2) where the sensors can be placed at both the lower and upper chords of the truss is shown in Fig. 3.21. It is observed from Fig. 3.21 that the difference between the errors of the two scenarios is negligible (less than 0.3%). Hence, for reliable damage detection results by the *DLV* method, the sensors can be placed at only the lower chord of the truss. In addition, the optimal locations to place the sensors always include the sensor collocated with the actuator.

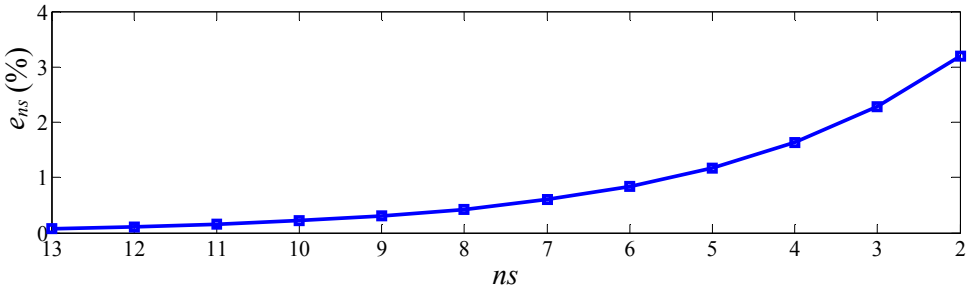

Fig. 3.20. Relationship between number of sensors and error in the identified stiffness matrix for the optimal sensor placement for 3-D modular truss structure (sensors can only be placed at the lower chord of the truss)

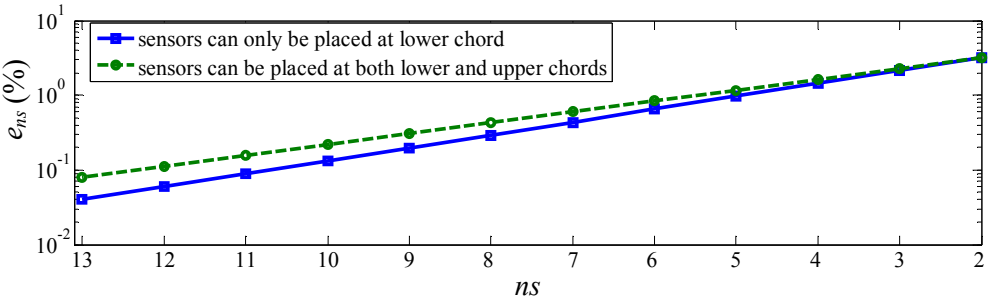

Fig. 3.21. Comparison between number of sensors and estimated errors in stiffness matrix for the case where sensors can be placed at the lower chords only and the case where sensors can be placed at both the lower and the upper chords of the 3-D modular truss structure

Table 3.7. Optimal sensor placement for 3-D modular truss structure (upper portion: sensors placed at the lower chord of the truss; lower portion: sensors placed at both lower and upper chords of the truss)

ns	Sensors at *DOF*	Sensors at nodes	e_{ns} (%)
13	(6, 9, 12, 15, 18, 21, 24, 27, 33, 36, 39, 42, 45)	(2, 3, 4, 5, 6, 7, 8, 9, 11, 12, 13, 14, 15)	0.0406
12	(9, 12, 15, 18, 21, 24, 27, 33, 36, 39, 42, 45)	(3, 4, 5, 6, 7, 8, 9, 11, 12, 13, 14, 15)	0.0596
11	(9, 15, 18, 21, 24, 27, 33, 36, 39, 42, 45)	(3, 5, 6, 7, 8, 9, 11, 12, 13, 14, 15)	0.0887
10	(9, 18, 21, 24, 27, 33, 36, 39, 42, 45)	(3, 6, 7, 8, 9, 11, 12, 13, 14, 15)	0.1322
9	(9, 18, 21, 24, 33, 36, 39, 42, 45)	(3, 6, 7, 8, 11, 12, 13, 14, 15)	0.1968
8	(9, 18, 21, 24, 36, 39, 42, 45)	(3, 6, 7, 8, 12, 13, 14, 15)	0.2932
7	(9, 18, 21, 24, 36, 39, 42)	(3, 6, 7, 8, 12, 13, 14)	0.4366
6	(18, 21, 24, 36, 39, 42)	(6, 7, 8, 12, 13, 14)	0.6503
5	(18, 21, 24, 39, 42)	(6, 7, 8, 13, 14)	0.9686
4	(18, 21, 24, 39)	(6, 7, 8, 13)	1.4426
3	(18, 21, 39)	(7, 8, 13)	2.1485
2	(21, 39)	(7, 13)	3.206
13	(9, 18, 21, 24, 36, 39, 42, 60, 63, 72, 75, 78, 81)	(3, 6, 7, 8, 12, 13, 14, 20, 21, 24, 25, 26, 27)	0.0818
12	(9, 18, 21, 24, 36, 39, 42, 60, 63, 75, 78, 81)	(3, 6, 7, 8, 12, 13, 14, 20, 21, 25, 26, 27)	0.1119
11	(9, 18, 21, 24, 36, 39, 42, 60, 63, 75, 78)	(3, 6, 7, 8, 12, 13, 14, 20, 21, 25, 26)	0.1564
10	(9, 18, 21, 24, 39, 42, 60, 63, 75, 78)	(3, 6, 7, 8, 13, 14, 20, 21, 25, 26)	0.2188
9	(9, 18, 21, 24, 39, 60, 63, 75, 78)	(3, 6, 7, 8, 13, 20, 21, 25, 26)	0.306
8	(18, 21, 24, 39, 60, 63, 75, 78)	(6, 7, 8, 13, 20, 21, 25, 26)	0.4279
7	(21, 24, 39, 60, 63, 75, 78)	(7, 8, 13, 20, 21, 25, 26)	0.5983
6	(21, 39, 60, 63, 75, 78)	(7, 13, 20, 21, 25, 26)	0.8367
5	(21, 39, 60, 63, 75)	(7, 13, 20, 21, 25)	1.1701
4	(21, 39, 60, 63)	(7, 13, 20, 21)	1.6363
3	(21, 39, 63)	(7, 13, 21)	2.2883
2	(21, 39)	(7, 13)	3.206

3.6 CONCLUDING REMARKS

The application of the *DLV* method to detect structural damage using dynamic responses is investigated for the case where the excitations are (*i*) known, and (*ii*) unknown. The difference between using dynamic responses from static responses in the *DLV* method to detect damage is the computation of the flexibility or stiffness matrix. The flexibility matrix can be obtained using the *ERA* algorithm in conjunction with an algorithm to compute flexibility coefficients from the realization matrices. Alternatively, the structural stiffness matrix can be computed from measured accelerations using the governing equations of motion and Newmark's time integration relationships. In this case, gradual change in the structural parameters with time can be discerned. Comparing the *NCE* of all elements for the cases where the excitations are

known and unknown, it is found as expected that the procedure with known excitations is more sensitive. Measured input excitations therefore should be integrated to the damage detection process to enhance the reliability of the result.

Numerical example of a 2-D warehouse structure showed that with unknown excitation, two damaged elements can be identified correctly using simulated accelerations which are contaminated with 10% noise. Besides, two elements with gradual reduction in element stiffnesses of approximately 4% per second can also be detected correctly. Assumption of known mass matrix is found reasonable in providing accurate estimations of the stiffness matrix for the cases where one or two elements are damaged, leading to significant reduction in the computation effort. The proposed method is also found applicable to identify two damaged elements using physically measured accelerations from an experiment of a 3-D modular truss structure.

In addition, an algorithm for optimal sensor placement is proposed to (*i*) find the optimal locations to place the *ns* available sensors and (*ii*) find the minimum number of sensors which is required to obtain reliable results by the *DLV* method. It is observed that the sensor collocated with the actuator is always present in the optimal sensor placement configuration. With 2 sensors available and are placed at the optimal locations, the error in the identified stiffness matrix is less than 5% and the damaged elements are still identified correctly in the set of *PDE*.

CHAPTER 4

SENSOR VALIDATION WITH *DLV* METHOD

4.1 INTRODUCTION

The *DLV* method is a model-based damage detection method in which the current flexibility matrix of the structure is identified based on current measurements and compared against the corresponding values of the reference structure. If discrepancy occurs, either the structure is damaged or the data from the sensors contains error or both. The reliability of structural damage assessment results is therefore dependent both on the accuracy of the *DLV* method and the quality of the measured signals. To enhance the reliability of structural damage detection using the *DLV* method following the proposed framework for structural damage detection in Fig. 4.1, the quality of measured signals (or *in situ* sensors) must be assessed *a priori* or in tandem with the detection. An algorithm for sensor validation in the context of structural damage detection using the *DLV* method is developed in this chapter. The objective of the algorithm is to identify measurements which are "suitable" to be used in the *DLV* method to detect structural damage.

Effect of error in flexibility matrix on the damage detection results using the *DLV* method is first discussed in Section 4.2. Definition of faulty sensors is then introduced in Section 4.3. The definition is adapted to two common sensors, namely displacement transducers and accelerometers. The algorithm for sensor validation is introduced in Section 4.4. From available sensors, different sets containing the same number of sensors is formulated. Change in flexibility matrices corresponding to different sets are then calculated based on which *SVD* is performed to compute the number of non-zero singular value (*NZV*). The set producing the smallest *NZV* may be

considered as comprising all "healthy" sensors and those sensors which do not belong to that set are classified as faulty. The performance of the proposed algorithm is verified using both simulated and experimental data from a 3-D modular truss structure for both single and multiple simultaneous faulty sensors in Sections 4.5 and 4.6.

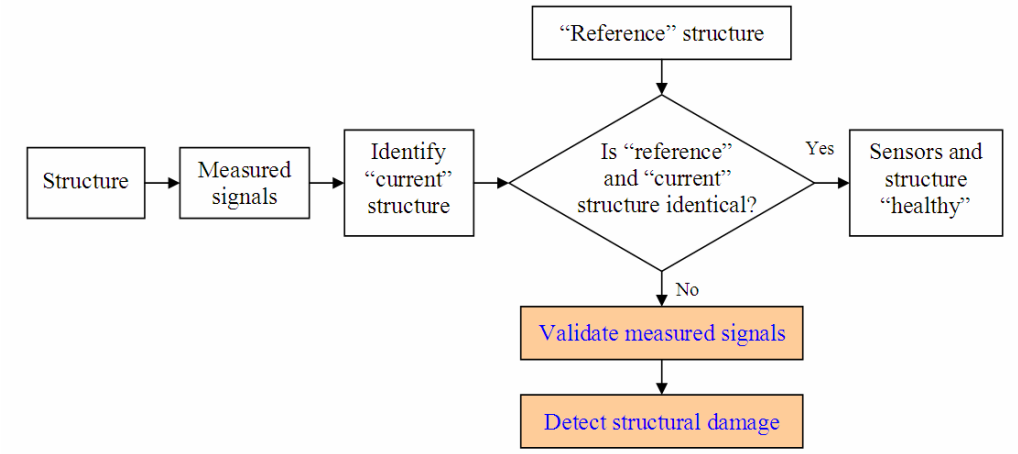

Fig. 4.1. Proposed framework for structural damage detection

4.2 EFFECT OF ERROR IN FLEXIBILITY MATRIX

4.2.1 Effect on damage detection result

To obtain *DLV*, flexibility matrix with respect to the sensor locations must be computed. From Eqs. (2.1) - (2.6) and (2.18) - (2.22), it can be observed that error in the flexibility matrix, if any, would propagate to the damage detection results. Performance of the *DLV* method under disturbance in the flexibility matrix is crucial and therefore will be investigated in this section.

For illustration, the 3-D modular truss structure shown in Fig. 2.8 with specifications summarized in Table 2.2 is simulated to obtain displacement responses at all nodes of the lower chord from which the flexibility matrices at the reference and the damaged states are estimated. Damaged state of the truss is generated by imposing 20% reduction in axial stiffness (*EA*) of element 86.

To investigate the effect of error in the flexibility matrix on the damage detection results, zero-mean white noises are added to both flexibility matrices. The *DLV* method is then performed using the contaminated flexibility matrices to identify a set of potential damaged elements (*PDE*). Of interest is the noise level beyond which the actual damaged element (element 86) is not a member of the *PDE* set, leading to erroneous damage detection results (Tran and Quek, 2006). For this purpose, various levels of noise are investigated, using a root mean square (*RMS*) value ranging from 0% to 30% in steps of 0.5%. The results are summarized in Table 4.1 which suggests a threshold noise level of 6.5% below which the *DLV* method may still be reliable. This is an extremely important and desirable feature of the *DLV* method since error is always present in any type of measurement in reality.

To investigate the variation of the threshold due to different damage severities, the entire range of reduction in axial stiffness of element 86 are generated and the same analysis as above performed. The results of one standard deviation below the mean plotted in Fig. 4.2 indicate that the threshold noise level of 6.5% can still be employed to differentiate the noise level below which the damage detection results by the *DLV* method can be reliable, provided that the damage severity is greater than 7%.

To investigate the effect of different damaged elements on the threshold noise level, one element at a time is prescribed as damaged with the reduction in the axial stiffness ranging from 7% to 99%. The same procedure described above is performed to determine the threshold noise level and the results of one standard deviation below the mean are summarized in Fig. 4.3, indicating a threshold value of 6.5% for this structure with any one element damage of more than 7% reduction in its axial stiffness. Fig. 4.2 indicates that the error level threshold at which the *DLV* method can accommodate monotonically increases with the damage severity. Hence, if more than

one element is damaged, the error level of 6.5% in the flexibility is conservative and can be safely adopted.

Table 4.1. Error level in flexibility matrices beyond which damaged element is not present in the identified *PDE* set (element 86 damaged)

Set No.	Sensors at nodes	No. of samples	Error level (%)		
			Mean	Standard deviation	One standard deviation below mean
1	[3,4,5,6,7,8,9,11,12,13,14,15]	30	9.4	2.9	6.5
2	[2,4,5,6,7,8,9,11,12,13,14,15]	30	11.3	3.8	7.5
3	[2,3,5,6,7,8,9,11,12,13,14,15]	30	11.1	3.1	8.0
4	[2,3,4,6,7,8,9,11,12,13,14,15]	30	10.0	3.5	6.5
5	[2,3,4,5,7,8,9,11,12,13,14,15]	30	11.8	2.8	9.0
6	[2,3,4,5,6,8,9,11,12,13,14,15]	30	10.3	3.8	6.5
7	[2,3,4,5,6,7,9,11,12,13,14,15]	30	13.7	3.2	10.5
8	[2,3,4,5,6,7,8,11,12,13,14,15]	30	13.1	4.1	9.0
9	[2,3,4,5,6,7,8,9,12,13,14,15]	30	14.6	4.1	10.5
10	[2,3,4,5,6,7,8,9,11,13,14,15]	30	13.1	3.6	9.5
11	[2,3,4,5,6,7,8,9,11,12,14,15]	30	10.9	3.4	7.5
12	[2,3,4,5,6,7,8,9,11,12,13,15]	30	13.7	4.2	9.5
13	[2,3,4,5,6,7,8,9,11,12,13,14]	30	12.5	4.0	8.5

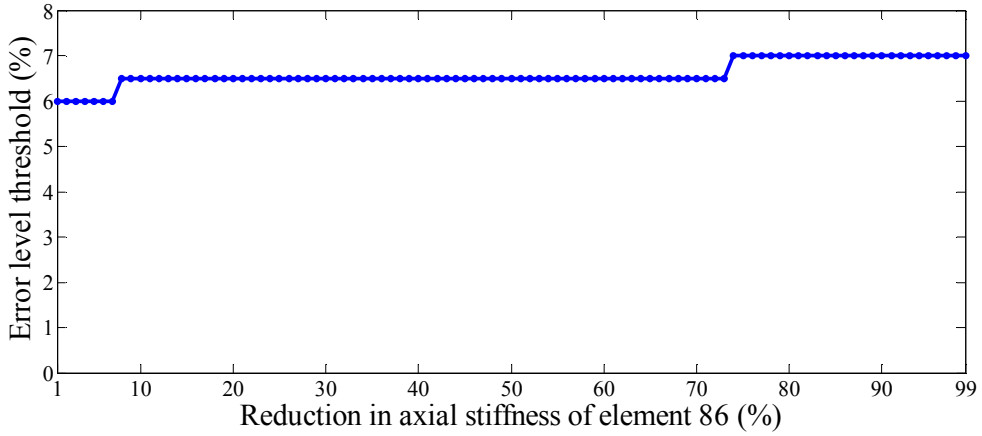

Fig. 4.2. Error threshold in flexibility matrices below which the *DLV* method can accommodate for various damage severities

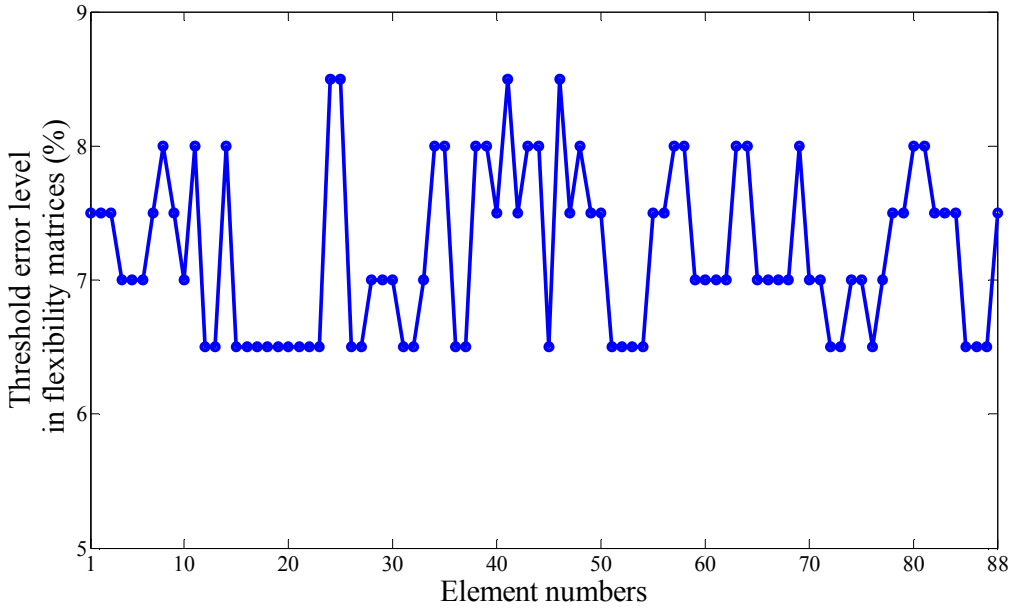

Fig. 4.3. Threshold error level in flexibility matrices below which the *DLV* method can accommodate (reduction in axial stiffness of each element ranging from 7% to 99%)

4.2.2 Effect on the *NZV*

From Eq. (2.2), the *DLV* is identified by examining the **Σ** matrix and partitioning into a portion which contains the non-zero diagonal values (*NZV*) and the remaining portion which contains zero diagonal values. Since **Σ** matrix is derived from the change in flexibility matrix, any *NZV* implies either the presence of noise or damage. The issue to be examined here is the effect of noise on *NZV* so that the presence of damage can be correctly ascertained.

The 3-D modular truss structure shown in Fig. 2.8 is utilized again to generate displacement responses from which the flexibility matrices at the reference and the damaged states are estimated. For the case where element 86 is damaged with 20% reduction in axial stiffness, zero-mean white noise with *RMS* ranging from 0% to 6.5% are introduced to the flexibility matrices based on which *SVD* is performed and **Σ** recorded. Since the structure has one element damaged, only the first diagonal value is non-zero, the magnitude being dependent on the severity of damage. The magnitudes

of the other diagonal values are not only dependent on the noise level but also the number of sensors used. To mitigate the effect of the number of sensors used, the ratio between a diagonal value and the first diagonal value is selected as criterion to classify *NZV*. Since the diagonal values are ordered in descending magnitude, the effect of noise may be studied by examining the ratio of the second diagonal value over the first diagonal value, which is plotted in Fig. 4.4a. Earlier, it is concluded that the tolerable error in the flexibility matrix is 6.5%. Using this value in Fig. 4.4a suggests a threshold value of 0.01 beyond which the second value may be classified as non-zero.

If one element at a time is prescribed as damaged with 20% reduction in the axial stiffness, Fig. 4.5 presents the threshold values for the cases where the error in the flexibility matrix is 0%, 2%, 4% and 6.5%. It is observed that the ratio between the second and the first diagonal values increases with higher error level in the flexibility matrix. Since 6.5% is the maximum error in the flexibility matrix below which the *DLV* method can be reliable, the mean value of 0.01 instead of the minimum value of 0.008 for the ratio between the second and the first diagonal values is proposed to discriminate zero diagonal values from non-zero diagonal values. If the reduction in axial stiffness of element 86 is not 20%, the threshold can be computed following the same procedure. Results in Fig. 4.4b show that the ratio between the second and the first diagonals increases with damage severity. Since the maximum error level of 6.5% is used to contaminate the flexibility matrices, the value of 0.01 is still suggested to classify *NZV* for cases of more than one damaged element because the ratio between the second and the first diagonal values monotonically increases with the severity of damage in element 86 as shown in Fig. 4.4b.

If the structure is healthy and the signals are contaminated, all diagonal values are not exactly zero. To be consistent with the above derivation where the structure is

damaged and the data is contaminated, the ratio between a diagonal and the first diagonal is still used as criterion to classify *NZV*. This makes the classification of *NZV* independent from the structural status (healthy or damaged) which is not known *a priori*. Since 6.5% is the maximal noise level below which the *DLV* method can accommodate, it is used to contaminate the flexibility matrices based on which the ratio between a diagonal and the first diagonal is computed. The procedure is repeated 30 times and results are presented in Table 4.2. Using the threshold value of 0.01 to classify *NZV*, the number of *NZV* obtained is 9 which means that the effect of noise on diagonal values is rather spread. This is different from the effect of structural damage which focuses on the first few diagonal values.

In summary, unless structure is not damaged, all sensors are healthy and measured signals are free of noise, the *NZV* will not be zero. A diagonal value in the singular value matrix will be classified as non-zero if it is greater than 0.01 times the first diagonal entry.

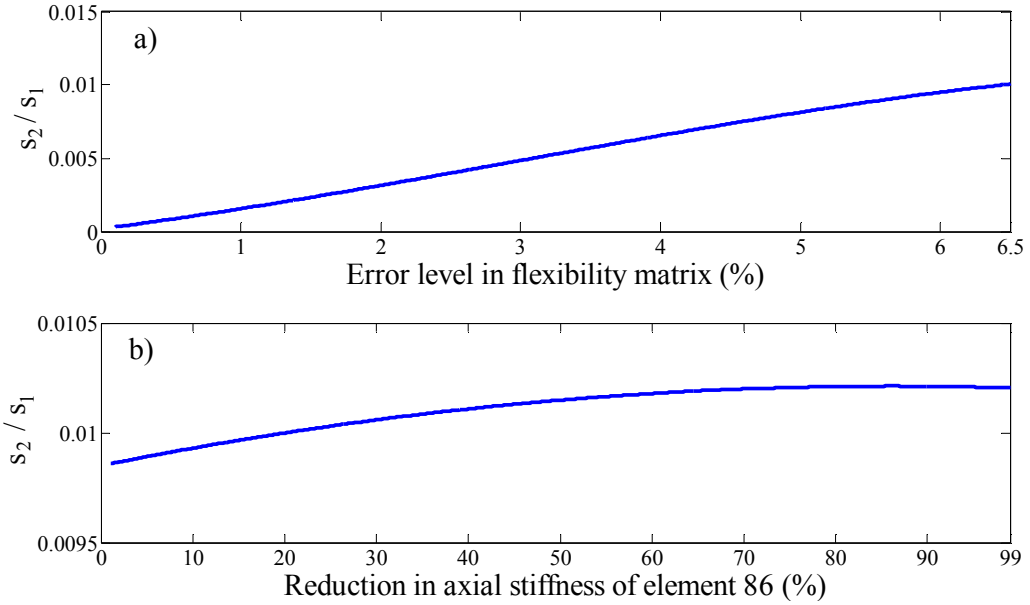

Fig. 4.4. Ratio between second and first diagonal values for: (a) 20% reduction in axial stiffness of element 86 with 0 to 6.5% error in flexibility matrices; (b) 6.5% error in flexibility matrices with damage severity ranging from 1 to 99%

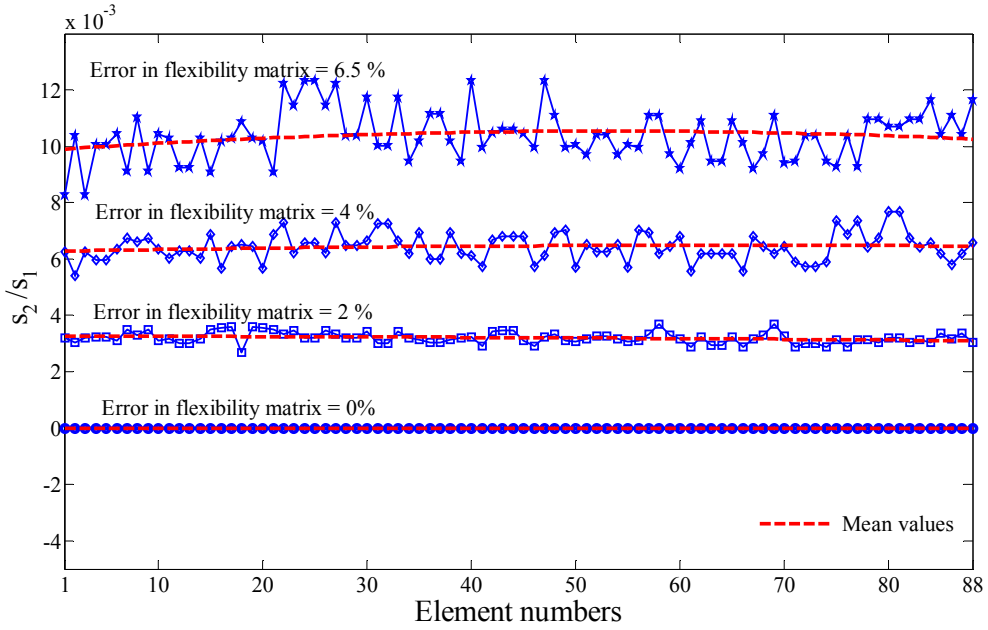

Fig. 4.5. Ratio between second and first diagonal values for various damaged elements and error levels in flexibility matrices

Table 4.2. Ratios between a diagonal value and the first diagonal value (6.5% error added)

Ratio	No. of samples	Mean	Standard deviation	One standard deviation below mean
s_2/s_1	30	0.900	0.225	0.675
s_3/s_1	30	0.453	0.112	0.341
s_4/s_1	30	0.265	0.065	0.200
s_5/s_1	30	0.158	0.038	0.120
s_6/s_1	30	0.094	0.024	0.071
s_7/s_1	30	0.050	0.013	0.037
s_8/s_1	30	0.026	0.007	0.020
s_9/s_1	30	0.013	0.003	0.010
s_{10}/s_1	30	0.007	0.002	0.006
s_{11}/s_1	30	0.004	0.001	0.003
s_{12}/s_1	30	0.001	0.000	0.001
s_{13}/s_1	30	0.000	0.000	0.000

4.3 DEFINITION OF FAULTY SENSORS

Two types of sensors are commonly used to measure structural responses, namely displacement transducers and accelerometers. Faulty sensors are generally perceived as those producing wild signals whereas in the context of structural health monitoring, they are referred to those which produces signals that deviate by a specified limit from the expected values. In this section, the limits to be specified are determined.

4.3.1 Faulty displacement transducers

For displacement readings, the procedure in Section 4.2 provides the threshold for deciding whether a sensor is unsuitable or "faulty" with respect to the *DLV* method. It should be noted that the user has to decide what the lowest tolerable damage level (7% in Section 3.2) is to arrive at the threshold. If the error in a displacement deviates

more than 6.5% from the true value, it is classified as faulty and vice versa. In practice, the true value is unknown and hence, the *NZV* in the matrix of the change in flexibility is utilized to identify faulty displacement transducer, as presented in the Section 4.2.

4.3.2 Faulty accelerometers

Faults in accelerometers are manifested either by additive error or random error or both. Details for additive error are given in Abdelghani and Friswell (2004). Random error may arise from calibration, noise and environmental effects such as that due to background excitation. It may be modeled as a zero-mean white noise added to the exact signal. Random error may also be considered as an extension of multiplicative error (Abdelghani and Friswell, 2004).

From the measured accelerations, the flexibility matrix with reference to the sensor locations can be obtained by adopting the eigensystem realization algorithm (*ERA*) (Juang and Pappa, 1985; Pappa et al., 1993; Juang, 1994) in conjunction with an algorithm to estimate the flexibility coefficients from state space results (Bernal and Gunes, 2004). The 3-D modular truss structure used in Section 4.2 is utilized again to generate acceleration responses by applying a dynamic load vertically at node 7. The load is simulated by a zero-mean white noise with *RMS* amplitude of 100 N. The amplitude of the applied load is selected such that the *RMS* of acceleration responses are approximately 20 m/s^2 which fall within the measurement range of the accelerometers used in this study (50 g). The vertical accelerations of all thirteen nodes at the lower chord of the truss are measured. Node 7 has a collocated sensor-actuator pair, which is the minimum requirement in the procedure to compute the flexibility matrix (see Fig. 2.8c for location of the nodes) (Bernal and Gunes, 2004). Damage in the structure is generated by a 20% reduction in the axial stiffness of element 86. By

varying the noise level such that the threshold error in the flexibility matrix established in Section 4.2 is reached, the error thresholds of the acceleration signals can be established.

Additive error threshold

If $\mathbf{a}_j^0(t)$ is the exact response acceleration at sensor j (j = 1, 2, …, ns) and $\mathbf{w}_a$ is a constant signal with magnitude ranging from 0% to 10% *RMS* of $\mathbf{a}_j^0(t)$, the contaminated response acceleration at sensor j by additive error can be generated as

$$\mathbf{a}_j(t) = \mathbf{a}_j^0(t) + \mathbf{w}_a \tag{4.1}$$

The flexibility matrix is then computed and compared with the known matrix. The procedure is repeated 30 times and the results are presented in Table 4.3. A reasonable threshold of 3.1% corresponding to one standard deviation below the mean is suggested as the additive error threshold beyond which the error in the identified flexibility matrix will exceed 6.5%. The variation of the additive error threshold with different single damaged member represented by 20% reduction in the axial stiffness is investigated using the same computational procedure with 30 runs. Results of one standard deviation below the mean are summarized in Fig. 4.6, indicating that the threshold of 3.1% additive error in the acceleration signals can still be employed to ensure reliable damage detection using the *DLV* method.

To investigate the effect of damage severity on the threshold, the entire range of reduction in axial stiffness of element 86 are generated. The threshold additive error for each damage severity level is computed and plotted in Fig. 4.7a. When the damage is more severe, $\mathbf{F}_d$ increases, resulting in higher additive error level the procedure can tolerate to obtain the same error in the identified flexibility matrices. From Fig. 4.7a, the value of 3.1% is still suggested as the additive error threshold beyond which the results from the *DLV* method are significantly affected. Fig. 4.7a also indicates that the

additive error threshold increases monotonically with damage severity and hence may be adopted for cases where more than one element are damaged.

It may be argued that the additive error threshold of 3.1% is too small to be practical. However, it is noted that the additive error is easier to detect being a *DC* shift by simple means and only small shift are harder to detect that methods, such as the one discussed here, are necessary. The proposed additive threshold is close to the 5% additive error employed by Friswell and Inman (1999) and Abdelghani and Friswell (2004).

Table 4.3. Additive error level beyond which error in identified flexibility matrices exceeds 6.5%

Set No.	Sensor numbers	Skipped sensors	No. of samples	Additive error level (%)		
				Mean	Standard deviation	One standard deviation below mean
1	[2,3,4,5,6,7,8,9,10,11,12,13]	1	30	4.2	1.1	3.1
2	[1,3,4,5,6,7,8,9,10,11,12,13]	2	30	4.6	1.4	3.2
3	[1,2,4,5,6,7,8,9,10,11,12,13]	3	30	4.5	1.4	3.1
4	[1,2,3,5,6,7,8,9,10,11,12,13]	4	30	4.9	1.7	3.2
5	[1,2,3,4,6,7,8,9,10,11,12,13]	5	30	4.8	1.7	3.1
6	[1,2,3,4,5,6,8,9,10,11,12,13]	7	30	4.5	1.4	3.1
7	[1,2,3,4,5,6,7,9,10,11,12,13]	8	30	4	0.5	3.5
8	[1,2,3,4,5,6,7,8,10,11,12,13]	9	30	4.9	1.8	3.1
9	[1,2,3,4,5,6,7,8,9,11,12,13]	10	30	4.4	1.2	3.2
10	[1,2,3,4,5,6,7,8,9,10,12,13]	11	30	4.6	1.0	3.6
11	[1,2,3,4,5,6,7,8,9,10,11,13]	12	30	4.8	1.5	3.3
12	[1,2,3,4,5,6,7,8,9,10,11,12]	13	30	4.3	0.8	3.5

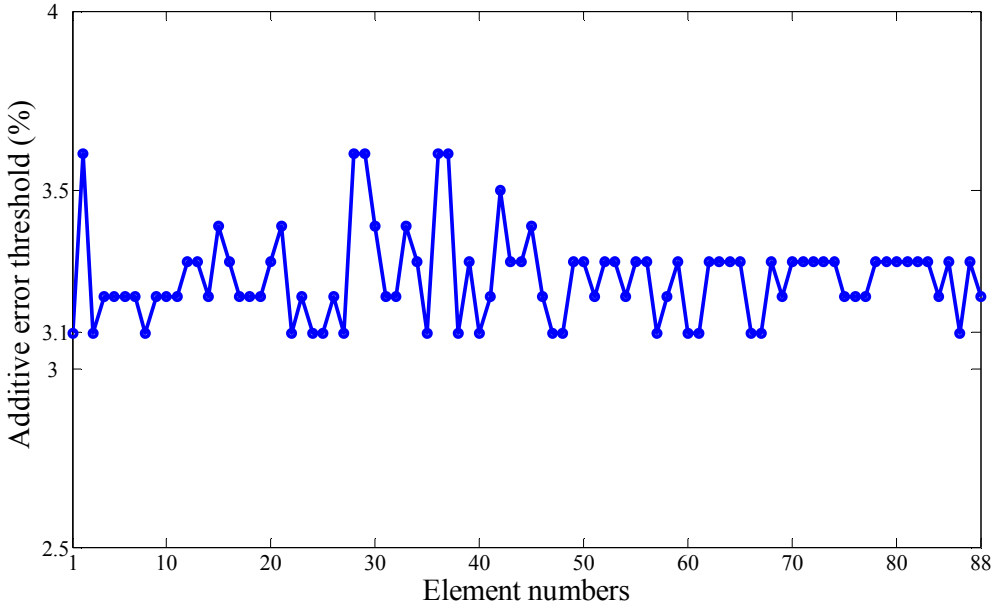

Fig. 4.6. Additive error thresholds in accelerations beyond which error in flexibility matrices will exceed 6.5%

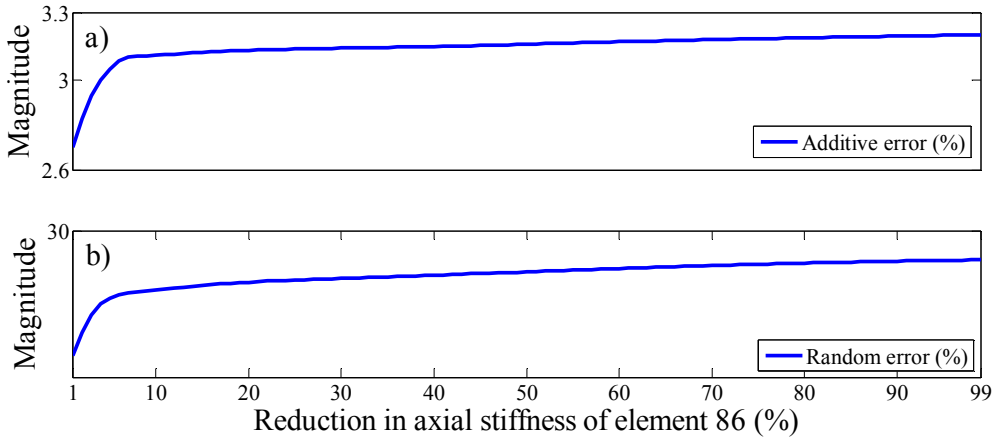

Fig. 4.7. (a) Additive error and (b) random error thresholds beyond which errors in identified flexibility matrices exceed 6.5% for various damage severities in element 86

Random error threshold

Similar to the case of additive error, if $\mathbf{a}_j^0(t)$ is the exact response acceleration measured by sensor j (j = 1, 2, …, ns) and $\mathbf{w}_r(t)$ is a zero-mean white noise signal with *RMS* ranging from 0% to 60% *RMS* of $\mathbf{a}_j^0(t)$, the contaminated response acceleration at sensor j by random error can be simulated as

$$\mathbf{a}_j(t) = \mathbf{a}_j^0(t) + \mathbf{w}_r(t) \tag{4.2}$$

From the contaminated accelerations, the flexibility matrix is computed and compared with the known matrix. The procedure is repeated 30 times and the results are summarized in Table 4.4 where element 86 is damaged with 20% reduction in axial stiffness. The value of 29% corresponding to one standard deviation below the mean can be selected as the threshold random error beyond which error in the identified flexibility matrices will exceed 6.5%, leading to erroneous in the damage detection results by the *DLV* method. The same procedure is repeated 30 times for the case where one element at a time is prescribed as damaged with 20% reduction in axial stiffness. Results which correspond to one standard deviation below the mean are plotted in Fig. 4.8, indicating that the threshold random error of 29% in the measured accelerations can still be employed to ensure reliable results by the *DLV* method.

The effect of damage severity on the random error threshold is similarly investigated by varying the reduction in the axial stiffness of element 86 and the results plotted in Fig. 4.7b. Similar to the case of additive error, the increment in damage severity makes $\mathbf{F}_d$ increase, leading to higher random error level the procedure can accommodate as shown in Fig. 4.7b. From Fig. 4.7b, the value of 29% is still suggested as threshold to demarcate the random error in the accelerations beyond which error in the identified flexibility matrix will exceed 6.5% and may lead to unreliable results from the *DLV* method (Tran and Quek, 2006). Results in Fig. 4.7b also indicate that the threshold random error increases monotonically with the damage severity of element 86, implying that the same threshold can be conservatively used if more than one element is damaged.

Table 4.4. Random error level beyond which error in identified flexibility matrices exceeds 6.5%

Set No.	Sensor numbers	Skipped sensors	No. of samples	Random error level (%)		
				Mean	Standard deviation	One standard deviation below mean
1	[2,3,4,5,6,7,8,9,10,11,12,13]	1	30	40.6	7.9	32.7
2	[1,3,4,5,6,7,8,9,10,11,12,13]	2	30	37.0	7.7	29.3
3	[1,2,4,5,6,7,8,9,10,11,12,13]	3	30	40.9	8.2	32.7
4	[1,2,3,5,6,7,8,9,10,11,12,13]	4	30	43.4	8.1	35.3
5	[1,2,3,4,6,7,8,9,10,11,12,13]	5	30	41.0	8.4	32.6
6	[1,2,3,4,5,6,8,9,10,11,12,13]	7	30	41.4	8.8	32.6
7	[1,2,3,4,5,6,7,9,10,11,12,13]	8	30	43.4	7.8	35.6
8	[1,2,3,4,5,6,7,8,10,11,12,13]	9	30	42.9	8.6	34.3
9	[1,2,3,4,5,6,7,8,9,11,12,13]	10	30	41.0	7.1	33.9
10	[1,2,3,4,5,6,7,8,9,10,12,13]	11	30	43.4	8.8	34.6
11	[1,2,3,4,5,6,7,8,9,10,11,13]	12	30	41.2	7.3	33.9
12	[1,2,3,4,5,6,7,8,9,10,11,12]	13	30	41.6	7.3	34.3

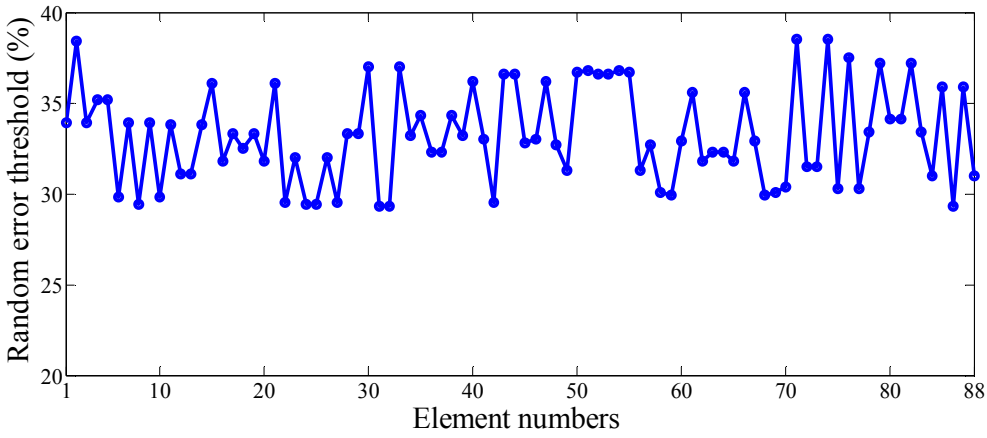

Fig. 4.8. Random error thresholds in accelerations beyond which error in flexibility matrices will exceed 6.5%

Hybrid error

Both the additive and random errors can occur simultaneously. To simulate this, all generated accelerations are shifted away by a value ranging from 0% to 3.1% to simulate additive error and zero-mean white noise with *RMS* ranging from 0% to 29% is added to generate random error. The contaminated acceleration at sensor *j* by hybrid error is modeled as

$$\mathbf{a}_j(t) = \mathbf{a}_j^0(t) + \mathbf{w}_a + \mathbf{w}_r(t) \tag{4.3}$$

where the symbols have been defined earlier. From the contaminated signals, the flexibility matrix is computed and compared with the known matrix to evaluate the error. The procedure is repeated 30 times and the values of additive error and random error corresponding to one standard deviation below the means are recorded. The relationship between additive error and random error beyond which error in the identified flexibility matrix will be greater than 6.5% is plotted in Fig. 4.9. For example, if the additive error of sensor *j* is 2%, it will be classified as faulty if the random error in sensor *j* is greater than 22.4%. The above results assume that the error is present in all sensors, which can be conservatively applied to real practice where not all sensors will have the same degree of error.

In summary, a displacement transducer is classified as faulty if its reading deviates by more than 6.5% from the exact value; an accelerometer is classified as faulty if its readings are shifted by more than 3.1% *RMS* from its exact values or if its noise level exceeds 29% *RMS* of the exact signal or any combination of additive and random errors that is outside the curve shown in Fig. 4.9.

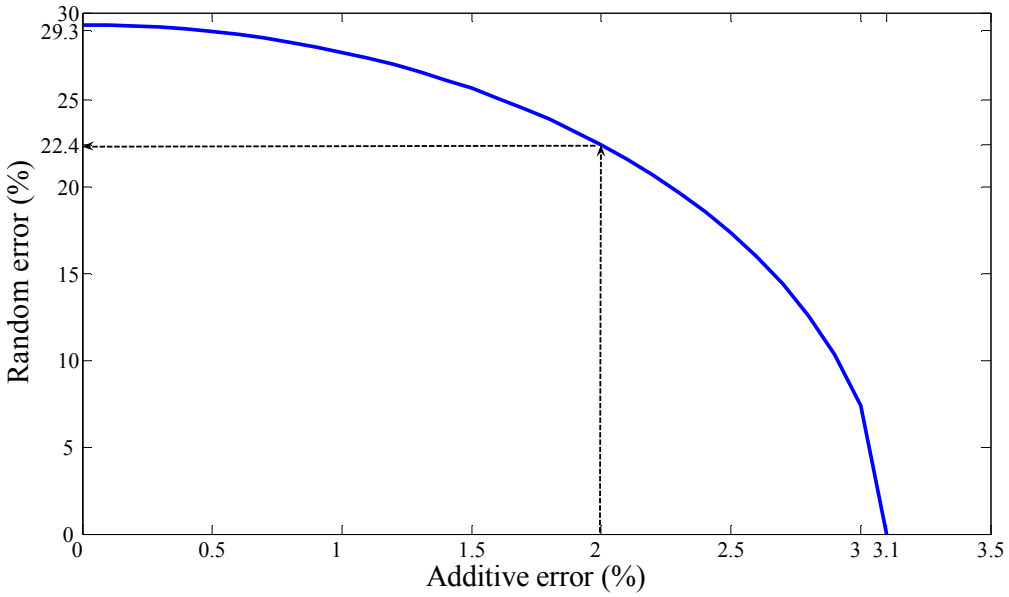

Fig. 4.9. Relationship between additive and random errors beyond which errors in identified flexibility matrices exceed 6.5%

4.4 SENSOR VALIDATION ALGORITHM

The sensor validation algorithm should start from the identified flexibility matrices obtained with reference to the *ns* sensor locations since this is the starting point of the *DLV* method irrespective of whether displacement transducers or accelerometers are used to measure structural responses.

The algorithm starts by forming all sets containing (*ns* - 1) sensors. Next, the change in flexibility matrix with respect to the (*ns* - 1) sensor locations of each set is computed, based on which *SVD* is performed to identify the *NZV*. The idea behind the sensor validation algorithm is that any significant error in the identified flexibility matrices will increase the *NZV*. Hence, the set producing the minimum *NZV* will contain all the "healthy" sensors and sensors which do not belong to this set may be classified as faulty. If more than one set, says N_1 sets, produces the smallest *NZV*, then the combinations of (*ns* - 2) sensors are next considered until the criterion that one set (N_1 = 1) produces the smallest *NZV* is met. The algorithm is also terminated if all sets

produce the same *NZV* (N_1 is assigned zero) or the remaining sensors for each set are 2. The former means that either all sensors are in good condition or they are all faulty (which is assumed unlikely). The latter implies that at least (*ns* - 1) sensors are faulty and it will be concluded that the data are unsuitable for damage assessment with the *DLV* method. The algorithm is summarized in Fig. 4.10.

The algorithm works provided that *ns* is greater than 2 since at least 2 measurements are required to form a matrix before any *SVD* can be performed to compute the *NZV*. With *ns* = 2, only 1 set of sensors can be formulated and the *NZV* cannot be compared to validate the sensors. This algorithm only assess whether the measurements can be used with the *DLV* method to obtain reliable damage detection results. It is unable to differentiate the types of errors, namely whether the error is an additive, random or hybrid. However, if an accelerometer is classified as faulty, the error will be either additive, random or hybrid as defined in Section 4.3.2.

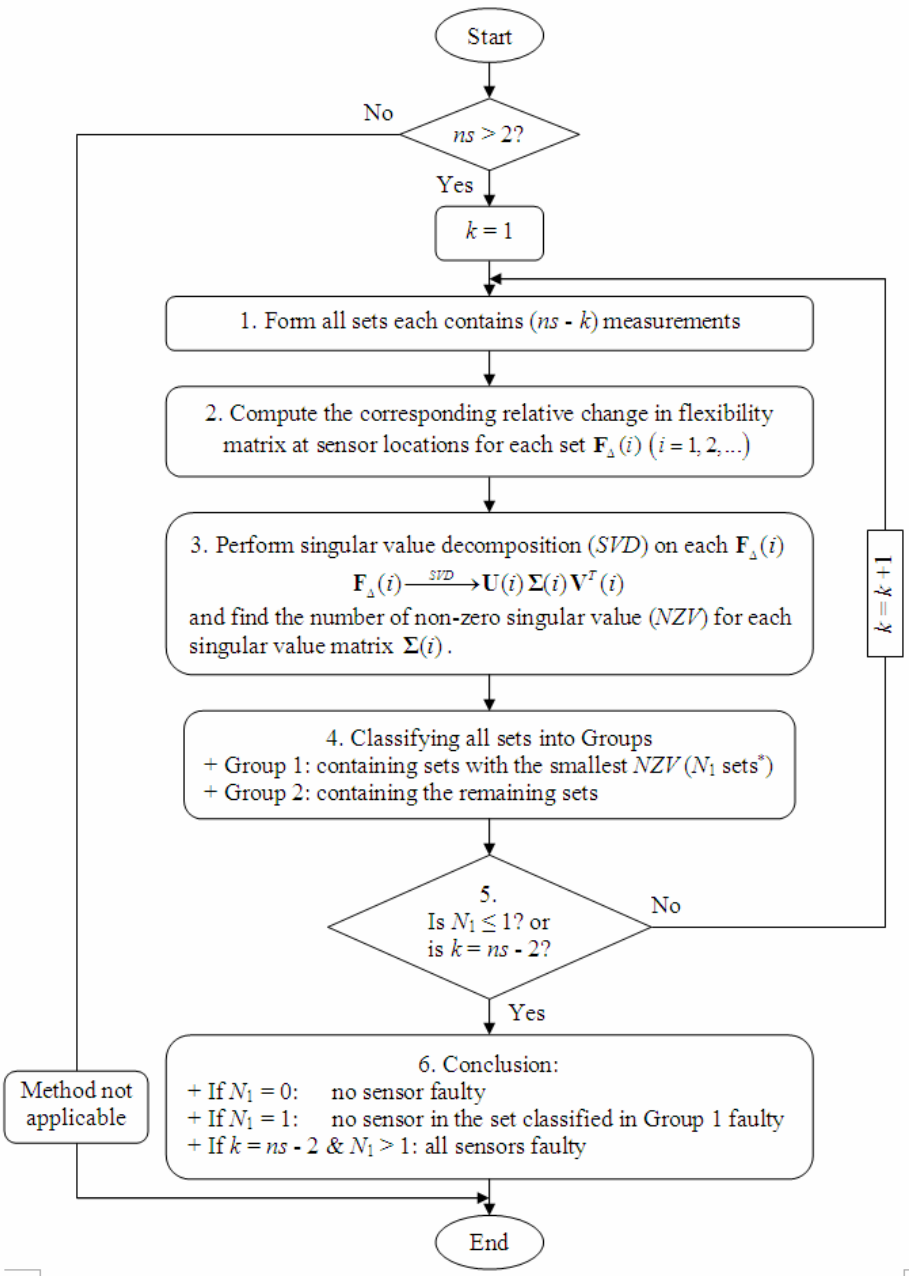

Fig. 4.10 Flow chart for sensor validation algorithm

* If all sets produce the same *NZV*, N_1 is assigned zero.

4.5 DISPLACEMENT TRANSDUCER VALIDATION

4.5.1 Numerical example

The 3-D modular truss structure shown in Fig. 2.8 with specifications of the truss members shown in Table 2.2 is used to generate displacement responses. Vertical

displacement responses of all 13 nodes at the lower chord of the truss are monitored. To generate displacement responses which fall within the range of the displacement transducers used (10 mm displacement transducers, model CDP), the magnitudes of the excited load is selected to be 921.5 N, resulting in displacement responses of approximately 2 mm. Damage in the truss is generated by equivalently imposing 20% reduction in axial stiffness of element 86. The reference or "healthy" state of the structure is associated with the case where all sensors are "healthy"; the damaged state of the structure is associated with the case where some sensors are faulty. Two cases of faulty sensors are investigated, namely (1) sensor 8 is faulty; and (2) sensors 8 and 10 are faulty. Locations of sensors are given in Fig. 2.8c. The fault is generated by 10% positive shift of the readings of the affected sensors from the actual readings. At first, it is assumed that all "healthy" sensors are noise free. The presence of noise in the "healthy" sensors will be investigated later in this section.

Sensor 8 faulty

From 13 sensors, 13 sets of signal data each comprising 12 sensors are formulated. From the response displacements of each set, the flexibility matrices with respect to the sensor locations at both the reference and the damaged states are computed following the procedure presented in Section 2.3. From the difference in flexibility matrices, *SVD* is performed to identify the *NZV*. The results in the upper portion of Table 4.5 show that only set number 8 produces the smallest *NZV* = 1, implying that $N_1 = 1$ and that set number 8 contains all healthy sensors. Sensor 8 which does not belong to set number 8 is suspected as faulty. To examine this result further, the sensor validation is performed on the 12 sensors belonging to set number 8. Similarly, 12 sets of signal data, each contains 11 sensors are formulated and the *NZV* for each set identified. Results in the lower portion of Table 4.5 show that the *NZV*

cannot be reduced to zero. Following the sensor validation algorithm, the 12 sensors are classified as healthy and the *NZV* in the 12 sets at the lower portion of Table 4.5 may be attributed to the presence of structural damage or the presence of measurement noise, reinforcing that set number 8 in the upper portion of Table 4.5 contains all healthy sensors and sensor 8 is faulty.

Table 4.5. Sensor validation results (element 86 damaged, sensor 8 faulty, $k = 1$

Set No.	Sensors	*NZV*	Set No.	Sensors	*NZV*
1	[2,3,4,5,6,7,8,9,10,11,12,13]	2	8	[1,2,3,4,5,6,7,9,10,11,12,13]	**1**
2	[1,3,4,5,6,7,8,9,10,11,12,13]	2	9	[1,2,3,4,5,6,7,8,10,11,12,13]	2
3	[1,2,4,5,6,7,8,9,10,11,12,13]	2	10	[1,2,3,4,5,6,7,8,9,11,12,13]	2
4	[1,2,3,5,6,7,8,9,10,11,12,13]	2	11	[1,2,3,4,5,6,7,8,9,10,12,13]	2
5	[1,2,3,4,6,7,8,9,10,11,12,13]	2	12	[1,2,3,4,5,6,7,8,9,10,11,13]	2
6	[1,2,3,4,5,7,8,9,10,11,12,13]	2	13	[1,2,3,4,5,6,7,8,9,10,11,12]	2
7	[1,2,3,4,5,6,8,9,10,11,12,13]				
1a	[2,3,4,5,6,7,9,10,11,12,13]	1	7a	[1,2,3,4,5,6,9,10,11,12,13]	1
2a	[1,3,4,5,6,7,9,10,11,12,13]	1	8a	[1,2,3,4,5,6,7,10,11,12,13]	1
3a	[1,2,4,5,6,7,9,10,11,12,13]	1	9a	[1,2,3,4,5,6,7,9,11,12,13]	1
4a	[1,2,3,5,6,7,9,10,11,12,13]	1	10a	[1,2,3,4,5,6,7,9,10,12,13]	1
5a	[1,2,3,4,6,7,9,10,11,12,13]	1	11a	[1,2,3,4,5,6,7,9,10,11,13]	1
6a	[1,2,3,4,5,7,9,10,11,12,13]	1	12a	[1,2,3,4,5,6,7,9,10,11,12]	1

Sensors 8 and 10 faulty

Following the same procedure as above, 13 sets each comprises 12 sensors are formulated to compute the corresponding flexibility matrices with respect to the sensor locations at the reference and the damaged states of the structure. From the difference in the flexibility matrices at each set, the *NZV* is computed and shown in Table 4.6. Set numbers 8 and 10 produce the smallest $NZV = 2$, implying that $N_1 = 2$. Since there are more than 1 set producing the smallest *NZV*, 78 combinatorial sets of 11 sensors are next considered. From each set of measurements, the flexibility matrices are computed for the reference and the damaged states of the structure based on which the *NZV* is identified and shown in upper portion of Table 4.7. The *NZV* is minimal for set number

65 where sensors 8 and 10 are not present, indicating that they may be faulty. For further investigation, the sensor validation algorithm is performed for the 11 sensors in set number 65. Results in the lower portion of Table 4.7 indicate that the *NZV* for each set cannot be further reduced. Following the sensor validation algorithm, the 11 sensors belonging to set number 65 in the upper portion of Table 4.7 are healthy, reinforcing that sensors 8 and 10 are in fact faulty.

Table 4.6. Sensor validation results (element 86 damaged, sensors 8 & 10 faulty, $k = 1$)

Set No.	Sensor	*NZV*	Set No.	Sensor	*NZV*
1	[2,3,4,5,6,7,8,9,10,11,12,13]	3	8	[1,2,3,4,5,6,7,9,10,11,12,13]	**2**
2	[1,3,4,5,6,7,8,9,10,11,12,13]	3	9	[1,2,3,4,5,6,7,8,10,11,12,13]	3
3	[1,2,4,5,6,7,8,9,10,11,12,13]	3	10	[1,2,3,4,5,6,7,8,9,11,12,13]	**2**
4	[1,2,3,5,6,7,8,9,10,11,12,13]	3	11	[1,2,3,4,5,6,7,8,9,10,12,13]	3
5	[1,2,3,4,6,7,8,9,10,11,12,13]	3	12	[1,2,3,4,5,6,7,8,9,10,11,13]	3
6	[1,2,3,4,5,6,8,9,10,11,12,13]	3	13	[1,2,3,4,5,6,7,8,9,10,11,12]	3
7	[1,2,3,4,5,6,7,9,10,11,12,13]	3			

Table 4.7. Sensor validation results (element 86 damaged, sensors 8 & 10 faulty, $k = 2$)

Set No.	Sensor	*NZV*	Set No.	Sensor	*NZV*
1	[3,4,5,6,7,8,9,10,11,12,13]	3	40	[1,2,3,5,6,7,8,9,10,12,13]	3
2	[2,4,5,6,7,8,9,10,11,12,13]	3	41	[1,2,3,5,6,7,8,9,10,11,13]	3
3	[2,3,5,6,7,8,9,10,11,12,13]	3	42	[1,2,3,5,6,7,8,9,10,11,12]	3
4	[2,3,4,6,7,8,9,10,11,12,13]	3	43	[1,2,3,4,7,8,9,10,11,12,13]	3
5	[2,3,4,5,7,8,9,10,11,12,13]	3	44	[1,2,3,4,6,8,9,10,11,12,13]	3
6	[2,3,4,5,6,8,9,10,11,12,13]	3	45	[1,2,3,4,6,7,9,10,11,12,13]	2
7	[2,3,4,5,6,7,9,10,11,12,13]	2	46	[1,2,3,4,6,7,8,10,11,12,13]	3
8	[2,3,4,5,6,7,8,10,11,12,13]	3	47	[1,2,3,4,6,7,8,9,11,12,13]	2
9	[2,3,4,5,6,7,8,9,11,12,13]	2	48	[1,2,3,4,6,7,8,9,10,12,13]	3
10	[2,3,4,5,6,7,8,9,10,12,13]	3	49	[1,2,3,4,6,7,8,9,10,11,13]	3
11	[2,3,4,5,6,7,8,9,10,11,13]	3	50	[1,2,3,4,6,7,8,9,10,11,12]	3
12	[2,3,4,5,6,7,8,9,10,11,12]	3	51	[1,2,3,4,5,8,9,10,11,12,13]	3
13	[1,4,5,6,7,8,9,10,11,12,13]	3	52	[1,2,3,4,5,7,9,10,11,12,13]	2
14	[1,3,5,6,7,8,9,10,11,12,13]	3	53	[1,2,3,4,5,7,8,10,11,12,13]	3
15	[1,3,4,6,7,8,9,10,11,12,13]	3	54	[1,2,3,4,5,7,8,9,11,12,13]	2
16	[1,3,4,5,7,8,9,10,11,12,13]	3	55	[1,2,3,4,5,7,8,9,10,12,13]	3
17	[1,3,4,5,6,8,9,10,11,12,13]	3	56	[1,2,3,4,5,7,8,9,10,11,13]	3
18	[1,3,4,5,6,7,9,10,11,12,13]	2	57	[1,2,3,4,5,7,8,9,10,11,12]	3
19	[1,3,4,5,6,7,8,10,11,12,13]	3	58	[1,2,3,4,5,6,9,10,11,12,13]	2
20	[1,3,4,5,6,7,8,9,11,12,13]	2	59	[1,2,3,4,5,6,8,10,11,12,13]	3
21	[1,3,4,5,6,7,8,9,10,12,13]	3	60	[1,2,3,4,5,6,8,9,11,12,13]	2
22	[1,3,4,5,6,7,8,9,10,11,13]	3	61	[1,2,3,4,5,6,8,9,10,12,13]	3
23	[1,3,4,5,6,7,8,9,10,11,12]	3	62	[1,2,3,4,5,6,8,9,10,11,13]	3
24	[1,2,5,6,7,8,9,10,11,12,13]	3	63	[1,2,3,4,5,6,8,9,10,11,12]	3
25	[1,2,4,6,7,8,9,10,11,12,13]	3	64	[1,2,3,4,5,6,7,10,11,12,13]	2
26	[1,2,4,5,7,8,9,10,11,12,13]	3	65	[1,2,3,4,5,6,7,9,11,12,13]	**1**
27	[1,2,4,5,6,8,9,10,11,12,13]	3	66	[1,2,3,4,5,6,7,9,10,12,13]	2
28	[1,2,4,5,6,7,9,10,11,12,13]	2	67	[1,2,3,4,5,6,7,9,10,11,13]	2
29	[1,2,4,5,6,7,8,10,11,12,13]	3	68	[1,2,3,4,5,6,7,9,10,11,12]	2
30	[1,2,4,5,6,7,8,9,11,12,13]	2	69	[1,2,3,4,5,6,7,8,11,12,13]	2
31	[1,2,4,5,6,7,8,9,10,12,13]	3	70	[1,2,3,4,5,6,7,8,10,12,13]	3
32	[1,2,4,5,6,7,8,9,10,11,13]	3	71	[1,2,3,4,5,6,7,8,10,11,13]	3
33	[1,2,4,5,6,7,8,9,10,11,12]	3	72	[1,2,3,4,5,6,7,8,10,11,12]	3
34	[1,2,3,6,7,8,9,10,11,12,13]	3	73	[1,2,3,4,5,6,7,8,9,12,13]	2
35	[1,2,3,5,7,8,9,10,11,12,13]	3	74	[1,2,3,4,5,6,7,8,9,11,13]	2
36	[1,2,3,5,6,8,9,10,11,12,13]	3	75	[1,2,3,4,5,6,7,8,9,11,12]	2
37	[1,2,3,5,6,7,9,10,11,12,13]	2	76	[1,2,3,4,5,6,7,8,9,10,13]	3
38	[1,2,3,5,6,7,8,10,11,12,13]	3	77	[1,2,3,4,5,6,7,8,9,10,12]	3
39	[1,2,3,5,6,7,8,9,11,12,13]	2	78	[1,2,3,4,5,6,7,8,9,10,11]	3
1a	[2,3,4,5,6,7,9,11,12,13]	1	7a	[1,2,3,4,5,6,9,11,12,13]	1
2a	[1,3,4,5,6,7,9,11,12,13]	1	8a	[1,2,3,4,5,6,7,11,12,13]	1
3a	[1,2,4,5,6,7,9,11,12,13]	1	9a	[1,2,3,4,5,6,7,9,12,13]	1
4a	[1,2,3,5,6,7,9,11,12,13]	1	10a	[1,2,3,4,5,6,7,9,11,13]	1
5a	[1,2,3,4,6,7,9,11,12,13]	1	11a	[1,2,3,4,5,6,7,9,11,12]	1
6a	[1,2,3,4,5,7,9,11,12,13]	1			

Sensor validation with noisy data

To investigate the effect of noise on the performance of the sensor validation algorithm, the above example is performed again where zero-mean white noise with *RMS* of 5% *RMS* of the displacement responses is added to all the displacement responses to generate contaminated data. For the case where sensor 8 is faulty, the *NZV* for the 13 sets of 12 sensors are computed and shown in the upper portion of Table 4.8. Though the number of *NZV* in set number 8 increases from 1 (corresponding to the case where the data is noise-free as shown in the upper portion of Table 4.5) to 2, sensor 8 is still correctly identified as faulty since set number 8, which produces the smallest *NZV* = 2, does not comprise sensor 8. This conclusion is reinforced by performing the sensor validation algorithm on the readings of the 12 sensors in set number 8. Results in the lower portion of Table 4.8 assure that sensor 8 is indeed faulty. Similar trend is also observed for the case where sensors 8 and 10 are faulty as the results shown in Tables 4.9-4.10.

Table 4.8. Sensor validation results (element 86 damaged, sensor 8 faulty, $k = 1$)

Set No.	Sensors	*NZV*	Set No.	Sensors	*NZV*
1	[2,3,4,5,6,7,8,9,10,11,12,13]	3	8	[1,2,3,4,5,6,7,9,10,11,12,13]	**2**
2	[1,3,4,5,6,7,8,9,10,11,12,13]	3	9	[1,2,3,4,5,6,7,8,10,11,12,13]	3
3	[1,2,4,5,6,7,8,9,10,11,12,13]	3	10	[1,2,3,4,5,6,7,8,9,11,12,13]	3
4	[1,2,3,5,6,7,8,9,10,11,12,13]	3	11	[1,2,3,4,5,6,7,8,9,10,12,13]	3
5	[1,2,3,4,6,7,8,9,10,11,12,13]	3	12	[1,2,3,4,5,6,7,8,9,10,11,13]	3
6	[1,2,3,4,5,7,8,9,10,11,12,13]	3	13	[1,2,3,4,5,6,7,8,9,10,11,12]	3
7	[1,2,3,4,5,6,8,9,10,11,12,13]	3			
1a	[2,3,4,5,6,7,9,10,11,12,13]	2	7a	[1,2,3,4,5,6,9,10,11,12,13]	2
2a	[1,3,4,5,6,7,9,10,11,12,13]	2	8a	[1,2,3,4,5,6,7,10,11,12,13]	2
3a	[1,2,4,5,6,7,9,10,11,12,13]	2	9a	[1,2,3,4,5,6,7,9,11,12,13]	2
4a	[1,2,3,5,6,7,9,10,11,12,13]	2	10a	[1,2,3,4,5,6,7,9,10,12,13]	2
5a	[1,2,3,4,6,7,9,10,11,12,13]	2	11a	[1,2,3,4,5,6,7,9,10,11,13]	2
6a	[1,2,3,4,5,7,9,10,11,12,13]	2	12a	[1,2,3,4,5,6,7,9,10,11,12]	2

Table 4.9. Sensor validation results (element 86 damaged, sensors 8 & 10 faulty, $k = 1$)

Set No.	Sensor	*NZV*	Set No.	Sensor	*NZV*
1	[2,3,4,5,6,7,8,9,10,11,12,13]	4	8	[1,2,3,4,5,6,7,9,10,11,12,13]	**3**
2	[1,3,4,5,6,7,8,9,10,11,12,13]	4	9	[1,2,3,4,5,6,7,8,10,11,12,13]	4
3	[1,2,4,5,6,7,8,9,10,11,12,13]	4	10	[1,2,3,4,5,6,7,8,9,11,12,13]	**3**
4	[1,2,3,5,6,7,8,9,10,11,12,13]	4	11	[1,2,3,4,5,6,7,8,9,10,12,13]	4
5	[1,2,3,4,6,7,8,9,10,11,12,13]	4	12	[1,2,3,4,5,6,7,8,9,10,11,13]	4
6	[1,2,3,4,5,6,8,9,10,11,12,13]	4	13	[1,2,3,4,5,6,7,8,9,10,11,12]	4
7	[1,2,3,4,5,6,7,9,10,11,12,13]	4			

Table 4.10. Sensor validation results (element 86 damaged, sensors 8 & 10 faulty, k = 1)

Set No.	Sensor	*NZV*	Set No.	Sensor	*NZV*
1	[3,4,5,6,7,8,9,10,11,12,13]	4	40	[1,2,3,5,6,7,8,9,10,12,13]	4
2	[2,4,5,6,7,8,9,10,11,12,13]	4	41	[1,2,3,5,6,7,8,9,10,11,13]	4
3	[2,3,5,6,7,8,9,10,11,12,13]	4	42	[1,2,3,5,6,7,8,9,10,11,12]	4
4	[2,3,4,6,7,8,9,10,11,12,13]	4	43	[1,2,3,4,7,8,9,10,11,12,13]	4
5	[2,3,4,5,7,8,9,10,11,12,13]	4	44	[1,2,3,4,6,8,9,10,11,12,13]	4
6	[2,3,4,5,6,8,9,10,11,12,13]	4	45	[1,2,3,4,6,7,9,10,11,12,13]	3
7	[2,3,4,5,6,7,9,10,11,12,13]	3	46	[1,2,3,4,6,7,8,10,11,12,13]	4
8	[2,3,4,5,6,7,8,10,11,12,13]	4	47	[1,2,3,4,6,7,8,9,11,12,13]	3
9	[2,3,4,5,6,7,8,9,11,12,13]	3	48	[1,2,3,4,6,7,8,9,10,12,13]	4
10	[2,3,4,5,6,7,8,9,10,12,13]	4	49	[1,2,3,4,6,7,8,9,10,11,13]	4
11	[2,3,4,5,6,7,8,9,10,11,13]	4	50	[1,2,3,4,6,7,8,9,10,11,12]	4
12	[2,3,4,5,6,7,8,9,10,11,12]	4	51	[1,2,3,4,5,8,9,10,11,12,13]	4
13	[1,4,5,6,7,8,9,10,11,12,13]	4	52	[1,2,3,4,5,7,9,10,11,12,13]	3
14	[1,3,5,6,7,8,9,10,11,12,13]	4	53	[1,2,3,4,5,7,8,10,11,12,13]	4
15	[1,3,4,6,7,8,9,10,11,12,13]	4	54	[1,2,3,4,5,7,8,9,11,12,13]	3
16	[1,3,4,5,7,8,9,10,11,12,13]	4	55	[1,2,3,4,5,7,8,9,10,12,13]	4
17	[1,3,4,5,6,8,9,10,11,12,13]	4	56	[1,2,3,4,5,7,8,9,10,11,13]	4
18	[1,3,4,5,6,7,9,10,11,12,13]	3	57	[1,2,3,4,5,7,8,9,10,11,12]	4
19	[1,3,4,5,6,7,8,10,11,12,13]	4	58	[1,2,3,4,5,6,9,10,11,12,13]	3
20	[1,3,4,5,6,7,8,9,11,12,13]	3	59	[1,2,3,4,5,6,8,10,11,12,13]	4
21	[1,3,4,5,6,7,8,9,10,12,13]	4	60	[1,2,3,4,5,6,8,9,11,12,13]	3
22	[1,3,4,5,6,7,8,9,10,11,13]	4	61	[1,2,3,4,5,6,8,9,10,12,13]	4
23	[1,3,4,5,6,7,8,9,10,11,12]	4	62	[1,2,3,4,5,6,8,9,10,11,13]	4
24	[1,2,5,6,7,8,9,10,11,12,13]	4	63	[1,2,3,4,5,6,8,9,10,11,12]	4
25	[1,2,4,6,7,8,9,10,11,12,13]	4	64	[1,2,3,4,5,6,7,10,11,12,13]	3
26	[1,2,4,5,7,8,9,10,11,12,13]	4	65	[1,2,3,4,5,6,7,9,11,12,13]	**2**
27	[1,2,4,5,6,8,9,10,11,12,13]	4	66	[1,2,3,4,5,6,7,9,10,12,13]	3
28	[1,2,4,5,6,7,9,10,11,12,13]	3	67	[1,2,3,4,5,6,7,9,10,11,13]	3
29	[1,2,4,5,6,7,8,10,11,12,13]	4	68	[1,2,3,4,5,6,7,9,10,11,12]	3
30	[1,2,4,5,6,7,8,9,11,12,13]	3	69	[1,2,3,4,5,6,7,8,11,12,13]	3
31	[1,2,4,5,6,7,8,9,10,12,13]	4	70	[1,2,3,4,5,6,7,8,10,12,13]	4
32	[1,2,4,5,6,7,8,9,10,11,13]	4	71	[1,2,3,4,5,6,7,8,10,11,13]	4
33	[1,2,4,5,6,7,8,9,10,11,12]	4	72	[1,2,3,4,5,6,7,8,10,11,12]	4
34	[1,2,3,6,7,8,9,10,11,12,13]	4	73	[1,2,3,4,5,6,7,8,9,12,13]	3
35	[1,2,3,5,7,8,9,10,11,12,13]	4	74	[1,2,3,4,5,6,7,8,9,11,13]	3
36	[1,2,3,5,6,8,9,10,11,12,13]	4	75	[1,2,3,4,5,6,7,8,9,11,12]	3
37	[1,2,3,5,6,7,9,10,11,12,13]	3	76	[1,2,3,4,5,6,7,8,9,10,13]	4
38	[1,2,3,5,6,7,8,10,11,12,13]	4	77	[1,2,3,4,5,6,7,8,9,10,12]	4
39	[1,2,3,5,6,7,8,9,11,12,13]	3	78	[1,2,3,4,5,6,7,8,9,10,11]	4
1a	[2,3,4,5,6,7,9,11,12,13]	2	7a	[1,2,3,4,5,6,9,11,12,13]	2
2a	[1,3,4,5,6,7,9,11,12,13]	2	8a	[1,2,3,4,5,6,7,11,12,13]	2
3a	[1,2,4,5,6,7,9,11,12,13]	2	9a	[1,2,3,4,5,6,7,9,12,13]	2
4a	[1,2,3,5,6,7,9,11,12,13]	2	10a	[1,2,3,4,5,6,7,9,11,13]	2
5a	[1,2,3,4,6,7,9,11,12,13]	2	11a	[1,2,3,4,5,6,7,9,11,12]	2
6a	[1,2,3,4,5,7,9,11,12,13]	2			

4.5.2 Experimental example

The experimental truss in Section 2.9.2 is employed again to generate displacement responses (refer to Fig. 2.18 for the experimental truss and Table 2.2 for specifications of the truss members). The node and element numbers of the structure are given in Fig. 2.8. Thirteen 10 mm displacement transducers (model CDP) and a data logger (model TDS-303) are employed to monitor the vertical displacements of all nodes at the lower chords of the truss. The positions and numbers of the displacement transducers are shown in Fig. 2.8c. A static load of 921.5 N, which can create displacement responses of approximately 2 mm, is shifted through all the 13 monitored nodes at the lower chord of the truss at both the reference and the damaged states to generate displacement responses to estimate the flexibility matrices formulated with respect to the sensor locations. Damage in the truss is generated by changing element 86 from steel to aluminum tube (specifications of the tubes are given in Table 2.2).

From readings of the 13 displacement transducers, 13 sets of 12 accelerometers are formulated. Next, flexibility matrices with respect to the sensor locations of all 13 sets are computed for both the reference and the damaged states of the structure. Singular value decompositions are then performed on the change in flexibility matrices to identify the *NZV* and results are tabulated in Table 4.11. Because all sets of 12 sensors produce the same $NZV = 2$, N_1 is assigned zero, indicating that all sensors are indeed healthy.

Table 4.11. Experimental results for sensor validation (element 86 damaged, $k = 1$)

Set No.	Sensors	*NZV*	Set No.	Sensors	*NZV*
1	[2,3,4,5,6,7,8,9,10,11,12,13]	2	8	[1,2,3,4,5,6,7,9,10,11,12,13]	2
2	[1,3,4,5,6,7,8,9,10,11,12,13]	2	9	[1,2,3,4,5,6,7,8,10,11,12,13]	2
3	[1,2,4,5,6,7,8,9,10,11,12,13]	2	10	[1,2,3,4,5,6,7,8,9,11,12,13]	2
4	[1,2,3,5,6,7,8,9,10,11,12,13]	2	11	[1,2,3,4,5,6,7,8,9,10,12,13]	2
5	[1,2,3,4,6,7,8,9,10,11,12,13]	2	12	[1,2,3,4,5,6,7,8,9,10,11,13]	2
6	[1,2,3,4,5,7,8,9,10,11,12,13]	2	13	[1,2,3,4,5,6,7,8,9,10,11,12]	2
7	[1,2,3,4,5,6,8,9,10,11,12,13]				

To further assess the performance of the sensor validation algorithm with measurement error using experimental data, 2 cases of faulty sensors are simulated, namely (1) fault in sensor 8; and (2) faults in both sensors 8 and 10. The fault is generated by multiplying the measured values with a constant of 1.5 (gain fault). Faulty sensors are associated with both the reference ("healthy") and damaged states of the structure. In other words, measured displacements by faulty sensors at both the reference and the damaged states are affected by the faults.

For the case where sensor 8 is faulty, 13 sets of 12 sensors are formulated and the flexibility matrices with respect to the sensor locations of all sets are computed, based on which the *NZV* is identified and summarized in the upper portion of Table 4.12. Since only set number 8 produces the smallest $NZV = 2$ ($N_1 = 1$), it comprises all healthy sensors and sensor 8 is suspected as faulty. This conclusion is confirmed by the results at the lower portion of Table 4.12 where the sensor validation algorithm is utilized to validate the 12 sensors in set number 8. Correct conclusion is also observed for the case where sensors 8 and 10 are faulty based on the summarized results in Tables 4.13-4.14.

Table 4.12. Experimental results for sensor validation (element 86 damaged, sensor 8 faulty, k= 1)

Set No.	Sensors	*NZV*	Set No.	Sensors	*NZV*
1	[2,3,4,5,6,7,8,9,10,11,12,13]	4	8	[1,2,3,4,5,6,7,9,10,11,12,13]	**2**
2	[1,3,4,5,6,7,8,9,10,11,12,13]	4	9	[1,2,3,4,5,6,7,8,10,11,12,13]	4
3	[1,2,4,5,6,7,8,9,10,11,12,13]	4	10	[1,2,3,4,5,6,7,8,9,11,12,13]	4
4	[1,2,3,5,6,7,8,9,10,11,12,13]	4	11	[1,2,3,4,5,6,7,8,9,10,12,13]	4
5	[1,2,3,4,6,7,8,9,10,11,12,13]	4	12	[1,2,3,4,5,6,7,8,9,10,11,13]	4
6	[1,2,3,4,5,7,8,9,10,11,12,13]	4	13	[1,2,3,4,5,6,7,8,9,10,11,12]	4
7	[1,2,3,4,5,6,8,9,10,11,12,13]				
1a	[2,3,4,5,6,7,9,10,11,12,13]	2	7a	[1,2,3,4,5,6,9,10,11,12,13]	2
2a	[1,3,4,5,6,7,9,10,11,12,13]	2	8a	[1,2,3,4,5,6,7,10,11,12,13]	2
3a	[1,2,4,5,6,7,9,10,11,12,13]	2	9a	[1,2,3,4,5,6,7,9,11,12,13]	2
4a	[1,2,3,5,6,7,9,10,11,12,13]	2	10a	[1,2,3,4,5,6,7,9,10,12,13]	2
5a	[1,2,3,4,6,7,9,10,11,12,13]	2	11a	[1,2,3,4,5,6,7,9,10,11,13]	2
6a	[1,2,3,4,5,7,9,10,11,12,13]	2	12a	[1,2,3,4,5,6,7,9,10,11,12]	2

Table 4.13. Experimental results for sensor validation (element 86 damaged, sensors 8 and 10 faulty, k = 1)

Set No.	Sensor	*NZV*	Set No.	Sensor	*NZV*
1	[2,3,4,5,6,7,8,9,10,11,12,13]	4	8	[1,2,3,4,5,6,7,9,10,11,12,13]	**3**
2	[1,3,4,5,6,7,8,9,10,11,12,13]	4	9	[1,2,3,4,5,6,7,8,10,11,12,13]	4
3	[1,2,4,5,6,7,8,9,10,11,12,13]	4	10	[1,2,3,4,5,6,7,8,9,11,12,13]	**3**
4	[1,2,3,5,6,7,8,9,10,11,12,13]	4	11	[1,2,3,4,5,6,7,8,9,10,12,13]	4
5	[1,2,3,4,6,7,8,9,10,11,12,13]	4	12	[1,2,3,4,5,6,7,8,9,10,11,13]	4
6	[1,2,3,4,5,6,8,9,10,11,12,13]	4	13	[1,2,3,4,5,6,7,8,9,10,11,12]	4
7	[1,2,3,4,5,6,7,9,10,11,12,13]	4			

Table 4.14. Experimental results for sensor validation (element 86 damaged, sensors 8 & 10 faulty, $k = 2$)

Set No.	Sensor	*NZV*	Set No.	Sensor	*NZV*
1	[3,4,5,6,7,8,9,10,11,12,13]	4	40	[1,2,3,5,6,7,8,9,10,12,13]	4
2	[2,4,5,6,7,8,9,10,11,12,13]	4	41	[1,2,3,5,6,7,8,9,10,11,13]	4
3	[2,3,5,6,7,8,9,10,11,12,13]	4	42	[1,2,3,5,6,7,8,9,10,11,12]	4
4	[2,3,4,6,7,8,9,10,11,12,13]	4	43	[1,2,3,4,7,8,9,10,11,12,13]	4
5	[2,3,4,5,7,8,9,10,11,12,13]	4	44	[1,2,3,4,6,8,9,10,11,12,13]	4
6	[2,3,4,5,6,8,9,10,11,12,13]	4	45	[1,2,3,4,6,7,9,10,11,12,13]	3
7	[2,3,4,5,6,7,9,10,11,12,13]	3	46	[1,2,3,4,6,7,8,10,11,12,13]	4
8	[2,3,4,5,6,7,8,10,11,12,13]	4	47	[1,2,3,4,6,7,8,9,11,12,13]	3
9	[2,3,4,5,6,7,8,9,11,12,13]	3	48	[1,2,3,4,6,7,8,9,10,12,13]	4
10	[2,3,4,5,6,7,8,9,10,12,13]	4	49	[1,2,3,4,6,7,8,9,10,11,13]	4
11	[2,3,4,5,6,7,8,9,10,11,13]	4	50	[1,2,3,4,6,7,8,9,10,11,12]	4
12	[2,3,4,5,6,7,8,9,10,11,12]	4	51	[1,2,3,4,5,8,9,10,11,12,13]	4
13	[1,4,5,6,7,8,9,10,11,12,13]	4	52	[1,2,3,4,5,7,9,10,11,12,13]	3
14	[1,3,5,6,7,8,9,10,11,12,13]	4	53	[1,2,3,4,5,7,8,10,11,12,13]	4
15	[1,3,4,6,7,8,9,10,11,12,13]	4	54	[1,2,3,4,5,7,8,9,11,12,13]	3
16	[1,3,4,5,7,8,9,10,11,12,13]	4	55	[1,2,3,4,5,7,8,9,10,12,13]	4
17	[1,3,4,5,6,8,9,10,11,12,13]	4	56	[1,2,3,4,5,7,8,9,10,11,13]	4
18	[1,3,4,5,6,7,9,10,11,12,13]	3	57	[1,2,3,4,5,7,8,9,10,11,12]	4
19	[1,3,4,5,6,7,8,10,11,12,13]	4	58	[1,2,3,4,5,6,9,10,11,12,13]	3
20	[1,3,4,5,6,7,8,9,11,12,13]	3	59	[1,2,3,4,5,6,8,10,11,12,13]	4
21	[1,3,4,5,6,7,8,9,10,12,13]	4	60	[1,2,3,4,5,6,8,9,11,12,13]	3
22	[1,3,4,5,6,7,8,9,10,11,13]	4	61	[1,2,3,4,5,6,8,9,10,12,13]	4
23	[1,3,4,5,6,7,8,9,10,11,12]	4	62	[1,2,3,4,5,6,8,9,10,11,13]	4
24	[1,2,5,6,7,8,9,10,11,12,13]	4	63	[1,2,3,4,5,6,8,9,10,11,12]	4
25	[1,2,4,6,7,8,9,10,11,12,13]	4	64	[1,2,3,4,5,6,7,10,11,12,13]	3
26	[1,2,4,5,7,8,9,10,11,12,13]	4	65	[1,2,3,4,5,6,7,9,11,12,13]	**2**
27	[1,2,4,5,6,8,9,10,11,12,13]	4	66	[1,2,3,4,5,6,7,9,10,12,13]	3
28	[1,2,4,5,6,7,9,10,11,12,13]	3	67	[1,2,3,4,5,6,7,9,10,11,13]	3
29	[1,2,4,5,6,7,8,10,11,12,13]	4	68	[1,2,3,4,5,6,7,9,10,11,12]	3
30	[1,2,4,5,6,7,8,9,11,12,13]	3	69	[1,2,3,4,5,6,7,8,11,12,13]	3
31	[1,2,4,5,6,7,8,9,10,12,13]	4	70	[1,2,3,4,5,6,7,8,10,12,13]	4
32	[1,2,4,5,6,7,8,9,10,11,13]	4	71	[1,2,3,4,5,6,7,8,10,11,13]	4
33	[1,2,4,5,6,7,8,9,10,11,12]	4	72	[1,2,3,4,5,6,7,8,10,11,12]	4
34	[1,2,3,6,7,8,9,10,11,12,13]	4	73	[1,2,3,4,5,6,7,8,9,12,13]	3
35	[1,2,3,5,7,8,9,10,11,12,13]	4	74	[1,2,3,4,5,6,7,8,9,11,13]	3
36	[1,2,3,5,6,8,9,10,11,12,13]	4	75	[1,2,3,4,5,6,7,8,9,11,12]	3
37	[1,2,3,5,6,7,9,10,11,12,13]	3	76	[1,2,3,4,5,6,7,8,9,10,13]	4
38	[1,2,3,5,6,7,8,10,11,12,13]	4	77	[1,2,3,4,5,6,7,8,9,10,12]	4
39	[1,2,3,5,6,7,8,9,11,12,13]	3	78	[1,2,3,4,5,6,7,8,9,10,11]	4
1a	[2,3,4,5,6,7,9,11,12,13]	2	7a	[1,2,3,4,5,6,9,11,12,13]	2
2a	[1,3,4,5,6,7,9,11,12,13]	2	8a	[1,2,3,4,5,6,7,11,12,13]	2
3a	[1,2,4,5,6,7,9,11,12,13]	2	9a	[1,2,3,4,5,6,7,9,12,13]	2
4a	[1,2,3,5,6,7,9,11,12,13]	2	10a	[1,2,3,4,5,6,7,9,11,13]	2
5a	[1,2,3,4,6,7,9,11,12,13]	2	11a	[1,2,3,4,5,6,7,9,11,12]	2
6a	[1,2,3,4,5,7,9,11,12,13]	2			

4.6 ACCELEROMETER VALIDATION

4.6.1 Numerical example

The 3-D modular truss structure shown in Fig. 2.8 is used again to generate acceleration responses. The truss is excited by a vertical zero-mean white noise load at node 7 and vertical accelerations of all 13 nodes at the lower chord of the truss are monitored. To generate acceleration responses which fall within the range of the accelerometers used (50 g), the *RMS* of magnitudes of the excited load is selected to be 100 N, resulting in acceleration responses of approximately 20 m/s^2 in *RMS* amplitude. Damage in the truss is generated by equivalently imposing 20% reduction in axial stiffness of element 86. The reference or "healthy" state of the structure is associated with the case where all sensors are "healthy"; the damaged state of the structure is associated with the case where some sensors are faulty. Two cases of faulty sensors are investigated, namely (1) sensor 8 is faulty; and (2) sensors 8 and 10 are faulty. Locations of sensors are given in Fig. 2.8c. The fault in sensor 8 is simulated by adding a zero-mean white noise signal (random error) having *RMS* equals to 35% *RMS* of the actual signal whereas the fault in sensor 10 is simulated by a positive shift (additive error) in its amplitudes by an amount equals to magnitude of 3.5% *RMS* of the actual signal. At first, it is assumed that all "healthy" sensors are noise free. The presence of noise in the "healthy" sensors will be investigated later in this section.

Sensor 8 faulty

From 13 sensors, 12 sets of signal data each comprising 12 sensors, which satisfy the minimum requirement that 1 sensor (sensor at node 7) is collocated with the actuator, are formulated. From the response accelerations of each set and the simulated excitation forces, the flexibility matrices with respect to the sensor locations at both the

reference and the damaged states are computed. Based on the difference in flexibility matrices, *SVD* is performed to identify the *NZV*. The results in the upper portion of Table 4.15 show that only set number 7 produces the smallest *NZV* (= 1), implying that N_1 = 1 and that set number 7 contains all healthy sensors. Sensor 8 which does not belong to set number 7 is classified as faulty. For further investigation, the sensor validation is performed on the 12 sensors belonging to set number 7. Similarly, 11 sets of signal data, each containing 11 sensors and satisfying the requirement that at least 1 sensor (sensor at node 7) is collocated with the actuator, are formulated and the *NZV* for each set identified. Results in the lower portion of Table 4.15 show that the *NZV* cannot be further reduced to zero. Following the sensor validation algorithm, the 12 sensors in set number 7 are classified as healthy and the *NZV* in the 11 sets at the lower portion of Table 4.15 may be attributed to the presence of structural damage or the round-off error, reinforcing that set number 7 in the upper portion of Table 4.15 contains all healthy sensors, implying that sensor 8 is faulty.

To investigate the robustness of the sensor validation algorithm, various zero-mean white noise levels with *RMS* ranging from 1% to 100% are added to the generated acceleration at sensor 8 to simulate the fault. Performing the same computational procedure as above, the number of *NZV* for 12 sets of 12 sensors are identified and plotted in Fig. 4.11. It can be observed that if the noise level is less than 29%, all sensors are classified as healthy since all sets produce the same *NZV* = 1 and hence N_1 is set to zero. If the noise level in sensor 8 is greater than 30%, sensor 8 is classified as faulty since set number 7 is the only set producing the smallest *NZV* = 1 (N_1 = 1).

Table 4.15. Sensor validation results (element 86 damaged, sensor 8 faulty, $k = 1$)

Set No.	Sensor numbers	Skipped Sensors	*NZV*	Set No.	Sensor numbers	Skipped Sensors	*NZV*
1	[2,3,4,5,6,7,8,9,10,11,12,13]	1	2	7	[1,2,3,4,5,6,7,9,10,11,12,13]	8	**1**
2	[1,3,4,5,6,7,8,9,10,11,12,13]	2	2	8	[1,2,3,4,5,6,7,8,10,11,12,13]	9	2
3	[1,2,4,5,6,7,8,9,10,11,12,13]	3	2	9	[1,2,3,4,5,6,7,8,9,11,12,13]	10	2
4	[1,2,3,5,6,7,8,9,10,11,12,13]	4	2	10	[1,2,3,4,5,6,7,8,9,10,12,13]	11	2
5	[1,2,3,4,6,7,8,9,10,11,12,13]	5	2	11	[1,2,3,4,5,6,7,8,9,10,11,13]	12	2
6	[1,2,3,4,5,6,8,9,10,11,12,13]	7	2	12	[1,2,3,4,5,6,7,8,9,10,11,12]	13	2
1a	[2,3,4,5,6,7,9,10,11,12,13]	1	1	7a	[1,2,3,4,5,6,7,10,11,12,13]	9	1
2a	[1,3,4,5,6,7,9,10,11,12,13]	2	1	8a	[1,2,3,4,5,6,7,9,11,12,13]	10	1
3a	[1,2,4,5,6,7,9,10,11,12,13]	3	1	9a	[1,2,3,4,5,6,7,9,10,12,13]	11	1
4a	[1,2,3,5,6,7,9,10,11,12,13]	4	1	10a	[1,2,3,4,5,6,7,9,10,11,13]	12	1
5a	[1,2,3,4,6,7,9,10,11,12,13]	5	1	11a	[1,2,3,4,5,6,7,9,10,11,12]	13	1
6a	[1,2,3,4,5,6,9,10,11,12,13]	7	1				

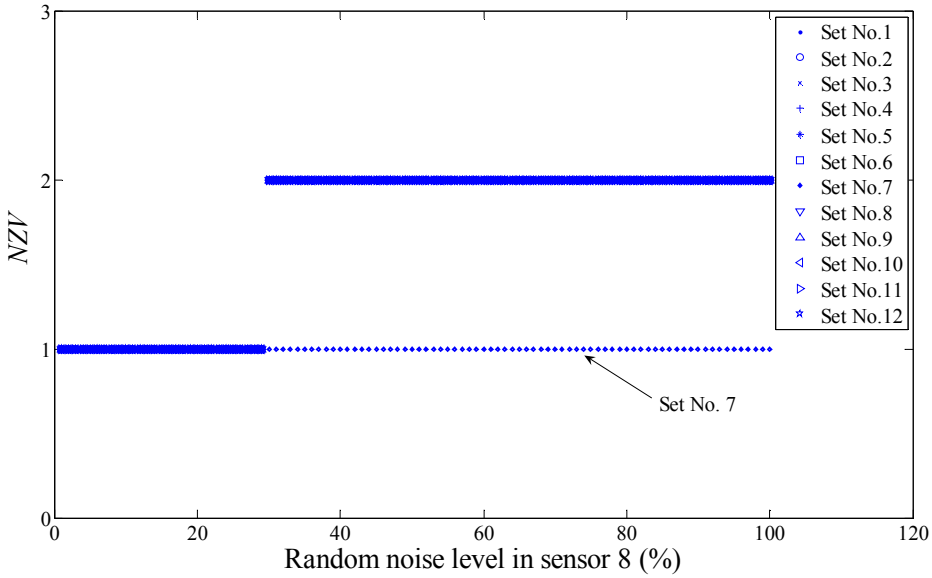

Fig. 4.11. Relationship between random error in sensor 8 and *NZV*

Sensors 8 and 10 faulty

Following the same procedure as above, 12 sets each comprises 12 sensors are formulated to compute the corresponding flexibility matrices with respect to the sensor locations at the reference and the damaged states of the structure. From the difference in the flexibility matrices at each set, the *NZV* is computed and shown in Table 4.16. Set numbers 7 and 9 produce the smallest *NZV* = 2, implying that $N_1 = 2$. Since there

are more than 1 sets producing the smallest *NZV*, 66 combinatorial sets of 11 sensors (since sensor at node 7 is required to be present in all sets of sensors) are next considered. From each set of measurements, the flexibility matrices are computed for the reference and the damaged states of the structure based on which the *NZV* is identified and shown in upper portion of Table 4.17. The *NZV* is minimal for set number 53 where sensors 8 and 10 are not present, indicating that they are faulty. For further investigation, the sensor validation algorithm is performed for the 11 sensors in set number 53. Results in the lower portion of Table 4.17 indicate that the *NZV* for each set cannot be further reduced. Following the sensor validation algorithm, the 11 sensors belonging to set number 53 in the upper portion of Table 4.17 are healthy, reinforcing that sensors 8 and 10 are in fact faulty.

To investigate the effect of additive error in sensor 10 on the sensor validation result, various additive errors ranging from 0% to 10% are employed to contaminate the simulated acceleration at sensor 10 whereas the random error in sensor 8 is kept constant at 35%. Following the above procedure by starting with $k = 1$, the *NZV* for all 12 sets of 12 sensors are computed and plotted in Fig. 4.12a. If the additive error in sensor 10 is less than 3.1%, only set number 7 produces the smallest $NZV = 1$ ($N_1 = 1$), indicating that sensor 8 is faulty. If the additive error in sensor 10 is greater than 3.1%, set numbers 7 and 9 produce the same smallest $NZV = 2$ ($N_1 = 2$). Continuing the sensor validation algorithm with $k = 2$, 66 combinatorial sets of 11 sensors are formulated and the results of *NZV* for set number 53 are plotted in Fig. 4.12b. Since sensors 8 and 10 do not belong to set number 53 which produces the smallest $NZV = 1$ ($N_1 = 1$), they are correctly classified as faulty.

Table 4.16. Sensor validation results (element 86 damaged, sensors 8 & 10 faulty, $k = 1$)

Set No.	Sensor numbers	Skipped sensors	*NZV*	Set No.	Sensor numbers	Skipped sensors	*NZV*
1	[2,3,4,5,6,7,8,9,10,11,12,13]	1	3	7	[1,2,3,4,5,6,7,9,10,11,12,13]	8	**2**
2	[1,3,4,5,6,7,8,9,10,11,12,13]	2	3	8	[1,2,3,4,5,6,7,8,10,11,12,13]	9	3
3	[1,2,4,5,6,7,8,9,10,11,12,13]	3	3	9	[1,2,3,4,5,6,7,8,9,11,12,13]	10	**2**
4	[1,2,3,5,6,7,8,9,10,11,12,13]	4	3	10	[1,2,3,4,5,6,7,8,9,10,12,13]	11	3
5	[1,2,3,4,6,7,8,9,10,11,12,13]	5	3	11	[1,2,3,4,5,6,7,8,9,10,11,13]	12	3
6	[1,2,3,4,5,6,8,9,10,11,12,13]	7	3	12	[1,2,3,4,5,6,7,8,9,10,11,12]	13	3

Table 4.17. Sensor validation results (element 86 damaged, sensors 8 & 10 faulty, $k = 2$)

Set No.	Sensor numbers	Skipped sensors	*NZV*	Set No.	Sensor	Skipped sensors	*NZV*
1	[3,4,5,6,7,8,9,10,11,12,13]	[1,2]	3	34	[1,2,3,5,6,7,8,10,11,12,13]	[4,9]	3
2	[2,4,5,6,7,8,9,10,11,12,13]	[1,3]	3	35	[1,2,3,5,6,7,8,9,11,12,13]	[4,10]	2
3	[2,3,5,6,7,8,9,10,11,12,13]	[1,4]	3	36	[1,2,3,5,6,7,8,9,10,12,13]	[4,11]	3
4	[2,3,4,6,7,8,9,10,11,12,13]	[1,5]	3	37	[1,2,3,5,6,7,8,9,10,11,13]	[4,12]	3
5	[2,3,4,5,6,8,9,10,11,12,13]	[1,7]	3	38	[1,2,3,5,6,7,8,9,10,11,12]	[4,13]	3
6	[2,3,4,5,6,7,9,10,11,12,13]	[1,8]	2	39	[1,2,3,4,6,8,9,10,11,12,13]	[5,7]	3
7	[2,3,4,5,6,7,8,10,11,12,13]	[1,9]	3	40	[1,2,3,4,6,7,9,10,11,12,13]	[5,8]	2
8	[2,3,4,5,6,7,8,9,11,12,13]	[1,10]	2	41	[1,2,3,4,6,7,8,10,11,12,13]	[5,9]	3
9	[2,3,4,5,6,7,8,9,10,12,13]	[1,11]	3	42	[1,2,3,4,6,7,8,9,11,12,13]	[5,10]	2
10	[2,3,4,5,6,7,8,9,10,11,13]	[1,12]	3	43	[1,2,3,4,6,7,8,9,10,12,13]	[5,11]	3
11	[2,3,4,5,6,7,8,9,10,11,12]	[1,13]	3	44	[1,2,3,4,6,7,8,9,10,11,13]	[5,12]	3
12	[1,4,5,6,7,8,9,10,11,12,13]	[2,3]	3	45	[1,2,3,4,6,7,8,9,10,11,12]	[5,13]	3
13	[1,3,5,6,7,8,9,10,11,12,13]	[2,4]	3	46	[1,2,3,4,5,6,9,10,11,12,13]	[7,8]	2
14	[1,3,4,6,7,8,9,10,11,12,13]	[2,5]	3	47	[1,2,3,4,5,6,8,10,11,12,13]	[7,9]	3
15	[1,3,4,5,6,8,9,10,11,12,13]	[2,7]	3	48	[1,2,3,4,5,6,8,9,11,12,13]	[7,10]	2
16	[1,3,4,5,6,7,9,10,11,12,13]	[2,8]	2	49	[1,2,3,4,5,6,8,9,10,12,13]	[7,11]	3
17	[1,3,4,5,6,7,8,10,11,12,13]	[2,9]	3	50	[1,2,3,4,5,6,8,9,10,11,13]	[7,12]	3
18	[1,3,4,5,6,7,8,9,11,12,13]	[2,10]	2	51	[1,2,3,4,5,6,8,9,10,11,12]	[7,13]	3
19	[1,3,4,5,6,7,8,9,10,12,13]	[2,11]	3	52	[1,2,3,4,5,6,7,10,11,12,13]	[8,9]	2
20	[1,3,4,5,6,7,8,9,10,11,13]	[2,12]	3	53	[1,2,3,4,5,6,7,9,11,12,13]	[8,10]	**1**
21	[1,3,4,5,6,7,8,9,10,11,12]	[2,13]	3	54	[1,2,3,4,5,6,7,9,10,12,13]	[8,11]	2
22	[1,2,5,6,7,8,9,10,11,12,13]	[3,4]	3	55	[1,2,3,4,5,6,7,9,10,11,13]	[8,12]	2
23	[1,2,4,6,7,8,9,10,11,12,13]	[3,5]	3	56	[1,2,3,4,5,6,7,9,10,11,12]	[8,13]	2
24	[1,2,4,5,6,8,9,10,11,12,13]	[3,7]	3	57	[1,2,3,4,5,6,7,8,11,12,13]	[9,10]	2
25	[1,2,4,5,6,7,9,10,11,12,13]	[3,8]	2	58	[1,2,3,4,5,6,7,8,10,12,13]	[9,11]	3
26	[1,2,4,5,6,7,8,10,11,12,13]	[3,9]	3	59	[1,2,3,4,5,6,7,8,10,11,13]	[9,12]	3
27	[1,2,4,5,6,7,8,9,11,12,13]	[3,10]	2	60	[1,2,3,4,5,6,7,8,10,11,12]	[9,13]	3
28	[1,2,4,5,6,7,8,9,10,12,13]	[3,11]	3	61	[1,2,3,4,5,6,7,8,9,12,13]	[10,11]	2
29	[1,2,4,5,6,7,8,9,10,11,13]	[3,12]	3	62	[1,2,3,4,5,6,7,8,9,11,13]	[10,12]	2
30	[1,2,4,5,6,7,8,9,10,11,12]	[3,13]	3	63	[1,2,3,4,5,6,7,8,9,11,12]	[10,13]	2
31	[1,2,3,6,7,8,9,10,11,12,13]	[4,5]	3	64	[1,2,3,4,5,6,7,8,9,10,13]	[11,12]	3
32	[1,2,3,5,6,8,9,10,11,12,13]	[4,7]	3	65	[1,2,3,4,5,6,7,8,9,10,12]	[11,13]	3
33	[1,2,3,5,6,7,9,10,11,12,13]	[4,8]	2	66	[1,2,3,4,5,6,7,8,9,10,11]	[12,13]	3
1a	[2,3,4,5,6,7,9,11,12,13]	1	1	6a	[1,2,3,4,5,6,9,11,12,13]	7	1
2a	[1,3,4,5,6,7,9,11,12,13]	2	1	7a	[1,2,3,4,5,6,7,11,12,13]	9	1
3a	[1,2,4,5,6,7,9,11,12,13]	3	1	8a	[1,2,3,4,5,6,7,9,12,13]	11	1
4a	[1,2,3,5,6,7,9,11,12,13]	4	1	9a	[1,2,3,4,5,6,7,9,11,13]	12	1
5a	[1,2,3,4,6,7,9,11,12,13]	5	1	10a	[1,2,3,4,5,6,7,9,11,12]	13	1

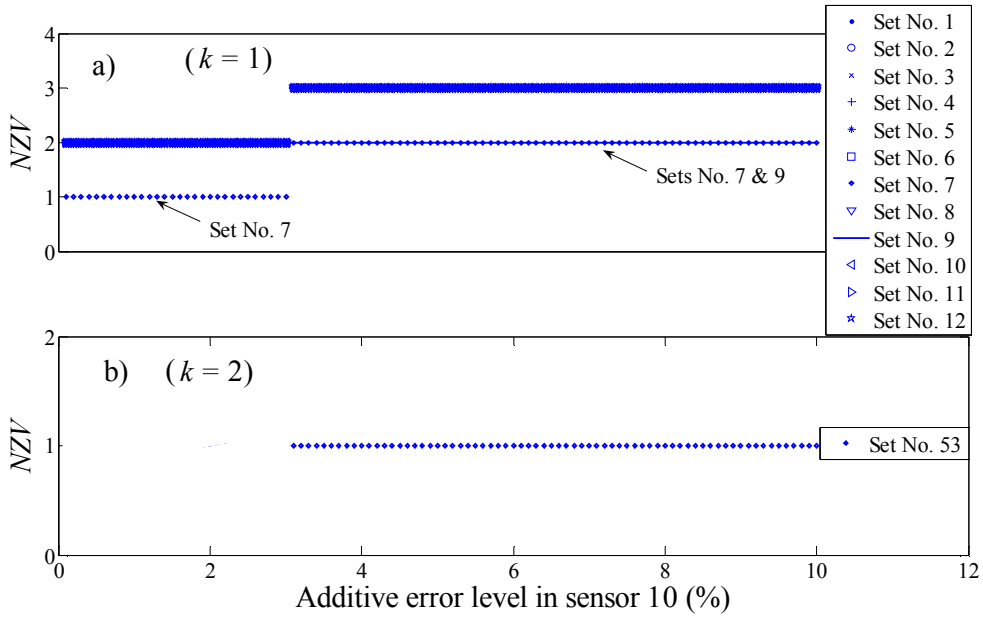

Fig. 4.12. Relationship between additive error in sensor 10 and *NZV* (35% noise in sensor 8)

Sensor validation with noisy data

To investigate the effect of noise on the performance of the sensor validation algorithm, the above example is performed again where zero-mean white noise with *RMS* of (*i*) 5%, and (*ii*) 10% *RMS* of the signal is added to all the response accelerations and the input force to generate contaminated data. For the case where sensor 8 is faulty, the *NZV* for the 12 sets of 12 sensors are computed and shown in the upper portion of Table 4.18. Though the number of *NZV* in set number 7 increases from 1 (corresponding to the case where the data is noise-free as shown in the upper portion of Table 4.15) to 2, sensor 8 is still correctly identified as faulty since set number 7, which produces the smallest *NZV* = 2, does not comprise sensor 8. The same computation is performed for the case where 10% noise is added and sensor 8 is faulty. Results of the *NZV* for all 12 sets of 12 sensors are shown in the lower portion of Table 4.18. The increment of noise level from 5% to 10% make the number of *NZV* in set number 7 increases from 2 to 3. Nevertheless, continuing with the sensor validation

algorithm, sensor 8 is still identified correctly as faulty. Similar trend is also observed for the case where sensors 8 and 10 are faulty as the results shown in Tables 4.19-4.20.

In summary, using the threshold of 0.01 introduced in Section 4.3.2 to classify *NZV*, the number of *NZV* increases as the signals get noisier. However, faulty sensors can still be identified correctly following the proposed sensor validation algorithm.

The sensor validation algorithm is able to accommodate the case where readings from each faulty sensor are: (*i*) positively shifted a value equal to 2.5% *RMS* of the measured signal; and (*ii*) added with a zero-mean white noise with *RMS* of 25% *RMS* of the measured signal (hybrid error). For the case where sensor 8 is faulty, performing the sensor validation algorithm, the computed *NZV* for all 12 sets containing 12 sensors in the upper portion of Table 4.21 identify that the fault is confined to sensor 8. For further validating the 12 sensors belonging to set number 7 which produces the smallest $NZV = 1$, the 11 sets each contains 11 sensors are formulated. The *NZV* for each set is then computed and shown in the lower portion of Table 4.21. Since all 11 sets produce the same $NZV = 1$, they are classified as healthy, confirming that sensor 8 is faulty. The same trend is also observed for the case where both sensors 8 and 10 are faulty though the results are not presented here.

Faulty sensor in undamaged structure

The sensor validation algorithm can still work well for the case where the structure is not damaged. Performing the algorithm for the case where the structure is not damaged and sensor 8 is faulty, the *NZV* for all 12 sets of 12 sensors are summarized in the upper portion of Table 4.22. Set number 7, which does not contains sensor 8, still produces the smallest $NZV = 0$, implying that sensor 8 is faulty. Performing the sensor validation algorithm on the 12 sensors in set number 7 confirms

that they are indeed healthy as results shown in the lower portion of Table 4.22. If the simulated accelerations from "healthy" sensors are contaminated with 5% noise, the faulty sensor can still be identified correctly based on the results shown in Table 4.23. By removing the readings from faulty sensor 8, the *DLV* method is able to confirm that the structure is healthy as shown in Table 4.24 following the intersection scheme. Particularly, from the readings of the remaining 12 sensors, the change in flexibility matrix with respect to the sensor locations is computed and 10 *DLV*s are identified. Applying these *DLV*s onto the reference structural model as nodal force vectors produces elements (20, 55, 73) as the set of potential damaged elements (*PDE*). The current intersected damaged set (*IDS*) therefore contains elements (20, 55, 73) and *ne* = 3. By omitting the readings of the sensor at node 11, the readings of the remaining 11 sensors are used to formulate the flexibility matrices at the reference and the damaged states. Performing *SVD* on the change in flexibility matrix, a set of 9 *DLV*s is identified and when applying onto the reference structural model as nodal force vector yields a set of *PDE* comprising elements (41, 45). Intersecting the set of *PDE* and the current *IDS* which contains elements (20, 55, 73) gives an empty set of *IDS* (*ne* = 0), indicating that no element is damaged. Correct conclusion is also observed for the case where sensors 8 and 10 are faulty although the results are not presented here. The results imply that the sensor validation algorithm can be integrated with the *DLV* method to identify signals that are corrupted besides performing damage detection.

Table 4.18. Sensor validation results (element 86 damaged, sensor 8 faulty, 5% & 10% noise, $k = 1$)

Set No.	Sensor numbers	Skipped sensors	*NZV*	Set No.	Sensor numbers	Skipped sensors	*NZV*
5% noise							
1	[2,3,4,5,6,7,8,9,10,11,12,13]	1	3	7	[1,2,3,4,5,6,7,9,10,11,12,13]	8	**2**
2	[1,3,4,5,6,7,8,9,10,11,12,13]	2	3	8	[1,2,3,4,5,6,7,8,10,11,12,13]	9	3
3	[1,2,4,5,6,7,8,9,10,11,12,13]	3	3	9	[1,2,3,4,5,6,7,8,9,11,12,13]	10	3
4	[1,2,3,5,6,7,8,9,10,11,12,13]	4	3	10	[1,2,3,4,5,6,7,8,9,10,12,13]	11	3
5	[1,2,3,4,6,7,8,9,10,11,12,13]	5	3	11	[1,2,3,4,5,6,7,8,9,10,11,13]	12	3
6	[1,2,3,4,5,6,8,9,10,11,12,13]	7	3	12	[1,2,3,4,5,6,7,8,9,10,11,12]	13	3
10% noise							
1	[2,3,4,5,6,7,8,9,10,11,12,13]	1	5	7	[1,2,3,4,5,6,7,9,10,11,12,13]	8	**3**
2	[1,3,4,5,6,7,8,9,10,11,12,13]	2	5	8	[1,2,3,4,5,6,7,8,10,11,12,13]	9	5
3	[1,2,4,5,6,7,8,9,10,11,12,13]	3	5	9	[1,2,3,4,5,6,7,8,9,11,12,13]	10	5
4	[1,2,3,5,6,7,8,9,10,11,12,13]	4	5	10	[1,2,3,4,5,6,7,8,9,10,12,13]	11	5
5	[1,2,3,4,6,7,8,9,10,11,12,13]	5	5	11	[1,2,3,4,5,6,7,8,9,10,11,13]	12	5
6	[1,2,3,4,5,6,8,9,10,11,12,13]	7	5	12	[1,2,3,4,5,6,7,8,9,10,11,12]	13	5

Table 4.19 Numerical results for sensor validation (element 86 damaged, sensors 8 & 10 faulty, 5% noise)

	Set No.	Sensor	*NZV*	Set No.	Sensor	*NZV*
(k = 1)	1	[2,3,4,5,6,7,8,9,10,11,12,13]	5	7	[1,2,3,4,5,6,7,9,10,11,12,13]	**3**
	2	[1,3,4,5,6,7,8,9,10,11,12,13]	5	8	[1,2,3,4,5,6,7,8,10,11,12,13]	5
	3	[1,2,4,5,6,7,8,9,10,11,12,13]	5	9	[1,2,3,4,5,6,7,8,9,11,12,13]	**3**
	4	[1,2,3,5,6,7,8,9,10,11,12,13]	5	10	[1,2,3,4,5,6,7,8,9,10,12,13]	5
	5	[1,2,3,4,6,7,8,9,10,11,12,13]	5	11	[1,2,3,4,5,6,7,8,9,10,11,13]	5
	6	[1,2,3,4,5,6,8,9,10,11,12,13]	5	12	[1,2,3,4,5,6,7,8,9,10,11,12]	5
(k = 2)	1	[3,4,5,6,7,8,9,10,11,12,13]	5	34	[1,2,3,5,6,7,8,10,11,12,13]	5
	2	[2,4,5,6,7,8,9,10,11,12,13]	5	35	[1,2,3,5,6,7,8,9,11,12,13]	3
	3	[2,3,5,6,7,8,9,10,11,12,13]	5	36	[1,2,3,5,6,7,8,9,10,12,13]	5
	4	[2,3,4,6,7,8,9,10,11,12,13]	5	37	[1,2,3,5,6,7,8,9,10,11,13]	5
	5	[2,3,4,5,6,8,9,10,11,12,13]	5	38	[1,2,3,5,6,7,8,9,10,11,12]	5
	6	[2,3,4,5,6,7,9,10,11,12,13]	3	39	[1,2,3,4,6,8,9,10,11,12,13]	5
	7	[2,3,4,5,6,7,8,10,11,12,13]	5	40	[1,2,3,4,6,7,9,10,11,12,13]	3
	8	[2,3,4,5,6,7,8,9,11,12,13]	3	41	[1,2,3,4,6,7,8,10,11,12,13]	5
	9	[2,3,4,5,6,7,8,9,10,12,13]	5	42	[1,2,3,4,6,7,8,9,11,12,13]	3
	10	[2,3,4,5,6,7,8,9,10,11,13]	5	43	[1,2,3,4,6,7,8,9,10,12,13]	5
	11	[2,3,4,5,6,7,8,9,10,11,12]	5	44	[1,2,3,4,6,7,8,9,10,11,13]	5
	12	[1,4,5,6,7,8,9,10,11,12,13]	5	45	[1,2,3,4,6,7,8,9,10,11,12]	5
	13	[1,3,5,6,7,8,9,10,11,12,13]	5	46	[1,2,3,4,5,6,9,10,11,12,13]	3
	14	[1,3,4,6,7,8,9,10,11,12,13]	5	47	[1,2,3,4,5,6,8,10,11,12,13]	5
	15	[1,3,4,5,6,8,9,10,11,12,13]	5	48	[1,2,3,4,5,6,8,9,11,12,13]	3
	16	[1,3,4,5,6,7,9,10,11,12,13]	3	49	[1,2,3,4,5,6,8,9,10,12,13]	5
	17	[1,3,4,5,6,7,8,10,11,12,13]	5	50	[1,2,3,4,5,6,8,9,10,11,13]	5
	18	[1,3,4,5,6,7,8,9,11,12,13]	3	51	[1,2,3,4,5,6,8,9,10,11,12]	5
	19	[1,3,4,5,6,7,8,9,10,12,13]	5	52	[1,2,3,4,5,6,7,10,11,12,13]	3
	20	[1,3,4,5,6,7,8,9,10,11,13]	5	53	[1,2,3,4,5,6,7,9,11,12,13]	**2**
	21	[1,3,4,5,6,7,8,9,10,11,12]	5	54	[1,2,3,4,5,6,7,9,10,12,13]	3
	22	[1,2,5,6,7,8,9,10,11,12,13]	5	55	[1,2,3,4,5,6,7,9,10,11,13]	3
	23	[1,2,4,6,7,8,9,10,11,12,13]	5	56	[1,2,3,4,5,6,7,9,10,11,12]	3
	24	[1,2,4,5,6,8,9,10,11,12,13]	5	57	[1,2,3,4,5,6,7,8,11,12,13]	3
	25	[1,2,4,5,6,7,9,10,11,12,13]	3	58	[1,2,3,4,5,6,7,8,10,12,13]	5
	26	[1,2,4,5,6,7,8,10,11,12,13]	5	59	[1,2,3,4,5,6,7,8,10,11,13]	5
	27	[1,2,4,5,6,7,8,9,11,12,13]	3	60	[1,2,3,4,5,6,7,8,10,11,12]	5
	28	[1,2,4,5,6,7,8,9,10,12,13]	5	61	[1,2,3,4,5,6,7,8,9,12,13]	3
	29	[1,2,4,5,6,7,8,9,10,11,13]	5	62	[1,2,3,4,5,6,7,8,9,11,13]	3
	30	[1,2,4,5,6,7,8,9,10,11,12]	5	63	[1,2,3,4,5,6,7,8,9,11,12]	3
	31	[1,2,3,6,7,8,9,10,11,12,13]	5	64	[1,2,3,4,5,6,7,8,9,10,13]	5
	32	[1,2,3,5,6,8,9,10,11,12,13]	5	65	[1,2,3,4,5,6,7,8,9,10,12]	5
	33	[1,2,3,5,6,7,9,10,11,12,13]	3	66	[1,2,3,4,5,6,7,8,9,10,11]	5

Table 4.20 Numerical results for sensor validation (element 86 damaged, sensors 8 & 10 faulty, 10% noise)

	Set No.	Sensor	*NZV*	Set No.	Sensor	*NZV*
(k = 1)	1	[2,3,4,5,6,7,8,9,10,11,12,13]	7	7	[1,2,3,4,5,6,7,9,10,11,12,13]	**5**
	2	[1,3,4,5,6,7,8,9,10,11,12,13]	7	8	[1,2,3,4,5,6,7,8,10,11,12,13]	7
	3	[1,2,4,5,6,7,8,9,10,11,12,13]	7	9	[1,2,3,4,5,6,7,8,9,11,12,13]	**5**
	4	[1,2,3,5,6,7,8,9,10,11,12,13]	7	10	[1,2,3,4,5,6,7,8,9,10,12,13]	7
	5	[1,2,3,4,6,7,8,9,10,11,12,13]	7	11	[1,2,3,4,5,6,7,8,9,10,11,13]	7
	6	[1,2,3,4,5,6,8,9,10,11,12,13]	7	12	[1,2,3,4,5,6,7,8,9,10,11,12]	7
(k = 2)	1	[3,4,5,6,7,8,9,10,11,12,13]	7	34	[1,2,3,5,6,7,8,10,11,12,13]	7
	2	[2,4,5,6,7,8,9,10,11,12,13]	7	35	[1,2,3,5,6,7,8,9,11,12,13]	5
	3	[2,3,5,6,7,8,9,10,11,12,13]	7	36	[1,2,3,5,6,7,8,9,10,12,13]	7
	4	[2,3,4,6,7,8,9,10,11,12,13]	7	37	[1,2,3,5,6,7,8,9,10,11,13]	7
	5	[2,3,4,5,6,8,9,10,11,12,13]	7	38	[1,2,3,5,6,7,8,9,10,11,12]	7
	6	[2,3,4,5,6,7,9,10,11,12,13]	5	39	[1,2,3,4,6,8,9,10,11,12,13]	7
	7	[2,3,4,5,6,7,8,10,11,12,13]	7	40	[1,2,3,4,6,7,9,10,11,12,13]	5
	8	[2,3,4,5,6,7,8,9,11,12,13]	5	41	[1,2,3,4,6,7,8,10,11,12,13]	7
	9	[2,3,4,5,6,7,8,9,10,12,13]	7	42	[1,2,3,4,6,7,8,9,11,12,13]	5
	10	[2,3,4,5,6,7,8,9,10,11,13]	7	43	[1,2,3,4,6,7,8,9,10,12,13]	7
	11	[2,3,4,5,6,7,8,9,10,11,12]	7	44	[1,2,3,4,6,7,8,9,10,11,13]	7
	12	[1,4,5,6,7,8,9,10,11,12,13]	7	45	[1,2,3,4,6,7,8,9,10,11,12]	7
	13	[1,3,5,6,7,8,9,10,11,12,13]	7	46	[1,2,3,4,5,6,9,10,11,12,13]	5
	14	[1,3,4,6,7,8,9,10,11,12,13]	7	47	[1,2,3,4,5,6,8,10,11,12,13]	7
	15	[1,3,4,5,6,8,9,10,11,12,13]	7	48	[1,2,3,4,5,6,8,9,11,12,13]	5
	16	[1,3,4,5,6,7,9,10,11,12,13]	5	49	[1,2,3,4,5,6,8,9,10,12,13]	7
	17	[1,3,4,5,6,7,8,10,11,12,13]	7	50	[1,2,3,4,5,6,8,9,10,11,13]	7
	18	[1,3,4,5,6,7,8,9,11,12,13]	5	51	[1,2,3,4,5,6,8,9,10,11,12]	7
	19	[1,3,4,5,6,7,8,9,10,12,13]	7	52	[1,2,3,4,5,6,7,10,11,12,13]	5
	20	[1,3,4,5,6,7,8,9,10,11,13]	7	53	[1,2,3,4,5,6,7,9,11,12,13]	**4**
	21	[1,3,4,5,6,7,8,9,10,11,12]	7	54	[1,2,3,4,5,6,7,9,10,12,13]	5
	22	[1,2,5,6,7,8,9,10,11,12,13]	7	55	[1,2,3,4,5,6,7,9,10,11,13]	5
	23	[1,2,4,6,7,8,9,10,11,12,13]	7	56	[1,2,3,4,5,6,7,9,10,11,12]	5
	24	[1,2,4,5,6,8,9,10,11,12,13]	7	57	[1,2,3,4,5,6,7,8,11,12,13]	5
	25	[1,2,4,5,6,7,9,10,11,12,13]	5	58	[1,2,3,4,5,6,7,8,10,12,13]	7
	26	[1,2,4,5,6,7,8,10,11,12,13]	7	59	[1,2,3,4,5,6,7,8,10,11,13]	7
	27	[1,2,4,5,6,7,8,9,11,12,13]	5	60	[1,2,3,4,5,6,7,8,10,11,12]	7
	28	[1,2,4,5,6,7,8,9,10,12,13]	7	61	[1,2,3,4,5,6,7,8,9,12,13]	5
	29	[1,2,4,5,6,7,8,9,10,11,13]	7	62	[1,2,3,4,5,6,7,8,9,11,13]	5
	30	[1,2,4,5,6,7,8,9,10,11,12]	7	63	[1,2,3,4,5,6,7,8,9,11,12]	5
	31	[1,2,3,6,7,8,9,10,11,12,13]	7	64	[1,2,3,4,5,6,7,8,9,10,13]	7
	32	[1,2,3,5,6,8,9,10,11,12,13]	7	65	[1,2,3,4,5,6,7,8,9,10,12]	7
	33	[1,2,3,5,6,7,9,10,11,12,13]	5	66	[1,2,3,4,5,6,7,8,9,10,11]	7

Table 4.21. Sensor validation results (element 86 damaged, sensor 8 faulty with hybrid error, k=1)

Set No.	Sensors	*NZV*	Set No.	Sensors	*NZV*
1	[2,3,4,5,6,7,8,9,10,11,12,13]	3	7	[1,2,3,4,5,6,7,9,10,11,12,13]	**1**
2	[1,3,4,5,6,7,8,9,10,11,12,13]	3	8	[1,2,3,4,5,6,7,8,10,11,12,13]	3
3	[1,2,4,5,6,7,8,9,10,11,12,13]	3	9	[1,2,3,4,5,6,7,8,9,11,12,13]	3
4	[1,2,3,5,6,7,8,9,10,11,12,13]	3	10	[1,2,3,4,5,6,7,8,9,10,12,13]	3
5	[1,2,3,4,6,7,8,9,10,11,12,13]	3	11	[1,2,3,4,5,6,7,8,9,10,11,13]	3
6	[1,2,3,4,5,6,8,9,10,11,12,13]	3	12	[1,2,3,4,5,6,7,8,9,10,11,12]	3
1a	[2,3,4,5,6,7,9,10,11,12,13]	1	7a	[1,2,3,4,5,6,7,10,11,12,13]	1
2a	[1,3,4,5,6,7,9,10,11,12,13]	1	8a	[1,2,3,4,5,6,7,9,11,12,13]	1
3a	[1,2,4,5,6,7,9,10,11,12,13]	1	9a	[1,2,3,4,5,6,7,9,10,12,13]	1
4a	[1,2,3,5,6,7,9,10,11,12,13]	1	10a	[1,2,3,4,5,6,7,9,10,11,13]	1
5a	[1,2,3,4,6,7,9,10,11,12,13]	1	11a	[1,2,3,4,5,6,7,9,10,11,12]	1
6a	[1,2,3,4,5,7,9,10,11,12,13]	1			

Table 4.22. Sensor validation results (structure healthy, sensor 8 faulty, k = 1)

Set No.	Sensors	*NZV*	Set No.	Sensors	*NZV*
1	[2,3,4,5,6,7,8,9,10,11,12,13]	1	7	[1,2,3,4,5,6,7,9,10,11,12,13]	**0**
2	[1,3,4,5,6,7,8,9,10,11,12,13]	1	8	[1,2,3,4,5,6,7,8,10,11,12,13]	1
3	[1,2,4,5,6,7,8,9,10,11,12,13]	1	9	[1,2,3,4,5,6,7,8,9,11,12,13]	1
4	[1,2,3,5,6,7,8,9,10,11,12,13]	1	10	[1,2,3,4,5,6,7,8,9,10,12,13]	1
5	[1,2,3,4,6,7,8,9,10,11,12,13]	1	11	[1,2,3,4,5,6,7,8,9,10,11,13]	1
6	[1,2,3,4,5,6,8,9,10,11,12,13]	1	12	[1,2,3,4,5,6,7,8,9,10,11,12]	1
1a	[2,3,4,5,6,7,9,10,11,12,13]	0	7a	[1,2,3,4,5,6,7,10,11,12,13]	0
2a	[1,3,4,5,6,7,9,10,11,12,13]	0	8a	[1,2,3,4,5,6,7,9,11,12,13]	0
3a	[1,2,4,5,6,7,9,10,11,12,13]	0	9a	[1,2,3,4,5,6,7,9,10,12,13]	0
4a	[1,2,3,5,6,7,9,10,11,12,13]	0	10a	[1,2,3,4,5,6,7,9,10,11,13]	0
5a	[1,2,3,4,6,7,9,10,11,12,13]	0	11a	[1,2,3,4,5,6,7,9,10,11,12]	0
6a	[1,2,3,4,5,7,9,10,11,12,13]	0			

Table 4.23. Sensor validation results (structure healthy, sensor 8 faulty, 5% noise, k = 1)

Set No.	Sensors	*NZV*	Set No.	Sensors	*NZV*
1	[2,3,4,5,6,7,8,9,10,11,12,13]	9	7	[1,2,3,4,5,6,7,9,10,11,12,13]	**8**
2	[1,3,4,5,6,7,8,9,10,11,12,13]	9	8	[1,2,3,4,5,6,7,8,10,11,12,13]	9
3	[1,2,4,5,6,7,8,9,10,11,12,13]	9	9	[1,2,3,4,5,6,7,8,9,11,12,13]	9
4	[1,2,3,5,6,7,8,9,10,11,12,13]	9	10	[1,2,3,4,5,6,7,8,9,10,12,13]	9
5	[1,2,3,4,6,7,8,9,10,11,12,13]	9	11	[1,2,3,4,5,6,7,8,9,10,11,13]	9
6	[1,2,3,4,5,6,8,9,10,11,12,13]	9	12	[1,2,3,4,5,6,7,8,9,10,11,12]	9
1a	[2,3,4,5,6,7,9,10,11,12,13]	8	7a	[1,2,3,4,5,6,7,10,11,12,13]	8
2a	[1,3,4,5,6,7,9,10,11,12,13]	8	8a	[1,2,3,4,5,6,7,9,11,12,13]	8
3a	[1,2,4,5,6,7,9,10,11,12,13]	8	9a	[1,2,3,4,5,6,7,9,10,12,13]	8
4a	[1,2,3,5,6,7,9,10,11,12,13]	8	10a	[1,2,3,4,5,6,7,9,10,11,13]	8
5a	[1,2,3,4,6,7,9,10,11,12,13]	8	11a	[1,2,3,4,5,6,7,9,10,11,12]	8
6a	[1,2,3,4,5,7,9,10,11,12,13]	8			

Table 4.24. Damage detection results using Intersection Scheme and readings of 12 healthy sensors

	Sensor numbers	Skipped sensors	No. of *DLV*	*PDE*	Eliminated elements	*IDS*	*ne*
ns =12	[1,2,3,4,5,6,7,9,10,11,12,13]		10	[20,55,73]		[20,55,73]	3
k=ns- 1= 11	[1,2,3,4,5,6,7,10,11,12,13]	9	9	[41, 45]	[20,55,73]	[]	0

4.6.2 Experimental example

The experiment truss in Section 3.5 is employed again to physically generate acceleration readings (refer to Fig. 3.12 for the experimental truss and Table 2.2 for specifications of the truss members). The node and element numbers of the structure are given in Fig. 2.8. Thirteen 50 g accelerometers are used to physically measure acceleration responses at all nodes at the lower chord of the structure (see Fig. 2.8c for accelerometer numbers and positions). Zero-mean white noise load is generated by a shaker with capacity of 75 lbs (334 N) and is applied vertically onto the structure at node 7. The *RMS* amplitude of the excited load is selected to be 100 N such that acceleration responses are within the measurement range of the accelerometers. Applied load onto the structure is measured by a force sensor with capacity of 100 lbs

(445 N). Damage in the structure is generated by changing element 86 from steel to aluminum tube (specifications of the tubes are given in Table 2.2).

From 13 accelerometers, 12 sets of 12 accelerometers, each satisfying the requirement that 1 sensor (at node 7) is collocated with the shaker, are formulated. From the readings of the accelerometers and the force sensor, flexibility matrices with respect to the sensor locations of all 12 sets are computed for both the reference and the damaged states of the structure. Singular value decompositions are then performed on the change in flexibility matrices to identify the *NZV* and results are tabulated in Table 4.25. Because all sets of 12 sensors produce the same $NZV = 2$, N_1 is assigned zero, indicating that all sensors are indeed healthy.

Table 4.25. Experimental results for sensor validation (element 86 damaged, $k = 1$)

Set No.	Sensors	*NZV*	Set No.	Sensors	*NZV*
1	[2,3,4,5,6,7,8,9,10,11,12,13]	2	7	[1,2,3,4,5,6,7,9,10,11,12,13]	2
2	[1,3,4,5,6,7,8,9,10,11,12,13]	2	8	[1,2,3,4,5,6,7,8,10,11,12,13]	2
3	[1,2,4,5,6,7,8,9,10,11,12,13]	2	9	[1,2,3,4,5,6,7,8,9,11,12,13]	2
4	[1,2,3,5,6,7,8,9,10,11,12,13]	2	10	[1,2,3,4,5,6,7,8,9,10,12,13]	2
5	[1,2,3,4,6,7,8,9,10,11,12,13]	2	11	[1,2,3,4,5,6,7,8,9,10,11,13]	2
6	[1,2,3,4,5,6,8,9,10,11,12,13]	2	12	[1,2,3,4,5,6,7,8,9,10,11,12]	2

To further assess the performance of the sensor validation algorithm with measurement error using experimental data, 2 cases of faulty sensors are simulated, namely (1) fault in sensor 8; and (2) faults in both sensors 8 and 10. Similar to Kerschen et al. (2005), the fault in sensor 8 is simulated by multiplying the measured signal with a constant of 1.5 (gain fault) whereas measured acceleration by sensor 10 is replaced by a zero-mean white noise sequence of the same *RMS* (failure) to generate sensor fault. Faulty sensors are associated with both the reference ("healthy") and damaged states of the structure. In other words, measured accelerations by faulty sensors at both the reference and the damaged states are affected by the faults.

For the case where sensor 8 is faulty, 12 sets of 12 sensors are formulated and the flexibility matrices with respect to the sensor locations of all sets are computed, based on which the *NZV* is identified and summarized in the upper portion of Table 4.26. Since only set number 7 produces the smallest *NZV* = 1 (N_1 = 1), it comprises all healthy sensors and sensor 8 is classified as faulty. This conclusion is confirmed by the results at the lower portion of Table 4.26 where the sensor validation algorithm is performed to validate the 12 sensors in set number 7. Correct conclusion is also observed for the case where sensors 8 and 10 are faulty based on the summarized results in Tables 4.26-4.27.

Table 4.26. Experimental results for sensor validation (element 86 damaged, sensor 8 faulty, *k*= 1)

Set No.	Sensors	*NZV*	Set No.	Sensors	*NZV*
1	[2,3,4,5,6,7,8,9,10,11,12,13]	4	7	[1,2,3,4,5,6,7,9,10,11,12,13]	**2**
2	[1,3,4,5,6,7,8,9,10,11,12,13]	4	8	[1,2,3,4,5,6,7,8,10,11,12,13]	4
3	[1,2,4,5,6,7,8,9,10,11,12,13]	4	9	[1,2,3,4,5,6,7,8,9,11,12,13]	4
4	[1,2,3,5,6,7,8,9,10,11,12,13]	4	10	[1,2,3,4,5,6,7,8,9,10,12,13]	4
5	[1,2,3,4,6,7,8,9,10,11,12,13]	4	11	[1,2,3,4,5,6,7,8,9,10,11,13]	4
6	[1,2,3,4,5,6,8,9,10,11,12,13]	4	12	[1,2,3,4,5,6,7,8,9,10,11,12]	4
1a	[2,3,4,5,6,7,9,10,11,12,13]	2	7a	[1,2,3,4,5,6,7,10,11,12,13]	2
2a	[1,3,4,5,6,7,9,10,11,12,13]	2	8a	[1,2,3,4,5,6,7,9,11,12,13]	2
3a	[1,2,4,5,6,7,9,10,11,12,13]	2	9a	[1,2,3,4,5,6,7,9,10,12,13]	2
4a	[1,2,3,5,6,7,9,10,11,12,13]	2	10a	[1,2,3,4,5,6,7,9,10,11,13]	2
5a	[1,2,3,4,6,7,9,10,11,12,13]	2	11a	[1,2,3,4,5,6,7,9,10,11,12]	2
6a	[1,2,3,4,5,7,9,10,11,12,13]	2			

Table 4.27. Experimental results for sensor validation (element 86 damaged, sensors 8 and 10 faulty, *k* = 1)

Set No.	Sensors	*NZV*	Set No.	Sensors	*NZV*
1	[2,3,4,5,6,7,8,9,10,11,12,13]	4	7	[1,2,3,4,5,6,7,9,10,11,12,13]	**3**
2	[1,3,4,5,6,7,8,9,10,11,12,13]	4	8	[1,2,3,4,5,6,7,8,10,11,12,13]	4
3	[1,2,4,5,6,7,8,9,10,11,12,13]	4	9	[1,2,3,4,5,6,7,8,9,11,12,13]	**3**
4	[1,2,3,5,6,7,8,9,10,11,12,13]	4	10	[1,2,3,4,5,6,7,8,9,10,12,13]	4
5	[1,2,3,4,6,7,8,9,10,11,12,13]	4	11	[1,2,3,4,5,6,7,8,9,10,11,13]	4
6	[1,2,3,4,5,6,8,9,10,11,12,13]	4	12	[1,2,3,4,5,6,7,8,9,10,11,12]	4

Table 4.28. Experimental results for sensor validation (element 86 damaged, sensors 8 & 10 faulty, $k = 2$)

Set No.	Sensors	*NZV*	Set No	Sensors	*NZV*
1	[3,4,5,6,7,8,9,10,11,12,13]	4	34	[1,2,3,5,6,7,8,10,11,12,13]	4
2	[2,4,5,6,7,8,9,10,11,12,13]	4	35	[1,2,3,5,6,7,8,9,11,12,13]	3
3	[2,3,5,6,7,8,9,10,11,12,13]	4	36	[1,2,3,5,6,7,8,9,10,12,13]	4
4	[2,3,4,6,7,8,9,10,11,12,13]	4	37	[1,2,3,5,6,7,8,9,10,11,13]	4
5	[2,3,4,5,6,8,9,10,11,12,13]	4	38	[1,2,3,5,6,7,8,9,10,11,12]	4
6	[2,3,4,5,6,7,9,10,11,12,13]	3	39	[1,2,3,4,6,8,9,10,11,12,13]	4
7	[2,3,4,5,6,7,8,10,11,12,13]	4	40	[1,2,3,4,6,7,9,10,11,12,13]	3
8	[2,3,4,5,6,7,8,9,11,12,13]	3	41	[1,2,3,4,6,7,8,10,11,12,13]	4
9	[2,3,4,5,6,7,8,9,10,12,13]	4	42	[1,2,3,4,6,7,8,9,11,12,13]	3
10	[2,3,4,5,6,7,8,9,10,11,13]	4	43	[1,2,3,4,6,7,8,9,10,12,13]	4
11	[2,3,4,5,6,7,8,9,10,11,12]	4	44	[1,2,3,4,6,7,8,9,10,11,13]	4
12	[1,4,5,6,7,8,9,10,11,12,13]	4	45	[1,2,3,4,6,7,8,9,10,11,12]	4
13	[1,3,5,6,7,8,9,10,11,12,13]	4	46	[1,2,3,4,5,6,9,10,11,12,13]	3
14	[1,3,4,6,7,8,9,10,11,12,13]	4	47	[1,2,3,4,5,6,8,10,11,12,13]	4
15	[1,3,4,5,6,8,9,10,11,12,13]	4	48	[1,2,3,4,5,6,8,9,11,12,13]	3
16	[1,3,4,5,6,7,9,10,11,12,13]	3	49	[1,2,3,4,5,6,8,9,10,12,13]	4
17	[1,3,4,5,6,7,8,10,11,12,13]	4	50	[1,2,3,4,5,6,8,9,10,11,13]	4
18	[1,3,4,5,6,7,8,9,11,12,13]	3	51	[1,2,3,4,5,6,8,9,10,11,12]	4
19	[1,3,4,5,6,7,8,9,10,12,13]	4	52	[1,2,3,4,5,6,7,10,11,12,13]	3
20	[1,3,4,5,6,7,8,9,10,11,13]	4	53	[1,2,3,4,5,6,7,9,11,12,13]	**2**
21	[1,3,4,5,6,7,8,9,10,11,12]	4	54	[1,2,3,4,5,6,7,9,10,12,13]	3
22	[1,2,5,6,7,8,9,10,11,12,13]	4	55	[1,2,3,4,5,6,7,9,10,11,13]	3
23	[1,2,4,6,7,8,9,10,11,12,13]	4	56	[1,2,3,4,5,6,7,9,10,11,12]	3
24	[1,2,4,5,6,8,9,10,11,12,13]	4	57	[1,2,3,4,5,6,7,8,11,12,13]	3
25	[1,2,4,5,6,7,9,10,11,12,13]	3	58	[1,2,3,4,5,6,7,8,10,12,13]	4
26	[1,2,4,5,6,7,8,10,11,12,13]	4	59	[1,2,3,4,5,6,7,8,10,11,13]	4
27	[1,2,4,5,6,7,8,9,11,12,13]	3	60	[1,2,3,4,5,6,7,8,10,11,12]	4
28	[1,2,4,5,6,7,8,9,10,12,13]	4	61	[1,2,3,4,5,6,7,8,9,12,13]	3
29	[1,2,4,5,6,7,8,9,10,11,13]	4	62	[1,2,3,4,5,6,7,8,9,11,13]	3
30	[1,2,4,5,6,7,8,9,10,11,12]	4	63	[1,2,3,4,5,6,7,8,9,11,12]	3
31	[1,2,3,6,7,8,9,10,11,12,13]	4	64	[1,2,3,4,5,6,7,8,9,10,13]	4
32	[1,2,3,5,6,8,9,10,11,12,13]	4	65	[1,2,3,4,5,6,7,8,9,10,12]	4
33	[1,2,3,5,6,7,9,10,11,12,13]	3	66	[1,2,3,4,5,6,7,8,9,10,11]	4

4.7 CONCLUDING REMARKS

Definition of faulty displacement transducers and accelerometers in the context of the *DLV* method for structural damage detection was introduced in Section 4.3. Displacement transducers and accelerometers are classified as faulty if based on their readings error in the identified flexibility matrix exceeds 6.5%. An algorithm for

sensor validation was then developed in Section 4.4 to identify the "suitable" measured signals before further processing in the *DLV* method to detect structural damage. Center to the algorithm is the performance of *SVD* on different flexibility matrices formulated with respect to different sets containing the same number of sensors to identify the *NZV*, based on which the relative quality among different sets of sensors is assessed. The set which produces the smallest *NZV* is considered as containing all healthy sensors and sensors which do not belong to this set are suspected as faulty.

The sensor validation algorithm is found applicable to identify both faulty displacement transducers and faulty accelerometers. With the presence of 5% noise in the simulated displacements, the 2 faulty displacement transducers can still be identified correctly. Whereas, 2 faulty accelerometers can also be assessed accurately for the case where all simulated accelerations are contaminated by 10% noise. The sensor validation algorithm is found applicable to identify faulty sensors for both cases, namely whether the structure is healthy or damaged. This characteristic of the sensor validation algorithm makes it possible to be integrated with the *DLV* method to identify signals that are not "suitable" besides performing damage detection. The performance of the sensor validation algorithm in detecting faulty displacement transducers and accelerometers are illustrated using experimental data from a 3-D modular truss structure where both gain fault, which is manifested by multiplying the actual measured signal with a constant of 1.5, and sensor failure, which is manifested by replacing actual measurement by a zero-mean white noise with the same *RMS* of magnitude, can be identified correctly. By ignoring completely the measurement of faulty sensors, structural parameters can still be identified correctly using the measurements of the remaining sensors.

Since the sensor validation algorithm is applicable on the measurement of each sensor, its accuracy does not depend on the type of the host structure. Nevertheless, for structures other than the 3D truss structure used in this study, the value of 7% for detectable level of damaged elements may be set differently, resulting in different threshold of noise level below which the damage detection results by the *DLV* method is still reliable.

CHAPTER 5

DAMAGE DETECTION VIA *DLV* USING WIRELESS SENSORS

5.1 INTRODUCTION

For reliable damage detection results using the *DLV* method, adequate number of quality sensors must be used and these sensors are traditionally connected to data-loggers or oscilloscopes with lengthy wires. The cost of installing and maintaining such wired sensors can be substantial and they may interfere with the normal operations of the structures (Lynch, 2004). The implementation of wireless sensors aims to overcome such difficulties.

Wireless sensors are being implemented in many applications, including structural damage detection and various enhancements have been reported in the last few years such as the improvement on sampling rate (Hou et al., 2008), the improvement on transmission topology (Mechitov et al., 2004). Although measured data on board of sensors has been digitalized, when transmitting the raw measured data from the sensor nodes to the base station, Nagayama (2007) noted that the percentage of lost data is random and can be as high as 86%. Therefore, one challenge in the application of wireless sensors in structural damage detection is the improvement in the quality of measured data. In this chapter, the set-up of wireless sensor for data acquisition is presented in Section 5.2. A data reconstruction algorithm for wireless sensors is proposed to estimate lost values resulting from radio frequency (RF) transmission problem and will be presented in Section 5.3. Numerical examples are performed to assess the robustness of the algorithm in Section 5.4. Comparison with

the existing methods in estimating lost data of a signal is also performed to illustrate the advantages and limitations of the proposed algorithm. Finally, the performance of the lost data reconstruction algorithm and the feasibility of its integration with the *DLV* method to detect structural damage are examined using experimental data from a 3-D modular truss structure in Section 5.5.

5.2 WIRELESS SENSOR NETWORK

5.2.1 Hardware platforms

The Wireless Sensor Network (WSN) used in this study has been constructed using some modifications of the following hardware designed by the University of California Berkeley researchers and commercialized by Crossbow Technology, Inc:

- MICAz mote: MICAz is the latest generation in the Mote families from Crossbow Technology. Each MICAz module (2400 MHz to 2483.5 MHz band) contains a microprocessor and a radio frequency transceiver. The onboard microprocessor (Atmega128L) is programmed using TinyOS-based application programs before implementation. The radio (Chipcon CC2420) facilitates communication between the sensor and the base station. MICAz supports up to 250k bits/sec radio data rate, which is much higher than the previous version MICA2 with 38.4k bits/sec. The outdoor transmission range of MICAz mote is ranging from 75 m to 100 m.
- MTS310 sensor and data acquisition board: MTS310 is a flexible sensor board with a variety of sensing modalities: microphone, sounder, light sensor, thermistor, 2-axis accelerometer, and 2-axis magnetometer. In this study, only the onboard accelerometer is used and all the other sensing modules are shut off to improve sampling rate. The accelerometer on MTS310 sensor board is a

MEMS surface micro-machined 2-axis device, ADXL202JE. The accelerometer features a low current draw of less than 1mA. It provides an analog signal which is passed through an on-board 10-bit Analog to Digital Converter (ADC).

- MIB520 USB interface board: MIB520 USB interface board is used to program or download compiled codes onto a MICAz mote. The MICAz mote has to be plugged onto the MIB520 board which is connected to the control PC via a USB port. The MICAz node when connected to the MIB520 USB interface board functions as a base station for data transfer.
- A control computer (Windows based, 1GB or more of free space in destination drive, 550MB or more of space in C drive).

Each sensor node is built by connecting a MICAz mote to a MTS310 board whereas a base station is built by connecting a MICAz mote to a MIB520 USB interface board.

5.2.2 Software platforms

TinyOS developed by UC Berkeley is used as the primary operating system for the WSN. TinyOS architecture is a totally open source and can support an extensive variety of applications by providing tiny foot-print, event driven system, and several component libraries. This facilitates easy modification for specific applications with high efficiency and reliability.

Multi-hop protocol is adopted in this study, facilitating the use of mesh topology. Unlike the star topology in which each node only communicates with the base station, multi-hop protocol enables nodes to communicate with each other and send data, by hopping if necessary, to reach the destination node or the base station. Compared with

star topology, mesh topology achieves more reliable communication within the network as more than one communication channels can be utilized, and is especially useful for WSN in rough outdoor environment.

To implement multi-hop protocol, the MintRoute algorithm is employed herein. MintRoute is a pro-active routing protocol in which the nodes send periodic routing messages to declare their local states. It is widely used in single base mesh network, providing best-effort multi-hop convergence routing by managing the Neighborhood and Route Tables.

5.2.3 Communication between sensor nodes and base station

In the WSN used in this study, the base station sends a "start measurement" message to all the sensor nodes. Upon receiving the "start measurement" message, the sensor nodes start to sample accelerations at a user-defined sampling rate (in this case, 100 Hz) based on their respective time delay values. The acceleration data are digitalized by an inherent ADC on each sensing node before transmitting to the base station. Each data packet containing four temporal data points is sent to the base station sequentially. The base station receives data and temporarily saves them in the MICAz. Acknowledgement (ACK) message indicating the data packet number will be sent back to the sensor nodes upon receiving the data packets. If the ACK message for a data packet is not received, the sensor node resends the lost data packet while continuously collects and saves the latest acceleration data in its flash memory. Upon receiving the "stop measurement" message from the base station, the sensor nodes stop sampling the accelerations. The communication between the sensor nodes and the base station is summarized in Fig. 5.1. Some possible causes for the loss of data during RF (in this case, 2.4 GHz) communication are:

- A number of wireless sensors send data packets at the same time, leading to clashes.
- The distances between the sensor nodes and the base station are out of the communication range.
- The acknowledgement (ACK) messages of the lost packets are lost. If the ACK messages indicating the lost packet numbers are not received by the sensor node, the lost packets are not resent.

The data loss phenomenon has been experimentally examined by Nagayama (2007). The loss percentage of 20% commonly found in the experiment can pose a huge challenge in the application of WSN for reliable structural damage detection (Nagayama, 2007). However, signal containing lost values is still better than totally faulty signal which is represented by a random time history since some characteristics of the signal may still be retrieved by some data processing procedures. Ongoing research has been carrying out to improve the hardware, software and transmission topology to mitigate the loss of data (Chintalapudj, 2006; Yang, 2007; Spencer et al., 2008). In the next section, numerical reconstruction of lost data is explored in relation to structural damage identification using the *DLV* method.

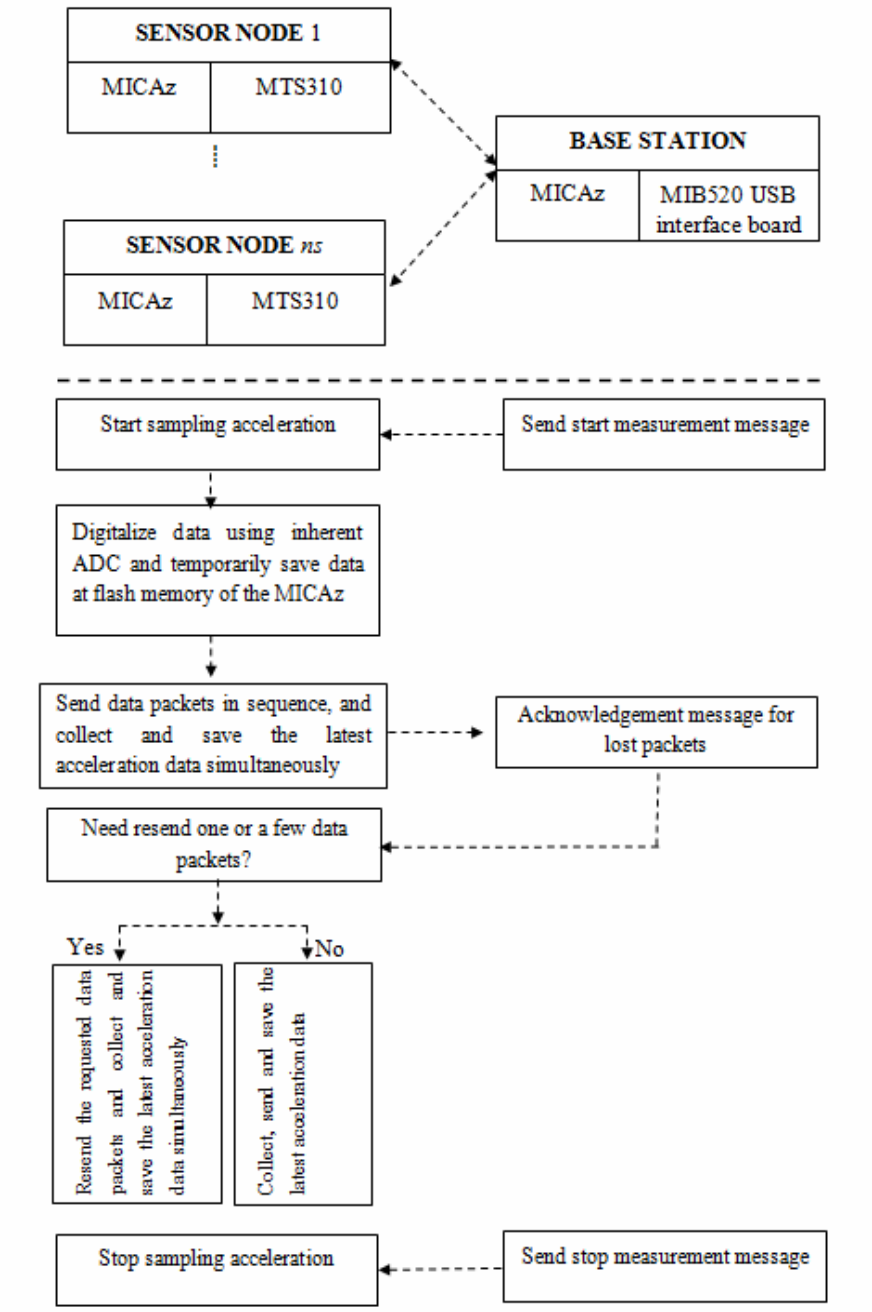

Fig. 5.1. Flow chart for data transmission from sensor nodes to base station

5.3 LOST DATA RECONSTRUCTION FOR WIRELESS SENSORS

In general, virtually all structural response signals can be decomposed into Fourier components at various discrete frequencies. On this basis, if the proportion of data that is lost is not significant, then reconstruction is possible by making use of the

available signal to identify the significant frequencies. For example, for a signal with ξ equally-spaced points of which m measured points are intact and ξ-m points are lost, by setting the latter to zeroes, Fourier transform will yield coefficients (or power spectral values, *PSV*) at various frequencies. By classifying significant frequencies as those with *PSV* normalized by the maximum *PSV* exceeding a threshold of 1%, a set of *nfreq* number of significant frequencies can be filtered, where $nfreq < 0.5\xi$. This threshold of 1% is selected on the basis that if the signal has no lost data, reconstructed signal using all significant frequencies and the corresponding Fourier coefficients will yield less than 1% error relative to the exact signal.

Using these *nfreq* significant frequencies and the m measured signal values, a system of m simultaneous equations can be formed with the Fourier coefficients A_k corresponding to the significant frequencies as unknowns using the following relationship

$$x_n = \frac{1}{\xi}\sum_{k=1}^{nfreq}\left[A_k \exp(\mathrm{j}n\frac{2\pi(k-1)}{\xi})\right] \tag{5.1}$$

where j denotes the imaginary unit. Physically, Eq. (5.1) is the inverse FFT to retrieve signal values at the nth discrete point from *nfreq* number of frequencies and their corresponding Fourier coefficients (A_k). The Fourier coefficients are determined by least-squares fit (requiring that $m > nfreq$ or $m > 0.5\xi$), from which lost portions is estimated using Eq. (5.1) again. Replacing lost data values by estimated values, the complete reconstructed signal is obtained. Performing Fourier transform on the reconstructed signal, a new set of significant frequencies which may not be the same as the previously identified significant frequencies is calculated. This latest set of frequencies is then used as before to compute the Fourier coefficients based on least-squares fit of the m measured data points. A new signal can then be reconstructed and

compared with the previously reconstructed signal. The relative difference, *Rerr*, between the two consecutive reconstructed lost portions of the signal is defined as

$$Rerr = \sqrt{\frac{\sum_{k=1}^{\xi-m}\left(g_k^i - g_k^{i-1}\right)^2}{\sum_{k=1}^{\xi-m}\left(g_k^i\right)^2}} \times 100\% \tag{5.2}$$

where g_k^i, g_k^{i-1} are the estimated lost values at iterations i and (i-1), respectively. This procedure is iterated until *Rerr* is less than 1%. The proposed lost data reconstruction algorithm is summarized in Fig. 5.2. It is noted that the algorithm to reconstruct lost data presented here is performed individually for the signals of each sensor collected at the base station.

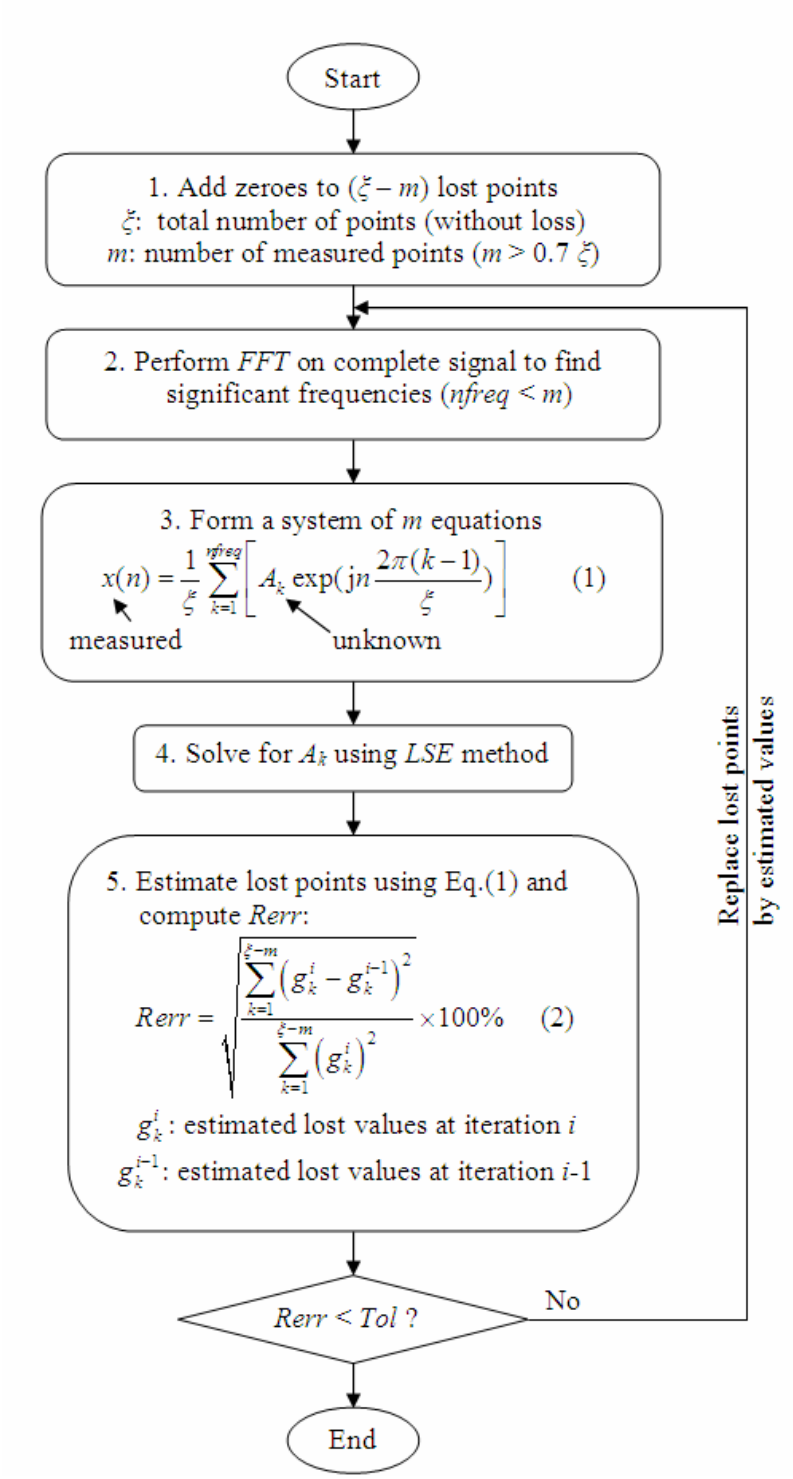

Fig. 5.2. Block diagram for lost data reconstruction algorithm

5.4 NUMERICAL EXAMPLES

A simulated random signal shown in Fig. 5.3a containing 1600 data points, sampled at the rate of 1 kHz is considered. The number of data points for each transmission is 4. The frequency domain of the signal is plotted in Fig. 5.3b.

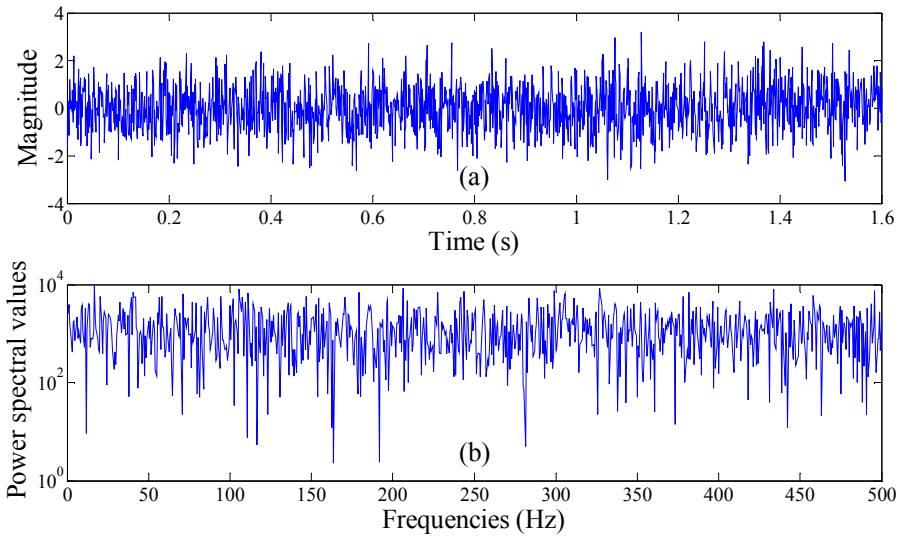

Fig. 5.3. Random signal with sampling rate of 1 kHz: (a) variation of magnitude with time, and (b) variation of power spectral values with frequencies

Determining Significant Frequencies

For determining whether a frequency is significant, a threshold of 1% for the ratio between its *PSV* and the maximum *PSV* in the signal is adopted. To estimate the error due to neglecting the insignificant frequencies, the signal with no missing data is Fourier transformed to identify significant frequencies and the corresponding Fourier coefficients. In theory, 800 frequencies and the corresponding Fourier coefficients can be identified based on 1600 data points. By using only the significant frequencies with their corresponding Fourier coefficients, a complete signal can be reconstructed using Eq. (5.1), and its relative error with respect to the exact signal is estimated using Eq. (5.2) (by taking the summation for all points since there is no lost data point). If the threshold of 1% is employed to demarcate the significant frequencies, 762 frequencies

(see Fig. 5.4a) are identified and used to reconstruct the signal, yielding a relative error of 0.9% (Fig. 5.4b). If a 5% relative error is considered acceptable, Fig. 5.4 indicates that a threshold of 20% to demarcate the significant frequencies is adequate. Zero error is obtained only if all frequencies (in this case, 800 frequencies) are used in the reconstruction process. Note that this relative error is the difference between the reconstructed and the exact complete signals and is different from that of Eq. (5.2) which is the relative difference of lost portions between two consecutive reconstructed signals. Nevertheless, this gives a sense of the minimum *Rerr* that can be imposed in the reconstruction procedure.

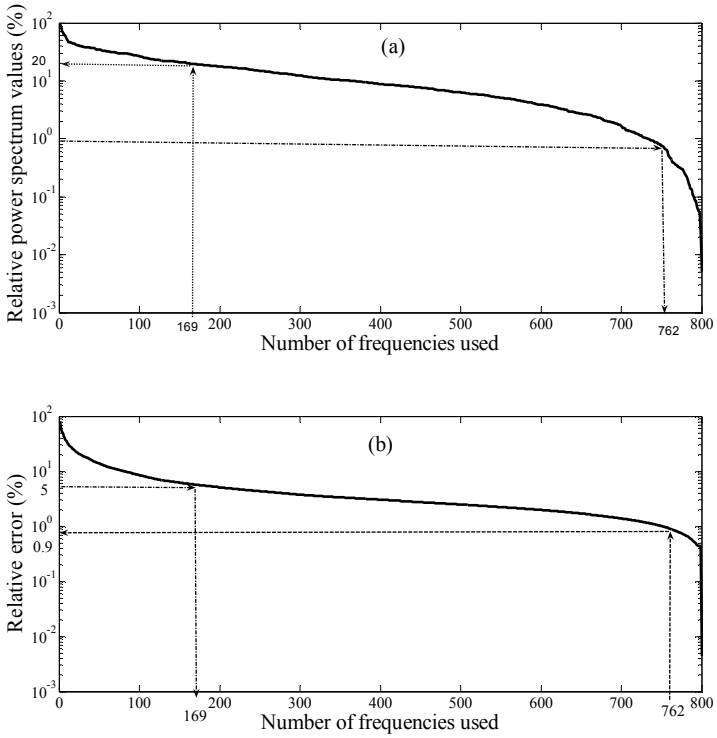

Fig. 5.4. Relationship between number of frequencies used and (a) relative power spectral values; and (b) relative error between reconstructed and exact signals

To investigate the effect of the cut-off frequency threshold of 1% on the accuracy of the reconstructed signals with different lengths, the same procedure as above is performed on signals with 100, 200, 500, 1000, 3200, 6400 and 12800 data

points that are extracted or combined from the original signal in Fig. 5.3. The results in terms of the number of significant frequencies and relative error of the reconstructed signals are shown in Fig. 5.5. The relative error of the reconstructed signal estimated using Eq. (5.2) varies slightly from 0.88% to 0.93% whereas the number of significant frequencies is found almost proportional to the number of data points of the signal. From these results, the threshold value of 1% is still suggested to demarcate significant frequencies.

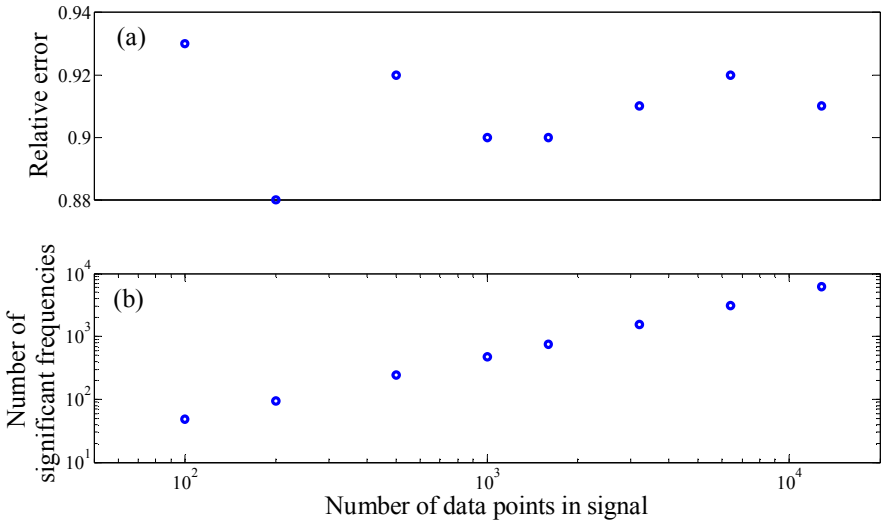

Fig. 5.5. Relationship between signal length and: (a) reconstruction error; and (b) number of significant frequencies

Reliability of Reconstruction

To study the reliability of the reconstruction methodology, the discrete signal in Fig. 5.3 is used again where random portions of the data are padded with zeroes to simulate loss of data packets during transmission (a multiplicative of 4 consecutive points are prescribed lost at a location). The reconstruction procedure is then performed and the relative error plotted in Fig. 5.6. With a threshold of 1% for both *Rerr* and the *PSV* to demarcate significant frequencies, the minimum relative error for

the lost portions achievable is 5%. For data loss beyond 28%, the relative error using this reconstruction procedure grows exponentially from 10%, beyond which it becomes unattractive for practical applications. Hence, this reconstruction procedure is practical for approximately $m > 0.7\xi$ or less than 30% data is lost. The same signal is used to obtain results for thresholds of 10%, 2% and 0.5% for both the significant frequencies and *Rerr*. The results in Fig. 5.6 show that the accuracy of the reconstructed signal is improved significantly when the threshold is reduced from 10% to 2%, but only slightly when it is reduced from 2% to 0.5%. Thus, the proposed value of 1% appears adequate.

To investigate the robustness of the 1% *Rerr* threshold to terminate the iteration in Eq. (5.2), the reconstruction process is iterated for 10, 20 and 50 additional cycles after the threshold of 1% is achieved. Results in Fig. 5.7 testify that the relative differences between the estimated lost portions at iterations *i* (at which the threshold of 1% is reached) and the additional computation cycles of 10, 20 and 50 show little improvement, indicating that the 1% *Rerr* threshold is fairly optimal. Furthermore, the number of required iterations at which the *Rerr* threshold of 1% is reached is not proportional to the lost percentages. This phenomenon may be explained by the fact that the number of iterations required depends not only on the lost percentages but also on the distribution of the lost values along the signals.

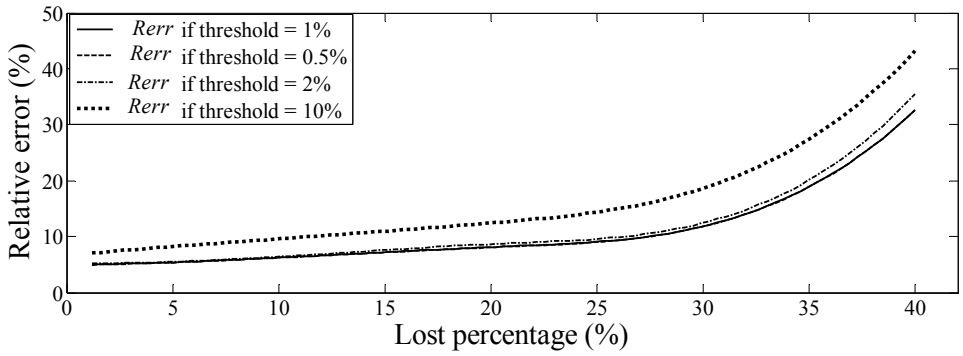

Fig. 5.6. Relationship between lost percentage and *Rerr* for different thresholds

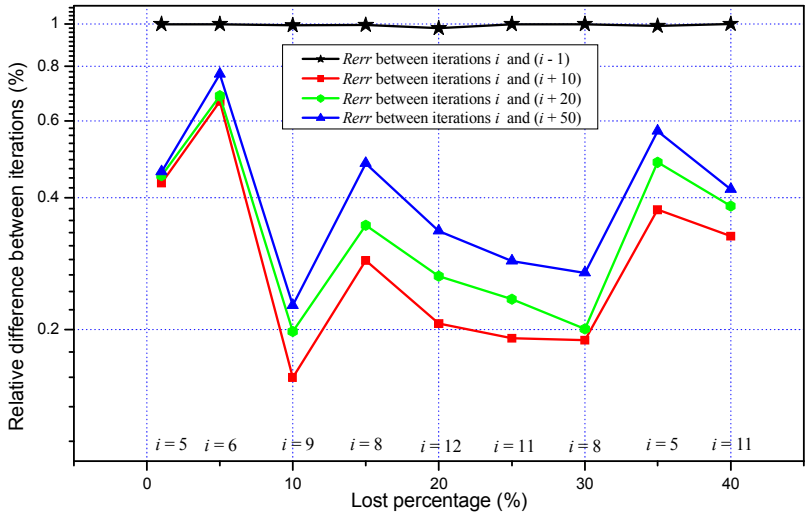

Fig. 5.7. Relative difference of lost portions with additional iterations

Comparison with other Algorithms

To further illustrate the effectiveness of the lost data reconstruction algorithm, the above-mentioned signal shown in Fig. 5.3 with different lost percentages (based on packet of 4 data points per transmission) is reconstructed using different methods, namely (*i*) linear interpolation method; (*ii*) cubic interpolation method; (*iii*) Hsu and Lo (2006) method; and (*iv*) the current method. Comparison of the reconstructed signals using different methods for the case of 20% lost data is shown in Fig. 5.8a with a zoom-in near 0.7s shown in Fig. 5.8b. The number of iterations required and the

relative error with respect to the exact signal for different methods are plotted in Fig. 5.9. Because interpolation methods are non-iterative, the number of iteration required is stated as one. Due to the presences of consecutive lost points, cubic interpolation method produces larger error than linear interpolation method. This may be explained as follows: From 2 measured data points at the 2 ends of few consecutive lost points, linear interpolation method produces the estimated values which are almost the mean of the lost points. Cubic interpolation method, however, tries to make sure the smoothness of the estimated data at the 2 measured data points of the few consecutive lost points. Since cubic interpolation method does not produce any flexible point within these consecutive lost points, the estimated values lie on one side compared to the mean value, either above or below, resulting in larger error compared to the linear interpolation method.

The two methods proposed by Hsu and Lo (2006) produce almost identical error although the number of iterations required is slightly different. The relative errors using the two methods proposed by Hsu and Lo (2006) are significantly improved compared to the two interpolation methods. This may be explained by the satisfaction of the periodic boundary conditions when Fourier transformed is employed on the pre-processed signal which is generated by superposing the original signal with a pre-computed signal. Subtracting the pre-computed signal from the reconstructed signal gives the estimated signal. Nevertheless, the relative errors using the two methods proposed by Hsu and Lo (2006) may still be too high for implementation in a SHM algorithm to assess structural damage since the minimum relative error achievable is approximately 20%. On the other hand, the current method produces a reasonable error of less than 10% where the lost percentage is less 30% and may be acceptable to many algorithms for structural damage detection.

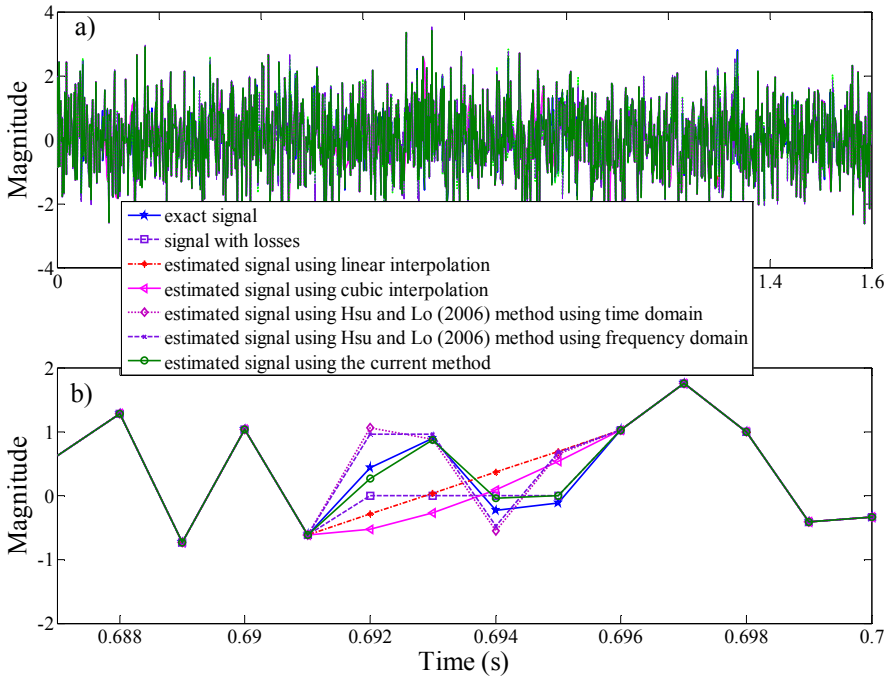

Fig. 5.8. Comparison between exact and estimated signals using different methods (20% data lost)

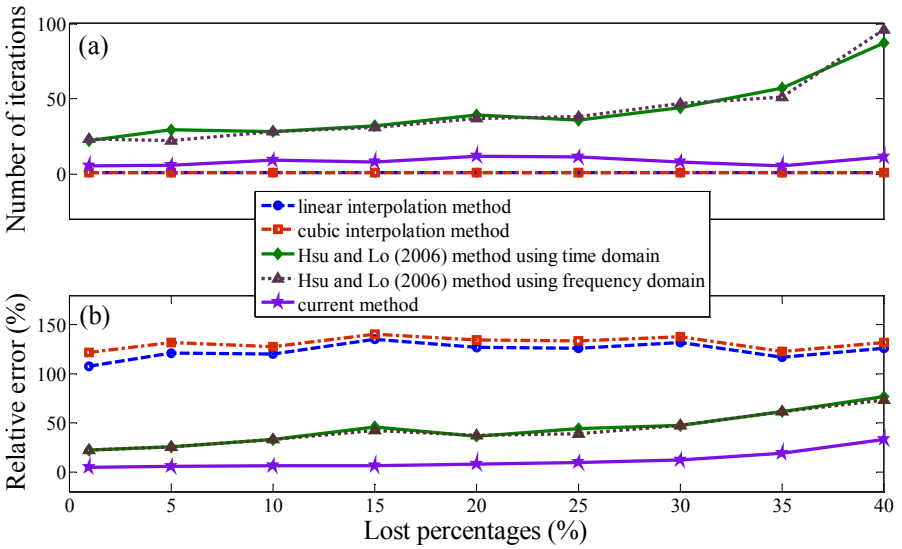

Fig. 5.9. Relationship between lost percentages and: (a) number of iterations, and (b) relative error

5.5 EXPERIMENTAL EXAMPLE

A 3-D modular truss structure comprising 23 aluminum tubes and 1 pre-tensioned cable is set up in this experiment as shown in Fig. 5.10. The geometrical and material properties of truss members are listed in Table 5.1 whereas element and node numbers are plotted in Fig. 5.11. Damage in the structure is simulated by cutting the pre-tensioned cable member mid-way through the test. Zero-mean white noise load with *RMS* of 50 N is generated using a shaker with capacity of 75 lbs (334 N) to act vertically on the truss at node 1. Acceleration responses are captured by 6 wireless sensors (locations are given in Fig. 5.10) and the corresponding lost percentages resulting from actual transmission loss (ranging from 19% to 25% are registered) are shown in the upper portion of Table 5.2. Examining the distribution of lost data packets along time axis, it is observed that the lost data packets are distributed randomly and are not synchronized among the 6 measurements.

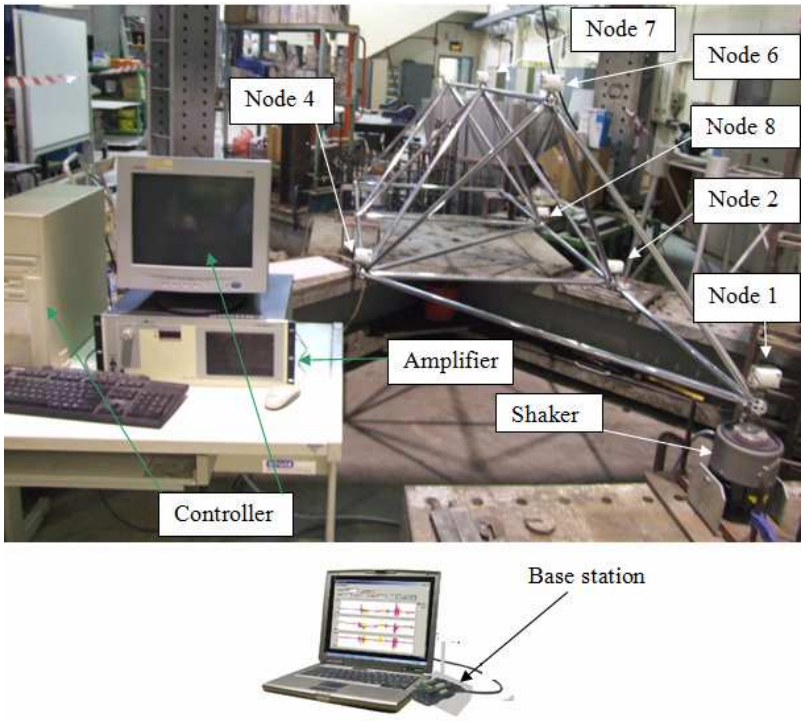

Fig. 5.10. Experimental set-up

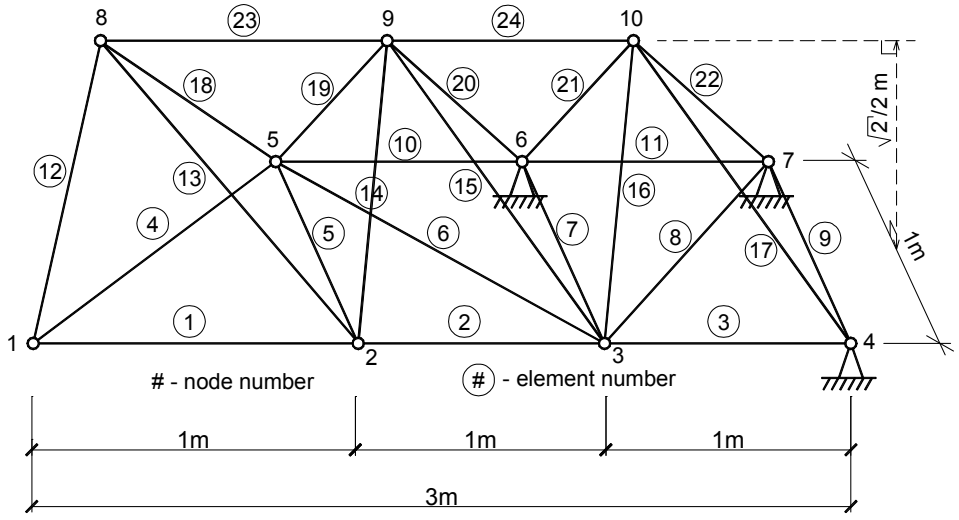

Fig. 5.11. Element and node numbers for experimental truss

Table 5.1. Geometric and material properties of truss members

	Aluminum tubular members	Pre-tensioned cable members
Outside diameter, (mm)	20.0	4.0
Thickness, (mm)	1.0	-
Young's modulus, (N/m^2)	6.8×10^{10}	1.6×10^{11}
Mass density, (kg/m^3)	2690.0	7500.0
Pre-tensioned force, (N)	-	2000.0

Table 5.2. Computational details for signal reconstruction at 6 sensor nodes

	Node 1	Node 2	Node 4	Node 6	Node 7	Node 8
Number of lost points	352	380	392	376	304	372
Total number of points	1600	1600	1600	1600	1600	1600
Lost percentage (%)	22.00	23.75	24.50	23.50	19.00	23.25
Number of iterations	12	14	14	11	14	10
Number of frequencies used in the last iteration	479	467	495	367	479	343
Relative error at the last iteration (%)	0.62	0.33	0.55	0.72	0.87	0.83

Note: see Fig. 5.10 for sensor node locations

With the lost percentage ranging from 19% to 25%, reconstruction error of lost portions is expected to fall between 8% and 9% based on Fig. 5.6. Performing the data

reconstruction algorithm in Section 5.3 on the measured signals, the number of iterations taken, the number of significant frequencies used and the relative error estimated for the last iteration are summarized in the lower portion of Table 5.2. It is observed that the number of iterations required is small, ranging from 10 to 14 and is not proportional to the lost percentage since the distribution of the lost data packets along the signal is another controlling factor. Results for the sensor at node 4 are demonstrated in Fig. 5.12, including an inset in Fig. 5.12a to show a segment of lost data. Fig. 5.12b gives a better indication of the locations of the lost data points based on the "corrected" values. Fig. 5.12c compares in frequency domain the raw signal against the reconstructed signal which shows no drastic change in the trend or general characteristics, as inherent in the proposed methodology.

Since the accelerometers and the shaker are not synchronized, only the reconstructed accelerations are fed into the method proposed in Section 3.3 to identify structural stiffness matrix since the procedure to identify structural flexibility method presented in Section 3.2 requires the measurement of excitation. From the reconstructed accelerations, 15 segments each of which contains 109 time steps can be used to feed in the proposed algorithm in Section 3.3 to estimate the structural stiffness matrix coefficients and some selected results are plotted in Fig. 5.13. Of the 6 stiffness coefficients plotted in Fig. 5.13, only K_{88} shows significant reduction since its value is contributed directly by the stiffness of the pre-tensioned cable member which is cut. The cut made mid-way through the experiment and the resulting transient oscillations towards dynamical equilibrium of the new system is manifested by the varying stiffness coefficients estimated for time segments 7, 8, and 9 (from 7 to 11 seconds). The identified stiffness coefficients stabilized from segment 10 (11^{th} second) onwards.

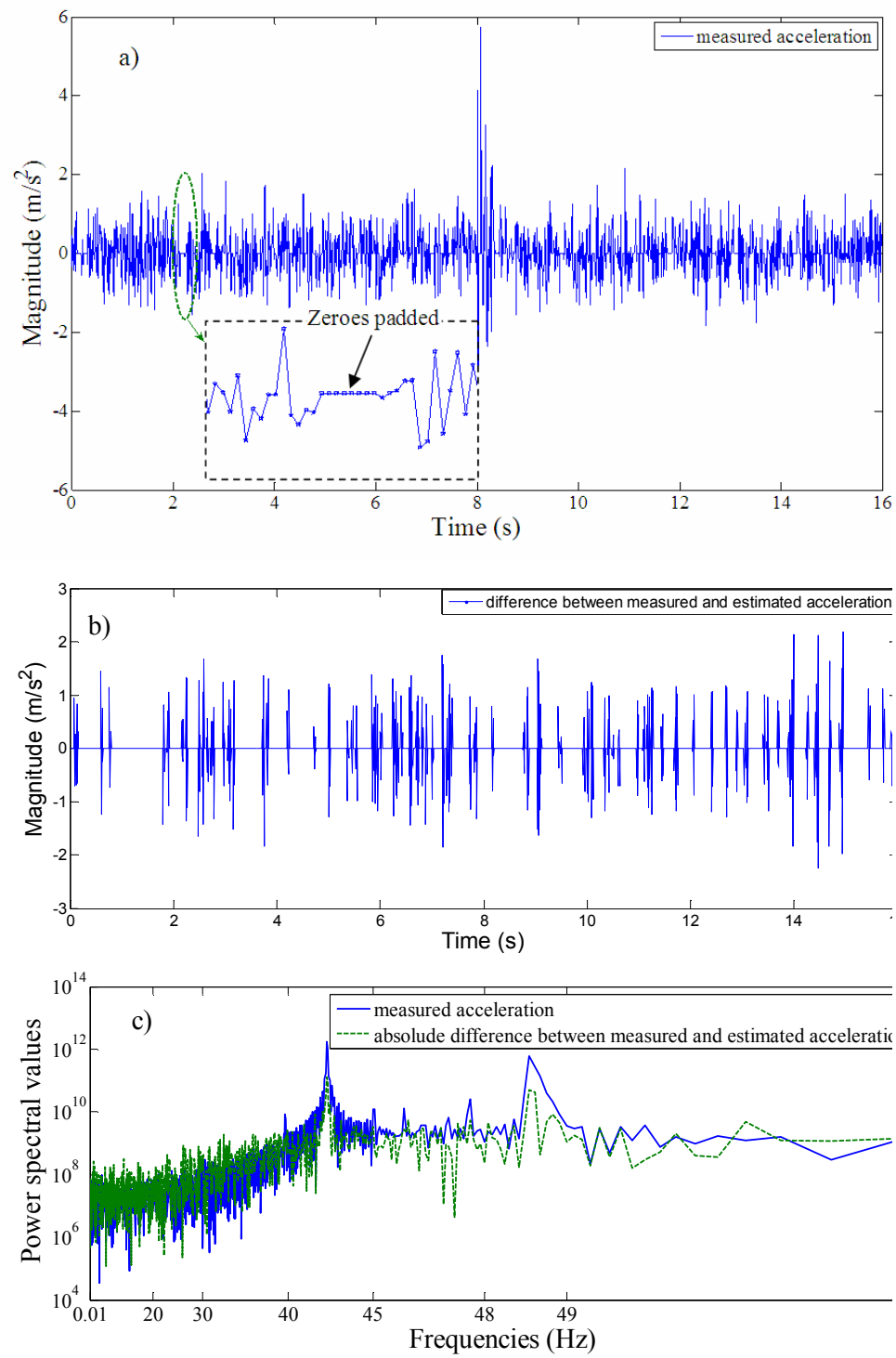

Fig. 5.12. Accelerations at sensor node 4: a) variation of magnitude with time where lost values are padded with zeroes; b) variation of the difference in magnitude between measured and reconstructed signals with time; and c) variation of power spectral values with frequencies for measured and reconstructed signals

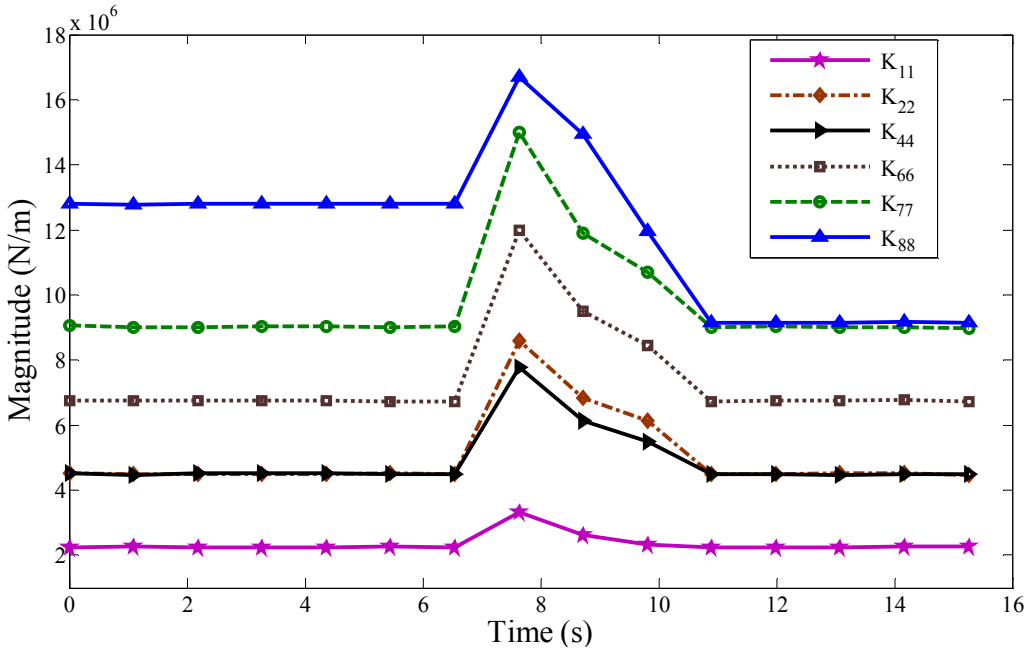

Fig. 5.13. Variation of structural stiffness coefficients with time

Based on the identified stiffness coefficients at segments 1 (first) and 15 (last), the change in stiffness matrix is calculated from which the set of *DLV*s is identified. Applying these *DLV*s to the reference structural model as nodal displacement vectors, the *NCE* of all elements are computed and the set of *PDE* comprising elements (1, 8) is identified. The current *IDS* therefore comprises elements (1, 8), and *ne* = 2. By omitting readings of the sensor at nodes 9, which is far away from the members of the current *IDS* set, the readings of the remaining 5 sensors are used to estimate the structural stiffness matrix for different time segments. Comparing the stiffness matrices identified for the first and the last time segments, the change in the stiffness matrix is evaluated. Performing *SVD* on the change in stiffness matrix, a set of 3 *DLV*s is obtained and applied to the reference model as nodal displacement vectors. The set of *PDE* identified comprises elements (4, 5, 8, 12, 14). Taking the intersection between the set of *PDE* and the current *IDS* containing elements (1, 8) gives the new *IDS* with element 8 as the only member (*ne* = 1). Similarly, by omitting the readings of the

sensor at node 1, which is far away from the only member of the current *IDS* set, instead of the sensor at node 9, another set of *PDE* comprising elements (1, 4, 8, 12) is identified. Intersecting the set of *PDE* and the current *IDS* which contains element 8 only gives element 8 as the new *IDS* (*ne* = 1). Since the *IDS* for 2 consecutive steps are identical, the iteration is terminated, and element 8 is concluded as damage. The whole procedure is summarized in Table 5.3.

Table 5.3. Damage detection results for experimental truss structure

		Set of sensors includes sensors at nodes	No. of *DLV*	*PDE*	Eliminated elements	*IDS*	*ne*
	ns =6	[1, 2, 3, 5, 8, 9]	4	[1,8]		[1, 8]	2
k=*ns* -1=5	*i* =1	[1, 2, 3, 5, 8]	3	[4, 5, 8, 12, 14]	1	[8]	1
	i =2	[2, 3, 5, 8, 9]	3	[1, 4, 8, 12]		[8]	1

If the differences in the identified stiffness matrices at segments 8, 9 and 10 with respect to that at segment 1 are utilized to evaluate the change in structural stiffness matrix which is then employed in the *DLV* method, no damaged element is identified as results shown in Table 5.4 a-c as the structure is in the transient stage of damage. If the difference in the identified stiffness matrices at segments 11 and 1 is used in the *DLV* method instead, element 8 is correctly detected as damaged, shown in Table 5.4d. As another check, if the difference in the identified stiffness matrices between segments 7 and 1 is utilized to assess damage using the *DLV* method, no damaged element is detected which is rightly so since at time segment 7, the pre-tensioned member has not been cut yet.

Table 5.4 Detect damage in experiment truss using difference in stiffness matrices between data segments 1 and 8 (a); 9 (b); 10 (c); and 11 (d)

	Set No.	Sensors at nodes	Potential damaged elements																					
(a)	1	[1, 2, 3, 5, 8, 9]	**1**			**4**	5		7	8		**12**												
	2	[1, 2, 5, 8, 9]	**1**	2		**4**						**12**												
	3	[1, 2, 3, 5, 8]			3				7	8											18		24	
(b)	1	[1, 2, 3, 5, 8, 9]	1					6	7	8														24
	2	[1, 2, 3, 5, 9]												14	15	16	17	18						
(c)	1	[1, 2, 3, 5, 8, 9]	**1**			4						12												
	2	[1, 2, 3, 5, 8]	**1**				5						13									23		
	3	[1, 2, 5, 8, 9]		2							10							18	21					
(d)	1	[1, 2, 3, 5, 8, 9]	1							**8**														
	2	[1, 2, 3, 5, 8]							5	**8**		14			15	16	17							
	3	[2, 3, 5, 8, 9]	1	4						**8**	12													

For this example, measured accelerations with losses from the 6 wireless sensors (where the lost data values are padded with zeroes) are used in the algorithm proposed in Section 3.3 to identify stiffness coefficients at different time segments and selected results are plotted in Fig. 5.14. From the difference in stiffness matrices at the first (1) and last (15) segments no *DLV* set is calculated to perform damage assessment. It may be explained by the fact that poor quality of the measured signals propagates to the identified stiffness matrices through the proposed algorithm to compute the stiffness matrices proposed in Section 3.3. Based on the inaccurate identified stiffness matrices, no *DLV* can be calculated, illustrating the importance of the data loss reconstruction procedure.

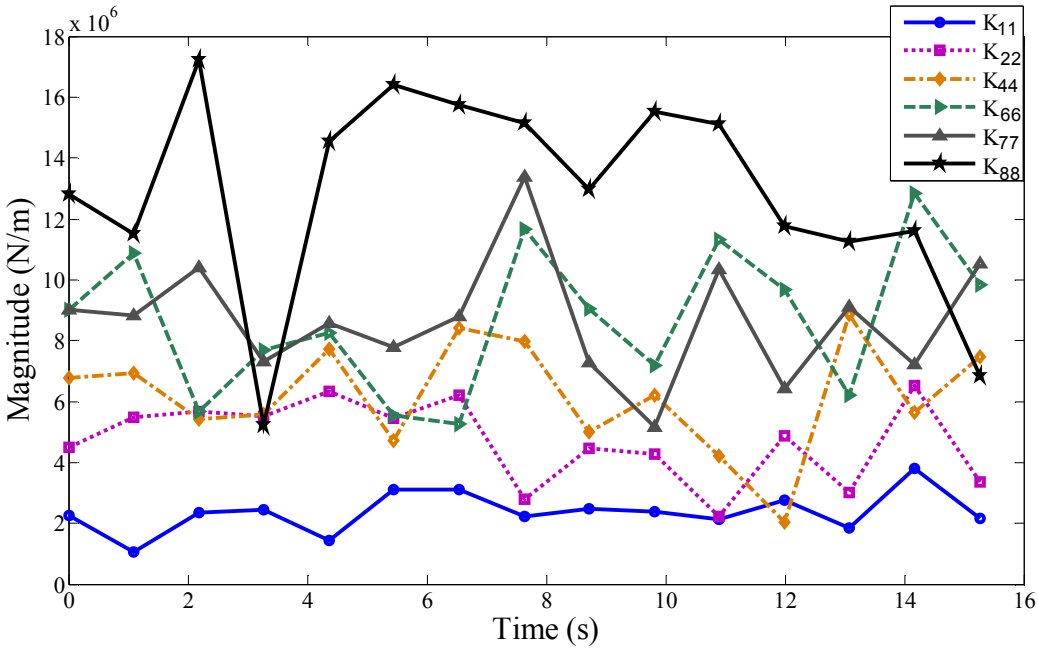

Fig. 5.14. Variation of structural stiffness coefficients with time estimated from raw measured data (where lost values are padded with zeroes)

5.6 CONCLUDING REMARKS

This chapter demonstrated that actual transmission loss in wireless sensor network can be as high as 25% and it is necessary to reconstruct the lost data before the signals can be used for reliable damage detection via the *DLV* method. Due to the presence of consecutive lost data points, methods for data loss reconstruction in the open literature such as by linear interpolation, cubic interpolation, methods proposed by Hsu and Lo (2006) are found not suitable for most algorithms for structural damage detection. On the other hand, the proposed Fourier-based lost data reconstruction algorithm with identified *PSV* and relative error thresholds of 1% is demonstrated to be feasible whereby data with approximately 30% transmission loss can be reconstructed with 10% relative error in the lost portions. Using a 3-D modular truss with 23 aluminum tubes, one pre-tensioned cable member and 6 wireless sensors with 1 base station, it is demonstrated that the reconstructed signals when used with the *DLV* method is able to identify the damage element correctly. By using different segments

of the data, the results indicated that data close to the time of perturbation (or damage) should not be used as the effect of the damage may not be accurately detected during this brief transient stage. The experimental results also confirm the necessity of using the lost data reconstruction algorithm for wireless sensors to enhance the robustness of the *DLV* method for structural damage detection.

CHAPTER 6

CONCLUSIONS AND RECOMMENDATIONS FOR FUTURE RESEARCH

6.1 CONCLUSIONS

To re-cap, the main objective of this research is to further develop the damage locating vector (*DLV*) method for structural damage detection accounting for: (a) structures comprising beam, column and truss elements with varied and constant cross-sectional area; (b) the availability of either static or dynamic responses; (c) the availability of excitation measurements; (d) the limitation of number of sensors used due to unavailability and malfunctioning; (e) the quality of measured data; and (f) the loss of data during wireless transmission from sensor nodes to the base station. The work has been presented as following:

The physical meaning of the *DLV*, its advantages and shortcomings are discussed and various enhancements to extend its practical applications beyond truss structures are detailed in Chapter 2. These enhancements include: (*i*) extending its formulation to accommodate multi-stress state elements and the variation of internal forces and capacity along the length of each element; (*ii*) proposing two schemes to identify damaged elements for the case of imperfect measurements; (*iii*) proposing a simple algorithm to assess the severity of the damage; and (*iv*) proposing an algorithm to detect damage for the case where the applied static load is unknown. Chapter 2 focuses on static responses whereas Chapter 3 is devoted to the use of dynamic responses for structural damage detection under the *DLV* framework. The difference between the use of static and dynamic responses is the formulation of flexibility/stiffness matrix from structural responses. Formulation of flexibility matrix from dynamic responses and

known excitation is summarized. An algorithm to formulate the stiffness matrix from acceleration responses only is proposed. Besides, a simple algorithm for optimal sensor placement is suggested to (*i*) identify the optimal configuration for placing the available sensors; and (*ii*) estimate the minimal number of sensors required for reliable damage detection results. For the methodology to work, reasonably good quality data must be available. Chapter 4 addresses the issue of validating the measured data where an algorithm is proposed to admit only "quality" data as input into the *DLV* method to enhance its reliability in the damage detection. With the advancement in sensor technology, wireless sensors will be a common component of most structural damage detection system in the near future. One critical issue at this stage is the loss of data packets during transmission. An algorithm to estimate lost values due to RF transmission is proposed in Chapter 5 and compared with other techniques available in open literature.

The conclusions drawn based on the above study can be summarized as follows.

1. From energy principle, it can be deduced that when the change in flexibility is used to compute the *DLV*, the latter has force as physical quantity. The force vector is orthogonal to the vector of the relative change in displacement vector from the reference to the damage state, formulated with respect to the sensor locations. If the change in stiffness is used to compute the *DLV* instead, the *DLV* is physically the displacement vector, which is orthogonal to the relative change in nodal force vector.
2. The original *DLV* method has been applied to truss structures and this study has extended the formulation to include more general elements by proposing the normalized cumulative energy (*NCE*) as damage indicator. The formulation caters for (*i*) different types of structural elements such as beam, column and truss

elements, (*ii*) variation of internal forces along the length of each element, and (*iii*) variation of capacity along the length of each element. The performance of the *NCE*-based *DLV* method has been illustrated using static responses simulated from a 2-D warehouse structure which comprises elements with multi-state stresses and varied cross-sectional areas. The method is workable for the case where 3 elements are damaged and the simulated data is contaminated with 5% noise. In an experiment of a 3-D modular truss structure comprising 88 members and 28 nodes, 2 damaged elements can be identified correctly using measured data from 7 displacement transducers.

3. Due to the presence of noise and the use of limited number of sensors, not all identified elements are actually damaged. Two implementation schemes of the *DLV* method were proposed to filter out the actual damaged elements, namely, (*i*) an intersection scheme and (*ii*) a two-stage analysis. The former makes use of the intersection of different identified sets of potential damaged elements derived using data from various combinations of sensors. The latter identifies possible damaged regions in the first stage using the relative change in flexibility matrix and then uses the *DLV* method in the second stage to identify damaged elements within the damaged regions. Though the two schemes are different in their approaches, they produced the same results for both the numerical and experimental examples. The performance of the two schemes has been illustrated using displacement responses simulated from the 2-D warehouse structure comprising frame and truss elements with varied and constant cross-sectional areas. With 10 displacement sensors used and 5% noise, the intersection scheme can provide reliable results within 3 combinations of sensors. The two-stage analysis can identify the 3 damaged elements correctly using 10 displacement sensors. If the noise level in the

displacement data exceeds 10%, unreliable damaged detection results are observed. Furthermore, displacement responses from an experiment of the 3-D modular truss structure are employed to assess the performance of the two schemes. The intersection scheme can identify the 2 damaged elements correctly with 7 displacement transducers used. However, the number of combinations of sensors increases from 3 for the case where 13 displacement transducers are used to 4 for the case where 7 displacement sensors are used. Nevertheless, the damaged elements can still be identified correctly. The two-stage analysis can also identify the 2 damaged elements correctly with 7 sensors used.

4. The original *DLV* method has not been developed to assess the damage severity of the identified damaged elements. An algorithm to assess damage severities of the identified damaged elements was developed. Penalty function method has been adopted to minimize the difference between the first singular values of the two flexibility matrices with respect to the sensor locations. One flexibility matrix ($\mathbf{F}_n$) is constructed using numerical model of the structure at the reference state. The other flexibility matrix ($\mathbf{F}_d$) is computed from measured data of the structure at the current (damaged) state. In other words, $\mathbf{F}_n$ is mapped to $\mathbf{F}_d$ by adjusting the stiffnesses of the identified damaged elements. When $\mathbf{F}_n$ approaches $\mathbf{F}_d$, the severity of the damaged elements is estimated. In the numerical example of the 2-D warehouse structure, using data with 5% noise, the damage severity of the damaged elements can be assessed with approximately 1% error within 10 iterations. In the experimental example of the 3-D modular truss structure, using measured data from 7 displacement transducers, the damage severity of the two damaged elements can also be assessed within 15 iterations and approximately 2% error.

5. The magnitude of the static load, which is used to actuate the structure, needs not be the same when performing for the reference and the damaged structures as they may be done at different times which may be months or years apart. In some cases, the magnitudes of the static loads are not known. An algorithm was proposed to detect structural damage for such case where the ratio between the magnitudes of the static loads at the reference and the damaged state are estimated from measured displacements. Using this algorithm and the *NCE*-based *DLV* method, three damaged elements can be identified using simulated displacements which are contaminated with 5% noise in a numerical example of the 2-D warehouse structure where the applied static loads are unknown. Although the static loads at the reference and damaged states are unknown in the experiment of the 3-D modular truss structure, the two damaged elements can also be identified correctly using the proposed algorithm in conjunction with the *NCE*-based *DLV* method.
6. Recognizing that measurement of the dynamic excitations is expensive, difficult or in some cases impossible, a direct method was proposed to identify structural stiffness matrix when the excitations are unknown and only limited acceleration responses are measured. Central to the method is the formulation of a system of nonlinear equations based on the equations of motion of structure at all *DOF* using Newmark-β method to relate the displacements and velocities between different time steps in terms of their initial values. This system of nonlinear equations is then solved using the Newton Raphson method to identify the structural stiffness matrix. The method works provided that at least two acceleration measurements are available. Integrating the direct method with the *NCE*-based *DLV* method, two damaged elements can be identified numerically using the 2-D warehouse structure. Furthermore, two elements with gradual reduction in element stiffnesses

(0.05% reduction in element stiffness per measurement segment) can also be identified correctly. In an experimental example of the 3-D modular truss structure, the two damaged elements can also be identified correctly using the direct method and the *NCE*-based *DLV* method. Comparing the *NCE* of all elements for the cases where the excitations are known and unknown, it is found as expected that the procedure with known excitations is more sensitive although the two methods can provide the same set of potential damaged elements for both cases. Measured input excitations therefore should be integrated to the damage detection process to enhance the reliability of the result.

7. The reliability of a structural health monitoring system is very dependent on the quality of signals which are acquired and fed into the damage detection algorithm. Although the integrity of sensors can be assessed offline, the practical challenge is to be able to detect faulty signals as they are being collected and processed through a structural damage detection algorithm. This is important for cases where it is difficult to predict when severe or accidental loads occur to facilitate *a priori* validation of the sensors. An algorithm for sensor validation in the context of the *DLV* method for structural damage detection was devised to increase the reliability of the damage detection results. Using simulated data from the 3-D modular truss structure which is contaminated with 10% noise, the two faulty sensors can be identified simultaneously. Using physically measured data from the same 3-D modular truss structure, gain fault, which is manifested by multiplying the actual measurement with a constant of 1.5, and sensor failure, which is manifested by replacing actual measurement by a zero-mean white noise signal with the same *RMS* of the magnitude, can be also be identified correctly. The algorithm is necessary because (*i*) it is important to differentiate between structural damage and

the case of faulty sensors; and (*ii*) it would increase the reliability of damage detection result by using only "suitable" measurements in the damage detection computation.

8. As wireless sensor technology has contributed to new developments in structural damage detection since there are significant advantages over wired sensors, the research and implementation of the *DLV* methodology have to take into account the possible use of wireless sensors and their associated practical issues. Transmitting data from various sensor nodes to the base station using radio frequency (RF) commonly experiences intermittent loss although the raw data on sensor nodes is digitalized. An algorithm was developed to reconstruct the lost data where wireless sensors are employed to collect acceleration responses. The algorithm makes use of frequencies which contribute significant amount of energy in the signal based on Fourier transform. As the amplitudes are uncertain due to lost data, the Fourier amplitudes are estimated based on least-squares fit of only the measured portions of the signal. The lost portions are reconstructed through inverse Fourier transform. The procedure is iterated until the discrepancy between the estimated lost portions of two consecutive iterations is below a set threshold. The proposed relative error thresholds of 1% was demonstrated to be feasible whereby data with approximately 30% transmission loss can be reconstructed with 10% relative error in the lost portions. Incorporating wireless sensors with the *DLV* method for structural damage detection is shown possible in an experimental example of a 3-D modular truss structure comprising 23 aluminum tubes and 1 pre-tensioned where 6 wireless sensors and 1 base station are used. The actual transmission loss in the experiment can be as high as 25% whereas the damaged element can be identified correctly using the *DLV* method and reconstructed

accelerations. By using different segments of the data, the results indicated that data close to the time of perturbation (or damage) should not be used as the effect of the damage may not be accurately detected during this brief transient stage. The experimental results also confirm the necessity of using the lost data reconstruction algorithm for wireless sensors to enhance the robustness of the *DLV* method for structural damage detection.

6.2 RECOMMENDATIONS FOR FUTURE RESEARCH

This study also brings to light four significant improvements on the *DLV* methodology that requires substantial work as summarized in the following.

1. Though the proposed methodologies seem to work well with numerical or laboratory model, their performance in real environment has not been proved yet. It is the real conditions that may bring about other factors which might negatively affect the performance of the proposed methodologies such as wind, humidity and temperature. A full scale experiment on existing structures such as buildings, bridges, or offshore platforms is thus suggested for future study. Based on full scale experiment results on existing structures the need for adjustment on some proposed thresholds may emerge. However, to perform such experiment, two conditions need to be fulfilled. The first condition is the financial support since it may cost few millions US dollar per one experiment as acknowledged by Celebi (2002). The second condition is the permission of authorities who are in charge of the structures. The authorities often do not allow or welcome such work being done on their structures quoting safety and interference from the normal operations associated with such structures.

2. To further popularize wireless sensors, another way to mitigate the effect of data loss due to radio frequency (RF) transmission is to decentralize structural damage detection, limiting the amount of data to be wirelessly transmitted from the sensor nodes to the base station. In particular, local integrity of structure is expected to be analyzed at the sensor board and data transmission is required only if damage appears at the sensor locality. To achieve this objective, two parallel works need to be fulfilled, namely (*i*) to develop a smart wireless sensors generation which can perform some engineering analysis; and (*ii*) to develop an algorithm to interrogate local integrity of structure using continuous measuring data from one sensor. The former is on-going at the University of Illinois at Urbana-Champaign (Spencer et al., 2008). The latter has just reached the stage of using measurements of some neighbouring sensors to assess local integrity of structure such as the introduction of the Distributed Computing Strategy, denoted as DCS, (Gao, 2005). However, if this algorithm is employed, communication among sensor nodes using RF transmission is still required and the lost data phenomenon still exists. Much effort is therefore expected before the latter is fully realized.
3. To produce a commercial tool for online structural damage detection using the enhanced *DLV* method. Despite the fact that the proposed methodologies are automation in data analysis and applicable for online damage detection, a commercial tool for detecting damage of an existing structure has not been achieved yet at this stage. This work is expected to be time consuming and expensive since measured data from various simulated configurations of structures such as 3-D frame structures, plate and shell structures as well as

existing structures such as buildings, bridges, and offshore platforms is required to test the performance of such tool.

4. For some large and/or complicated structures, the presence of damage in some elements may not significantly change the structural flexibility/stiffness matrix formulated with respect to the sensor locations to facilitate the computation of the *DLV* for damage interrogation purpose. In such cases, measured displacements and accelerations should be used in conjunction with measured strain to localize the damage. Incorporating strain measurement into the *DLV* method for damage localization is promising since the damaged structure may be best illustrated by the entire stress strain curve. The work is expected to be experimentally examined on existing structures where the local effect of few damaged elements is best manifested.

REFERENCES

[1] Abdelghani M., and Friswell M. I., Sensor validation for structural systems with multiplicative sensor faults. *Mechanical Systems and Signal Processing* **21** (1) (2007) 270-279.

[2] Abdelghani M., and Friswell M. I., Sensor validation for structural systems with additive sensor faults. *Structural Health Monitoring* **3** (3) (2004) 265-275.

[3] Alampalli S., Fu G., and Dillon E.W., Signal versus noise in damage detection by experimental modal analysis. *Journal of Structural Engineering* **123** (2) (1997) 237-245.

[4] Alvandi A., and Cremona C., Assessment of vibration-based damage identification techniques. *Journal of Sound and Vibration* **292**(1-2) (2006) 179-202.

[5] Alvin K. F., Robertson A. N., Reich G. W., and Park K. C., Structural system identification: From reality to models. *Computers & Structures* **81** (12) (2003) 1149-1176.

[6] Aoki Y., and Byon O. I., Damage detection of CFRP pipes and shells by using localized flexibility method. *Advanced Composite Materials* **10** (2-3) (2001) 189-198.

[7] ATmega128(L) Complete Technical Documents, http://www.atmel.com/dyn/resources/prod documents/doc2467.pdf.

[8] Auweraer H. V. D., and Peeters B., International research projects on Structural Health Monitoring. *Structural Health Monitoring* **2**(4) (2003) 341-358.

[9] Bakir B. S., and Akis E., Analysis of a highway embankment failure associated with the 1999 Duzce, Turkey earthquake. *Soil Dynamics and Earthquake Engineering* **25** (3) (2005) 251-260.

[10] Balasko M., Veresb I., Molnar G. Y., Balasko Z. S., and Svab E., Composite structure of helicopter rotor blades studied by neutron- and X-ray radiography. *Physical B* **350** (1) (2004) 107-109.

[11] Banan M. R., Banan M. R., and Hjelmstad K. D., Parameters estimation of structures from static response. I. Computational aspects. *Journal of Structural Engineering* **120** (11) (1994a) 3243-3258.

[12] Banan M. R., Banan M. R., and Hjelmstad K. D., Parameters estimation of structures from static response. I. Numerical simulation studies. *Journal of Structural Engineering* **120** (11) (1994b) 3259-3283.

[13] Banks H. T., Inman D. J., Leo D. J., and Wang Y., An experimentally validated damage detection theory in smart structures. *Journal of Sound and Vibration* **191** (5) (1996) 859-880.

[14] Barer R. D., and Peters B. F., *Why metals fail*. Gordon and Breach Science Publishers, New York, 1970.

[15] Barroso L. R., and Rodriguez R., Damage detection utilizing the damage index method to a benchmark structure. *Journal of Engineering Mechanics* **130** (2) (2004) 142-151.

[16] Beck J. L., and Jennings P. C., Structural identification using linear models and earthquake engineering records. *International Journal of Earthquake Engineering and Structural Dynamics* **8** (2) (1980) 145-160.

[17] Bernal D., Load vectors for damage localization. *Journal of Engineering Mechanics* **128** (1) (2002) 7-14.

[18] Bernal D., and Gunes B., Flexibility based approach for damage characterization: benchmark application. *Journal of Engineering Mechanics* **130** (1) (2004) 61-70.

[19] Bernal D., Modal scaling from known mass perturbations. *Journal of Engineering Mechanics* **130** (9) (2004) 1083-1088.

[20] Bernal D., Flexibility-based damage localization from stochastic realization result. *Journal of Engineering Mechanics* **132** (6) (2006) 651-658.

[21] Bhuptani N. N., and Khosla N. K., Prediction of lost data in virtual control system with networked sensors. *Proceeding of international conference on computational intelligence for modeling control and automation, and international conference on intelligent agents, web technologies and internet commerce, 29th Nov -1st December 2006, Sydney, Australia,* (2006) 1-16.

[22] Bray D., and McBride D., *Non-Destructive Testing Techniques*, John Wiley and Sons Inc., New York, 1992.

[23] Campa G., Thiagarajan M., Krishnamurty M., Napolitano M. R., and Gautam M., A neural network based sensor validation scheme for heavy-duty diesel engines. *Journal of Dynamic Systems, Measurement and Control* **130** (2) (2008) 0210081-02100810.

[24] Cawley P., A high frequency coin-tap method of non-destructive testing. *Mechanical Systems and Signal Processing* **5** (1) (1991) 1-11.

[25] Castello D. A., Stutz L. T., and Rochinha, F. A., A structural defect identification approach based on a continuum damage model. *Computers & Structures* **80** (5-6) (2002) 417-437.

[26] Celebi M., *Seismic Instrumentation of Buildings (With Emphasis on Federal Buildings)*, Technical Report No. 0-7460-68170, United States Geological Survey, Menlo Park, CA, USA, 2002.

[27] Cha P. D., and Tuck-Lee J. P., Updating structural system parameters using frequency response data. *Journal of Engineering Mechanics* **126** (12) (2000) 1240-1246.

[28] Chang P. C., Flatau A., and Liu S. C., Review paper: Health monitoring of civil infrastructure. *Structural Health Monitoring* **2** (3) (2003) 257-267.

[29] Chase J. G., Begoc V., and Barroso L. R., Efficient Structural Health Monitoring for a benchmark structure using adaptive recursive least squares filter. *Computers & Structures* **83** (8-9) (2005) 639-647.

[30] Chen H. L., Spyrakos C. C., and Venkatesh G., Evaluating structural deterioration by dynamic response. *Journal of Structural Engineering* **121** (8) (1995) 1197-1204.

[31] Chen H. P., and Bicanic N., Assessment of damage in continuum structures based on incomplete modal information. *Computers & Structures* **74** (5) (2000) 559-570.

[32] Chen J., and Li J., Simultaneous identification of structural parameters and input time history from output only measurements. *Computational Mechanics* **33** (5) (2004) 365-374.

[33] Chen Q., Chan Y. W., and Worden K., Structural fault diagnosis and isolation using neural networks based on response-only data. *Computers & Structures* **81** (22-23) (2003) 2165-2172.

[34] Chintalapudj K. K., Design of wireless sensor network based Structural Health Monitoring system, PhD Thesis, University of South California, USA, 2006.

[35] Crawley E. F., and Aubert A. C., Identification of nonlinear structural elements by force-state mapping. *AIAA Journal* **24** (1) (1986) 155-162.

[36] Delatte N., Failure of cold-formed steel beams during concrete placement. *Journal of Performance of Constructed Facilities* **19** (2) (2005) 178-181.

[37] Diaz S. H. V., and Soutis C., Delamination detection in composite laminates from variations of their modal characteristics. *Journal of Sound and Vibration* **228** (1) (1999) 1-9.

[38] Doebling S. W., Minimum-rank optimal update of elemental stiffness parameters for structural damage identification. *AIAA Journal* **34** (12) (1996) 2615-2621.

[39] Doebling S. W., Farrar C. R., Prime M. B., and Shevitz D. W., *Damage identification and health monitoring of structural and mechanical systems from*

changes in their vibration characteristics: A literature review, Technical report LA-13070, Los Alamos National Laboratory, Los Alamos, NM, USA, 1996.

[40] Doebling S. W., Measurement of structural flexibility matrices for experiments with incomplete reciprocity, PhD Thesis, Colorado University, Colorado, 1996.

[41] Dry C., Procedures developed for self repair of polymer matrix composite materials. *Composite Structures* **35** (3) (1996) 263-269.

[42] Duan Z., Yan G., Ou J., and Spencer Jr. B. F., Damage localization in ambient vibration by constructing proportional flexibility matrix. *Journal of Sound and Vibration* **284** (1-2) (2005) 455-466.

[43] Dunia R., Win S. J., Edgar T. F., and McAvoy T. J., Identification of faulty sensors using principal component analysis. *AIChE Journal* **42** (10) (1996) 2797-2812.

[44] Elghazouli A. Y., and Izzuddin B. A., Failure of lightly reinforced concrete members under fire. II: Parametric studies and design considerations. *Journal of Structural Engineering* **130** (1) (2004) 18-31.

[45] Escobar J. A., Sosa J. J., and Gomez R., Structural damage detection using the transformation matrix. *Computers & Structures* **83** (4-5) (2005) 357-368.

[46] Evensen G., Sequential data assimilation with a nonlinear quasi-geotropic model using Monte Carlo methods to forecast error statistics. *Journal of Geophysical Research* **99** (5) (1994) 10143-10162.

[47] Farrar C. R., *Historical Overview of Structural Health Monitoring*, Lecture Notes on Structural Health Monitoring Using Statistical Pattern Recognition, Los Alamos Dynamics, Los Alamos, NM, USA, 2001.

[48] Farrar C. R., Worden K., Todd M. D., Park G., Nichols J., Adams D. E., Bement M. T., and Farinholt K., *Nonlinear system identification for damage detection*, Technical report LA-14353, Los Alamos National Laboratory, Los Alamos, NM, USA, 2007.

[49] Farrar C. R., and James G. H. I., System identification from ambient vibration measurements on a bridge. *Journal of Sound and Vibration* **205** (1) (1997) 1-18.

[50] Feng Z., Wang Q., and Shida K., A review of self-validating sensor technology. *Sensor Review* **27** (1) (2007) 48-56.

[51] Fraser M. S., Development and implementation of an integrated framework for Structural Health Monitoring, PhD Thesis, University of California, San Diego, USA, 2006.

[52] Fritzen C. P., and Jennewein D., Damage detection based on model updating methods. *Mechanical Systems and Signal Processing* **12** (1) (1998) 163-186.

[53] Friswell M. I., and Inman D. J., Sensor validation for smart structure. *Journal of Intelligent Material Systems and Structures* **10** (12) (1999) 973-982.

[54] Friswell M. I, and Mottershead J. E., *Finite element model updating in structural dynamics*, Kluwer Academic, Dordrecht, the Netherlands, 1995.

[55] Gao Y., and Spencer Jr. B. F., Damage localization under ambient vibration using change in flexibility. *Earthquake Engineering and Engineering Vibration* **1** (1) (2002) 136-144.

[56] Gao Y., Spencer Jr. B. F., and Bernal D., Experimental verification of the flexibility based damage locating vector method. *Journal of Engineering Mechanics* **133** (10) (2007) 1043-1049.

[57] Gao Y., Structural Health Monitoring strategies for smart sensor networks, PhD Thesis, University of Illinois at Urbana-Champaign, USA, 2005.

[58] Gao Y., and Spencer Jr. B. F., Online damage diagnosis for civil infrastructure employing a flexibility-based approach. *Smart Materials and Structures* **15** (1) (2006) 9-19.

[59] Getting Stared Guide, Crossbow Technology Inc., 2005.

[60] Gibson R. F., Modal vibration response measurements for characterization of composite materials and structures. *Composites Science and Technology* **60** (15) (2000) 2769-2780.

[61] Glaser S. D., Li H., Wang M. L., Ou J., and Lynch J., Sensor technology innovation for the advancement of Structural Health Monitoring: a strategic program of US-China research for the next decade. *Smart Structures and Systems* **3** (2) (2007) 221-244.

[62] Green R. E., Non-contact ultrasonic techniques. *Ultrasonics* **42** (1) (2004) 9-16.

[63] Hac A., and Spanos P. D., Time Domain Method for Parameter System Identification. *Journal of Vibration and Acoustic* **112** (3) (1990) 281-287.

[64] Haldar A., Martinez F. R., and Katkhuda H., Crack Detection in Existing Structures using Noise Contaminated Dynamic Responses. *Journal of Theoretical and Applied Fracture Mechanics* **50** (1) (2008) 74-80.

[65] Haldar A., Structural health assessment using noise-contaminated minimum dynamic response information. (*Chapter 17 of the book Frontier Technologies for Infrastructure Engineering*, edited by S S Chen and A. H S Ang, CRC Press/Balkema, 383-408, 2009) (2009).

[66] Haldar A., Is the Inverse Problem Technique Appropriate for Structural Health Assessment?. *Current Science* **97** (8) (2009) 1-9.

[67] Hamid M., Soroosh S., Hoshin V. G., and Paul R. H., Dual state parameter estimation of hydrological models using ensemble Kalman filter. *Advances in Water Resources* **28** (2) (2005) 135-147.

[68] Halling M. W., Ikhsan M., and Womack K. C., Dynamic field testing for condition assessment of bridge bents. *Journal of Structural Engineering* **127** (2) (2001) 161-167.

[69] Hasan K., Rene M., and Haldar A., Health assessment at local level with unknown input excitation. *Journal of Structural Engineering* **131** (6) (2005) 956-965.

[70] Hjelmstad K. D., Banan M. R., and Banan M. R., Time domain parameters estimation algorithm for structures. I. Computational aspects. *Journal of Engineering Mechanics* **121** (3) (1995a) 424-434.

[71] Hjelmstad K. D., Banan M. R., and Banan M. R., Time domain parameters estimation algorithm for structures. II. Computational aspects. *Journal of Engineering Mechanics* **121** (3) (1995b) 435-447.

[72] Hjelmstad K. D., and Shin S., Damage detection and assessment of structures from static response. *Journal of Engineering Mechanics* **123** (6) (1997) 568-576.

[73] Ho B. L., and Kalman R. E., Effective construction of linear state variable models from input/output data. *Proceedings of the 3rd annual Allerton conference on circuits and systems theory, Monticello, IL, USA*, (1965) 449-459.

[74] Hou J. P., and Jeronimidis G., Vibration of delaminated thin composite plates. *Composites: Part A* **30** (8) (1999) 989-995.

[75] Hou X. Y., Qin F., and Quek S. T., A wireless sensor network with continuous high frequency sampling and time synchronization for structural dynamic testing. *Proceeding of the fourth European workshop, Kracow, Poland, July 2-4, 2008*, 1-13.

[76] Hou Z., Noori M., and Amand R. St., Wavelet-based approach for structural damage detection. *Journal of Engineering Mechanics* **126** (7) 677-683.

[77] Hsiao T. S., Sensor fault detection and fault tolerant control with application to vehicle lateral control system, PhD Thesis, University of California at Berkeley, USA, 2005.

[78] Hsu C. Y., and Lo T. M., Signal reconstruction with boundary-matching via iterative algorithm. *IEICE Transactions on Fundamentals of Electronics, Communications and Computer Sciences* **E89-A** (11) (2006) 3283-3289.

[79] Ibargüengoytia P. H., Vadera S., and Sucar L. E., A probabilistic model for information and sensor validation. *The Computer Journal* **49** (1) (2006) 113-126.

[80] Imamovic N., Model validation of large finite element model using test data, PhD Thesis, Imperial College London, London, 1998.

[81] Izzuddin B. A., and Elghazouli A. Y., Failure of lightly reinforced concrete members under fire. I: Analytical modeling. *Journal of Structural Engineering* **130** (1) (2004) 3-17.

[82] Jaishi B., and Ren W.X., Structural finite element model updating using ambient vibration test results. *Journal of Structural Engineering* **131** (4) (2005) 617-628.

[83] Jama H. A., Hussein E. M. A., and Sullivan P. L., Detection of debonding in composite-aluminum joints using Gamma-ray Compton scattering. *Non-destructive Evaluation and Testing International* **31** (2) (1998) 99-103.

[84] Kalman R. E., and Bucy R. S., New results in linear filtering and prediction theory. *Transactions of the ASME, Series D, Journal of Basic Engineering* **83** (1961) 95-108.

[85] Kammer D. C., and Brillhart R. D., Optimal sensor placement for modal identification using system realization methods. *Journal of Guidance, Control and Dynamics* **19** (3) (1996) 729-731.

[86] Kao C. Y., and Hung S. L., Detection of structural damage via free vibration responses generated by approximating artificial neural networks. *Computers & Structures* **81** (28-29) (2003) 2631-2644.

[87] Katkhuda M., and Haldar A., Health assessment at local level with unknown input excitation. *Journal of Structural Engineering* **131** (6) (2005) 956-965.

[88] Katkluda H. and Haldar A., A Novel Health Assessment Technique with Minimum Information. *Structural Control and Health Monitoring* **15** (6) (2008) 82l-838.

[89] Khan A. Z., Stanbridge A. B., and Ewins D. J., Detecting damage in vibrating structures with a scanning LDV. *Optics and Lasers in Engineering* **32** (6) (2000) 583-592.

[90] Kerschen G., Pascal B., Jean C. G., and Keith W., Sensor validation using principal component analysis. *Smart Materials and Structures* **14** (1) (2005) 36-42.

[91] Kerschen G., Worden K., Vakakis A. F., and Golinval J-C, Past, Present and Future of Nonlinear System Identification in Structural Analysis. *Mechanical Systems and Signal Processing* **20** (3) (2006) 505- 592.

[92] Kessler S., Spearing M., Atalla M. J., Cesnik C. E. S., and Soutis C., Damage detection in composite materials using frequency response methods. *Composites: Part B* **33** (1) (2002) 87-95.

[93] Kim H. Y., Vibration-based damage identification using reconstructed FRFs in Composite Structures. *Journal of Sound and Vibration* **259** (5) (2003) 1131-1146.

[94] Kodur V. K. R., and Bisby L. A., Evaluation of fire endurance of concrete slabs reinforced with fiber-reinforced polymer bars. *Journal of Structural Engineering* **131** (1) (2005) 34-43.

[95] Koh C.G., See M., and Balendra T., Estimation of structural parameters in time domain: a substructure approach. *Earthquake Engineering and Structural Dynamics* **20** (8) (1991) 787-801.

[96] Koh C. G., and See M., Identification and uncertainty estimation of structural parameters. *Journal of Engineering Mechanics* **120** (6) (1994) 1219-1236.

[97] Koh C. G., See L. M., and Balendra T., Damage detection of buildings: numerical and experimental studies. *Journal of Engineering Mechanics* **121** (8) (1995) 1155-1160.

[98] Koh C. G., Hong B., and Liaw C. Y., Parameter identification of large structural systems in time domain. *Journal of Structural Engineering* **126** (8) (2000) 957-963.

[99] Koh C. G., Chen Y. F., and Liaw C. Y., A hybrid computational strategy for identification of structural parameters. *Computers and Structure* **81** (2) (2003a) 107-117.

[100] Koh C. G., Hong B., and Liaw C. Y., Substructural and progressive structural identification methods. *Engineering Structures* **25** (12) (2003b) 1551-1563.

[101] Koh C. G., and Shankar K., Substructural identification method without interface measurement. *Journal of Engineering Mechanics* **129** (7) (2003c) 769-776.

[102] Law S. S., Li X. Y., Zhu X. Q., and Chan S. L., Structural damage detection from wavelet packet sensitivity. *Engineering Structures* **27** (9) (2005) 1339-1348.

[103] Law S. S., Shi Z. Y., and Zhang L. M., Structural damage detection from incomplete and noisy modal test data. *Journal of Engineering Mechanics* **124** (11) (1998) 1280-1288.

[104] Leahy M. J., Henry M. P., and Clarke D. W., Sensor validation in biomedical applications. *Control Engineering Practice* **5** (12) (1997) 1753-1758.

[105] Lee D. E., Hwang I., Valente C. M. O., Oliveira J. F. G., and Dornfeld D. A., Precision manufacturing process monitoring with acoustic emission. *International Journal of Machine Tools and Manufacture* **46** (2) (2006) 176-188.

[106] Lee J. W., and Kim J. D., Health monitoring method for bridges under ordinary traffic loadings. *Journal of Sound and Vibration* **257** (2) (2002) 247-264.

[107] Li Z., Koh B. H., and Nagarajaiah S., Detecting sensor failure via decoupled error function and inverse input-output model. *Journal of Engineering Mechanics* **133** (11) (2007) 1222-1228.

[108] Liang Y. C., and Hwu C., On-line identification of holes/cracks in Composite Structures. *Smart Materials and Structures* **10** (4) (2001) 599-609.

[109] Lin C. S., Location of modeling errors using modal test data. *AIAA Journal* **28** (9) (1995) 1650-1654.

[110] Ling X., and Haldar A., Element level system identification with unknown input with Rayleigh damping. *Journal of Engineering Mechanics* **130** (8) (2004) 877-885.

[111] Ling Z., Structural Health Monitoring and damage identification using best approximated dead load stress redistribution, PhD Thesis, University of Delaware, Delaware, USA, 2004.

[112] Lipetzky K. G., and Bandos B. G., Composite Structures and adhesive joints: NDE techniques for naval applications. *SAMPE Journal* **39** (5) (2003) 66- 74.

[113] Liu P. L., and Chian C. C, Parametric identification of truss structures using static strains. *Journal of Structural Engineering* **123** (7) (1997) 927-933.

[114] Liu Y., and Shepard Jr. W. S., Dynamic force identification based on enhanced least squares and total least squares schemes in the frequency domain. *Journal of Sound and Vibration* **282** (1-2) (2004) 37-60.

[115] Lu C. J., and Hsu Y. T., Vibration analysis of an inhomogeneous string for damage detection by wavelet transform. *International Journal of Mechanical Sciences* **44** (4) (2002) 745-754.

[116] Lu Z. R., and Law S. S., Force identification based on sensitivity in time domain. *Journal of Engineering Mechanics* **132** (10) (2006) 1050-1056.

[117] Lu Z. R., and Law S. S., Identification of system parameters and input force from output only. *Mechanical System and Signal Processing* **21** (5) (2007) 2099-2111.

[118] Lus H., Betti R., Yu J., and Angelis M. D., Investigation of a system identification methodology in the context of the ASCE benchmark problem. *Journal of Engineering Mechanics* **130** (1) (2004) 71-84.

[119] Lynch J. P., Overview of wireless sensors for real time health monitoring of civil structures. *Proceedings of the 4th international workshop on structural control and monitoring, 10-11 June 2004, New York City, NY, USA*, (2004) 1-6.

[120] Lynch J. P., Sundararajan A., Law K. H., Kiremidjian A. S., Kenny T., and Carryer E., Embedment of structural monitoring algorithms in a wireless sensing unit. *Structural Engineering and Mechanics* **15** (3) (2003) 285-297.

[121] Lynch J. P., and Loh K., A summary review of wireless sensors and sensor networks for Structural Health Monitoring. *Shock and Vibration Digest* **38** (2) (2006) 91-128.

[122] Maeck J., Wahab M. A., Peeters B., De Roeck G., De Visscher J., De Wilde W. P., Ndambi, J.-M., and Vantomme, J., Damage identification in reinforced concrete structures by dynamic stiffness determination. *Engineering Structures* **22** (10) (2000) 1339-1349.

[123] Marks R. J., Restoring lost samples from an oversampled band-limited signal. *IEEE Transactions on Acoustics, Speech, and Signal Processing* **31** (3) (1983) 752-755.

[124] Martinez F. R., Katkhuda H., and Haldar A., A Novel Health Assessment Technique with Minimum Information: Verification. *International Journal of Performability Engineering* **4** (2) (2008) 12l-140.

[125] Marvasti F. A., Clarkson P. M., Dokic M. V., Goenchanart U., and Liu C., Reconstruction of speech signals with lost samples. *IEEE Transactions on Signal Processing* **40** (12) (1992) 2897-2903.

[126] Masri S. F., and Caughey T. K., A nonparametric identification technique for nonlinear dynamic problems. *Journal of Applied Mechanics* **46** (2) (1979) 433–447.

[127] Mechitov K. A., Kim W., Agha G. A., and Nagayama T., High-frequency distributed sensing for structure monitoring. *Proceeding of the 1st international workshop on networked sensing systems, Tokyo, Japan* (2004) 101-105.

[128] Mesbahi E., An intelligent sensor validation and fault diagnostic technique for diesel engines. *Journal of Dynamic Systems, Measurement and Control* **123** (1) (2001) 141-144.

[129] Mevel L., Benveniste A., Basseville M., Goursat M., Peeters B., Auweraer H. V., and Vecchio A., Input/output versus output-only data processing for structural identification-Application to in-flight data analysis. *Journal of Sound and Vibration* **295** (3-5) (2006) 531-552.

[130] MICAz Data Sheet, Crossbow Technology Inc., 2006.

[131] Michael J. P., Modified genetic algorithm approach to system identification with structural and offshore application, PhD Thesis, National University of Singapore, Singapore, 2006.

[132] Moslem K., and Nafaspour R., Structural damage detection by genetic algorithms. *AIAA Journal* **40** (7) (2002) 1395-1401.

[133] MOTE-VIEW 1.2 User's Manual, Crossbow Technology Inc, 2006.

[134] Moteworks Software Platform, Crossbow Technology Inc., 2006.

[135] MPR/MIB User's Manual, Crossbow Technology Inc., 2006.

[136] Nagayama T., Structural Health Monitoring using smart sensors, PhD Thesis, University of Illinois at Urbana-Champaign, USA, 2007.

[137] Napolitano M. R., Silvestri G., Windon D. A. II, Casanova J. L., and Innocenti M., Sensor validation using hardware-based on-line learning neural networks. *IEEE Transactions on Aerospace and Electronic Systems* **34** (2) (1998) 456-468.

[138] Narayana K. L., and Jebaraj C., Sensitivity analysis of local/global modal parameters for identification of a crack in a beam. *Journal of Sound and Vibration* **228** (5) (1999) 977-994.

[139] Nasrellah H. A., Dynamic State Estimation Techniques for Identification of Parameters of Finite Element Structural Models, PhD thesis, Indian Institute of Science, Bangalore, India, 2009.

[140] Nelles O., *Nonlinear System Identification: from classical approaches to neural networks and fuzzy models*, Springer-Verlag, 2001.

[141] Omika Y., Fukuazwa E., Koshika N., Morikawa H., and Fukuda R., Structural responses of world trade center under aircraft attacks. *Journal of Structural Engineering* **131** (1) (2005) 6-15.

[142] Pandey A. K., Biswas M., and Samman M. M., Damage detection from changes in curvature mode shapes. *Journal of Sound and Vibration* **145** (2) (1991) 321-332.

[143] Pandey A. K., and Biswas M., Damage detection in structures using changes in flexibility. *Journal of Sound and Vibration* **169** (1) (1994) 3-17.

[144] Pang J. W. C., and Bond I. P., Bleeding composites - Damage detection and self repair using a biomimetic approach. *Composites: Part A* **36** (2) (2005) 183-188.

[145] Papadimitriou J. L., Beck J. L., and Au S. K., Entropy based optimal sensor location for structural model updating. *Journal of Vibration and Control* **6** (5) (2000) 781-800.

[146] Park S., Yun C. B., and Inman D. J., Wireless Structural Health Monitoring using an active sensing node. *Steel Structures* **6** (5) (2006) 361-368.

[147] Pranatyasto T. N., and Qin S. J., Sensor validation and process fault diagnosis for FCC units under MPC feedback. *Control Engineering Practice* **9** (8) (2001) 877-888.

[148] Qin S. J., Yue H., and Dunia R., Self-validating inferential sensors with application to air emission monitoring. *Industrial and Engineering Chemistry Research* **36** (5) (1997) 1675-1685.

[149] Qu G. M., Li Y. Y., Cheng L., and Wang B., Vibration analysis of a piezoelectric composite plate with cracks. *Composite Structures* **72** (1) (2006) 111-118.

[150] Quek S. T., Wang W., and Koh C. G., System identification of linear MDOF structure under ambient excitation. *Earthquake Engineering and Structural Dynamics* **28** (1) (1999) 61-77.

[151] Quek S. T., Tua P. S., and Wang Q., Detecting anomaly in beams and plate based on Hilbert-Huang transform of real signals. *Smart Materials and Structures* **12** (3) (2003) 447-460.

[152] Quek S. T., Tran V. A., Duan W. H., and Hou X. Y., Structural damage detection using wireless sensors accounting for data loss. *Proceeding of the 16th SPIE international conference on sensors and smart structure technologies for civil, mechanical and aerospace system, 8-12 March 2009, San Diego, California, USA*, (2009) 7292-9.

[153] Rajasekaran S., and Varghese S. P., Damage detection in beams and plates using wavelet transforms. *Computers and Concrete* **2** (6) (2005) 481-498.

[154] Ratcliffe C. P., Damage detection using a modified Laplacian operator on mode shape data. *Journal of Sound and Vibration* **204** (3) (1997) 505-517.

[155] Ray L. R., and Tian L., Damage detection in smart structures through sensitivity enhancing feedback control. *Journal of Sound and Vibration* **227** (5) (1999) 987-1002.

[156] Reichle R. H., McLaughlin D., Entekhabi D., Hydrologic data assimilation with the ensemble Kalman filter. *Monthly Weather Review* **130** (1) (2002) 103-114.

[157] Rizzo A., and Xibilia M. G., An innovative intelligent system for sensor validation in Tokamak machines. *IEEE Transactions on Control Systems Technology* **10** (3) (2002) 421-431.

[158] Safak, E., Adaptive modeling, identification and control of dynamic structural system: I. Theory. *Journal of Engineering Mechanics* **115** (11) (1989) 2386-2405.

[159] Safak, E., Adaptive modeling, identification and control of dynamic structural system: II. Applications. *Journal of Engineering Mechanics* **115** (11) (1989) 2406-2426.

[160] Sain T., and Kishen J. M. C., Damage assessment in beams using inverse method. *Journal of Engineering Mechanics* **32** (4) (2006) 337-344.

[161] Salawu O. S., and Williams C., Review of full-scale dynamic testing of bridge structures. *Engineering Structures* **17 (2)** (1995) 113-121.

[162] Salawu O. S., and Williams C., Bridge assessment using forced-vibration testing. *Journal of Structural Engineering* **121** (2) (1995) 161-173.

[163] Sanayei M., and Saletnik M. J., Parameter estimation of structures from static strain measurements. I: Formulation. *Journal of Structural Engineering* **122** (5) (1996a) 555-562.

[164] Sanayei M., and Scampoli S., Structural element stiffness identification from static test data. *Journal of Engineering Mechanics* **117** (5) (1991) 1021-1036.

[165] Sanayei M., and Saletnik M. I., Parameter estimation of structures from static strain measurements. II: Error sensitivity analysis. *Journal of Structural Engineering* **122** (5) (1996b) 563-572.

[166] Schiff D., *Dynamic analysis and failure modes of simple structures*, Wiley-Interscience Inc., New York, 1990.

[167] Shi Z. Y., Law S. S., and Zhang L. M., Structural damage detection from modal strain energy change. *Journal of Engineering Mechanics* **126** (12) (2000) 1216-1223.

[168] Shi Z. Y., Law S. S., and Zhang L. M., Improved damage quantification from elemental modal strain energy change. *Journal of Engineering Mechanics* **128** (5) (2002) 512-529.

[169] Sim S. H., Jang S. A., Spencer Jr. B. F., and Song J., Reliability-based evaluation of the performance of the damage locating vector method. *Probabilistic Engineering Mechanics* **23** (4) (2008) 489-495.

[170] Soong T. T. and Cimellaro G. P., Future directions in structural control. *Structural Control and Health Monitoring* **16** (1) (2009) 7-16.

[171] Spencer B. F., Jr., Nagayama T., and Rice J. A., Decentralized Structural Health Monitoring using smart sensors. *Proceeding of the 15th SPIE international conference on sensors and smart structure technologies for civil, mechanical and aerospace system, 9 - 13 March 2008, San Diego, California, USA*, (2008) 639202.

[172] Su Z., and Ye L., An intelligent signal processing and pattern recognition technique for defect identification using an active sensor network. *Smart Materials & Structures* **13** (4) (2004) 957-969.

[173] Swamidas A. S. J., and Chen Y., Monitoring crack growth through monitoring of modal parameters. *Journal of Sound and Vibration* **186** (2) (1995) 325-343.

[174] Tenek L. H., Henneke G., and Guzburger M., Vibration of delaminated composite plates and some applications to non-destructive testing. *Composite Structures* **23** (3) (1995) 253-262.

[175] Thornton J., Enhanced radiography for aircraft materials and components. *Engineering Failure Analysis* **11** (2) (2004) 207-220.

[176] Torkamani M. A. M., and Ahmadi A. K., Stiffness identification of two and three dimensional frames. *International Journal of Earthquake Engineering and Structural Dynamics* **16** (8) (1988) 1157-1176.

[177] Tran V. A., and Quek S. T., Damage locating vector for identifying structural damage using limited sensors. *Proceeding of the 19th KKCNN symposium on civil engineering, 10-12 December 2006, Kyoto University, Japan*, (2006) 121-124.

[178] Tran V. A., and Quek S. T., Structural damage assessment with limited sensors. *Proceeding of the fifth international conference on advances in steel structures, 5-7 December 2007, Singapore*, (2007a) 677-682.

[179] Tran V. A., and Quek S. T., Sensor validation in the context of the damage locating vector method. *Proceeding of the 20th KKCNN symposium on civil engineering, 4 - 5 October 2007, Jeju, Korea*, (2007b) 79-82.

[180] Tran V. A., Duan W. H., and Quek S. T., Structural damage detection using damage locating vector with unknown excitation. *Proceeding of the 21st KKCNN symposium on civil engineering, 27-28 October 2008, Singapore*, (2008a) 105-108.

[181] Tran V. A., Duan W. H., and Quek S. T., Structural damage assessment using damage locating vector with limited sensors. *Proceeding of the 15th SPIE international conference on sensors and smart structure technologies for civil, mechanical and aerospace system, 9 - 13 March 2008, San Diego, California, USA*, (2008b) 693226.

[182] Tsuda H., Ultrasound and damage detection in CFRP using fibre bragg grating sensors. *Composites Science and Technology* **66** (5) (2006) 676-683.

[183] Tua P. S., Quek S. T., and Wang Q., Detection of cracks in plates using piezo-actuated lamb waves. *Smart Materials and Structures* **13** (4) (2004) 643-660.

[184] Tua P. S., Quek S. T., and Wang Q., Detection of cracks in cylindrical pipes and plates using piezo-actuated lamb waves. *Smart Materials and Structures* **14** (6) (2005) 1325-1342.

[185] Vo P. H., and Haldar A., Health assessment of beams - experimental investigations. *Journal of Structural Engineering* **131** (6) (2005) 23-30.

[186] Wahab M. M. A., De Roeck G., and Peeters B., Parameterization of damage in reinforced concrete structures using model updating. *Journal of Sound and Vibration* **228** (4) (1999) 717-730.

[187] Wahab M. M. A., and De Roeck G., Damage detection in bridges using modal curvatures: Applications to a real damage scenario. *Journal of Sound and Vibration* **226** (2) (1999) 217-235.

[188] Wang D., and Haldar A., Element level system identification with unknown input. *Journal of Engineering Mechanics* **120** (1) (1994) 159-176.

[189] Wang D., and Haldar A., System identification with limited observations and without input. *Journal of Engineering Mechanics* **123** (5) (1997) 504-511.

[190] Wang L., *Support vector machines: theory and application*, Springer, Berlin, 2005.

[191] Wang X., Hu N., Fukunaga H., and Yao Z. H., Structural damage identification using static test data and changes in frequencies. *Engineering Structures* **23** (6) (2001) 610-621.

[192] Wang Y., Wireless sensing and decentralized control for civil structures: Theory and Implementation, PhD Thesis, Stanford University, USA, 2007.

[193] Waszczyszyn Z., and Ziemianski L., Neural networks in mechanics of structures and materials - new results and prospects of applications. *Computers & Structures* **79** (22) (2001) 2261-2276.

[194] Wong M. B., Size effect on temperatures of structural steel in fire. *Journal of Structural Engineering* **131** (1) (2005) 16-20.

[195] Woo A., Tong T., and Culler D., Taming the underlying challenges of reliable multi-hop routing in sensor networks. *Proceedings of the 1st International Conference on Embedded Networked Sensor Systems, 5-7 November 2003, Los Angeles California, USA*, (2003) 14-273.

[196] Worden K., and Dulieu-Barton J. M., An overview of intelligent fault detection in systems and structures. *Structural Health Monitoring* **3** (1) (2004) 85-98.

[197] Worden K., Farrar C. R., Manson G., and Park G, The Fundamental Axioms of Structural Health Monitoring. *Proceedings of the Royal Society A: Mathematical, Physical and Engineering Sciences,* **463** (2082) (2007) 1639-1664.

[198] Worden K., and Burrows A. P., Optimal sensor placement for fault detection. *Engineering Structures* **23** (8) (2001) 885-901.

[199] Worden, K., Farrar, C. R., Haywood, J. and Todd, M., A review of nonlinear dynamics applications to structural health monitoring. *Structural Control and Health Monitoring* **15** (4) (2008) 540-567.

[200] Wu C., and Hao H., Numerical study of characteristics of underground blast induced surface ground motion and their effect on above-ground structures.

Part I. Ground motion characteristics. *Soil Dynamics and Earthquake Engineering* **25** (1) (2005a) 27-38.

[201] Wu C., and Hao H., Numerical study of characteristics of underground blast induced surface ground motion and their effect on above-ground structures. Part II. Effects on structural responses. *Soil Dynamics and Earthquake Engineering* **25** (1) (2005b) 39-53.

[202] Xu Y. L., and Chen J., Structural damage detection using empirical mode decomposition: Experimental investigation. *Journal of Engineering Mechanics* **130** (11) (2004) 1279-1288.

[203] Yan A. M., and Golinval J. C., Structural damage localization by combining flexibility and stiffness methods. *Engineering Structures* **27** (12) (2005) 1752-1761.

[204] Yan Y. J., Cheng L., Wu Z. Y., and Yam L. H., Development in vibration based structural damage detection technique. *Mechanical Systems and Signal Processing* **21** (4) (2007) 2198-2111.

[205] Yang J. N., Lei Y., Pan S., and Huang N., System identification of linear structures based on Hilbert-Huang spectral analysis. Part 1: Normal modes. *Earthquake Engineering and Structural Dynamics* **32** (9) (2003a) 1443-1467.

[206] Yang J. N., Lei Y., Pan S., and Huang N., System identification of linear structures based on Hilbert-Huang spectral analysis. Part 2: Complex modes. *Earthquake Engineering and Structural Dynamics* **32** (9) (2003b) 1533-1554.

[207] Yang J. N., and Lin S., Online identification of nonlinear hysteretic structures using an adaptive tracking technique. *International Journal of Non-linear Mechanics* **39** (9) (2004) 1481 -1491.

[208] Yang J. N., and Lin S., Identification of parametric variations of structures based on least squares estimation and adaptive tracking technique. *Journal of Engineering Mechanics* **131** (3) (2005) 290-298.

[209] Yang J. N., Huang H. W., and Lin S., Sequential non-linear least-square estimation for damage identification of structures. *International Journal of Non-linear Mechanics* **41** (1) (2005) 124-140.

[210] Yang J. N., Pan S., and Lin S., Least squares estimation with unknown excitations for damage identification of structure. *Journal of Engineering Mechanics* **133**(1) (2007) 12-21.

[211] Yang J. N., and Huang H., Sequential non-linear least-square estimation for damage identification of structures with unknown inputs and unknown outputs. *International Journal of Non-linear Mechanics* **42** (5) (2007) 789-801.

[212] Yang Q. W., and Liu J. K., Structural damage identification based on residual force vector. *Journal of Sound and Vibration* **305** (1-2) (2007) 298-307.

[213] Yang J. N., Lei Y., Lin S., and Huang N., Hibert-Huang based approach for structural damage detection. *Journal of Engineering Mechanics* **130** (1) (2004) 85-95.

[214] Yuen K. V., and Lam H. F., On the complexity of artificial neural networks for smart structures monitoring. *Engineering Structures* **28** (7) (2006) 977-984.

[215] Yuen M. M. F., A numerical study of the eigen-parameters of a damaged cantilever. *Journal of Sound and Vibration* **103** (3) (1985) 301-310.

[216] Yuito M., and Matsuo N., A new sample-interpolation method for recovering missing speech samples in packet voice communications. *Proceeding of international conference on acoustics, speech and signal processing, 23-26 May 1989, Glasgow, UK,* **1** (1989) 381-384.

[217] Zou Y, Tong L., and Steven G. P., Vibration-based model-dependent damage identification and health monitoring for Composite Structures. *Journal of Sound and Vibration* **230** (2) (2000) 357-378.

APPENDIX A – *DLV* PROPERTY JUSTIFICATION

A.1 Justification for the case of determinate structure

Consider a determinate structure with two portions: (1) unaltered portion with ne_1 elements and stiffnesses $(E_jI_j)_1$, $(G_jA_j)_1$, $(E_jA_j)_1$ and length L_{j1}, where j = 1, 2, ..., ne_1; and (2) altered portion with ne_2 elements, and length L_{j2}, where j = 1, 2, …, ne_2. The stiffness of the altered portion are $(E_jI_j)_2$, $(G_jA_j)_2$, $(E_jA_j)_2$ and $(E_jI_j)_3$, $(G_jA_j)_3$, $(E_jA_j)_3$ corresponding to the reference and the altered states. Assuming that if element j is damaged: $(E_jI_j)_2 > (E_jI_j)_3$, $(G_jA_j)_2 > (G_jA_j)_3$, $(E_jA_j)_2 > (E_jA_j)_3$ and the opposite holds if element j is strengthened.

Assume that $\mathbf{P}$ is a ($ns \times 1$) static load vector which satisfies Eq. (2.1); ns is the number of sensors attached to the structure to measure displacement responses; and $\mathbf{F}_u$ and $\mathbf{F}_d$ are the flexibility matrices formulated with respect to the sensor locations at the reference and the altered states, respectively. Since the structure is deterministic, applying $\mathbf{P}$ to the reference and the altered states at the sensor locations yields the same set of internal forces in the structure, denoted as M_{j1}, Q_{j1}, N_{j1} and M_{j2}, Q_{j2}, N_{j2} for the unaltered and the altered portions, respectively. The energy induced by the load $\mathbf{P}$ at the reference (Ξ_1) and the altered (Ξ_2) states can be expressed as follows

$$\begin{aligned}\Xi_1 = &\sum_{ne_1}\left[\int_{L_{j1}}\frac{M_{j1}M_{j1}}{2\left(E_jI_j\right)_1}ds+\int_{L_{j1}}\nu\frac{Q_{j1}Q_{j1}}{2\left(G_jA_j\right)_1}ds+\int_{L_{j1}}\frac{N_{j1}N_{j1}}{2\left(E_jA_j\right)_1}ds\right]\\ &+\sum_{ne_2}\left[\int_{L_{j2}}\frac{M_{j2}M_{j2}}{2\left(E_jI_j\right)_2}ds+\int_{L_{j2}}\nu\frac{Q_{j2}Q_{j2}}{2\left(G_jA_j\right)_2}ds+\int_{L_{j2}}\frac{N_{j2}N_{j2}}{2\left(E_jA_j\right)_2}ds\right]=\frac{1}{2}\mathbf{P}^T\left(\mathbf{F}_u\mathbf{P}\right)\end{aligned} \tag{A.1}$$

$$\Xi_2 = \sum_{ne_1}\left[\int_{L_{j1}} \frac{M_{j1}M_{j1}}{2\left(E_jI_j\right)_1}ds + \int_{L_{j1}} \nu\frac{Q_{j1}Q_{j1}}{2\left(G_jA_j\right)_1}ds + \int_{L_{j1}} \frac{N_{j1}N_{j1}}{2\left(E_jA_j\right)_1}ds\right] + \sum_{ne_2}\left[\int_{L_{j2}} \frac{M_{j2}M_{j2}}{2\left(E_jI_j\right)_3}ds + \int_{L_{j2}} \nu\frac{Q_{j2}Q_{j2}}{2\left(G_jA_j\right)_3}ds + \int_{L_{j2}} \frac{N_{j2}N_{j2}}{2\left(E_jA_j\right)_3}ds\right] = \frac{1}{2}\mathbf{P}^T\left(\mathbf{F}_d\mathbf{P}\right) \tag{A.2}$$

Subtracting Eq. (A.2) from Eq. (A.1), and using Eq. (2.1) gives

$$\sum_{ne_2}\left[\int_{L_{j2}} \frac{M_{j2}M_{j2}}{\left(E_jI_j\right)_2}\left(1-\frac{\left(E_jI_j\right)_2}{\left(E_jI_j\right)_3}\right)ds + \int_{L_{j2}} \nu\frac{Q_{j2}Q_{j2}}{\left(G_jA_j\right)_2}\left(1-\frac{\left(G_jA_j\right)_2}{\left(G_jA_j\right)_3}\right)ds + \int_{L_{j2}} \frac{N_{j2}N_{j2}}{\left(E_jA_j\right)_2}\left(1-\frac{\left(E_jA_j\right)_2}{\left(E_jA_j\right)_3}\right)ds\right] = 0 \tag{A.3}$$

If the altered elements are damaged, implying that $(E_jI_j)_2 > (E_jI_j)_3$, $(G_jA_j)_2 > (G_jA_j)_3$, $(E_jA_j)_2 > (E_jA_j)_3$ or $\left(1-\frac{\left(E_jI_j\right)_2}{\left(E_jI_j\right)_3}\right) < 0$, $\left(1-\frac{\left(G_jA_j\right)_2}{\left(G_jA_j\right)_3}\right) < 0$, $\left(1-\frac{\left(E_jA_j\right)_2}{\left(E_jA_j\right)_3}\right) < 0$.

Each term in Eq. (A.3) is smaller than or equal to zero. Hence, Eq. (A.3) is satisfied if and only if $M_{j2} = 0$, $Q_{j2} = 0$, $N_{j2} = 0$ for all j.

If the altered elements are strengthened, implying that $(E_jI_j)_2 < (E_jI_j)_3$, $(G_jA_j)_2 < (G_jA_j)_3$, $(E_jA_j)_2 < (E_jA_j)_3$ or $\left(1-\frac{\left(E_jI_j\right)_2}{\left(E_jI_j\right)_3}\right) > 0$, $\left(1-\frac{\left(G_jA_j\right)_2}{\left(G_jA_j\right)_3}\right) > 0$, $\left(1-\frac{\left(E_jA_j\right)_2}{\left(E_jA_j\right)_3}\right) > 0$.

Each term in Eq. (A.3) is larger than or equal to zero. Thus, Eq. (A.3) is also satisfied if and only if $M_{j2} = 0$, $Q_{j2} = 0$, $N_{j2} = 0$ for all j.

The above derivations implied that

$$\int_{L_{j2}} \frac{M_{j2}M_{j2}}{2\left(E_jI_j\right)_2}ds = 0, \int_{L_{j2}} \nu\frac{Q_{j2}Q_{j2}}{2\left(G_jA_j\right)_2}ds = 0, \int_{L_{j2}} \frac{N_{j2}N_{j2}}{2\left(E_jA_j\right)_2}ds = 0 \tag{A.4}$$

or

$$\int_{L_{j2}} \frac{M_{j2}M_{j2}}{2\left(E_jI_j\right)_2}ds + \int_{L_{j2}} \nu\frac{Q_{j2}Q_{j2}}{2\left(G_jA_j\right)_2}ds + \int_{L_{j2}} \frac{N_{j2}N_{j2}}{2\left(E_jA_j\right)_2}ds = 0 \tag{A.5}$$

which means that the energy induced by the load vector **P** satisfying Eq. (2.1), that is the *DLV*, in the altered element(s) at the reference state is zero.

A.2 Justification for the case of indeterminate structure

For indeterminate structures, applying a load vector **P** onto the reference and the altered structure will yield two different sets of internal forces. The derivation in Section A.1 is thus no longer applicable and modification is needed. In this section, an indeterminate structure with two portions, namely unaltered and altered, and with *nr* redundant connections is considered. Under a static load vector **P** satisfying Eq. (2.1), that is *DLV*, internal forces in the redundant connections are $\mathbf{R}_{i1}$ and $\mathbf{R}_{i2}$ for the reference and the altered structures, respectively, where $i = 1, 2,\ldots, nr$.

Internal forces of the indeterminate structural behavior under a static load vector **P** can be considered as combination of (1) internal forces of the determinate structure under **P**; and (2) internal forces of the determinate structure under $\mathbf{R}_{i1}$ or $\mathbf{R}_{i2}$ corresponding to the reference or the altered structure. Hence, the derivation in Section A.1 is a special case of the derivation in this section with $\mathbf{R}_{i1}=\mathbf{R}_{i2}=0$ for all i.

From the distribution of internal forces principle, if a static load P is applied onto the reference and the damaged structures, internal forces in the undamaged elements increase whereas internal forces in damaged elements decrease. Since the redundant connections are not damaged, they experience increment in internal forces, that is, $\mathbf{R}_{i2} \geq \mathbf{R}_{i1}$. In other words, internal forces (in term of absolute values) induced by $\mathbf{R}_{i2}$ in every members of the determinate structure are greater than or equal to internal forces generated by $\mathbf{R}_{i1}$. The opposite holds if the structure is strengthened.

Applying the static load vector **P** onto the determinate structure, the internal forces of the unaltered and altered portions are $M_{j1\mathbf{P}}$, $Q_{j1\mathbf{P}}$, $N_{j1\mathbf{P}}$, and $M_{j2\mathbf{P}}$, $Q_{j2\mathbf{P}}$, $N_{j2\mathbf{P}}$, respectively. Applying $\mathbf{R}_{i1}$ onto the determinate structure, the internal forces of the

unaltered and altered portions are $M_{j1\mathbf{R}_1}, Q_{j1\mathbf{R}_1}, N_{j1\mathbf{R}_1}$ and $M_{j2\mathbf{R}_1}, Q_{j2\mathbf{R}_1}, N_{j2\mathbf{R}_1}$, respectively. Applying $\mathbf{R}_{i2}$ onto the determinate structure, the internal forces of the unaltered and altered portions are $M_{j1\mathbf{R}_2}, Q_{j1\mathbf{R}_2}, N_{j1\mathbf{R}_2}$ and $M_{j2\mathbf{R}_2}, Q_{j2\mathbf{R}_2}, N_{j2\mathbf{R}_2}$, respectively. Hence, applying the static load vector $\mathbf{P}$ onto the indeterminate structure at the reference and the altered states, the corresponding energy are Ξ_1 and Ξ_2, respectively, where

$$\begin{aligned}\Xi_1 = &\sum_{ne_1}\left[\int_{L_{j1}}\frac{M_{j1\mathbf{P}}M_{j1\mathbf{P}}}{2\left(E_jI_j\right)_1}ds+\int_{L_{j1}}\nu\frac{Q_{j1\mathbf{P}}Q_{j1\mathbf{P}}}{2\left(G_jA_j\right)_1}ds+\int_{L_{j1}}\frac{N_{j1\mathbf{P}}N_{j1\mathbf{P}}}{2\left(E_jA_j\right)_1}ds\right]\\
&+\sum_{ne_2}\left[\int_{L_{j2}}\frac{M_{j2\mathbf{P}}M_{j2\mathbf{P}}}{2\left(E_jI_j\right)_2}ds+\int_{L_{j2}}\nu\frac{Q_{j2\mathbf{P}}Q_{j2\mathbf{P}}}{2\left(G_jA_j\right)_2}ds+\int_{L_{j2}}\frac{N_{j2\mathbf{P}}N_{j2\mathbf{P}}}{2\left(E_jA_j\right)_2}ds\right]\\
&+\sum_{ne_1}\left[\int_{L_{j1}}\frac{M_{j1\mathbf{R}_1}M_{j1\mathbf{R}_1}}{2\left(E_jI_j\right)_1}ds+\int_{L_{j1}}\nu\frac{Q_{j1\mathbf{R}_1}Q_{j1\mathbf{R}_1}}{2\left(G_jA_j\right)_1}ds+\int_{L_{j1}}\frac{N_{j1\mathbf{R}_1}N_{j1\mathbf{R}_1}}{2\left(E_jA_j\right)_1}ds\right]\\
&+\sum_{ne_2}\left[\int_{L_{j2}}\frac{M_{j2\mathbf{R}_1}M_{j2\mathbf{R}_1}}{2\left(E_jI_j\right)_2}ds+\int_{L_{j2}}\nu\frac{Q_{j2\mathbf{R}_1}Q_{i2\mathbf{R}_1}}{2\left(G_jA_j\right)_2}ds+\int_{L_{j2}}\frac{N_{j2\mathbf{R}_1}N_{j2\mathbf{R}_1}}{2\left(E_jA_j\right)_2}ds\right]=\frac{1}{2}\mathbf{P}^T\left(\mathbf{F}_u\mathbf{P}\right)\end{aligned} \tag{A.6}$$

$$\begin{aligned}\Xi_2 = &\sum_{ne_1}\left[\int_{L_{j1}}\frac{M_{j1\mathbf{P}}M_{j1\mathbf{P}}}{2\left(E_jI_j\right)_1}ds+\int_{L_{j1}}\nu\frac{Q_{j1\mathbf{P}}Q_{j1\mathbf{P}}}{2\left(G_jA_j\right)_1}ds+\int_{L_{j1}}\frac{N_{j1\mathbf{P}}N_{j1\mathbf{P}}}{2\left(E_jA_j\right)_1}ds\right]\\
&+\sum_{ne_2}\left[\int_{L_{j2}}\frac{M_{j2\mathbf{P}}M_{j2\mathbf{P}}}{2\left(E_jI_j\right)_3}ds+\int_{L_{j2}}\nu\frac{Q_{j2\mathbf{P}}Q_{j2\mathbf{P}}}{2\left(G_jA_j\right)_3}ds+\int_{L_{j2}}\frac{N_{j2\mathbf{P}}N_{j2\mathbf{P}}}{2\left(E_jA_j\right)_3}ds\right]\\
&+\sum_{ne_1}\left[\int_{L_{j1}}\frac{M_{j1\mathbf{R}_1}M_{j1\mathbf{R}_1}}{2\left(E_jI_j\right)_1}ds+\int_{L_{j1}}\nu\frac{Q_{j1\mathbf{R}_1}Q_{j1\mathbf{R}_1}}{2\left(G_jA_j\right)_1}ds+\int_{L_{j1}}\frac{N_{j1\mathbf{R}_1}N_{j1\mathbf{R}_1}}{2\left(E_jA_j\right)_1}ds\right]\\
&+\sum_{ne_2}\left[\int_{L_{j2}}\frac{M_{j2\mathbf{R}_1}M_{j2\mathbf{R}_1}}{2\left(E_jI_j\right)_3}ds+\int_{L_{j2}}\nu\frac{Q_{j2\mathbf{R}_1}Q_{i2\mathbf{R}_1}}{2\left(G_jA_j\right)_3}ds+\int_{L_{j2}}\frac{N_{j2\mathbf{R}_1}N_{j2\mathbf{R}_1}}{2\left(E_jA_j\right)_3}ds\right]=\frac{1}{2}\mathbf{P}^T\left(\mathbf{F}_d\mathbf{P}\right)\end{aligned} \tag{A.7}$$

Subtracting Eq. (A.7) from Eq. (A.6), and using Eq.(2.1) gives

$$\sum_{ne_2}\left[\begin{array}{l}\int_{L_{j2}}\frac{M_{j2\mathbf{P}}M_{j2\mathbf{P}}}{(E_jI_j)_2}\left(1-\frac{(E_jI_j)_2}{(E_jI_j)_3}\right)ds+\int_{L_{j2}}\nu\frac{Q_{j2\mathbf{P}}Q_{j2\mathbf{P}}}{(GA)_{j2}}\left(1-\frac{(G_jA_j)_2}{(G_jA_j)_3}\right)ds\\+\int_{L_{j2}}\frac{N_{j2\mathbf{P}}N_{j2\mathbf{P}}}{(E_jA_j)_2}\left(1-\frac{(E_jA_j)_2}{(E_jA_j)_3}\right)ds\end{array}\right]$$
$$+\sum_{ne_1}\left[\begin{array}{l}\int_{L_{j1}}\frac{(M_{j1\mathbf{R}_1}M_{j1\mathbf{R}_1}-M_{j1\mathbf{R}_2}M_{j1\mathbf{R}_2})}{(E_jI_j)_1}ds+\int_{L_{j1}}\nu\frac{Q_{j1\mathbf{R}_1}Q_{j1\mathbf{R}_1}-Q_{j1\mathbf{R}_2}Q_{j1\mathbf{R}_2}}{(G_jA_j)_1}ds\\+\int_{L_{j1}}\frac{N_{j1\mathbf{R}_1}N_{j1\mathbf{R}_1}-N_{j1\mathbf{R}_2}N_{j1\mathbf{R}_2}}{(E_jA_j)_1}ds\end{array}\right]$$
$$+\sum_{ne_2}\left[\begin{array}{l}\int_{L_{j2}}\left(\frac{M_{j2\mathbf{R}_1}M_{j2\mathbf{R}_1}}{(E_jI_j)_2}-\frac{M_{j2\mathbf{R}_2}M_{j2\mathbf{R}_2}}{(E_jI_j)_3}\right)ds+\int_{L_{j2}}\nu\left(\frac{Q_{j2\mathbf{R}_1}Q_{j2\mathbf{R}_1}}{(G_jA_j)_2}-\frac{Q_{j2\mathbf{R}_2}Q_{j2\mathbf{R}_2}}{(G_jA_j)_3}\right)ds\\+\int_{L_{j2}}\left(\frac{N_{j2\mathbf{R}_1}N_{j2\mathbf{R}_1}}{(E_jA_j)_2}-\frac{N_{j2\mathbf{R}_2}N_{j2\mathbf{R}_2}}{(E_jA_j)_3}\right)ds\end{array}\right]=0 \quad \text{(A.8)}$$

If the structure is damaged, $(E_jI_j)_2 > (E_jI_j)_3$, $(G_jA_j)_2 > (G_jA_j)_3$, $(E_jA_j)_2 > (E_jA_j)_3$ or $\left[1-\frac{(E_jI_j)_2}{(E_jI_j)_3}\right]<0$, $\left[1-\frac{(G_jA_j)_2}{(G_jA_j)_3}\right]<0$, $\left[1-\frac{(E_jA_j)_2}{(E_jA_j)_3}\right]<0$, and $|M_{j1\mathbf{R}_1}|\le|M_{j1\mathbf{R}_2}|$, $|Q_{j1\mathbf{R}_1}|\le|Q_{j1\mathbf{R}_2}|$, $|N_{j1\mathbf{R}_1}|\le|N_{j1\mathbf{R}_2}|$, $|M_{j2\mathbf{R}_1}|\le|M_{j2\mathbf{R}_2}|$, $|Q_{j2\mathbf{R}_1}|\le|Q_{j2\mathbf{R}_2}|$, $|N_{j2\mathbf{R}_1}|\le|N_{j2\mathbf{R}_2}|$, or $\left[M^2_{j1\mathbf{R}_1}-M^2_{j1\mathbf{R}_2}\right]\le 0$, $\left[Q^2_{j1\mathbf{R}_1}-Q^2_{j1\mathbf{R}_2}\right]\le 0$, $\left[N^2_{j1\mathbf{R}_1}-N^2_{j1\mathbf{R}_2}\right]\le 0$, $\Rightarrow$ $\left[\frac{M^2_{j2\mathbf{R}_1}}{(E_jI_j)_2}-\frac{M^2_{j2\mathbf{R}_2}}{(E_jI_j)_3}\right]\le 0$, $\left[\frac{Q^2_{j2\mathbf{R}_1}}{(G_jA_j)_2}-\frac{Q^2_{j2\mathbf{R}_2}}{(G_jA_j)_3}\right]\le 0$, $\left[\frac{N^2_{j2\mathbf{R}_1}}{(E_jA_j)_2}-\frac{N^2_{j2\mathbf{R}_2}}{(E_jA_j)_3}\right]\le 0$. Every term in Eq. (A.8) is smaller than or equal to zero. Thus, Eq. (A.8) is satisfied if and only if $M_{j2\mathbf{P}}=0$, $Q_{j2\mathbf{P}}=0$, $N_{j2\mathbf{P}}=0$, $M_{j1\mathbf{R}_1}=0$, $Q_{j1\mathbf{R}_1}=0$, $N_{j1\mathbf{R}_1}=0$, $M_{j1\mathbf{R}_2}=0$, $Q_{j1\mathbf{R}_2}=0$, $N_{j1\mathbf{R}_2}=0$, $M_{j2\mathbf{R}_1}=0$, $Q_{j2\mathbf{R}_1}=0$, $N_{j2\mathbf{R}_1}=0$ for all j.

If the structure is strengthened, $(E_jI_j)_2 < (E_jI_j)_3$, $(G_jA_j)_2 < (G_jA_j)_3$, $(E_jA_j)_2 < (E_jA_j)_3$ or $\left[1-\frac{(E_jI_j)_2}{(E_jI_j)_3}\right]>0$, $\left[1-\frac{(G_jA_j)_2}{(G_jA_j)_3}\right]>0$, $\left[1-\frac{(E_jA_j)_2}{(E_jA_j)_3}\right]>0$ and $|M_{j1\mathbf{R}_1}|\ge|M_{j1\mathbf{R}_2}|$,

$\left|Q_{j1\mathbf{R}_1}\right| \geq \left|Q_{j1\mathbf{R}_2}\right|$, $\left|N_{j1\mathbf{R}_1}\right| \geq \left|N_{j1\mathbf{R}_2}\right|$, $\left|M_{j2\mathbf{R}_1}\right| \geq \left|M_{j2\mathbf{R}_2}\right|$, $\left|Q_{j2\mathbf{R}_1}\right| \geq \left|Q_{j2\mathbf{R}_2}\right|$, $\left|N_{j2\mathbf{R}_1}\right| \geq \left|N_{j2\mathbf{R}_2}\right|$, or

$\left[M_{j1\mathbf{R}_1}^2 - M_{j1\mathbf{R}_2}^2\right] \geq 0$, $\left[Q_{j1\mathbf{R}_1}^2 - Q_{j1\mathbf{R}_2}^2\right] \geq 0$, $\left[N_{j1\mathbf{R}_1}^2 - N_{j1\mathbf{R}_2}^2\right] \geq 0$, $\Rightarrow$

$\left[\frac{M_{j2\mathbf{R}_1}^2}{\left(E_jI_j\right)_2} - \frac{M_{j2\mathbf{R}_2}^2}{\left(E_jI_j\right)_3}\right] \geq 0$, $\left[\frac{Q_{j2\mathbf{R}_1}^2}{\left(G_jA_j\right)_2} - \frac{Q_{j2\mathbf{R}_2}^2}{\left(G_jA_j\right)_3}\right] \geq 0$, $\left[\frac{N_{j2\mathbf{R}_1}^2}{\left(E_jA_j\right)_2} - \frac{N_{j2\mathbf{R}_2}^2}{\left(E_jA_j\right)_3}\right] \geq 0$. Every term in Eq. (A.8) is greater than or equal to zero. Thus, Eq. (A.8) is satisfied if and only if $M_{j2\mathbf{P}} = 0$, $Q_{j2\mathbf{P}} = 0$, $N_{j2\mathbf{P}} = 0$, $M_{j1\mathbf{R}_1} = 0$, $Q_{j1\mathbf{R}_1} = 0$, $N_{j1\mathbf{R}_1} = 0$, $M_{j1\mathbf{R}_2} = 0$, $Q_{j1\mathbf{R}_2} = 0$, $N_{j1\mathbf{R}_2} = 0$, $M_{j2\mathbf{R}_1} = 0$, $Q_{j2\mathbf{R}_1} = 0$, $N_{j2\mathbf{R}_1} = 0$ for all j.

The above derivations imply that

$$\begin{aligned}
&\int_{L_{j2}} \frac{M_{j2\mathbf{P}}M_{j2\mathbf{P}}}{2\left(E_jI_j\right)_2}ds = 0, \int_{L_{j2}} \nu\frac{Q_{j2\mathbf{P}}Q_{j2\mathbf{P}}}{2\left(G_jA_j\right)_2}ds = 0, \int_{L_{j2}} \frac{N_{j2\mathbf{P}}N_{j2\mathbf{P}}}{2\left(E_jA_j\right)_2}ds = 0, \\
&\int_{L_{j2}} \frac{M_{j2\mathbf{R}_1}M_{j2\mathbf{R}_1}}{2\left(E_jI_j\right)_2}ds = 0, \int_{L_{j2}} \nu\frac{Q_{j2\mathbf{R}_1}Q_{j2\mathbf{R}_1}}{2\left(G_jA_j\right)_2}ds = 0, \int_{L_{j2}} \frac{N_{j2\mathbf{R}_1}N_{j2\mathbf{R}_1}}{2\left(E_jA_j\right)_2}ds = 0
\end{aligned} \tag{A.9}$$

or

$$\begin{aligned}
&\int_{L_{j2}} \frac{M_{j2\mathbf{P}}M_{j2\mathbf{P}}}{2\left(E_jI_j\right)_2}ds + \int_{L_{j2}} \nu\frac{Q_{j2\mathbf{P}}Q_{j2\mathbf{P}}}{2\left(G_jA_j\right)_2}ds + \int_{L_{j2}} \frac{N_{j2\mathbf{P}}N_{j2\mathbf{P}}}{2\left(E_jA_j\right)_2}ds \\
&+ \int_{L_{j2}} \frac{M_{j2\mathbf{R}_1}M_{j2\mathbf{R}_1}}{2\left(E_jI_j\right)_2}ds + \int_{L_{j2}} \nu\frac{Q_{j2\mathbf{R}_1}Q_{j2\mathbf{R}_1}}{2\left(G_jA_j\right)_2}ds + \int_{L_{j2}} \frac{N_{j2\mathbf{R}_1}N_{j2\mathbf{R}_1}}{2\left(E_jA_j\right)_2}ds = 0
\end{aligned} \tag{A.10}$$

or energy induced in the altered element(s) at the reference state by the static load vector **P** which satisfies Eq. (2.1), that is *DLV*, is zero.

APPENDIX B – PHYSICAL PROPERTIES OF *DLV*

B.1 Sub-problem

Performing *SVD* on an $(n \times n)$ matrix $\mathbf{A}$ with rank $r_{\mathbf{A}}$ gives

$$\mathbf{A} \xrightarrow{SVD} \mathbf{U}\boldsymbol{\Sigma}\mathbf{V}^T \tag{B.1}$$

where

$$\mathbf{A} = \begin{bmatrix} a_{11} & a_{12} & \cdots & a_{1n} \\ a_{21} & a_{22} & \cdots & a_{2n} \\ \cdots & \cdots & \cdots & \cdots \\ a_{n1} & a_{n2} & \cdots & a_{nn} \end{bmatrix}, \boldsymbol{\Sigma} = \begin{bmatrix} s_1 & 0 & \cdots & 0 \\ 0 & s_2 & \cdots & 0 \\ \cdots & \cdots & \cdots & \cdots \\ 0 & 0 & \cdots & s_n \end{bmatrix} \text{ in which } s_1 \geq s_2 \geq \cdots \geq s_n \geq 0,$$

$$\mathbf{U} = \begin{bmatrix} u_{11} & u_{12} & \cdots & u_{1n} \\ u_{21} & u_{22} & \cdots & u_{2n} \\ \cdots & \cdots & \cdots & \cdots \\ u_{n1} & u_{n2} & \cdots & u_{nn} \end{bmatrix} = \begin{bmatrix} \mathbf{u}_1 & \mathbf{u}_2 & \cdots & \mathbf{u}_n \end{bmatrix}, \text{ and}$$

$$\mathbf{V} = \begin{bmatrix} v_{11} & v_{12} & \cdots & v_{1n} \\ v_{21} & v_{22} & \cdots & v_{2n} \\ \cdots & \cdots & \cdots & \cdots \\ v_{n1} & v_{n2} & \cdots & v_{nn} \end{bmatrix} = \begin{bmatrix} \mathbf{v}_1^T & \mathbf{v}_2^T & \cdots & \mathbf{v}_n^T \end{bmatrix}^T$$

The transformation of column $\mathbf{x}$ vector to a column $\mathbf{y}$ vector through the transformation matrix $\mathbf{A}$ is expressed as

$$\mathbf{y} = \mathbf{A}\,\mathbf{x} \tag{B.2}$$

Invoking the definition of $\mathbf{A}$ in Eq. (B.1), Eq. (B.2) can be re-written as

$$\mathbf{y} = \mathbf{U}\begin{bmatrix} s_1 & 0 & \cdots & 0 \\ 0 & s_2 & \cdots & 0 \\ \cdots & \cdots & \cdots & \cdots \\ 0 & 0 & \cdots & s_n \end{bmatrix}\begin{bmatrix} \mathbf{v}_1 \\ \mathbf{v}_2 \\ \cdots \\ \mathbf{v}_n \end{bmatrix}.\mathbf{x} = \mathbf{U}\begin{bmatrix} s_1 & 0 & \cdots & 0 \\ 0 & s_2 & \cdots & 0 \\ \cdots & \cdots & \cdots & \cdots \\ 0 & 0 & \cdots & s_n \end{bmatrix}\begin{bmatrix} \mathbf{v}_1\mathbf{x} \\ \mathbf{v}_2\mathbf{x} \\ \cdots \\ \mathbf{v}_n\mathbf{x} \end{bmatrix} \tag{B.3}$$

Because **x** is a column vector, $\mathbf{v}_i$ is a row vector, and s_i is a scalar, Eq. (B.3) can be expanded as

$$\mathbf{y} = \mathbf{U}\begin{bmatrix} s_1\mathbf{v}_1\mathbf{x} \\ s_2\mathbf{v}_2\mathbf{x} \\ \cdots \\ s_n\mathbf{v}_n\mathbf{x} \end{bmatrix} = \begin{bmatrix}\mathbf{u}_1 & \mathbf{u}_2 & \cdots & \mathbf{u}_n\end{bmatrix}\begin{bmatrix} s_1\mathbf{v}_1\mathbf{x} \\ s_2\mathbf{v}_2\mathbf{x} \\ \cdots \\ s_n\mathbf{v}_n\mathbf{x} \end{bmatrix} = \sum_{i=1}^{n}(s_i\,\mathbf{v}_i.\mathbf{x})\,\mathbf{u}_i \tag{B.4}$$

Assuming that the input column vector **x** is equal to $\mathbf{v}_i^T$, and invoking the orthonormal property of $\mathbf{v}_i$, that is, $\mathbf{v}_i.\mathbf{v}_j^T = \begin{cases} 0 & \text{if } i \neq j \\ 1 & \text{if } i = j \end{cases}$, Eq. (B.4) can be expressed as

$$\mathbf{y} = \mathbf{U}\begin{bmatrix} s_1 & 0 & \cdots & 0 \\ 0 & s_2 & \cdots & 0 \\ \cdots & \cdots & \cdots & \cdots \\ 0 & 0 & \cdots & s_n \end{bmatrix}\begin{bmatrix} \mathbf{v}_1 \\ \mathbf{v}_2 \\ \cdots \\ \mathbf{v}_n \end{bmatrix}.\mathbf{v}_i^T = \begin{bmatrix}\mathbf{u}_1 & \mathbf{u}_2 & \cdots & \mathbf{u}_n\end{bmatrix}\begin{bmatrix} s_1 & 0 & \cdots & 0 \\ 0 & s_2 & \cdots & 0 \\ \cdots & \cdots & \cdots & \cdots \\ 0 & 0 & \cdots & s_n \end{bmatrix}\begin{bmatrix} 0 \\ \cdots \\ \mathbf{v}_i\,\mathbf{v}_i^T \\ 0 \end{bmatrix} \tag{B.5}$$

or

$$\mathbf{y} = \begin{bmatrix}\mathbf{u}_1 & \mathbf{u}_2 & \cdots & \mathbf{u}_n\end{bmatrix}\begin{bmatrix} s_1 & 0 & \cdots & 0 \\ 0 & s_2 & \cdots & 0 \\ \cdots & \cdots & \cdots & \cdots \\ 0 & 0 & \cdots & s_n \end{bmatrix}\begin{bmatrix} 0 \\ \cdots \\ 1 \\ 0 \end{bmatrix} = s_i\mathbf{u}_i \tag{B.6}$$

Remark:

+ If the right singular vector $\mathbf{v}_i$ of matrix **A** is considered input through the transformation in Eq. (B.2), output will be the left singular vector $\mathbf{u}_i$ of matrix **A** scaled by singular value quantity s_i of matrix **A**.

B.2 Main problem

a. Apply a ($ns \times 1$) load vector **P** to the reference and the altered structures and measure the corresponding ($ns \times 1$) displacement responses $\mathbf{d}_u$ and $\mathbf{d}_d$ at the *ns* sensor locations. Structural compatibility conditions at the sensor locations of the two states can be expressed respectively as follows

$$\mathbf{d}_u = \mathbf{F}_u\mathbf{P} \tag{B.7}$$

and

$$\mathbf{d}_d = \mathbf{F}_d \mathbf{P} \tag{B.8}$$

where $\mathbf{F}_u$ and $\mathbf{F}_d$ are the ($ns \times ns$) structural flexibility matrices formulated with respect to the sensor locations at the reference and the damaged states, respectively. Subtracting Eq. (B.7) from Eq. (B.8) gives

$$\mathbf{d}_d - \mathbf{d}_u = \left(\mathbf{F}_d - \mathbf{F}_u\right)\mathbf{P} \quad \text{or} \quad \mathbf{d}_\Delta = \mathbf{F}_\Delta \mathbf{P} \tag{B.9}$$

Decomposing $\mathbf{F}_\Delta$ using *SVD* gives

$$\mathbf{F}_\Delta \xrightarrow{SVD} \mathbf{U}_1 \, \mathbf{\Sigma}_1 \, \mathbf{V}_1^T \tag{B.10}$$

Equation (B.9) has the same form with the transformation of vector **x** to vector **y** in Eq. (B.2). Hence, employing the results of Section B.1 with $\mathbf{v}_{1i}^{\mathrm{T}}$ ($\mathbf{v}_{1i}$ is row i of $\mathbf{V}_1$) as the input load vector **P** gives

$$\mathbf{d}_{\Delta i} = s_{1i}\mathbf{u}_{1i} \tag{B.11}$$

where $\mathbf{u}_{1i}$ is column i of $\mathbf{U}_1$; and s_{1i} the ith singular value of $\mathbf{\Sigma}_1$. If $i = r_\mathbf{A}+1, r_\mathbf{A}+2, \ldots, ns$ ($r_\mathbf{A}$ is the rank of $\mathbf{F}_\Delta$) then $s_{1i} = 0$, and thus $\mathbf{d}_{\Delta i} = 0$. In other words, the same static load vector $\mathbf{P} = \mathbf{v}_{1i}^{\mathrm{T}}$ ($i = r_\mathbf{A}+1, r_\mathbf{A}+2, \ldots, ns$) generates the same displacements at sensor locations at the two states of the structure. Those input force vectors $\mathbf{P} = \mathbf{v}_{1i}^{\mathrm{T}}$ is called the *load vectors* in the *DLV* method proposed by Bernal (2002).

b. Apply a ($ns \times 1$) displacement vector **d** onto the ns sensor locations at the reference and the altered states while restrain the other *DOF*, the ($ns \times 1$) nodal force vector with respect to the sensor locations at the two states are $\mathbf{P}_u$ and $\mathbf{P}_d$, respectively. The compatibility conditions of the structure at the sensor locations for the two states can be expressed respectively as follows

$$\mathbf{P}_u = \mathbf{K}_u \mathbf{d} \tag{B.12}$$

and

$$\mathbf{P}_d = \mathbf{K}_d \mathbf{d} \tag{B.13}$$

where $\mathbf{K}_u$ and $\mathbf{K}_d$ are the ($ns \times ns$) structural stiffness matrices formulated with respect to the sensor locations at the reference and the altered states, respectively. Subtracting Eq. (B.13) from Eq. (B.12) gives

$$\mathbf{P}_u - \mathbf{P}_d = \left(\mathbf{K}_u - \mathbf{K}_d\right)\mathbf{d} \quad \text{or} \quad \mathbf{P}_\Delta = \mathbf{K}_\Delta \mathbf{d} \tag{B.14}$$

Decomposing $\mathbf{K}_\Delta$ using *SVD* gives

$$\mathbf{K}_\Delta \xrightarrow{SVD} \mathbf{U}_2\, \mathbf{\Sigma}_2\, \mathbf{V}_2^T \tag{B.15}$$

Equation (B.14) has the same form with the transformation of vector **x** to vector **y** in Eq. (B.2). Hence, applying the results of Section B.1 with $\mathbf{v}_{2i}^{\mathrm{T}}$ as input displacement vector **d** ($\mathbf{v}_{2i}$ is row i of $\mathbf{V}_2$) gives

$$\mathbf{P}_{\Delta i} = s_{2i}\mathbf{u}_{2i} \tag{B.16}$$

where $\mathbf{u}_{2i}$ is column i of $\mathbf{U}_2$; and s_{2i} the ith singular value of $\mathbf{\Sigma}_2$. If $i = r_{\mathbf{A}}+1, r_{\mathbf{A}}+2, \ldots, ns$ ($r_{\mathbf{A}}$ is the rank of $\mathbf{K}_\Delta$) then $s_{2i} = 0$, and thus $\mathbf{P}_{\Delta i} = 0$. In other words, the same displacement vector $\mathbf{d} = \mathbf{v}_{2i}^{\mathrm{T}}$ ($i = r_{\mathbf{A}}+1, r_{\mathbf{A}}+2, \ldots, ns$) creates the same nodal force vector at the sensor locations at the two states of the structure. Those input displacement vectors $\mathbf{d} = \mathbf{v}_{2i}^{\mathrm{T}}$ are called the *displacement vectors* for the *DLV* method.

APPENDIX C – PUBLISHCATION IN THIS RESEARCH

C.1 JOURNAL PAPERS

[1] Quek S. T., Tran V. A., and Hou X. Y., Structural damage detection accounting for loss of data in wireless network sensors. *Key engineering materials* 413-414 (2009), 125-132.

[2] Quek S. T., Tran V. A., Duan W. H., and Hou X. Y., Structural damage detection using enhanced damage locating vector method with limited wireless sensors. *Journal of sound and vibration* **328** (4-5) (2009) 411-427.

[3] Tran V. A., Quek S. T., and Duan W. H., Locating vector method for structural damage detection using noisy and limited static response data. *Journal of engineering structures* (2009) (under review).

[4] Tran V. A., Quek S. T., and Duan W. H., Sensor validation with damage locating vector method for structural health monitoring (2009) *International journal of structural stability and dynamics* (Accepted).

C.2 CONFERENCE PAPERS

[1] Tran V. A., and Quek S. T., Damage locating vector for identifying structural damage using limited sensors. *Proceeding of the 19th KKCNN symposium on civil engineering, 10-12 December 2006, Kyoto University, Japan*, 121-124, 2006.

[2] Tran V. A., and Quek S. T., Sensor validation in the context of the damage locating vector method. *Proceeding of the 20th KKCNN symposium on civil engineering, 4-5 October 2007, Jeju, Korea*, 79-82, 2007a.

[3] Tran V. A., and Quek S. T., Structural damage assessment with limited sensors. *Proceeding of the 5th international conference on advances in steel structures, 5-7 December 2007, Singapore*, 677-682, 2007b.

[4] Tran V. A., Duan W. H., and Quek S. T., Structural damage assessment using damage locating vector with limited sensors. *Proceeding of the 15th SPIE international conference on sensors and smart structure technologies for civil,*

mechanical and aerospace system, 10-13 March 2008, San Diego, California, USA, 693226, 2008a.

[5] Tran V. A., Duan W. H., and Quek S. T., Structural damage detection using damage locating vector with unknown excitation. *Proceeding of the 21st KKCNN symposium on civil engineering, 27-28 October 2008, Singapore*, 105-108, 2008b.

[6] Quek S. T., Tran V. A., Duan W. H., and Hou X. Y., Structural damage detection using wireless sensors accounting for data loss. *Proceeding of the 16th SPIE international conference on sensors and smart structure technologies for civil, mechanical and aerospace system, 8-12 March 2009, San Diego, California, USA*, 7292, 2009.

[7] Quek S. T., Tran V. A., and Hou X. Y., Structural damage detection accounting for loss of data in wireless network sensors. *Proceeding of the 8th international conference on damage assessment of structures, 3-5 August 2009, Beijing China*, 125-132, 2009.

[8] Quek S. T., and Tran V. A., Structural damage detection utilizing accelerations induced by moving load. *Proceeding of the 7th international workshop on structural health monitoring, 9-11 September 2009, Stanford University, Stanford, CA, USA*, (submitted), 2009.